SYNTHESIS, CHARACTERIZATION AND BIOLOGICAL ACTIVITIES OF SOME INDOLE DERIVATIVES AND THEIR METAL COMPLEXES

MOHAMED MUSTAFA MOHAMED IBRAHIM

A thesis submitted in fulfillment of the requirements for the degree of Doctor of Philosophy

Department of Chemistry
Faculty of Science
University of Malaya
2010

CONTENTS

Contents (continued)

Contents (continued)

Contents (continued)

Contents (continued)

Contents (continued)

Acknowledgments

A dissertation does not just appear out of nowhere, and although it is supposed to be a contribution by one person for a PhD, there are still many people who have helped me out over the years. I have been fortunate enough to have had the support of so many people and without it this would not have been possible. While most people did not help directly on the project, every one of them contributed in some way towards helping me to get where I am today, even things like just being a friend and going out and having fun. Others were responsible for giving me a push in the right direction in life, and for everyone listed here I am eternally grateful for their help.

Firstly, I would like to thank my supervisor Prof. Hapipah Mohd. Ali. I could not have imagined having a better advisor and mentor for my PhD, and without her common-sense, knowledge, perceptiveness and cracking-of-the-whip, I would never have finished. Besides being an excellent supervisor, Prof. Hapipah was as close as a relative and a good friend to me. I am really glad that I have come to get to know Prof. Hapipah in my life.

Secondly, I would like to express my thanks to my co-supervisor Dr. Mahmood Ameen Abdullah for his patience and help during all animal experiments which I performed, and without his help I will do nothing. Furthermore his suggestions and discussions are extremely useful.

Also thanks were conveyed to Prof. Ng Seik Weng and Prof. Ward T. Robinson for their help in X-ray crystallography and publications.

I would also like to thank all my colleagues at the Department of Chemistry, and Department of Molecular Medicine, University of Malaya, and all other UM staff and technicians for their instrumental and all other kinds of assistance.

Acknowledgement was also to the financial support of the work by the University Malaya via a postgraduate research grant scheme (PPP grant No. PS145/2007B), and I am indebted to the Institute of Postgraduate Studies (IPS) UM, for awarding a UM fellowship.

Finally I want to thank my family, the encouragement and support from my beloved wife Sulafa and our always positive and joyful children Amro and Amar who are a powerful source of inspiration and energy. A special thought is devoted to my parents, brother and sister for their never-ending support.

Now it is time to catch up on some sleep and have a holiday! (well, not really- there are still plenty of other work to do now).

UNIVERSITI MALAYA
ORIGINAL LITERARY WORK DECLARATION

Name of Candidate: Mohamed Mustafa Mohamed Ibrahim
(I.C/Passport No: 608648)
Registration/Matric No: SHC070009
Name of Degree: PhD
Title of Project Paper/Research Report/Dissertation/Thesis ("this Work"):

Synthesis, characterization and biological activities of some indole derivatives and their metal complexes

Field of Study: Inorganic chemistry

I do solemnly and sincerely declare that:
(1) I am the sole author/writer of this Work;
(2) This Work is original;
(3) Any use of any work in which copyright exists was done by way of fair dealing and for permitted purposes and any excerpt or extract from, or reference to or reproduction of any copyright work has been disclosed expressly and sufficiently and the title of the work and its authorship have been acknowledged in this Work;
(4) I do not have any actual knowledge nor do I ought reasonably to know that the making of this work constitutes an infringement of any copyright work;
(5) I hereby assign all and every rights in the copyright to this Work to the University of Malaya ("UM"), who henceforth shall be owner of the copyright in this work and that any reproduction or use in any form or by any means whatsoever is prohibited without the written consent of UM having been first had and obtained;
(6) I am fully aware that if in the course of making this Work I have infringed any copyright whether intentionally or otherwise, I may be subject to legal action or any other action as may be determined by UM.

Candidate's Signature Date: 6.06.2010

Subscribed and solemnly declared before,

Witness's Signature Date: 6.06.2010

Name: Hapipah Mohd. Ali
Designation: Prof./supervisor

ABSTRACT

Tryptamine (1H-indole-3-ethyleneamine) Schiff bases were prepared by the condensation reaction of ethanolic solution of tryptamine with: salicylaldehyde (TS), 5-chlorosalicylaldehyde (TCS), 5-nitrosalicylaldehyde (TNS), 3,5-di-tert-butyl-2-hydroxy benzaldehyde (TTET) and the ketones: 2-hydroxyacetophenone (THAP), 5-methyl-2-hydroxyacetophenone (TMeHAP), 5-methoxy-2-hydroxyacetophenone (TOMeHAP), 5-chloro-2-hydroxyacetophenone (TClHAP) and 5-bromo-2-hydroxyacetophenone (TBrHAP). The ligands were coordinated to Zn(II), Cu(II) and Ni(II) by the reaction of metal acetates with the corresponding ligand in a 1 : 2 metal to ligand ratio. The solid products formed were collected, washed with ethanol and recrystallized from a suitable solvent. All the ligands and complexes prepared have been characterized by spectroscopic methods using IR, ^{1}H and ^{13}C $\{^{1}H\}$ NMR spectroscopies, and UV-Visible spectrophotomerty. Single crystal X-ray structure analysis was carried out for TNS, $(TS)_2Zn$ complex, $(TS)_2Ni$ complex, $(TCS)_2Zn$ complex, $(TTET)_2Zn$ complex and $(THAP)_2Zn$ complex. Metal content was determined using atomic absorption spectroscopy. X-ray diffraction crystallography for (TNS) shows that it was exists in the zwitterionic form with the phenol H atom transferred to the imine group. Adjacent zwitterions are linked into a linear chain running along the axis by an indole–hydroxy N—H···O hydrogen bond. For zinc complexes the zinc atom is N, O-chelated by two deprotonated Schiff base monoanionic ligands in tetrahedral coordination geometry. In the case of nickel complex, Bis{2-[2-(1H-indol-3-yl)ethyliminomethyl] phenolato k^2N,O}nickel(II) N,N-dimethylformamide disolvate the nickel atom lies on a twofold rotation axis. It is N, O-chelated by the deprotonated Schiff base in a square-planar

coordination environment. The molecule is linked to a solvent molecule by an indole–dimethylformamide NH···O hydrogen bond.

Anti-ulcerogenic activities of the ligands and complexes have been investigated with Cimetidine as a standard drug. The screening was done on high and low doses (60 mg/kg and 30 mg/kg) respectively on six albino Sprague-Dawley rats in which ulcer was induced after dosing by absolute ethanol. The ulcer lesion of the stomachs were identified and counted, and then correlation between the different compound effects has been made. $(TS)_2Zn$ complex proved to be more effective in ulcer inhibition than its nickel and copper congeners.

The anti-oxidant properties for the prepared ligands and complexes have been evaluated against vitamin C and BHT as standard drugs. The complexes show comparable scavenging activity against DPPH radical than do the ligands. Copper complexes reveal the strongest radical scavenging activity among the compounds. However, none of the compounds were found to be better than vitamin C or BHT. $(TTET)_2Zn$, $(TTET)_2Cu$ complexes and TOMeHAP ligand exhibit better ferric reducing abilities than BHT in the FRAP assay. Acute toxicity studies proved that most of the prepared compounds were non-toxic and can be considered as safe.

Abstrak

Sebatian bes Schiff bagi triptamina (1H-indol-3-etilamina) telah disediakan melalui tindak balas kondensasi yang dilakukan di dalam larutan etanol yang setiap satunya mengandungi triptamina dan sebatian aldehid seperti salisilaldehid (TS), 5-klorosalisilaldehid (TCS), 5-nitrosalisilaldehid (TNS), 3,5-di-tert-butil-2-hidroksibenzaldehid (TTET) dan sebatian keton seperti 2-hidroksiasetofenon (THAP), 5-metil-2-hidroksiasetofenon (TMeHAP), 5-metoksi-2-hidroksiasetofenon (TOMeHAP), 5-kloro-2-hidroksiasetofenon (TClHAP) and 5-bromo-2-hidroksiasetofenon (TBrHAP). Semua ligan telah ditindakbalaskan dengan sebatian asetat logam Zn(II), Cu(II) dan Ni(II) dengan nisbah 1 asetat logam dan 2 ligan. Produk yang diperoleh telah dikumpulkan, dicuci dengan menggunakan etanol dan dilakukan pengkristalan semula dalam pelarut yang sesuai. Ligan dan kompleks telah dicirikan melalui kaedah-kaedah spektroskopi seperti IR, ^{1}H dan ^{13}C NMR dan UV-Vis. Analisis struktur bagi TNS, kompleks $Zn(TS)_2$, $Ni(TS)_2$, $Zn(TCS)_2$, $Zn(TTET)_2$ and $Zn(THAP)_2$ telah dijalankan dengan menggunakan kaedah X-ray kristal tunggal. Kandungan logam pula telah ditentukan melalui kaedah spektroskopi penyerapan atom. Kristalografi pembelauan X-ray menunjukkan bahawa TNS wujud sebagai zwitterions dengan atom H daripada fenol dipindahkan kepada kumpulan imina. Zwitterion bersebelahan pula dihubungkan dalam rantai linear melalui ikatan hidrogen indol-hidroksi N - H····· O. Sementara itu, atom zink terikat kepada N dan O pada dua bes Schiff monoanion dan menghasilkan bentuk tetrahedral. Atom nikel bagi kompleks bis{2-[2-(1H-indol-3-yl)] fenolato κ^2N, O} nikel(II) N,N-dimetilformamida tersolvat berada pada paksi putaran *twofold*. Atom

tersebut terikat pada N, O yang ternyahproton pada sebatian bes Schiff secara koordinasi *satah empat segi-sama*. Molekul tersebut dihubungkan kepada molekul pelarut melalui ikatan hidrogen indol - dimetilformamida NH····· O.

Aktiviti anti-ulser bagi semua ligan dan kompleks telah dikaji dengan menggunakan *cimetidine* sebagai sebatian kawalan. Ujian terhadap enam ekor tikus albino Sprague - Dawley telah dijalankan dengan menggunakan dos tinggi dan rendah (60 mg/kg dan 30 mg/kg) yang mana yang tikus - tikus tersebut telah diberikan etanol mutlak selepas sebatian ujian diberikan. Luka ulser di perut tikus telah dikenalpasti, dikira dan korelasi kesan yang ditunjukkan antara sebatian yang berbeza telah dikenalpasti. Kompleks $(TS)_2Zn$ didapati lebih efektif dalam merencatkan pembentukan ulser daripada kompleks nikel dan kuprum yang sepadan dengannya.

Sifat antioksidan bagi ligan dan kompleks yang telah disediakan juga telah dikaji dengan menggunakan Vitamin C dan BHT sebagai sebatian kawalan eksperimen. Sebatian kompleks menunjukkan aktiviti pemerangkapan radikal DPPH yang memberangsangkan berbanding aktiviti yang ditunjukkan oleh sebatian ligan. Sebatian-sebatian kompleks kuprum telah menunjukkan kesan aktiviti pemerangkapan radikal yang terkuat. Walau bagaimanapun, aktiviti bagi semua sebatian yang disintesis tidak mengatasi aktiviti Vitamin C atau BHT. $(TTET)_2Zn$, $(TTET)_2Cu$ dan TOMeHAP menunjukkan keupayaan menurunkan kadar ferik berbanding BHT dalam ujian FRAP. Toksisiti akut juga telah membuktikan bahawa kebanyakan sebatian yang disediakan adalah tidak toksik dan boleh dipertimbangkan sebagai sebatian yang selamat untuk digunakan.

List of abbreviations

Å	Angstrom
AAS	Atomic absorption spectroscopy
Abs.	Absorbance
ANOVA	Analysis of variance
Ar.	Aromatic ring
BHT	Butylated hydroxytoluene
Conc.	Concentration
CT	Charge transfer
Deg.	Degree
DMF	Dimethyl formamide
DMSO	Dimethyl sulphoxide
DPPH	Diphenylpicrylhydrazyl free radical
e.s.d	Estimated standard deviation
FRAP	Ferric reducing anti-oxidant power
%I	Percent inhibition
ICR	Institute of cancer research (United States)
IR	Infrared
kg	Kilogram
LD_{50}	Lethal dose which kills 50% of the animals
m	multiplet
μM	Micromolar
mg	Milligram

ml	Milliliter
nm	Nanometer
NMR	Nuclear magnetic resonance
p	Probability
PGs	Prostaglandines
pH	Hydrogen ion exponent
ppm	Part per million
s	Singlet
S.E.M	Standard error mean
t	Triplet
THF	Tetrahydrofurane
TPTZ	Tripyridyl triazine
U_{eq}	Equivalent isotropic displacement parameter
UI	Ulcer index
US	Ulcer surface
UV-Vis.	Ultra-violet-Visible spectroscopy
Vit C	Vitamin C

List of figures

List of tables

CHAPTER ONE

INTRODUCTION

1. Introduction

1.1 General and historical aspects:

The condensation of primary amines with carbonyl compounds was first reported in 1864 by Schiff [1, 2] and the condensation products are often referred to as Schiff bases. The experimental conditions depend on the nature of the amine and especially of the carbonyl compound which determine the position of the equilibrium:

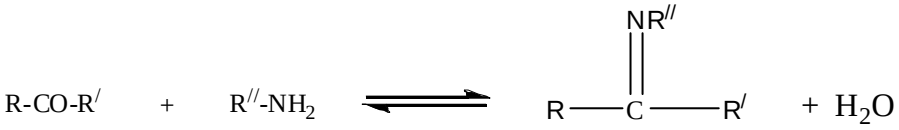

Aromatic aldehydes react smoothly under mild conditions and at relatively low temperature in a suitable solvent. In condensation of aromatic amines with aromatic aldehydes, electron attracting substituents in the para position of the amine decrease the rate of the reaction, while increasing it when on the aldehyde [3]. With ketones, especially aromatic ketones higher temperatures, longer reaction times and catalyst are usually required in addition to the removal of the water as it is formed, and the reaction is acid catalyzed [4].

The most characteristic respect in which compounds containing the C=N bond show basic properties in the formation of complexes is with metals. These complexes provide some very characteristic series of co-ordination compounds, and consequently a large number of them have been prepared and their properties were examined and compared [5-7]. The basic strength of the C=N group is insufficient by itself to permit for the formation of stable complexes by simple co-ordination of the lone pair to a metal ion. Therefore in order the stable compounds should be formed, it is necessary that there

should also be a molecule with a functional group with a replaceable hydrogen atom is present, preferably a hydroxyl group, near enough to the C=N group to permit the formation of a five or six membered ring by chelation to the metal atom.

Among the simplest compounds which meet this requirement are salicylaldimines [Fig1.1a] and their N-hydroxy derivative, salicyldoxime [Fig1.1b] and by far the most intensive studies have been made on the metal complexes of the former and their derivatives.

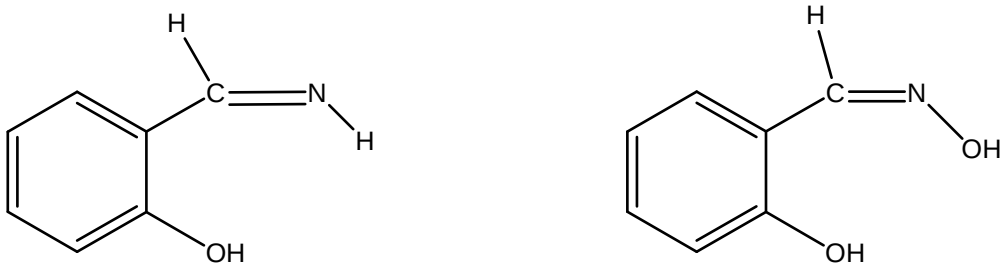

a b

Figure 1.1: Salicylaldimine (a) and Salicyldoxime (b)

The compounds formed with metals by these and other Schiff bases and known up to 1960's have been listed and their properties discussed in details by Holm, Everett and Chakravorthy [8] whilst some of the salicylaldimine complexes have formed the subject of reviews by Sacconi [9].

In 1840 Jorgensen and Werner Ettling [10-11] isolated a dark green crystalline product from the reaction of cupric acetate salicylaldehyde and aqueous ammonia. In 1869 Schiff

isolated the corresponding phenyl derivative as well as 1:2 metal – ligand stoichiometry [12 - 13].

The salicylaldimine complexes of the general type [Fig 1.2a] and [Fig 1.2b] can often be made by the direct interaction between the metal ion and the appropriate Schiff base in alcoholic or aqueous alcoholic solution and in the presence of a base such as sodium hydroxide or sodium acetate.

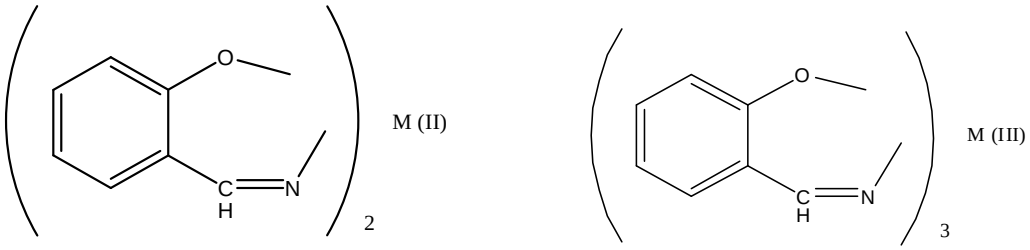

a b

Figure 1.2: Salicylaldimine complexes

Under these conditions the N-alkylsalicylaldimines tend to hydrolyse, however, so a more general useful method of preparation is to reflux the salicylaldehyde complex of the metal with a slight excess of the primary amine in a non aqueous solvent. This procedure was originally used by Schiff [12] who prepared a number of these compounds and proved their compositions.

The co-ordination complexes formed with divalent metal ions (Fig 1.2a) are of considerable interest as they vary in structure from coplanar to tetrahedral not only in dependence of the nature of the divalent metal, but also on the nature of the substituent on the nitrogen atom and the substituents on the aromatic ring of the salicylaldimine molecule.

A number of reasons make complexes of the first row transition metals with salicylaldehyde Schiff bases of significant importance, among them are a large variety of co-ordination geometries, and the complexes often exist in many crystalline modifications, besides the stereochemistry of these complexes is often labile so that very often the molecular configurations in solution are different from those in the solid state and conformational equilibria between different forms takes place.

It has been shown that the lability of the geometry of many metal complexes with Schiff bases also occurs in the solid state, giving rise to cases of anomalous isomorphism [14-15]. This phenomenon has been particularly investigated in complexes of 3d metals from Mn(II) to Zn(II) with N-methylsalicylaldimines having the general formula:

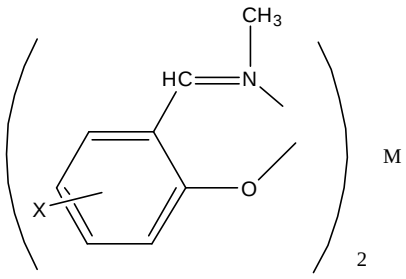

The Ni(II) complex was the first example of the magnetically anomalous complexes reported in the literature [16]. It exists in two planar diamagnetic forms the α-form (orthorhombic) and the β-form (monoclinic). Above 180^{o}C both forms transform to the γ-paramagnetic form. This form is insoluble in all inert solvents. For this reason a polymeric structure involving the sharing of oxygen atoms by the nickel atoms has been attributed to it.

The copper complex exists in three crystalline modifications, α- and γ- both orthorhombic and β- form which is monoclinic. The forms α- and β- are isomorphous with the corresponding forms of the nickel derivative. In these complexes the copper has planar co-ordination geometry [5].

The Mn(II), Co(II) and Zn(II) complexes with N-methyl salicylaldimine are mutually isomorphous. They exist as dimers in the solid state. The metal ion which is bound to three oxygen and two nitrogen atoms has a co-ordination number of five in a distorted trigonl bipyramidal environment [17].

Moreover, a significant amount of information related to the characterization of Schiff bases and their metal complexes with several metals has appeared in the literature [18-19] The spectroscopic properties of salicylaldimines and α-hydroxy naphthaldimines with copper(II), nickel(II) and iron(III) complexes were studied previously [20]. NMR results have shown the presence of keto-amine versus enol-imine equilibria:

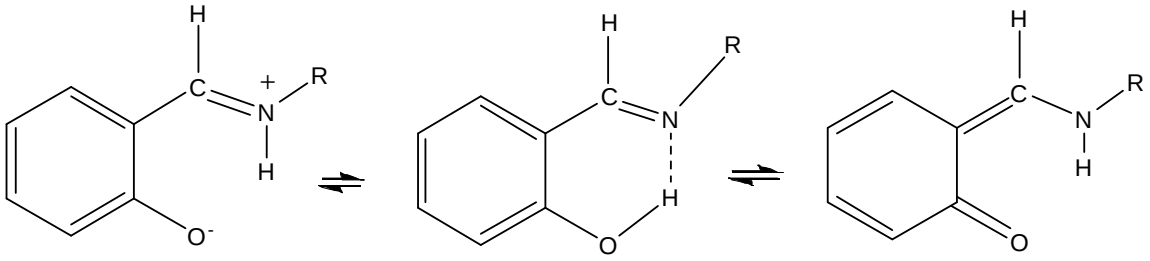

enol-imine keto-imine

Recently in 1986 M.G Martin Reyes, P. Gili and co-workers [21] have synthesized and characterized for the first time the Schiff base 1H-Indole-3-ethylene salicylaldimine from the coupling reaction of tryptamine and salicylaldehyde. The Cu(II), Ni(II) and Co(II) complexes were also studied. The results indicate that the ligands were co-ordinated

through oxygen and nitrogen atoms with the metal ions in different stereochemistry. The electronic spectra of the compounds revealed that the energy of the $\pi - \pi^*$ transition of the chelate ring of the ligand is characteristic of Schiff bases which exhibit delocalized systems with an intramolecular hydrogen bonding [22]. It was also been suggested that for the Cu(II) complex the position of UV bands at high wavelengths indicates the presence of a square planar environment around the copper ion in solution, shifted towards a pseudotetrahedral geometry in the solid state [23].

In 1989 P. Gili and co-workers extend the work and synthesized and characterized a Schiff bases: 3- and 5-methoxysalicylaldimine-3-ethlene-1H Indole and their Co(II), Ni(II) and Cu(II) complexes. X-ray structure for the Cu(II) complex indicates co-ordination of the Cu(II) complex is trans planar (CuO_2N_2) geometry [24] and also the two Ni(II) complexes (NiO_2N_2). The magnetic data for bis(1H-Indole-3-ethylene-5-methoxysalicylaldimine) Co(II) complex is consistent with an octahedral environment around the metal.

In 1990 P. Martin Zarza *et al* has extended the work further through the condensation reaction of tryptamine with 2-hydroxyacetophenone and other diketones [25]. They also prepared and characterized their Cu(II) complexes. The electronic diffuse reflectance spectra of the bidentate ligand complexes indicate a distorted pseudotetrahedral disposition around the Cu(II) ion attributed to the substitution of the hydrogen atom on the iminic carbon by methyl groups.

P. Gili extended his work in 1990 for related compounds with different substituents in order to study how the nature and position of the alkoxy group in the ligand and complexes affect their properties. Thus he described a new nickel complex of the ligand:

1H-Indole-3-ethylene-3-ethoxysalicylaldimine. He discovered that the geometry around the Ni atom is a square planar with the metal atom lying at the center of symmetry. There is an intermolecular hydrogen bonding between the nitrogen atom of the indole group and the phenolic oxygen of the ethoxysalicylaldiminate moiety. The six-membered chelate ring is observed puckered while in related compounds the equivalent rings are nearly planar probably due to the accommodation of the larger ethoxy groups in order to avoid steric hindrance [26]

Similar complexes of Cu(II) and Ni(II) with the ligand N-[2-(3-ethyl indole) pyridoxaldimine prepared by the condensation reaction of tryptamine with pyridoxal have been synthesized and characterized [27]. X-ray diffraction analysis for Ni(II) complex indicate that the co-ordination of the Ni(II) complex is trans planar NiN_2O_2 species and the spectroscopic data for the Cu(II) complexes suggest the same chromophore group CuN_2O_2 with a trans configuration in the solid phase. The nickel atom is lying at the center of symmetry and is four co-ordinated to the phenolic oxygen atoms and the imine nitrogen atoms of the two Schiff base units. The crystal structure can be described in terms of chains of complex units along the crystallographic b-axis. The complex units in the chains are held together by intermolecular hydrogen bonding. Each hydrogen bond is formed between the nitrogen atom of the indole group and the pyridine nitrogen atom of the pyridoxaldiminate group.

In 1997 manganous complexes containing Mn(II) and Mn(III) species have been introduced with the Schiff base: N-[2-(3-ethylindole)] pyridoxaldimine previously stated [28]. The compounds have been characterized by spectroscopic methods as well as magnetic measurements, thermogravimetric and calorimetric studies. The spectroscopic

and magnetic data indicate a tetrahedral co-ordination for the Mn(II) complex and a five co-ordination for the Mn(III) complex. Square pyramidal geometry was favored by such bulky ligands. However the observed geometries are usually intermediate between trigonal bipyramidal and square pyramidal. The steriochemical non-rigidity is common for penta co-ordinate complexes which thus can easily exhibit distorted geometries.

Lanthanide complexes of salicylaldehyde Schiff bases with salicyled hydrazide and anthranilic acid were synthesized and characterized [29]. Proton NMR spectra and infra red studies for the complexes reveal the bidentate binding of both Schiff base ligands to the lanthanide ion. Electronic spectra along with the conductance data for the complexes indicate a coordination number of six for the lanthanide ion in the complexes of both the Schiff bases.

1.2 Biological activities of Schiff bases and their metal complexes:

A great deal of information regarding the properties of synthetic Schiff bases of potential biological interest has arisen during the last few years [30-32]. Several of these compounds were characterized and used as models for a series of systems including nickel which has been found in few biological systems, but has recently been detected in very low amounts in jack-bean urease [33] and in some hydrogenases [34-35].

Also it is well known that several metalloproteins and metaloenzymes play important roles in natural biological systems. These functions are related to catalytic activity in reactions such as hydrogen exchange, hydrolysis of esters, carboxylation or decarboxilation. The functions of a metal ion in a metalloprotein are determined by structural characteristics which include, among others, the nature of its co-ordination

sphere. These functions also depend on the structural arrangement in the vicinity of the metallic ion but outside its co-ordination sphere [36-37].

Schiff base complexes are known to be dioxygen carriers and have been studied as potential reagents for oxygen separation and transportation. [2, 38-40]. The Co(II) complexes of Schiff bases such as bis(salicylaldehyde) ethylenediamine and its analogues have been the first and extensively investigated. Dian Chen *et al* [41] has synthesized a series of Co(II) Schiff base complexes and their oxygen affinities have been tested against the effect of substituents in the benzene ring. The substitution of methyl groups on the Schiff bases (α-substitution, acetophenone derivatives) increases the affinity for oxygen but also increasing the rate of degradation. Flourine substitution on the aromatic rings of the Schiff bases increasing the affinity for dioxygen by promoting 2:1 (binuclear) dioxygen complex formation. Sulphonation of the aromatic rings of the Schiff base increase the rate of degradation of the Co(II) complexes studied. Methoxy groups on the aromatic rings of the Schiff bases tends to increase the affinity of the Co(II) complex for dioxygen and favor 1:1 dioxygen complex formation. Combination of dioxygen with the Co(II) complexes of the pentadentate Schiff bases seems to be partially inhibited by steric effects, which are relieved by hydrogenation of the ligands. The Co(II) complexes of reduced ligands have much higher affinities for dioxygen than do the complexes of the corresponding Schiff bases.

The first report that a low molecular weight Cu(II) complex was effective against rheumatoid arthritis appears as early as 1941 [42]. Sorenson and Hangarter reviewed the treatment of some 1500 patients since then with a variety of copper Schiff base

compounds. Cupraline (formula (I), Figure1.3), alcuprin (formula (II), Figure 1.3) and dicuprene (formula (III), Figure 1.3) [43].

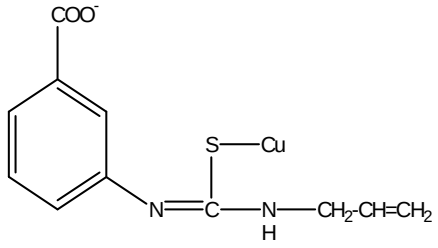

(I)

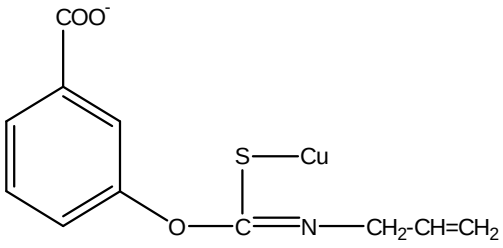

(II)

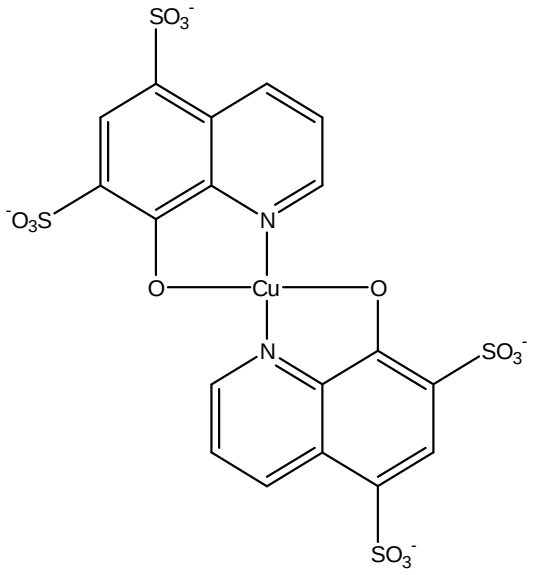

(III)

Figure 1.3: Cupraline(I) , Alcuprin(II) and Dicuprene (III)

These preparations all bring about marked reductions in inflammation and particularly show very few toxic reactions. Indeed they exhibit an antiulcer activity [44-45] which is significant because gastrointestinal irritation commonly necessitates treatment by many

antiarthritic drugs to be abandoned [46]. This in line with the role of copper in generally preventing gastrointestinal damage by acidic anti-inflammatory agents [47].

P.K Parashar *et al* studied the anti-inflammatory and anti ulcer activities of Schiff bases derived from salicylaldehydes and 2-substituted aniline and their metal chelates with Cu(II), Ni(II), and Co(II) [48]. The compound salicylidene anthranilic acid was found to possess antiflammatory and antiulcer activity, while the copper complexes showed an increased antiulcer activity. Similar study was carried out by K. D Rainsford and co-workers on a number of Cu(II) complexes [49]. Results show that Cu(II) preparations which are highly irritating outside the stomach, caused no ulceration when applied intra gastric, but always elicited a copious mucus effusion into the stomach. This non ulcerant effect was confirmed by light microscopic observations of formaline-fixed tissues stained with periodic acid Schiff reagent, Alcian blue (pH 2.5) or the haematoxylin and eosin stains.

Mucus discharge from the superficial and gastric pit mucous cells was clearly evident after administering $CuCl_2$ and those Cu(II) complexes which elicited a visible mucus effusion. Some disruption of parietal cells was also seen specially after giving high doses of Cu(II) compounds [49].

L.Araya and J.Vargas [36] studied a series of Cu(II) complexes derived from substituted anilines and bromosalicylaldehydes. They realize that biological and catalytic response of the complex may be increased or diminished by small changes in the ligand structure and this may be attributed to the redox activity and an interesting problem in bioinorganic chemistry has been the quantitative evaluation of the effect on the redox potential of changing the ligand structure.

Jan Vanco *et al* [50] recently described copper and zinc complexes with a tridentate ONO donor Schiff base derived from salicylaldehyde and β-alanine. Their biological activities have been evaluated by the anti-peroxynitrite activity assay and alloxan induced diabetes model. Significant antioxidant and anti-diabetic activities have been found in the case of Cu(II) complexes, but not significant in the case of Zn(II) complex. The biological results sets the potential use of Cu(II) complexes as nutritional supplements with biological activities relevant in prevention of diseases connected with progression of oxidative stress-like diabetes mellitus.

Pt(II) complexes with Schiff bases derived from salicylaldehyde and phenylene diamine have been studied along with their biological activities as anti-microbials [40] The results revealed that the complexes are more microbial toxic than the ligands. Chelation to the metal ion reduces the polarity of the metal mainly because of partial sharing of its positive charge with the donor groups and possible π-electron delocalization within the whole chelate ring. Also chelation increases the lipophelic nature of the central atom which subsequently favors its permeation through the lipid layer of the cell membrane.

Schiff bases derived from the reaction of salicylaldehyde and 2-amino-3-carboxy ethyl - 4, 5 dimethyl thiophene and their metal complexes with Mn(II), Fe(II), Co(II), Ni(II), Cu(II) and Zn(II) have also been studied and screened for their anti bacterial activities [51] It has been observed that the antibacterial activity of the ligand increased on chelation with the metal ions. Metal chelates of salicylaldimines derived from heterocyclic systems, which have known to be unstable, can be stabilized by suitable substitutions at the remaining positions of the thiophene ring by an ester group and two methyl groups. The resulting compound 2-amino-3-carboxyethyl-4, 5 dimethyl thiophene

has been condensed with salicylaldehyde to form a potentially tridentate Schiff base: (N-salicylidene)-3-carboxyethyl-4, 5 dimethyl thiophene containing an ONO doner sequence. It is also found that introduction of carboxyethyl group at position 3 of the thiophene ring has provided further scope of reactivity and a new coordination site. In addition highly substituted thiophenes have shown extensive potential in pharmaceutical industry, besides the structural diversities, bonding interactions, bioisosteric relationship of thiophene to benzene has lead to several structures of drug analogs in which benzene rings have been replaced by thiophene rings and the vivid applications of thiphene derivatives as important therapeutic agents which have been documented in literature [52]. It is expected that metal chelates containing thiophene ring system would carry bioisosteric relationship and therapeutic values thus introducing another class of metal-based thiophene derivatives.

The antibacterial property can be thought of as a result of geometry and charge distribution around the molecule [53]. If the geometry and charge distribution around the molecule are incompatible with those around the holes of the bacterial cell wall, penetration through the wall by the toxic agent cannot takes place and this in turn prevent the toxic reaction within the pores. The presence of co-ligand also plays a decisive role in determining the antibacterial property of metal complexes. The mode of action of the complexes also indulges in the formation of hydrogen-bonded interaction through the coordinated anion and the azomethine group, with the active centers of the cell constituents resulting in interference with the normal cell processes.

It has been also shown that Schiff base complexes derived from 4-hydroxysalicylaldehyde and amines have strong anticancer activity e.g. *Ehrlich ascites*

carcinoma as well as antifungal activity [54]. N-4-hydroxysalicylidene-glycylglycine, and its Mn(II), Co(II), Ni(II) and Cu(II) complexes have been synthesized, characterized and screened for antifungal activity towards *Candida albicans* and *Cryptococcus neoformans*. The results show that the ligand and its complexes exhibit strong inhibition towards *Cryptococcus neoformans* under the test conditions. All of the compounds have strong inhibitory action towards *Candida albicans* when the concentration is comparatively high. When the concentration of the compounds is 200 ppm the ligand N-4-hydroxysalicylidene-glycylglycine and its complexes exhibit strong antifungal activity to the two selected fungi except for copper complex.

Schiff base ligands containing cyclobutane and thiazole rings have been studied together with their Co(II), Cu(II), Ni(II) and Zn(II) complexes [55]. Anti microbial activities of the ligands and their complexes have been tested against eight different microorganisms. The ligands with the nitrogen and oxygen donor system might have inhibited enzyme production, since enzymes which require a free hydroxyl group for their activity appear to be especially susceptible to deactivation by the ions of the complexes. Chelation reduces the polarity of the central ion mainly because of the partial sharing of its positive charge with the donor groups and possible π-electron delocalization within the whole chelate ring. This chelation increases the liophilic nature of the central atom which favors its permeation through the lipid layer of the membrane.

To wide the scope of investigation on the coordination behavior of Schiff base ligands in biological systems towards organotin complexes, Han Dong *et al* [56] has reported six diorganotin(IV) derivatives of salicylaldehyde isonicontinylhydrazone. X-ray studies of the ligand and its di-tert-butyl Sn(IV) complex show that the Schiff base ligand is a

tridentate planar ligand, the tin atom lies in this plane and formed a five-membered and six-membered chelate ring with the ligand.

In 2006, Hapipah Mohd Ali *et al* [57] has introduced Ni(II) and Cd(II) complexes of Schiff base ligand derived from 4-nitrobenzhydrazide and 5-chloro-2-hydroxyacetophenone as well as their anti cancer activity. IR and UV spectra of the ligand and complexes indicate coordination of the ligand to the metal centers. The nickel complex is a square planar which changed to octahedral geometry in pyridine solution due to coordinated solvent molecules. The Schiff base ligand is more sensitive towards human breast cancer cells (MCF-7) than the unsubstituted ligand. However upon coordination to nickel the activity have been reduced to the same level as the positive control drug tamoxifen. The anti-oxidant properties of the Schiff base ligand exhibited higher activity than vitamin-E or quercetine. However the activity is lower than the unsubstiuted Schiff base ligand or the commercial anti-oxidant agent butylated hydroxytoluene (BHT).

1.3 The objectives of this work:

In this work we report the synthesis, characterization, anti ulcerogenic and antioxidant activities of Schiff bases derived from the condensation reaction of tryptamine with the aldehydes: salicylaldehyde, 5-chlorosalicylaldehyde, 5-nitrosalicylaldehyde, 3,5-di-tert-butyl-2-hydroxy benzaldehyde, and the ketones: 2-hydroxyacetophenone, 5-chloro-2-hydroxyacetophenone, 5-bromo-2-hydroxyacetophenone, 5-methyl-2-hydroxyacetophenone, and 5-methoxy-2-hydroxyacetophenone, together with their Zn(II), Ni(II) and Cu(II) complexes. All the prepared compounds were characterized by

spectroscopic methods including IR, ^{1}H and ^{13}C NMR, UV-Visible and X-ray diffraction whenever possible and applicable, as well as AAS for metal analysis.

The prepared compounds were screened for anti-ulcer test, the screening involved high (60 mg/kg) and low (30 mg/kg) dosage of compound onto a minimum number of 6 adult male and female albino Sprague-Dawley rats to determine the best dosage needed for the ulcer treatment. Rats were fasting for two days but were allowed to access to water. The rats were fed with synthetic compound in 10% Tween-20 and after 30 minutes absolute ethanol were administrated. They were left for another 30 minutes before sacrifice. The 1 day screening process includes negative control (10% Tween-20) and positive control (Cimetidine). After the rats sacrificed, the stomachs are removed, incised along its greater curvature and gastric juices as well as the mucus were collected. The stomachs were preserved in 10% formalin for gastric lesions measurement to determine mucosal erosion. The sum of the areas was expressed as ulcer index (mm^2). The mucus was weighted and juices were measured for pH. Values were expressed as mean ± S.E.M.

Acute toxicity studies for the ligands were checked and assessed in terms of LD_{50}.

CHAPTER TWO

EXPERIMENTAL

2. Experimental

2.1 Preparation of the ligands:

2.1.1 Preparation of: 1H-Indole-3-ethylenesalicylaldimine (TS):

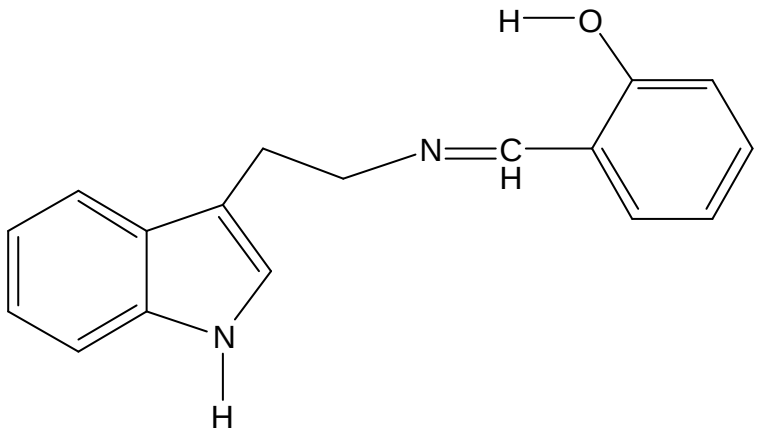

Tryptamine (0.3g, 1.87 mmol.) was dissolved in 50 ml of acidified ethanol (pH 4.5) and added to (0.228g, 1.86 mmol.) of salicylaldehyde in 50 ml acidified ethanol (pH 4.5). The mixture was stirred under reflux for 2 hours. The solid product was formed, filtered and recrystallized from hot ethanol (yield 71%).

2.1.2 Preparation of: 1H-Indole-3-ethylene-5-chlorosalicylaldimine (TCS):

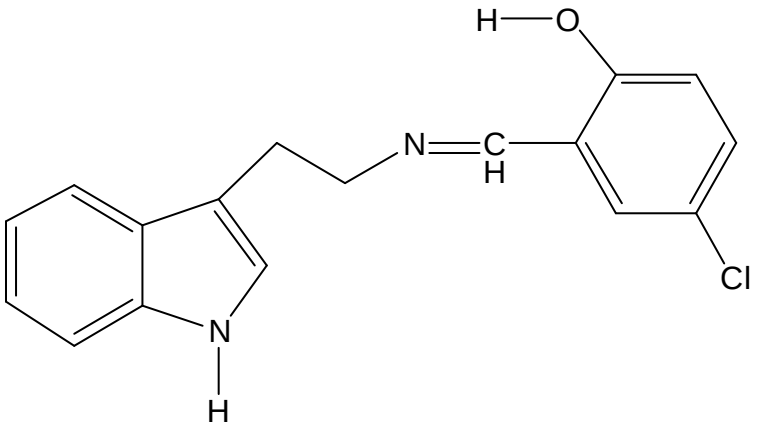

Tryptamine (0.3g, 1.87 mmol.) was dissolved in 50 ml of acidified ethanol (pH 4.5) and added to (0.29g, 1.80 mmol.) of 5-chlorosalicylaldehyde in 50 ml acidified ethanol (pH 4.5). The mixture was stirred under reflux for 2 hours. A solid product was formed, filtered and recrystallized from hot ethanol (yield 79%).

2.1.3 Preparation of: 1H-Indole-3-ethylene-5-nitrosalicylaldimine (TNS):

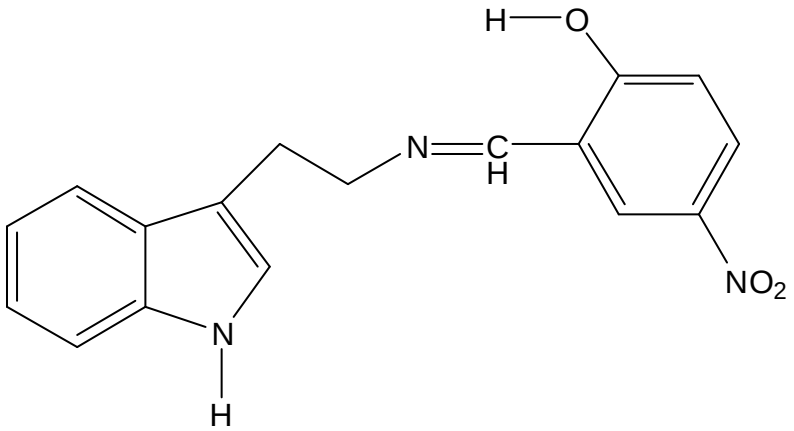

Tryptamine (0.3g, 1.87 mmol.) was dissolved in 50 ml of acidified ethanol (pH 4.5) and added to (0.33g 1.9 mmol.) of 5-nitrosalisylaldehyde in 50 ml of acidified ethanol (pH 4.5). The mixture was stirred for 2 hours under reflux. A solid product was formed, filtered, and recrystallized from hot THF (yield 54%).

2.1.4 Preparation of: 1H-Indole-3-ethylene-3-5-di-tertiarybutylsalicylaldimine (TTET):

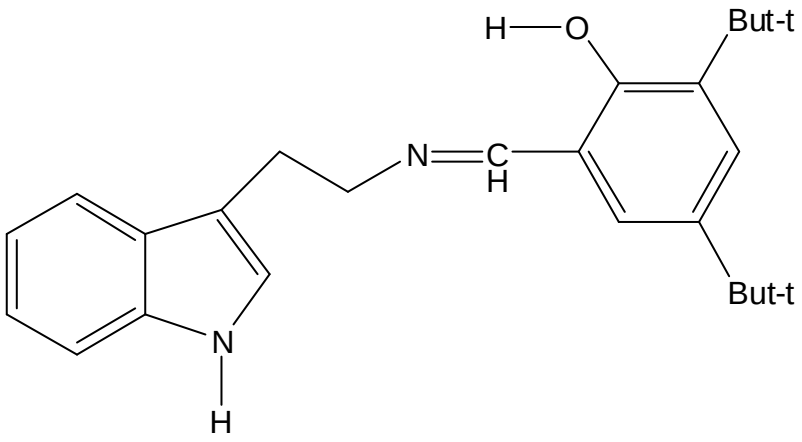

Tryptamine (0.5g, 3.12 mmol.) was dissolved in 50 ml of acidified ethanol and added to (0.73g, 3.12 mmol.) of 3, 5 ditertiarybutyl-2-hydroxybenzaldehyde in 50 ml acidified ethanol. The mixture was refluxed for 2 hours in a water bath. The product was collected after the evaporation of ethanol at room temperature, and recrystallized from hot ethanol (yield is 80%).

2.1.5 Preparation of: 2-{1-[2-(1H-Indole-3-yl)ethylimino]-ethyl}phenol (THAP):

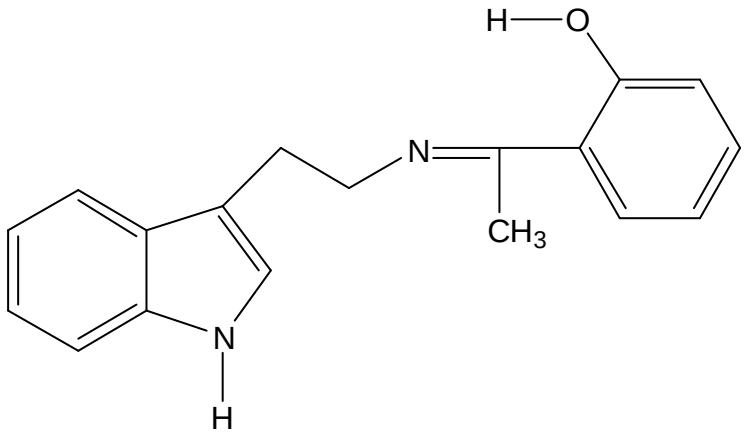

Tryptamine (0.5g, 3.12 mmol.) in 50 ml acidified ethanol was added to (0.426g, 3.13 mmol.) of 2-hydroxyacetophenone in 50 ml of acidified ethanol. The mixture was refluxed in a water bath for 2 hours. The solvent was reduced in a rotary evaporator, and the yellow product was collected by filtration, recrystallized from hot ethanol (yield is 79.4%).

2.1.6 Preparation of: 2-{1-[2-(1H-Indole-3-yl)-ethylimino]-ethyl}-4-methyl phenol (TMeHAP):

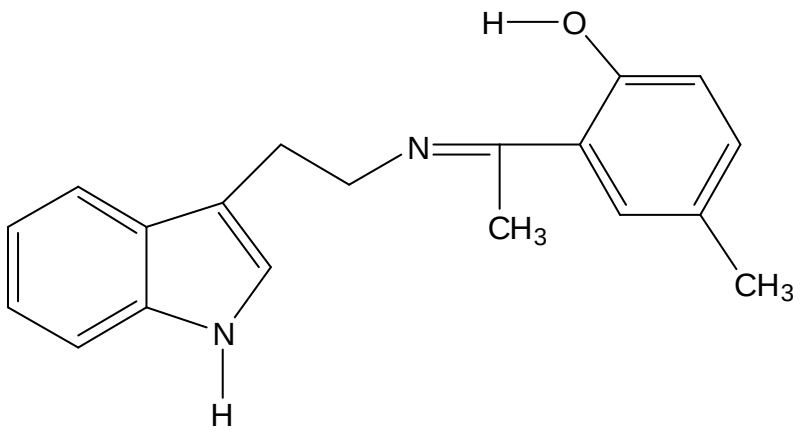

Tryptamine (0.5g, 3.12 mmol.) was dissolved in 50 ml of acidified ethanol, and added to (0.468g, 3.11 mmol.) of 5-methyl-2-hydroxyacetophenone in 50 ml of acidified ethanol. The reaction mixture was refluxed for 2 hours in a water bath. A solid product was formed, filtered and recrystallized from hot ethyl acetate (yield is 70%).

2.1.7 Preparation of: 2-{1-[2-(1H-Indole-3-yl)-ethylimino]-ethyl}-4-methoxy phenol (TOMeHAP):

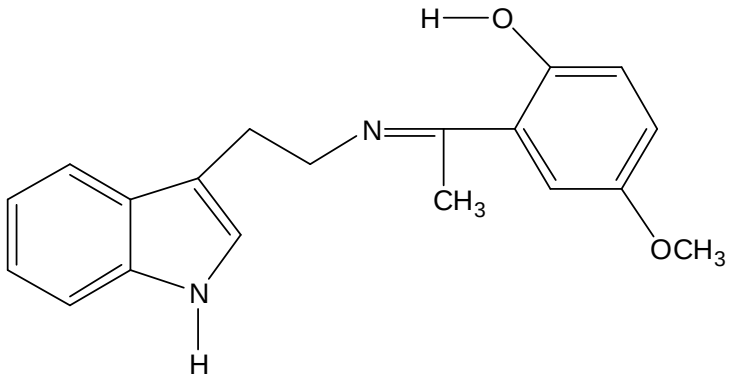

Tryptamine (1g, 6.24 mmol.) was dissolved in 50 ml of acidified ethanol, and added to (1.04g, 6.25 mmol.) of 5-methoxy-2-hydroxyacetophenone in 50 ml of ethanol. The reaction mixture was refluxed for 2 hours. The yellow product was formed after reduction of the solvent, filtered and recrystallized from hot ethyl acetate (percentage yield 72.2%).

2.1.8 Preparation of: 2-{1-[2-(1H-Indole-3-yl)-ethylimino]-ethyl}-4-chloro phenol (TClHAP):

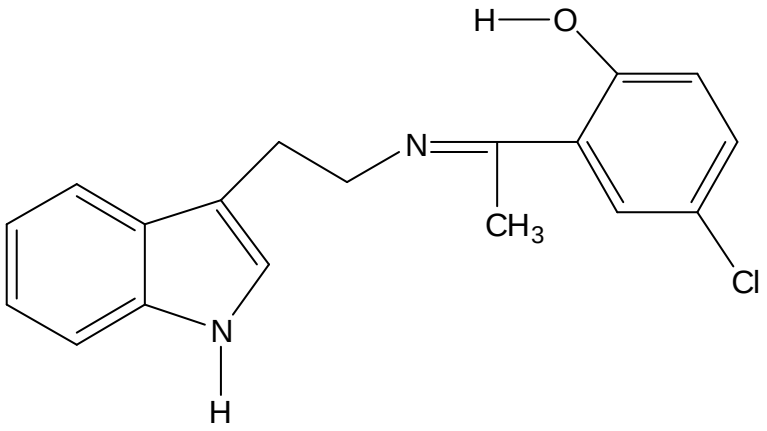

Tryptamine (1g, 6.24 mmol.) was dissolved in 50 ml of acidified ethanol at pH 4.5, and added to (1.06g, 6.21 mmol.) of 5-chloro-2-hydroxyacetophenone in 50 ml of acidified ethanol. The reaction mixture was refluxed in a water bath for 2 hours. After the reduction of the solvent, the yellow crystalline product was filtered, washed with ethanol, and dried at room temperature (percentage yield 81.2%).

2.1.9 Preparation of: 4-Bromo-2-{1-[2-(1H-Indole-3-yl)-ethylimino]-ethyl}-phenol (TBrHAP):

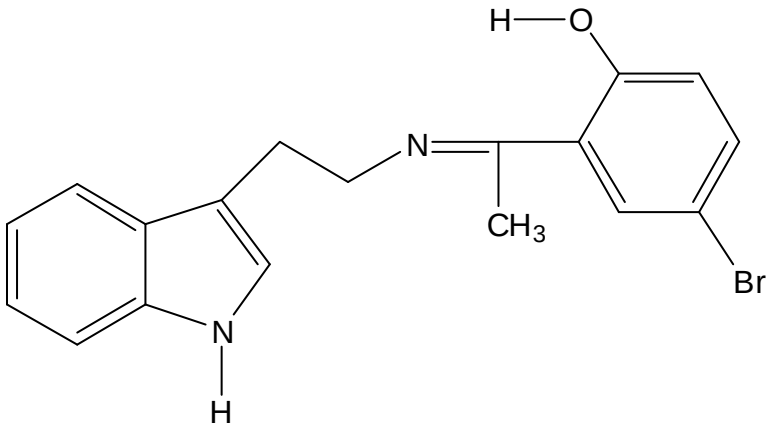

Tryptamine (1g, 6.24 mmol.) was dissolved in 50 ml of acidified ethanol, and added to (1.34g, 6.23 mmol.) of 5-bromo-2-hydroxyaceophenone in 50 ml acidified ethanol. The mixture was refluxed for 2 hours. A cotton yellow product was formed filtered and recrystallized from boiling ethanol (percentage yield 91.6 %).

2.2 Preparation of the complexes:

2.2.1 Preparation of: bis(1H-Indole-3-ethylenesalicylaldiminato-k^2N,O)Zn(II): $(TS)_2Zn$:

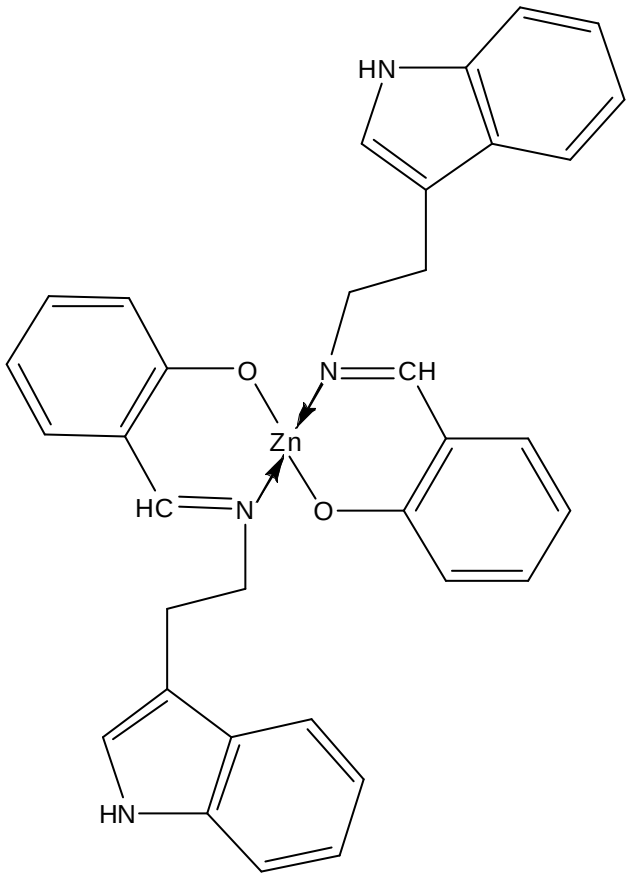

TS (0.5g, 1.89 mmol.) in 50 ml of ethanol and (0.21g, 0.956 mmol.) of zinc acetate dihydrate in 10 mls of ethanol was stirred and refluxed for 5 hours in the presence of few drops of triethylamine. The solid product formed was filtered and recrystallized from DMF (yield 0.458g, 82%).

2.2.2 Preparation of: bis(1H-Indole-3-ethylenesalicylaldiminato-k^2N,O)Ni(II): $(TS)_2Ni$:

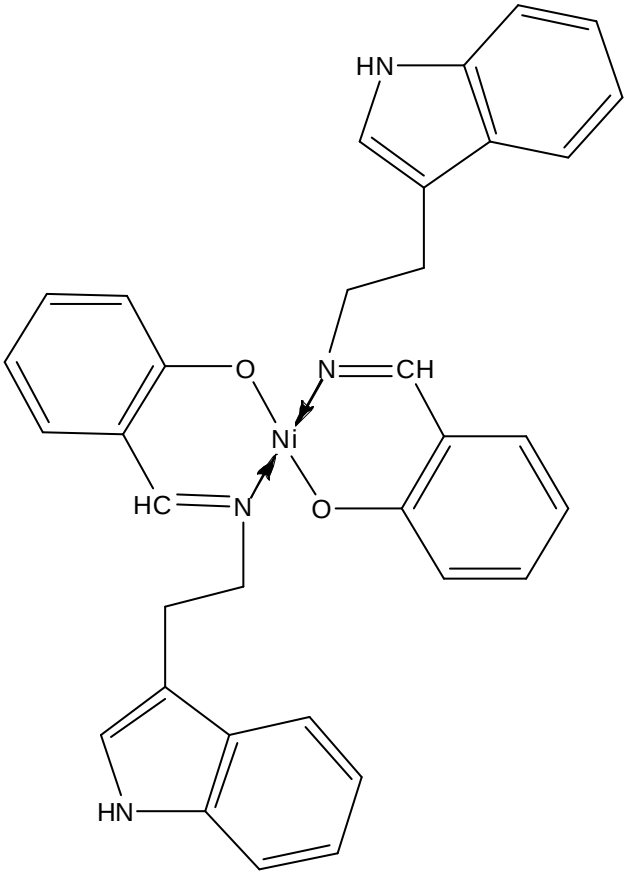

TS (0.506g, 1.91 mmol.) in 50 ml of ethanol and (0.231g, 0.930 mmol.) of nickel acetate tetrahydrate in 10 mls of ethanol was stirred and refluxed for 5 hours in the presence of few drops of triethylamine. The solid product formed was filtered and recrystallized from DMF (yield 0.464g, 82.8%).

2.2.3 Preparation of: bis(1H-Indole-3-ethylenesalicylaldiminato-k^{2}N,O)Cu(II): (TS)$_2$Cu:

TS (0.505g, 1.91 mmol.) in 50 ml of ethanol and (0.189g, 0.951 mmol.) of copper(II) acetate monohydrate in 10 mls of ethanol was stirred and refluxed for 5 hours in the presence of few drops of triethylamine. The solid product formed was filtered and recrystallized from DMF (yield 0.481g, 85%).

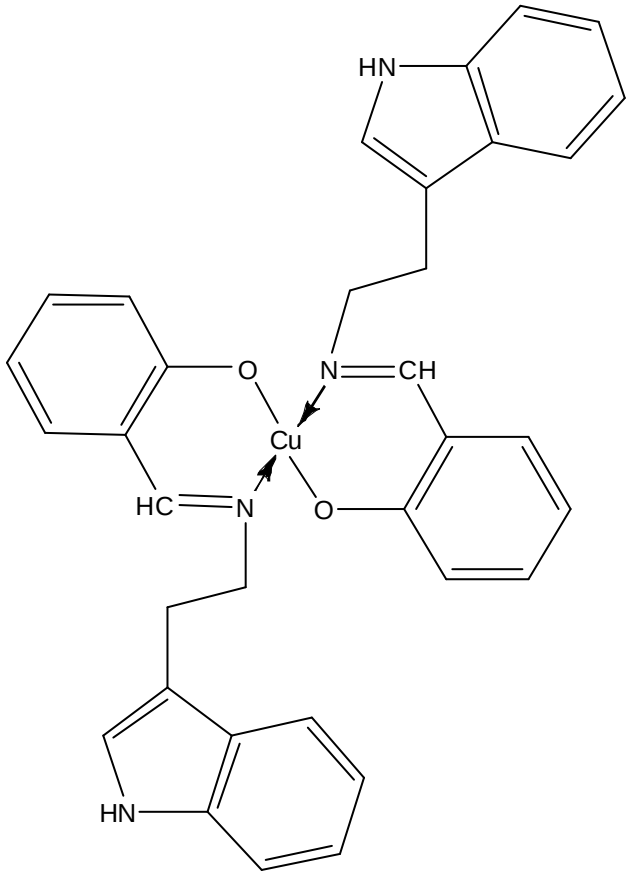

2.2.4 Preparation of: bis{4-chloro-2-[2-(1H-indol-3-yl)ethyliminomethyl] phenolato-κ2N, O} zinc(II): $(TCS)_2Zn$:

TCS (0.5g, 1.67 mmol.) in 50 ml of ethanol and (0.18g, 0.835 mmol.) of zinc acetate dihydrae in 10 mls of ethanol was stirred and refluxed for 5 hours in the presence of few drops of triethylamine. The solid product formed was filtered, and recrystallized from DMF (yield 0.321g, 58%).

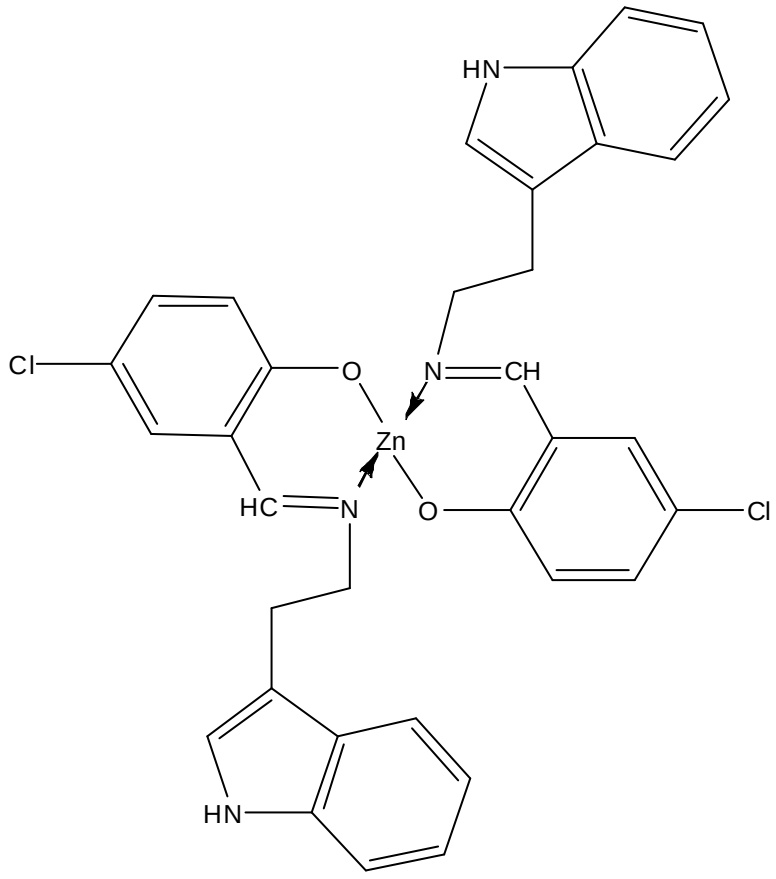

2.2.5 Preparation of: bis{4-chloro-2-[2-(1H-indol-3-yl)ethyliminomethyl] phenolato-κ2N, O} nickel(II): $(TCS)_2Ni$:

TCS (0.501g 1.67 mmol.) in 50 ml of ethanol and (0.207g, 8.35mmol.) of nickel acetate tetrahydrate in 10 mls of ethanol was stirred and refluxed for 5 hours in the presence of few drops of triethylamine. The solid product formed was filtered and recrystallized from DMF (yield 0.321g, 70%).

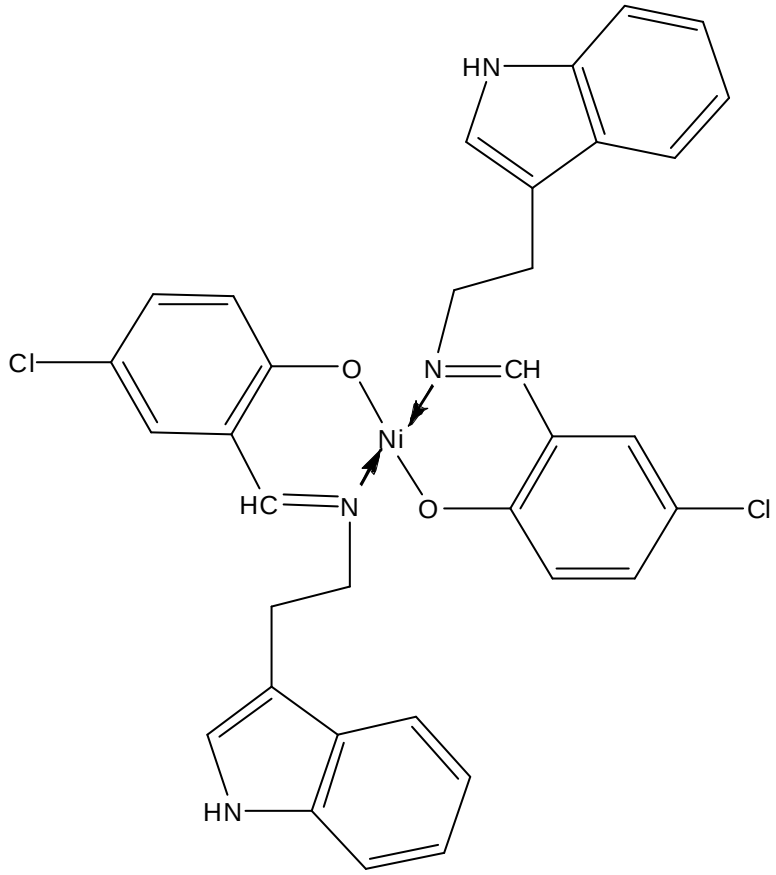

2.2.6 Preparation of: bis{4-chloro-2-[2-(1H-indol-3-yl)ethyliminomethyl] phenolato-κ2N, O} copper(II): $(TCS)_2Cu$:

TCS (0.505g, of 1.69 mmol.) in 50 ml of ethanol and (0.168g, 8.41 mmol.) of copper acetate monohydrate in 10 mls of ethanol was stirred and refluxed for 5 hours in the presence of few drops of triethylamine. The solid product formed was filtered and recrystallized from DMF (yield 0.474g, 85%).

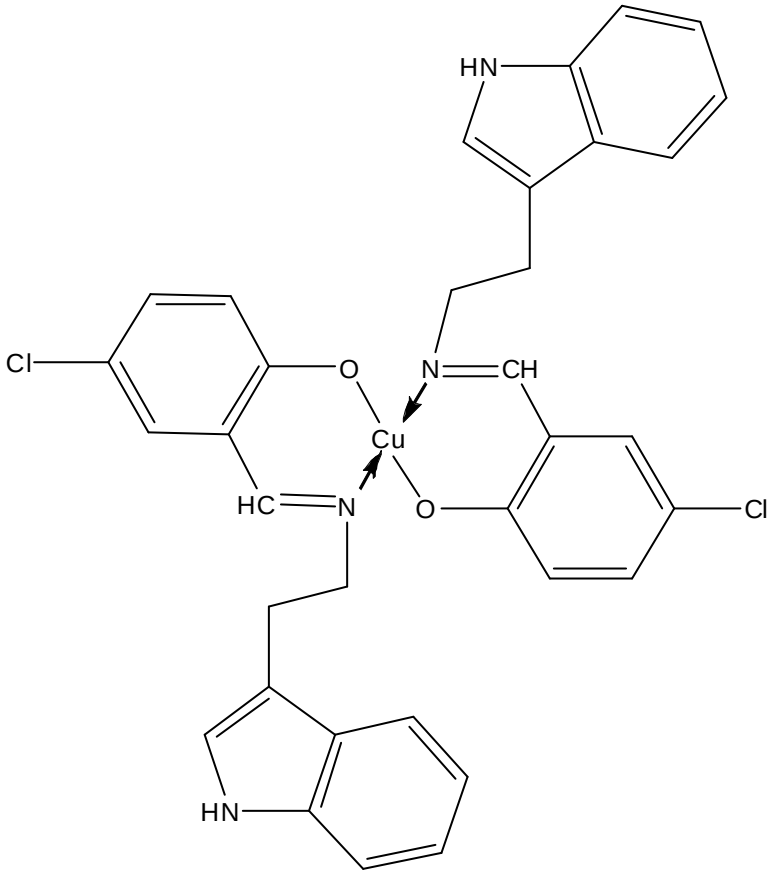

2.2.7 Preparation of the complex: bis{4-nitro-2-[2-(1H-indol-3-yl)ethyliminomethyl] phenolato-κ2N, O} zinc(II): $(TNS)_2Zn$:

TNS (0.502g, 1.62 mmol.) in 50 ml of THF and (0.192g, 0.876 mmol.) of zinc acetate dihydrate in 10 mls of ethanol was stirred and refluxed for 5 hours in the presence of few drops of triethylamine. The solid product formed was filtered and recrystallized from DMF (yield 0.326g, 59%).

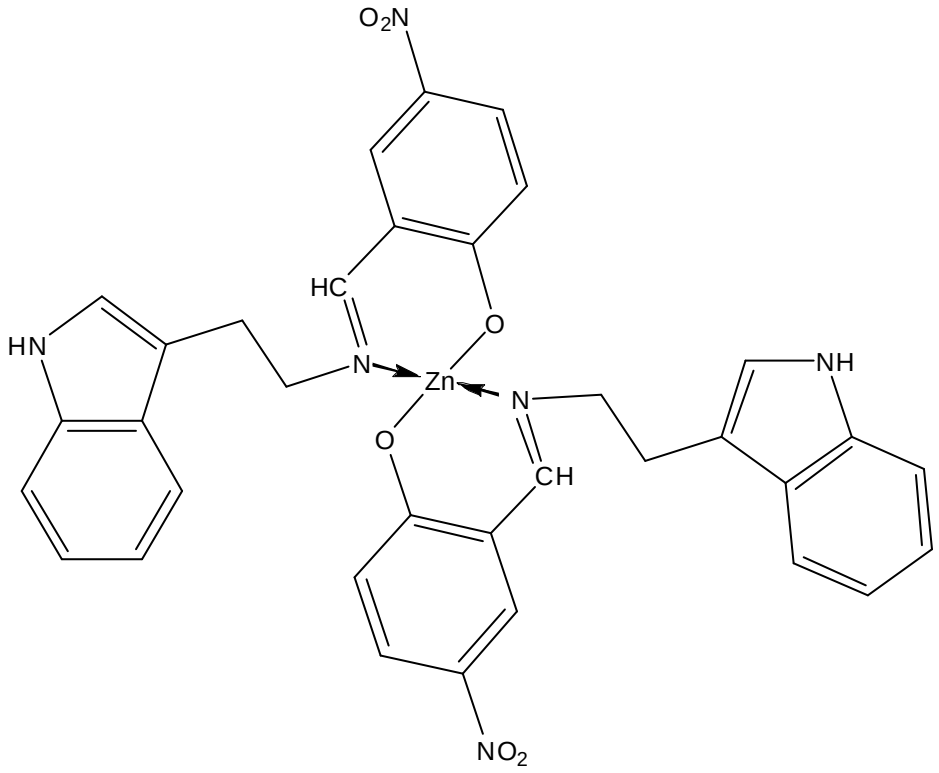

2.2.8 Preparation of: bis{4-nitro-2-[2-(1H-indol-3-yl)ethyliminomethyl] phenolato-κ2N, O} nickel(II): $(TNS)_2Ni$:

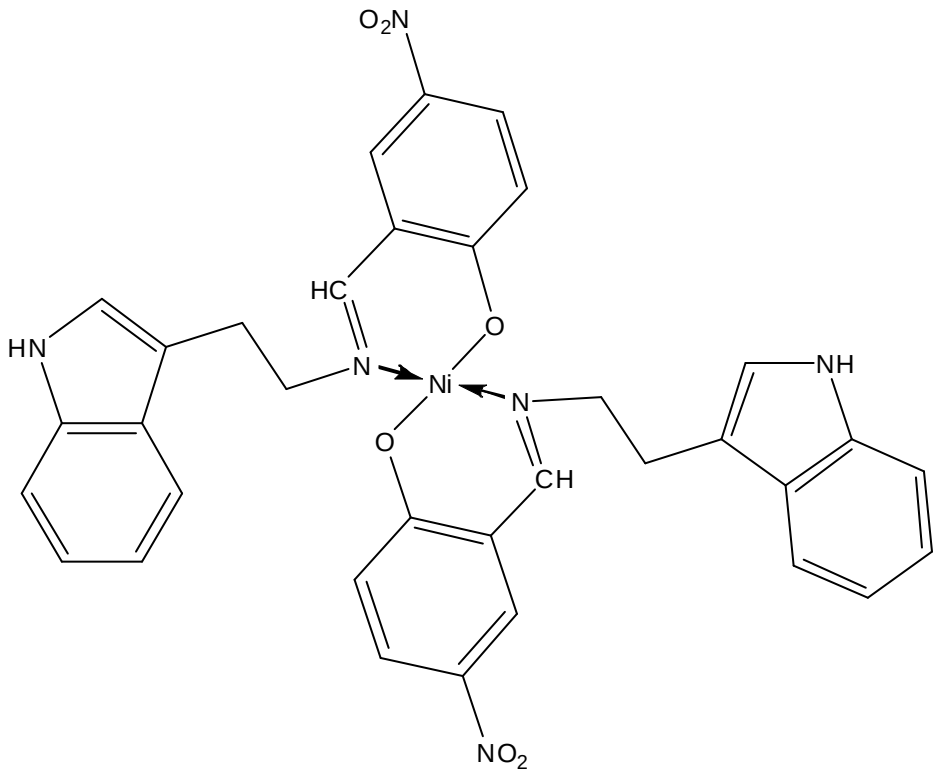

TNS (0.505g, 1.63 mmol.) in 50 ml of ethanol and (0.203g, 8.15 mmol.) of nickel acetate tetrahydrate in 10 mls of ethanol was stirred and refluxed for 5 hours in the presence of few drops of triethylamine. The solid product formed was filtered and recrystallized from DMF (yield 0.423g, 76.7%).

2.2.9 Preparation of: bis{4-nitro-2-[2-(1H-indol-3-yl)ethyliminomethyl] phenolato-κ2N, O} copper(II): $(TNS)_2Cu$:

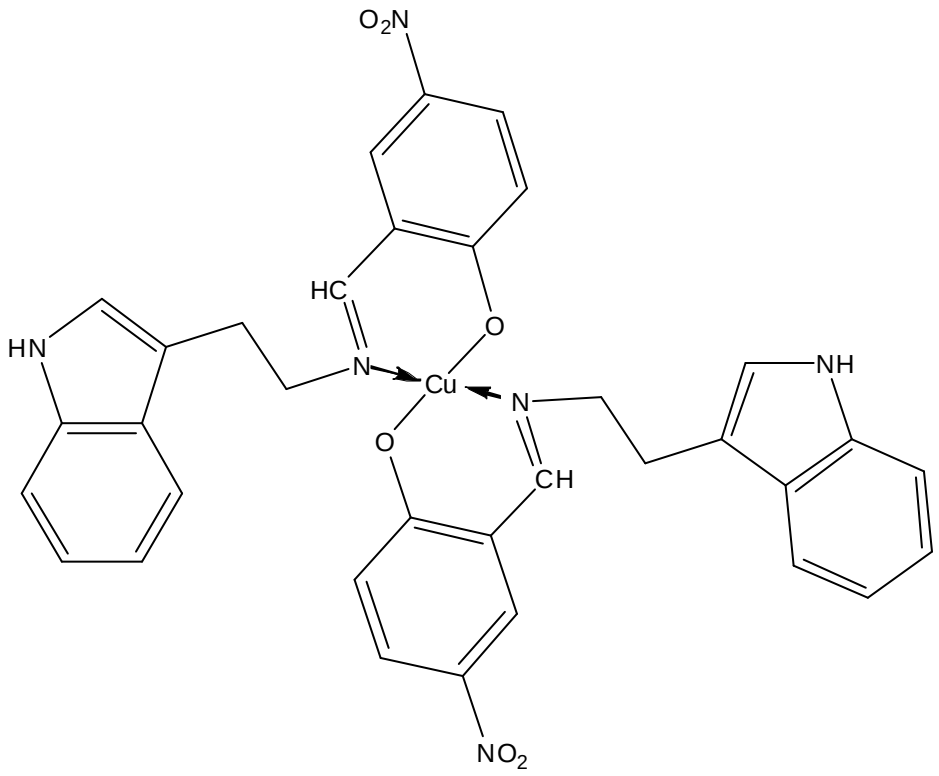

TNS (0.505g, 1.62 mmol.) in 50 ml of THF and (0.181g, 0.91 mmol.) of copper acetate monohydrate in 10 mls of ethanol was stirred and refluxed for 5 hours in the presence of few drops of triethylamine. The solid product formed was filtered and recrystallized from DMF (yield 0.423g, 76.2%).

2.2.10 Preparation of: bis(1H-Indole-3-ethylene-3-5-di-tertiarybutylsalicylaldiminato-k^2N,O)Zn(II): $(TTET)_2Zn$:

TTET (0.5g, 1.33 mmol) was dissolved in 50 ml of ethanol; and 20 ml (0.15g, 0.664 mmol.) of zinc acetate dihydrate was added to the solution. Few drops of triethylamine were then added, and the mixture was refluxed in a water bath for 5 hours. The pale yellow product formed was collected through a filter paper, and recrystallized from DMSO. (yield 0.31g, 71.9%).

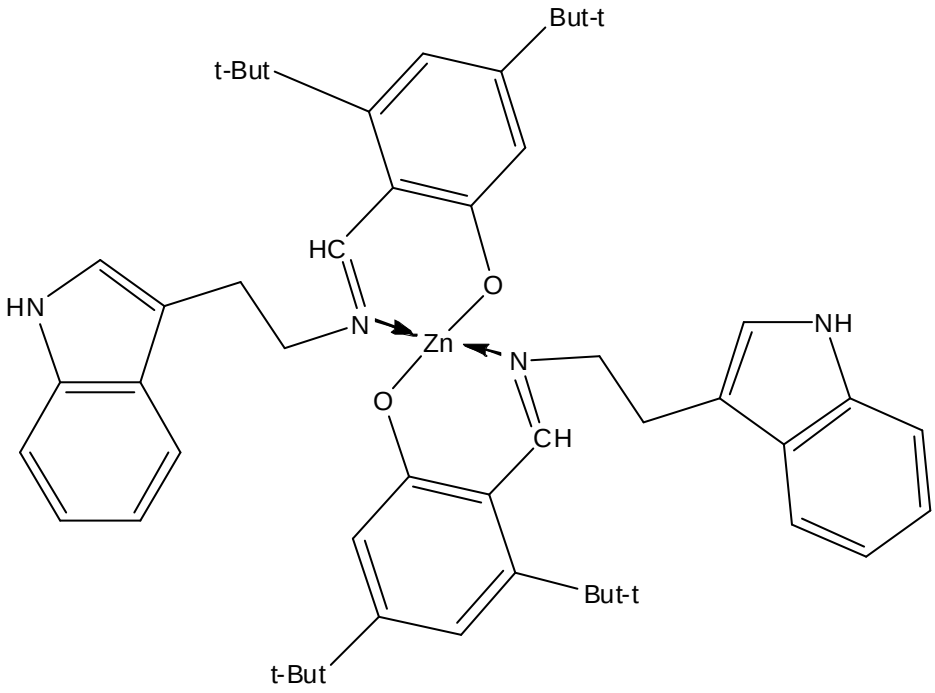

2.2.11 Preparation of: bis(1H-Indole-3-ethylene-3-5-di-tertiarybutylsalicylaldiminato-k^2N,O)Ni(II): $(TTET)_2Ni$:

TTET (0.5g, 1.33 mmol.) was dissolved in 50 ml of ethanol; 20 ml (0.165g, 0.663 mmol.) of nickel acetate tetrahydrate was then added together with few drops of triethylamine. The mixture was refluxed for 5 hours. The sticky product formed was treated with n-hexane whereby a brownish yellow precipitate was separated, filtered and washed several times with n-hexane (yield 0.126g, 23.46%).

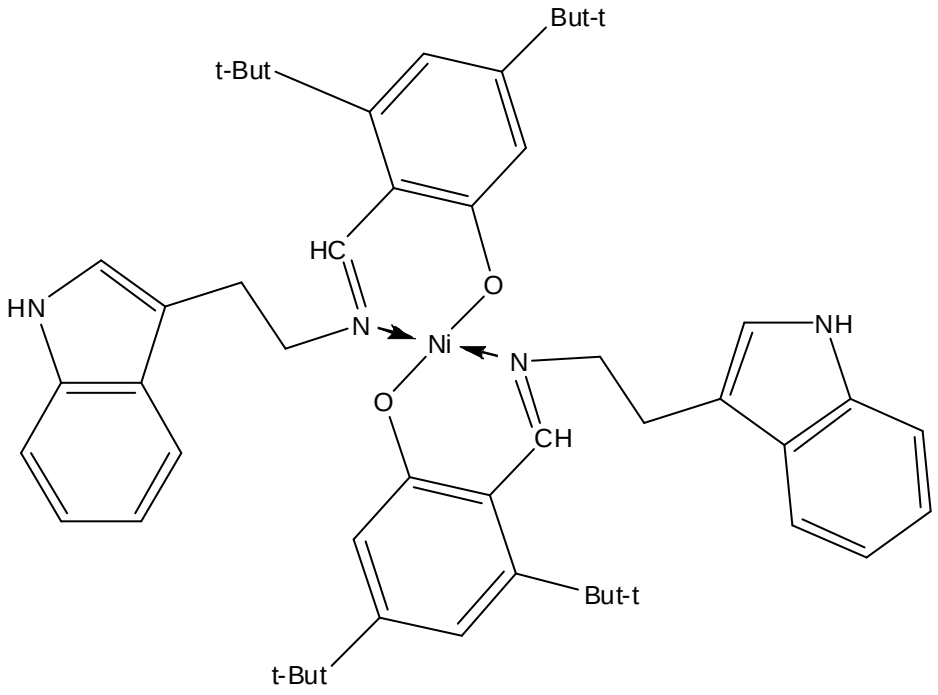

2.2.12 Preparation of: bis(1H-Indole-3-ethylene-3-5-di-tertiarybutylsalicylaldiminato-k^2N,O)Cu(II): $(TTET)_2Cu$:

TTET (0.5g, 1.33 mmol.) in 50 ml of ethanol was mixed with (0.13g, 0.651 mmol.) of copper acetate monohydrate in 20 ml of ethanol. Few drops of triethylamine were introduced to the reaction vesicle, and the mixture was refluxed for 5 hours. After the reduction of the solvent, a sticky product was formed, treated with n-hexane whereby a black precipitate was separated, filtered and washed with n-hexane.

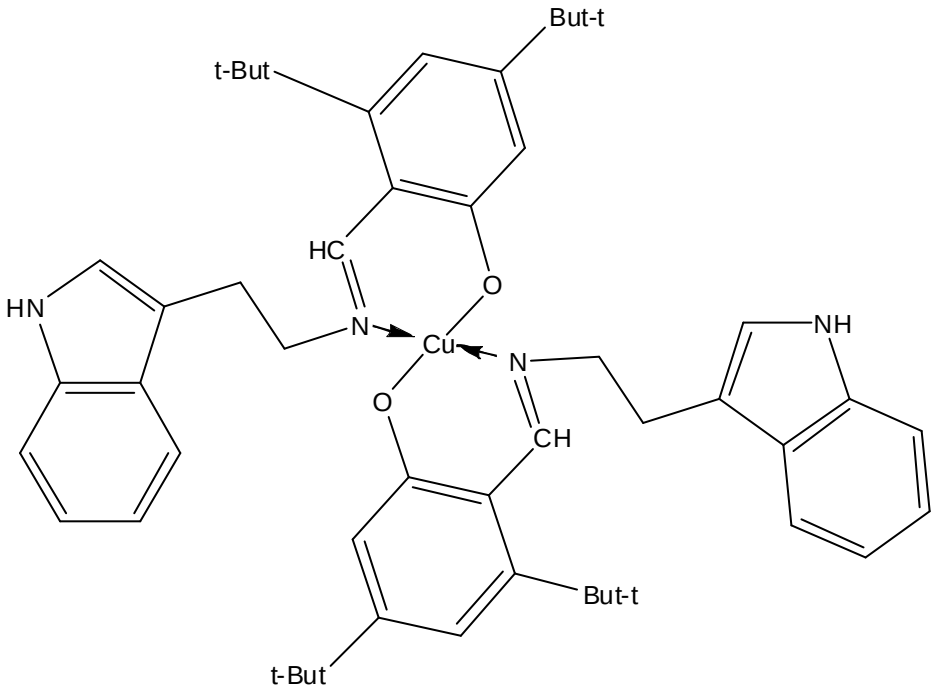

2.2.13 Preparation of:

dichloridobis(2-{1-[2-(1H-indol-3-yl)-ethyliminio]ethyl}phenolate-kO)zinc(II):

$(THAP)_2Zn$:

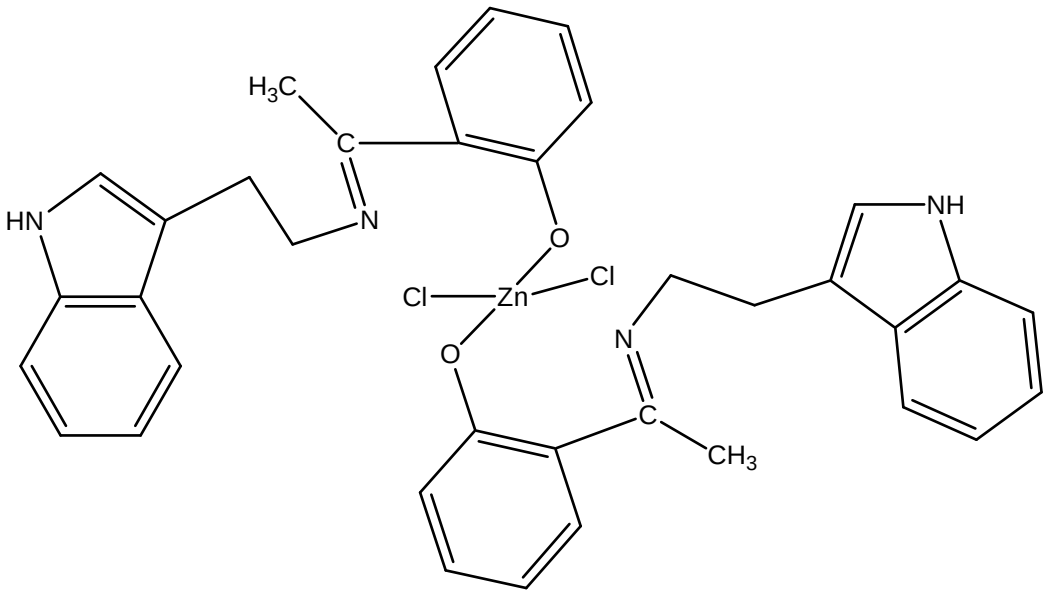

THAP (0.5g, 1.8 mmol.) was dissolved in 50 ml of ethanol, and added to (0.122g, 0.895 mmol.) of unhydrous zinc chloride in 20 ml of dry ethanol; 0.024g of sodium hydride was then added. The reaction mixture was brought into a vacuum line, evacuated from air and refluxed for 5 hours under nitrogen. The product formed was collected and recrystallized from hot ethanol.

2.2.14 Preparation of:

bis(2-{1-[2-(1H-indol-3-yl)- ethyliminio]ethyl}phenolato-k^2N, O)Ni(II): $(THAP)_2Ni$:

THAP (0.5g, 1.8 mmol.) in 20 ml of ethanol, 0.06g of NaH and (0.224g, 0.90 mmol.) of nickel acetate tetrahydrate in 20 ml of ethanol were mixed and refluxed for 3 hours in a water bath. After which the reaction volume was reduced to the third, then distilled water was added. The green precipitate formed was filtered, washed with water and ethanol and dried in the oven at 50 ^{0}C.

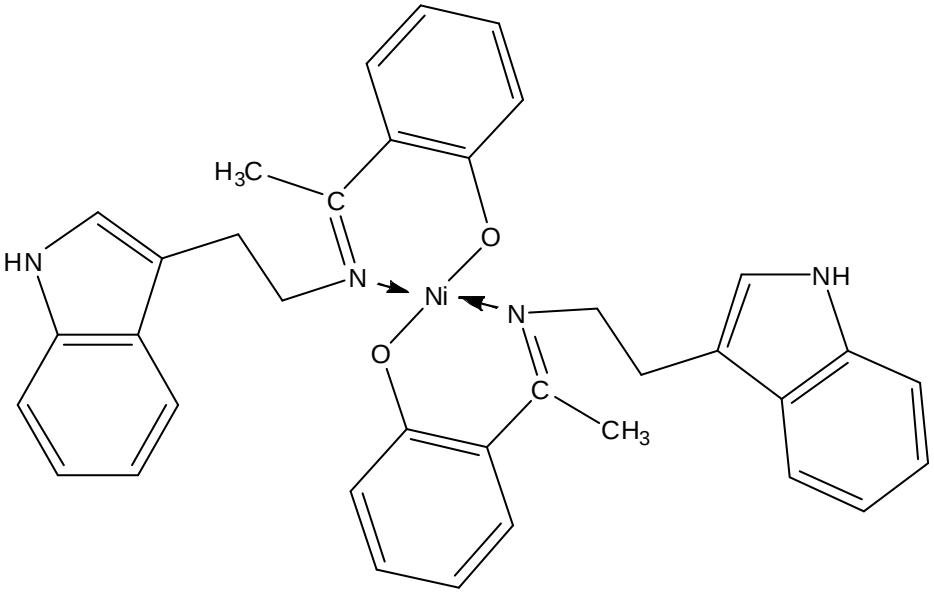

2.2.15 Preparation of:

bis(2-{1-[2-(1H-indol-3-yl)-ethyliminio]ethyl}phenolato-k^2N, O)Cu(II): $(THAP)_2Cu$:

THAP (0.5g, 1.8 mmol.) in 50 ml of ethanol, and (0.177g, 0.88 mmol.) of copper acetate monohydrate in 20 ml of ethanol were mixed. Few drops of triethylamine were added to

the reaction mixture, and the reaction was refluxed for 5 hours in a water bath. A brown product was formed, filtered, washed with ethanol and dried at room temperature. (percentage yield 28.4%).

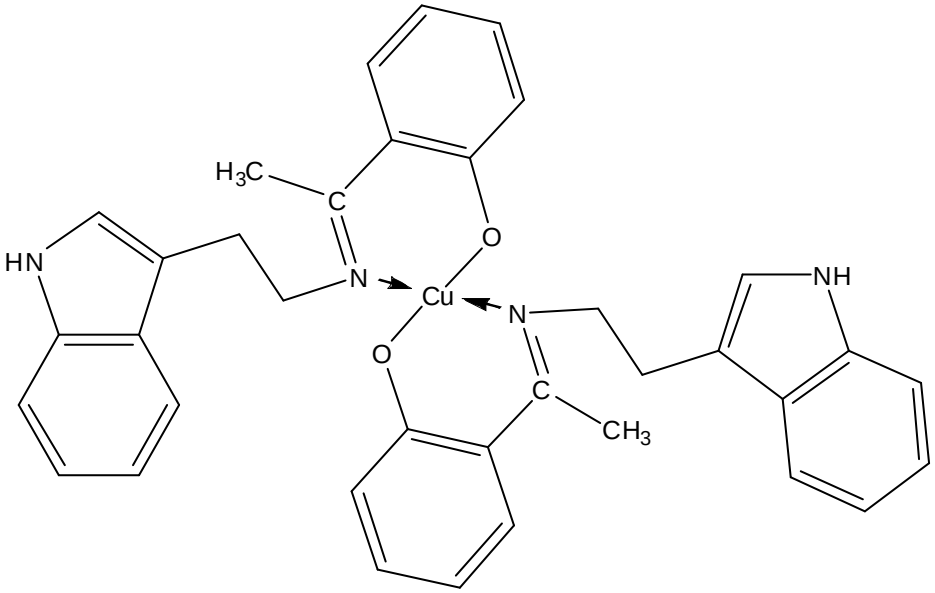

2.2.16 Preparation of:

bis{2-{1-[2-(1H-Indole-3-yl)-ethylimino]-ethyl}-4-methylphenolato-k^{2}N,O}Cu(II):

(TMeHAP)$_2$Cu:

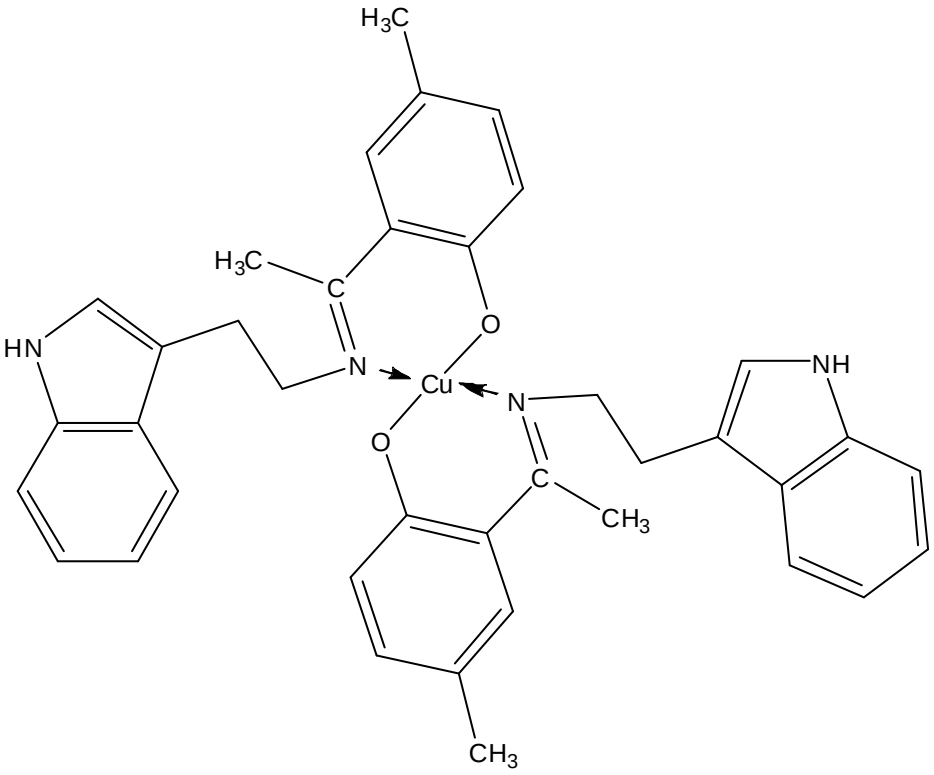

TMeHAP (0.5g, 1.71 mmol.) was dissolved in 50 ml of ethanol, and added to (0.173g, 0.866 mmol.) of copper acetate monohydrate in ethanol followed by few drops of triethylamine to make the reaction mixture slightly basic. The mixture was refluxed for 5 hours and the brown product formed was filtered, washed with ethanol and dried at room temperature (yield 34.6 %).

2.2.17 Preparation of:

bis{2-{1-[2-(1H-Indole-3-yl)-ethylimino]-ethyl}-4-methoxyphenolato-k^{2}N,O}Ni(II):

(TOMeHAP)$_2$Ni:

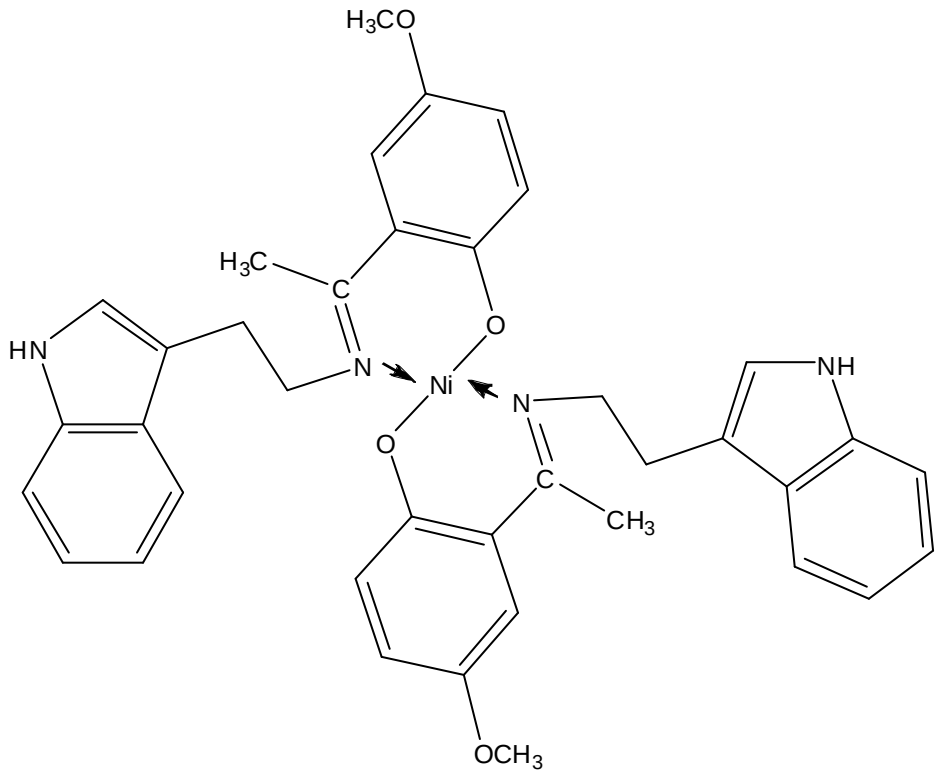

TOMeHAP (0.5g, 1.62 mmol.) was dissolved in 20 ml of ethanol, and added to (0.2g, 0.80 mmol.) of nickel acetate tetrahydrate in 20 ml of ethanol. 0.06g of NaH was introduced to the reaction mixture. The mixture was refluxed for 5 hours in a water bath after which time the volume of the reaction was reduced to the third. Distilled water was then added. A yellow product was separated, filtered, washed with water, ethanol and dried at 50 ^{0}C at the oven.

2.2.18 Preparation of:

bis{2-{1-[2-(1H-Indole-3-yl)-ethylimino]-ethyl}-4-methoxyphenolato-k^2N,O}Cu(II):

$(TOMeHAP)_2Cu$:

TOMeHAP (0.5g, 1.62 mmol.) was dissolved in 50 ml of ethanol, and added to (0.16g, 0.80 mmol.) of copper acetate monohydrate in 20 ml of ethanol. Few drops of triethylamine were then added. The mixture was refluxed in a water bath for 5 hours. The brown precipitate formed was then filtered, washed with ethanol and dried at room temperature (percentage yield 19.1%)

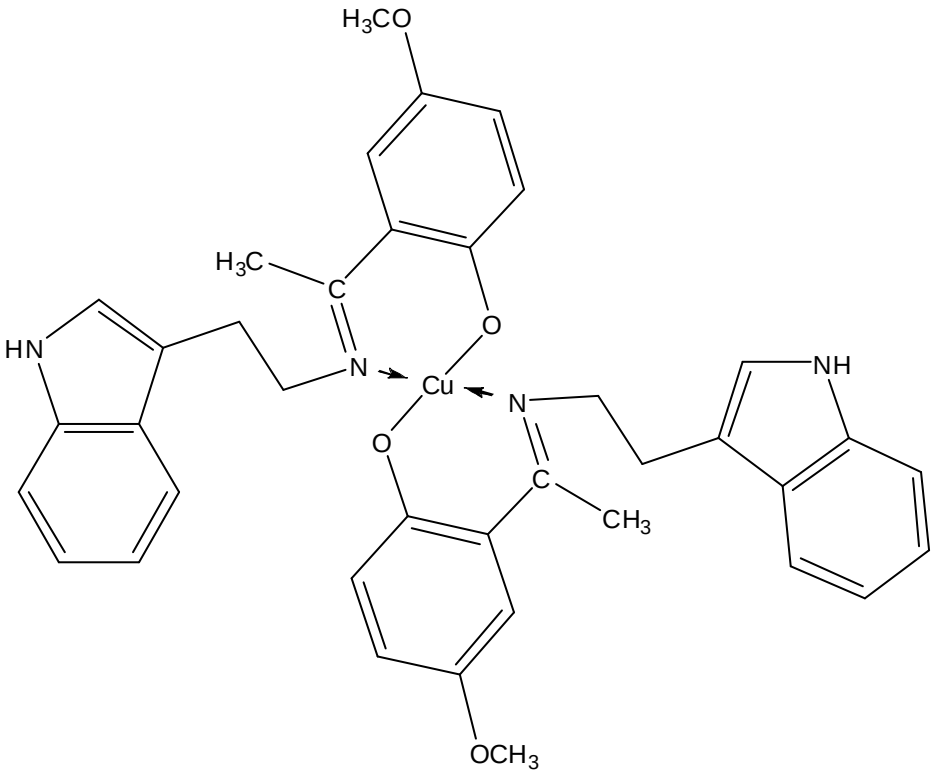

2.2.19 Preparation of:

bis{2-{1-[2-(1H-Indole-3-yl)-ethylimino]-ethyl}-4-chlorophenolato-k^2N,O}Ni(II):

$(TClHAP)_2Ni$:

The ligand (0.5g, 1.68 mmol.) was dissolved in 20 ml of ethanol, and added to (0.2g, 0.80 mmol.) of nickel acetate tetrahydrate in 20 ml of ethanol. 0.06g of NaH was then added. The mixture was refluxed for 3 hours after which the volume was reduced and water was added. A solid product was formed, filtered, washed with ethanol and water and dried in the oven at 50 ^{0}C.

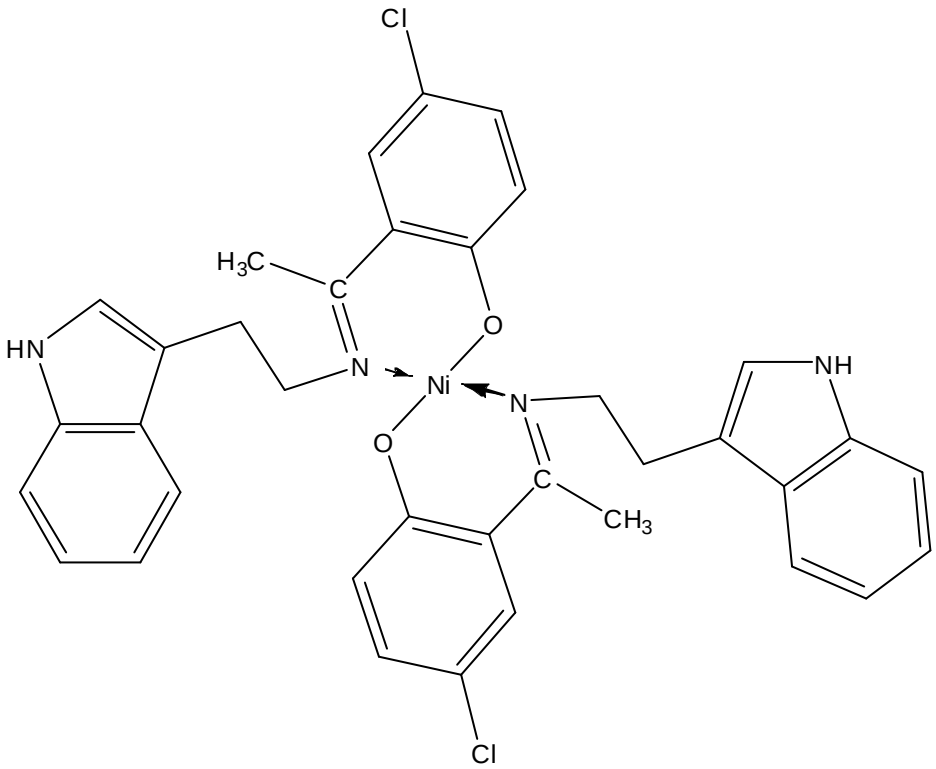

2.2.20 Preparation of:

bis{2-{1-[2-(1H-Indole-3-yl)-ethylimino]-ethyl}-4-chlorophenolato-k^2N,O}Cu(II):

$(TClHAP)_2Cu$:

The ligand (0.5g, 1.68 mmol.) was dissolved in 50 ml of ethanol and added to (0.16g, 0.80 mmol.) of copper acetate monohydrate in 20 ml of ethanol. Few drops of triethylamine were then added. The mixture was refluxed for 5 hours. A brown solid was formed, filtered, washed with ethanol and dried at room temperature.

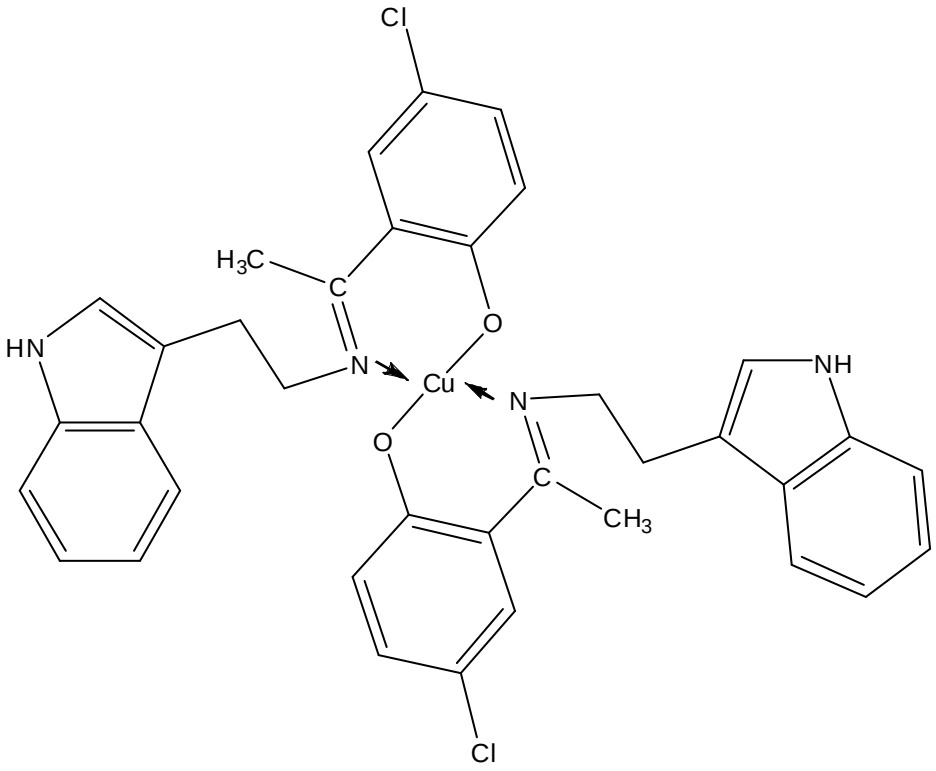

2.2.21 Preparation of:

bis{2-{1-[2-(1H-Indole-3-yl)-ethylimino]-ethyl}-4-bromophenolato-k^2N,O}Cu(II):

$(TBrHAP)_2Cu$:

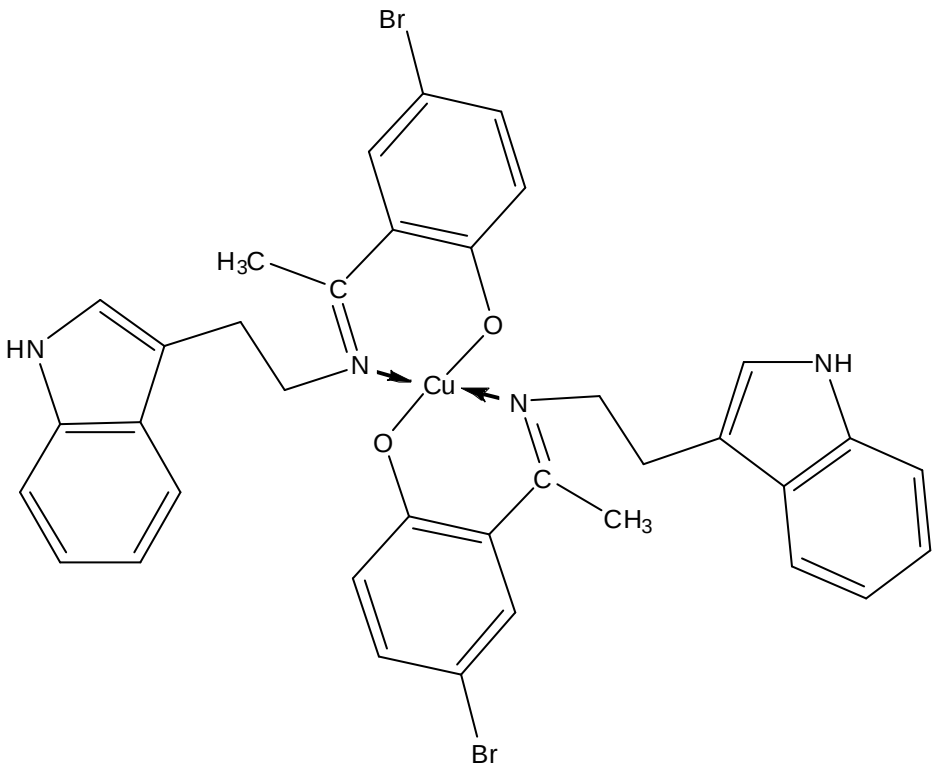

The ligand (0.5g, 1.40 mmol.) was dissolved in 50 ml of ethanol and added to 20 ml (0.137g, 0.68 mmol.) of copper acetate monohydrate in ethanol. Few drops of triethylamine were then added. The reaction mixture was refluxed for 5 hours. A brown solid was formed, filtered, washed with ethanol and dried at room temperature (percentage yield 41%).

2.3 Metal analysis by atomic absorption spectroscopy (AAS):

An accurately weighted amount (see table 2.1) of the complex sample was taken and digested with 10 mls of concentrated nitric acid in a hot plate heater, after the evolution of the brown nitrogen dioxide gas has ceased, 10 mls of concentrated sulphuric acid was then added and the heating continued until all the brown vapors of nitrogen dioxide was completely stopped and the solution becomes clear. The solution was then cooled, diluted with distilled water to 100 ml volumetric flask. From this solution, 0.4 ml was taken and diluted further to 10 ml volumetric flask. Concentration measurements was carried out and the results were summarized in table (2.1)

Experimental percentage has been calculated according to the formula:

$$\%^{age} \text{ of copper} = \text{conc. (ppm)} \times 0.25 / \text{weight of sample taken}$$

Table (2.1): Results of Cu analysis by AAS:

No.	Name of complex	Weight taken (g)	Conc. Value (ppm)	Experimental percentage	Theoretical percentage
1	$(TS)_2Cu$	0.0463	1.8963	10.24	10.77
2	$(TCS)_2Cu$	0.0518	2.0650	9.96	9.65
3	$(TNS)_2Cu$	0.0534	1.8892	8.84	9.35

Table 2.1 contiued

No.	Name of complex	Weight taken (g)	Conc. Value (ppm)	Experimental percentage	Theoretical percentage
4	$(TTET)_2Cu$	0.0643	1.9235	7.48	7.80
5	$(THAP)_2Cu$	0.0487	2.0142	10.33	10.27
6	$(TMeHAP)_2Cu$	0.0506	2.0136	9.94	9.83
7	$(TOMeHAP)_2Cu$	0.0534	1.9172	8.97	9.36
8	$(TClHAP)_2Cu$	0.0544	1.9645	9.03	9.24
9	$(TBrHAP)_2Cu$	0.0613	1.8039	7.35	8.18

2.4 Physical properties of the prepared ligands and complexes:

The physical properties of all the prepared ligands and complexes throughout this work including color, molecular weights, melting points and CHN elemental analysis were listed in appendix (A).

CHAPTER THREE

RESULTS AND DISCUSSION

3. Characterization of ligands and complexes

3.1 IR spectra of ligands and complexes:

3.1.1 IR spectra of the ligand: 1H-Indole-3-ethylenesalicylaldimine (TS) and its Zn, Ni, and Cu complexes:

The IR spectra of the ligand and its associated complexes was summarized in table (3.1) and shown in Fig 3.1, 3.2., 3.3 and 3.4

Table (3.1) IR data of TS and its Zn, Ni, and Cu complexes:

Compound	N-H	O-H	C-H aliphatic	C=N	C-O	C-H Out of plane Ar	M-O	M-N
TS	3420	3049-2857 broad	2936	1630	1281	746	-	-
$(TS)_2Zn$	3411	-	3170-2924	1623	1302	738	596	489
$(TS)_2Ni$	3447	-	2926	1612	1332	740	597	421
$(TS)_2Cu$	3424	-	2901	1623	1326	743	579	427

It has been shown that by comparing the IR spectra of the ligand precursor, salicylaldehyde and the ligand itself, the absence of the characteristic aldehydic carbonyl group stretching band near 1700 cm^{-1}, and the appearance of the azomethine –C=N band at 1630 cm^{-1} indicating the formation of the Schiff base. The broad band at 3049-2857 cm^{-1} could be attributed to the intramolecular hydrogen-bonded O-H group [58]. The hydrogen bond arises between the azomethine nitrogen atom and the proton of the hydroxyl group [21]. The sharp band at 3420 cm^{-1} is due to the N-H stretching of the indole group. The C-O phenolic band appears at 1281 cm^{-1}, and the strong band at 746 cm^{-1} is attributed to the C-H out- of- plane aromatic bend.

In the case of $(TS)_2Zn$ complex, it is clear that the hydroxyl band at 3049 cm^{-1} of the ligand was disappeared indicating deprotonation of the ligand, and confirming co-ordination of the phenolic oxygen atom to the metal [59]. This fact can also be supported further by the shifting of the C-O stretching band with respect to the same band in the free ligand. The azomethine stretching band in the free ligand shifts from 1630 cm^{-1} to 1623 cm^{-1} in the complex. This supports the participation of the azomethine nitrogen atom in coordinate bond to the metal center.

A new bands at 596 cm^{-1} and 489 cm^{-1} could be assigned to vibrations associated with Zn-O, and Zn-N bonds respectively [21,61].

For $(TS)_2Ni$ complex, the band at 1612 cm^{-1} could be assigned to the shifted azomethine –C=N stretch upon complexation. C-O phenolic band shifts to 1332 cm^{-1} and Ni-O and Ni-N vibrations appear at 597 cm^{-1} and 421 cm^{-1} respectively.

Same explanations can be given to the copper complex $(TS)_2Cu$ indicating similar co-ordination manner for the three metal ions. The -C=N band for the copper complex appears at 1623 cm^{-1} just like its zinc congener, C-O at 1326 cm^{-1} , Cu-O at 579 cm^{-1} and Cu-N at 427 cm^{-1}.

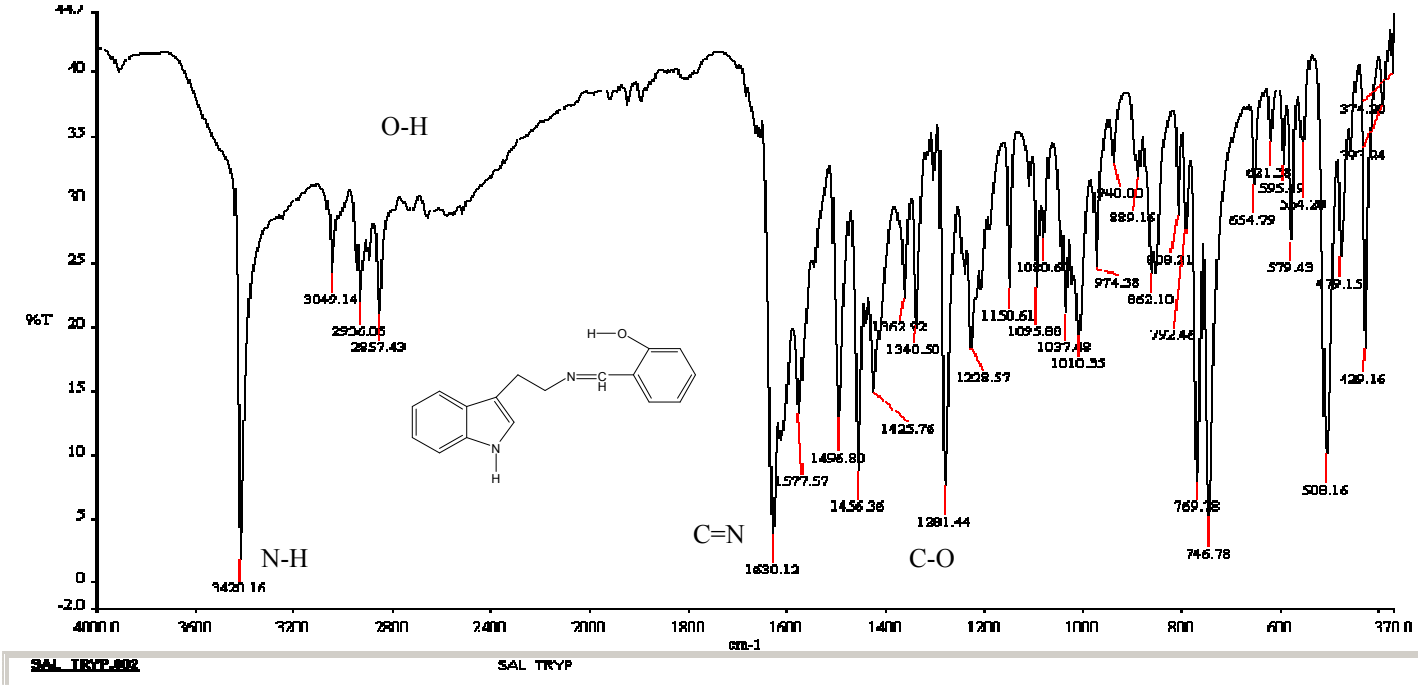

Fig 3.1: IR spectra of: 1H-Indole-3-ethylenesalicylaldimine (TS)

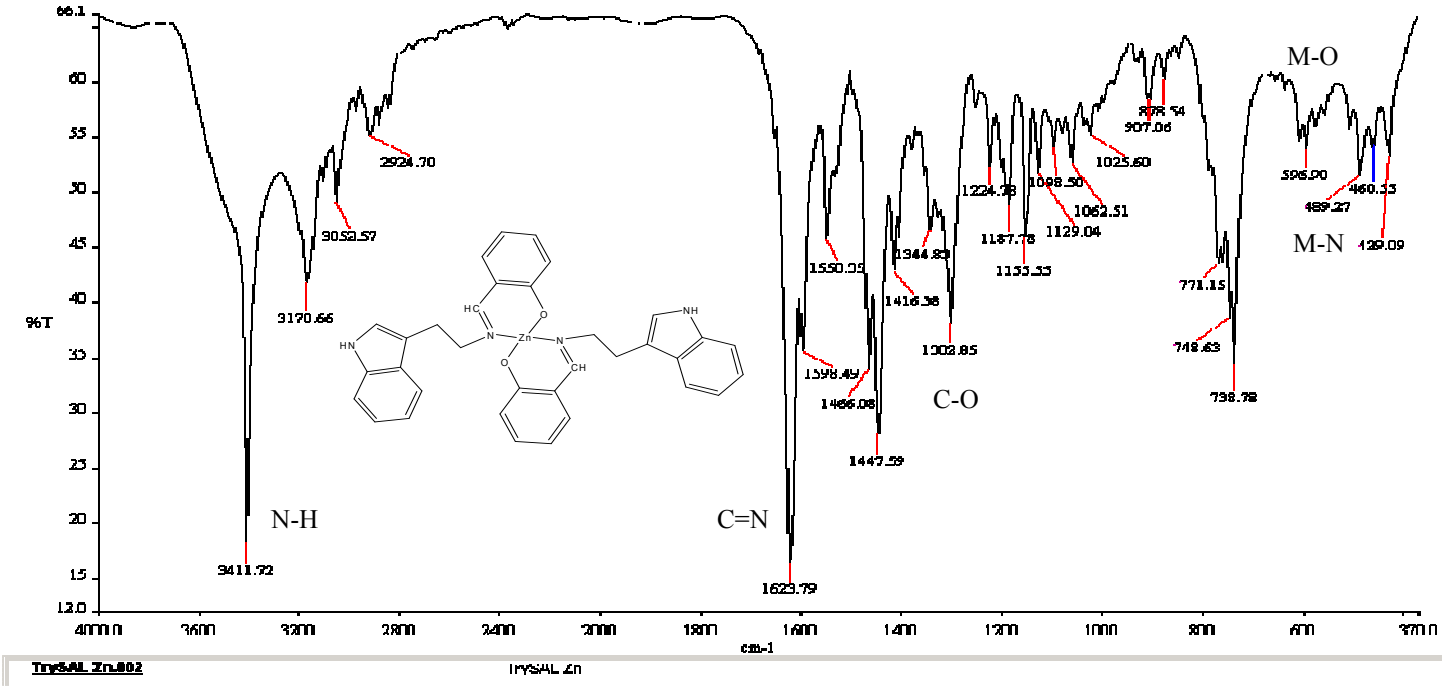

Fig 3.2: IR spectra of: Bis(1H-Indole-3-ethylenesalicylaldiminato-k^{2}N,O)Zn(II) $(TS)_2Zn$

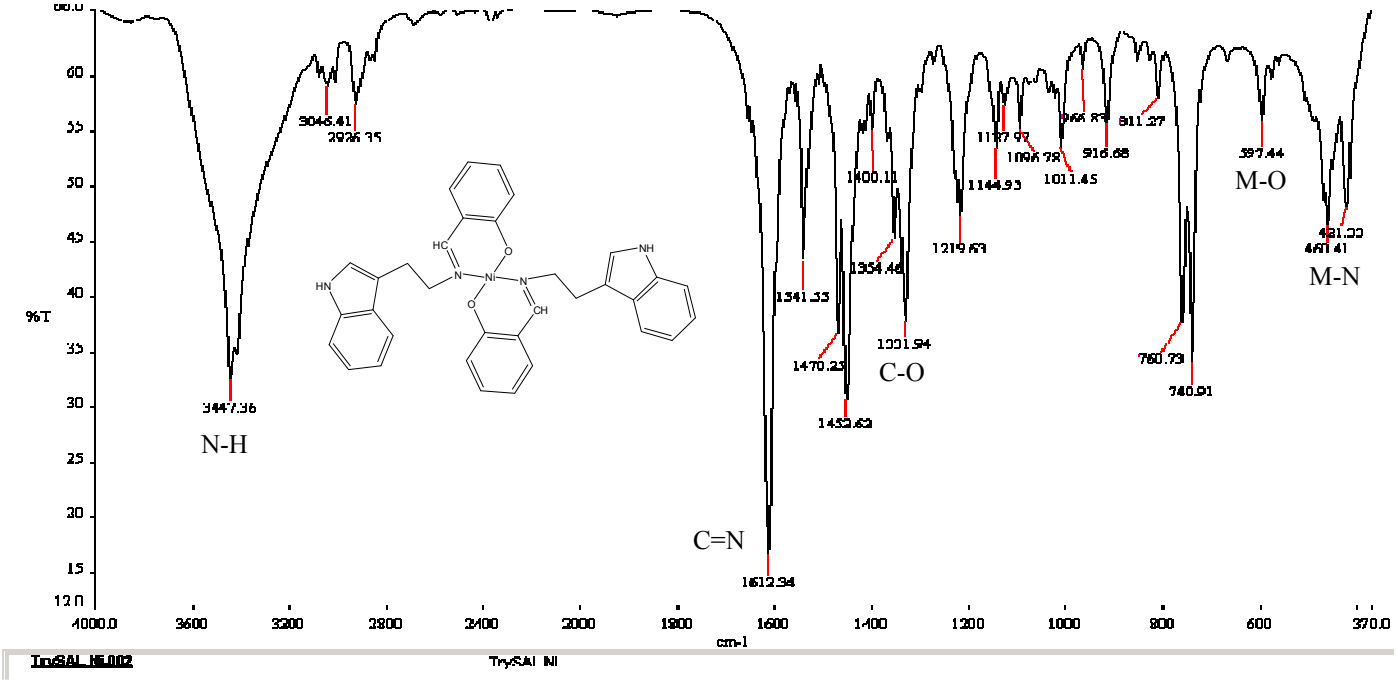

Fig 3.3: IR spectra of: Bis(1H-Indole-3-ethylenesalicylaldiminato-k^{2}N,O)Ni(II) $(TS)_2Ni$

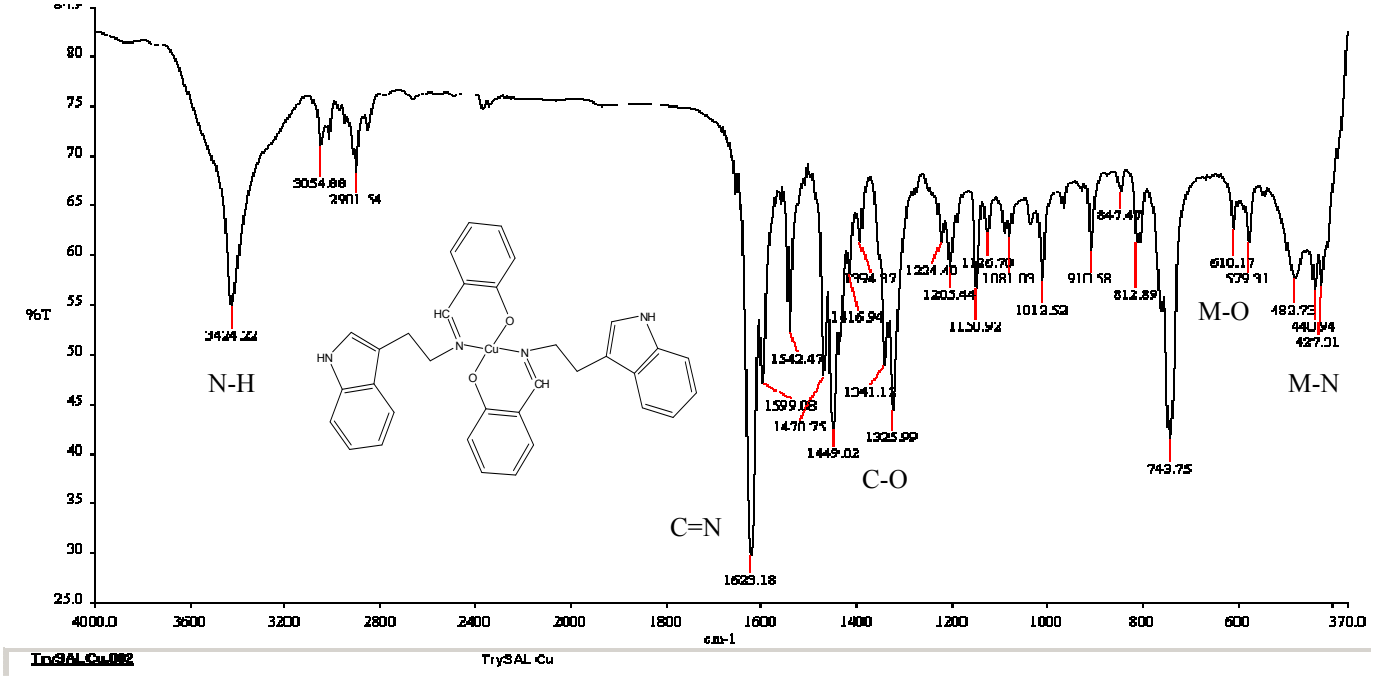

Fig 3.4: IR spectra of: Bis(1H-Indole-3-ethylenesalicylaldiminato-k^{2}N,O)Cu(II) $(TS)_2Cu$

3.1.2 IR spectra of the ligand: 1H-Indole-3-ethylene-5-chlorosalicylaldimine (TCS) and its Zn, Ni, and Cu complexes:

The IR spectra of the ligand and its associated complexes were summarized in table (3.2) and shown in Fig 3.5, 3.6, 3.7 and 3.8

Table (3.2): IR spectra of TCS and its Zn, Ni, and Cu complexes:

Compound	N-H	O-H	C-H aliphatic	C=N	C-O	C-H Out of plane Ar	M-O	M-N
TCS	3434	3054	2919	1630	1281	746	-	-
$(TCS)_2Zn$	3409	-	2920	1630	1311	739	580	425
$(TCS)_2Ni$	3431	-	2918	1617	1326	739	463	420
$(TCS)_2Cu$	3431	-	2913	1622	1324	739	453	421

It can be shown from the table that for the free ligand, the N-H indolic stretching frequency appears at 3434 cm^{-1} a little bit higher than TS ligand. The phenolic O-H band appears at 3054 cm^{-1} as a broad band. The azomethine –C=N band appears at the same frequency 1630 cm^{-1} as TS ligand indicating that the chlorine substituent in the fifth position of the phenolic ring does not affect the position of this band. Further more the C-O stretching vibration appears at 1281 cm^{-1}, and the aromatic out-of-plane bending vibration at 746 cm^{-1}.

In the spectra of $(TCS)_2Zn$ complex, the O-H band of the ligand at 3054 cm^{-1} was also similarly disappeared indicating co-ordination through the phenolic oxygen to the zinc atom. This fact also reinforced by the shifting of the C-O band from 1281 cm^{-1} in the ligand to 1311 cm^{-1} in the complex . The bands observed at the region 580 cm^{-1} and 425 cm^{-1} can be related to Zn-O and Zn-N stretching respectively.

The spectra of $(TCS)_2Ni$ looks somewhat similar to the zinc complex except the azomethine –C=N band has shifted to lower frequency to be at 1617 cm^{-1}, C-O band at 1326 cm^{-1} and bands due to Ni-O and Ni-N at 463 cm^{-1} and 420 cm^{-1} respectively supporting the proposed structure.

The same explanation could be described for the copper complex of the ligand. Both –C=N and C-O stretching frequencies shifts to 1622 cm^{-1} and 1324 cm^{-1} in comparison to the free ligand because of complex formation. Cu-O and Cu-N bands observed at 453 cm^{-1} and 421 cm^{-1} respectively.

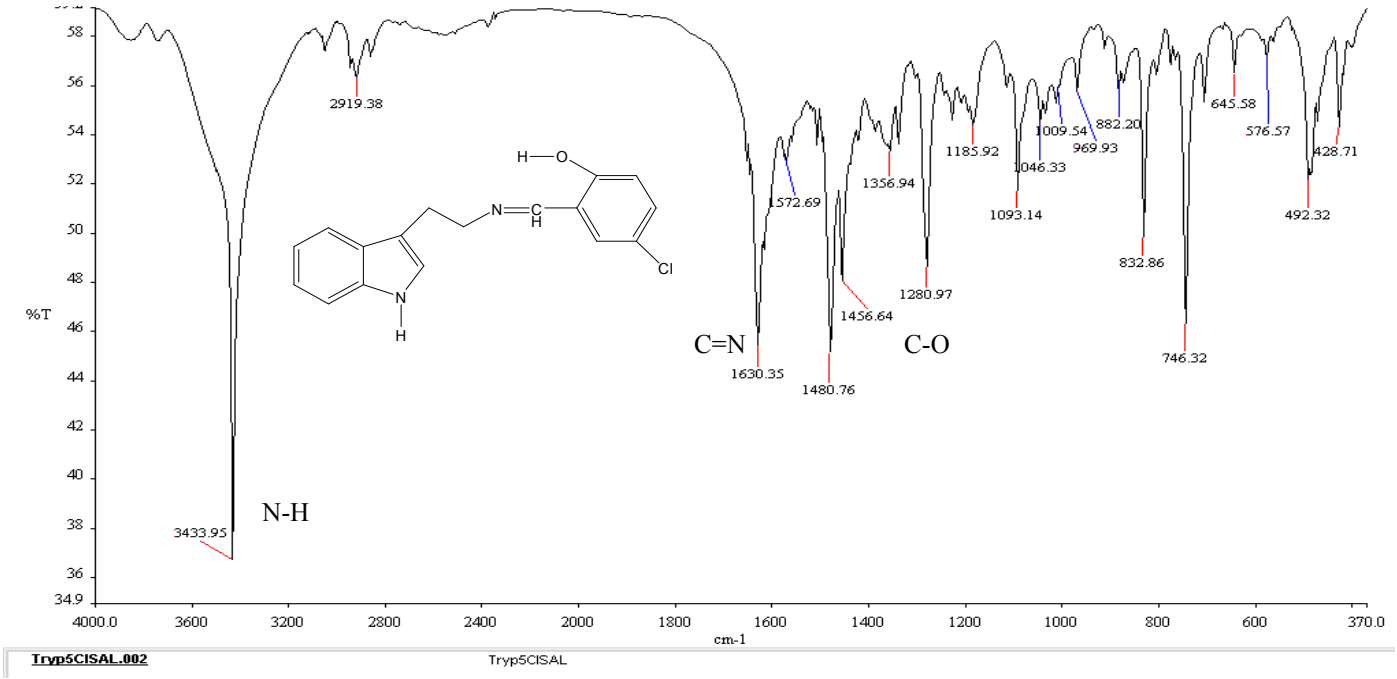

Fig 3.5: IR spectra of: 1H-Indole-3-ethylene-5-chlorosalicylaldimine (TCS)

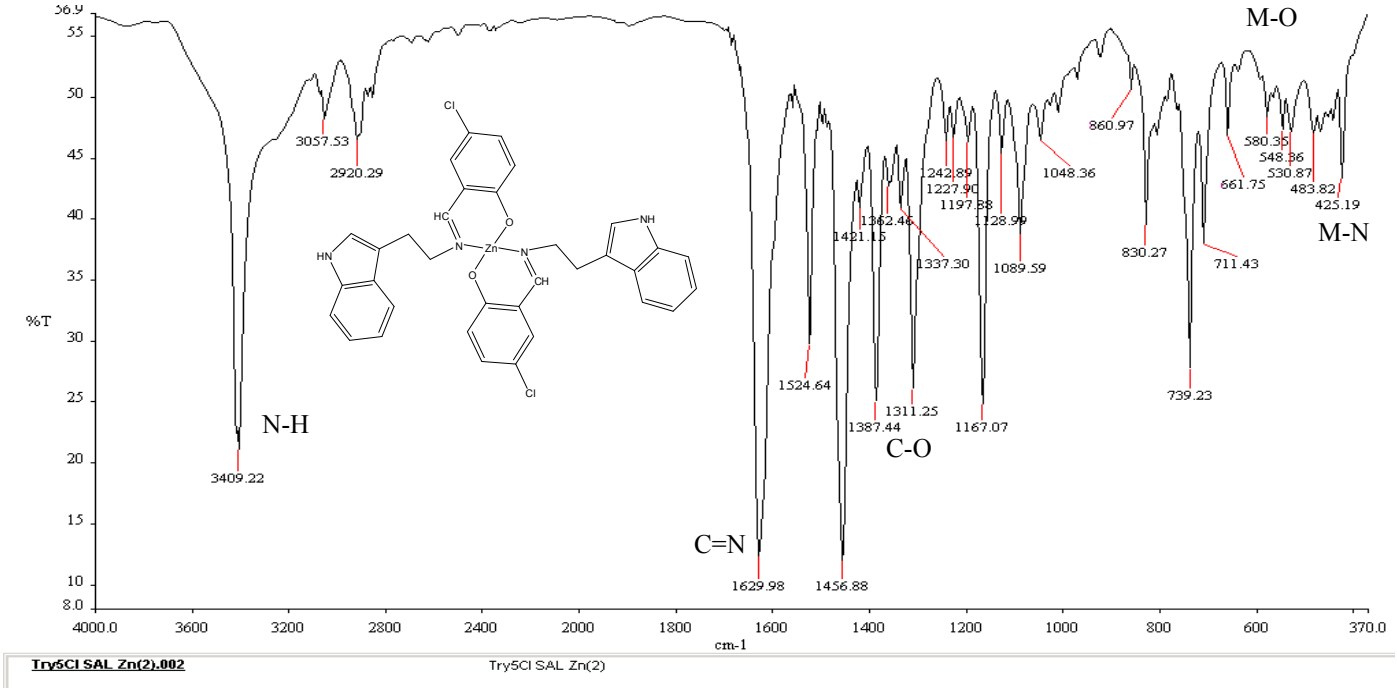

Fig 3.6: IR spectra of: Bis{4-chloro-2-[2-(1H-indol-3-yl)ethyliminomethyl]phenolato-κ2N,O}zinc(II) $(TCS)_2Zn$

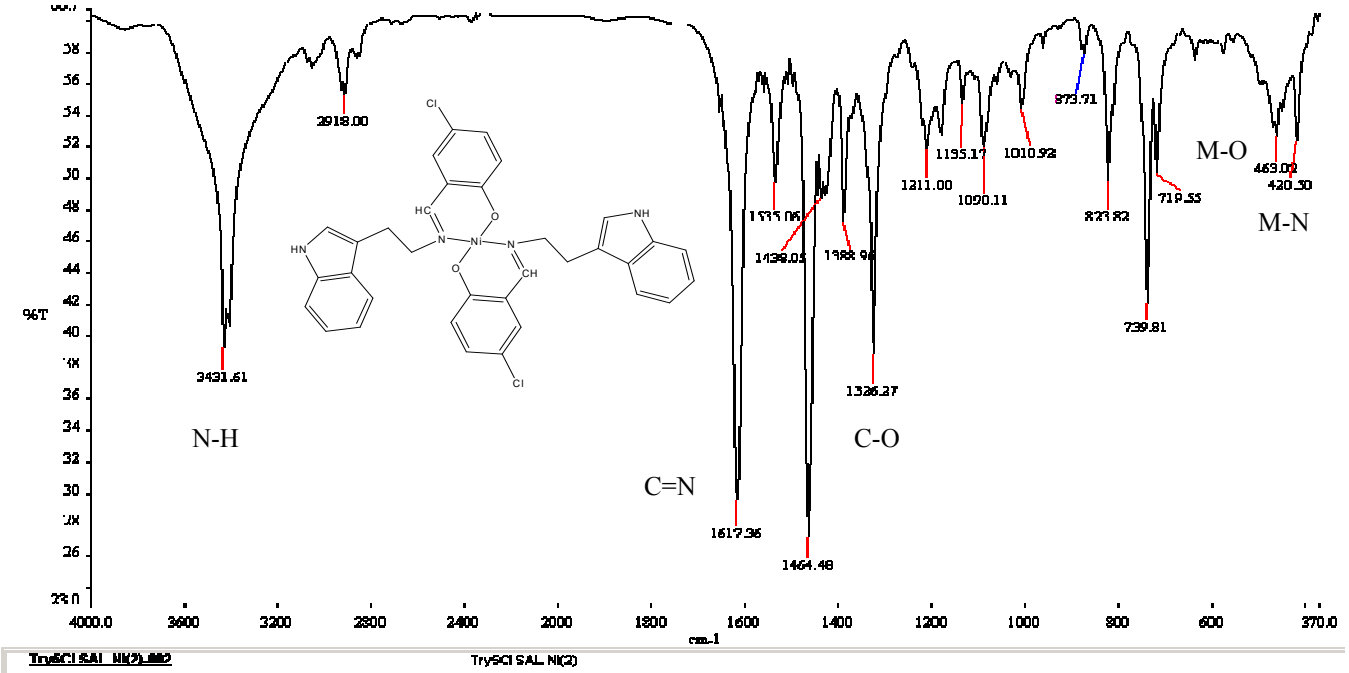

Fig 3.7: IR spectra of: Bis{4-chloro-2-[2-(1H-indol-3-yl)ethyliminomethyl]phenolato-κ2N,O}nickel(II) $(TCS)_2Ni$

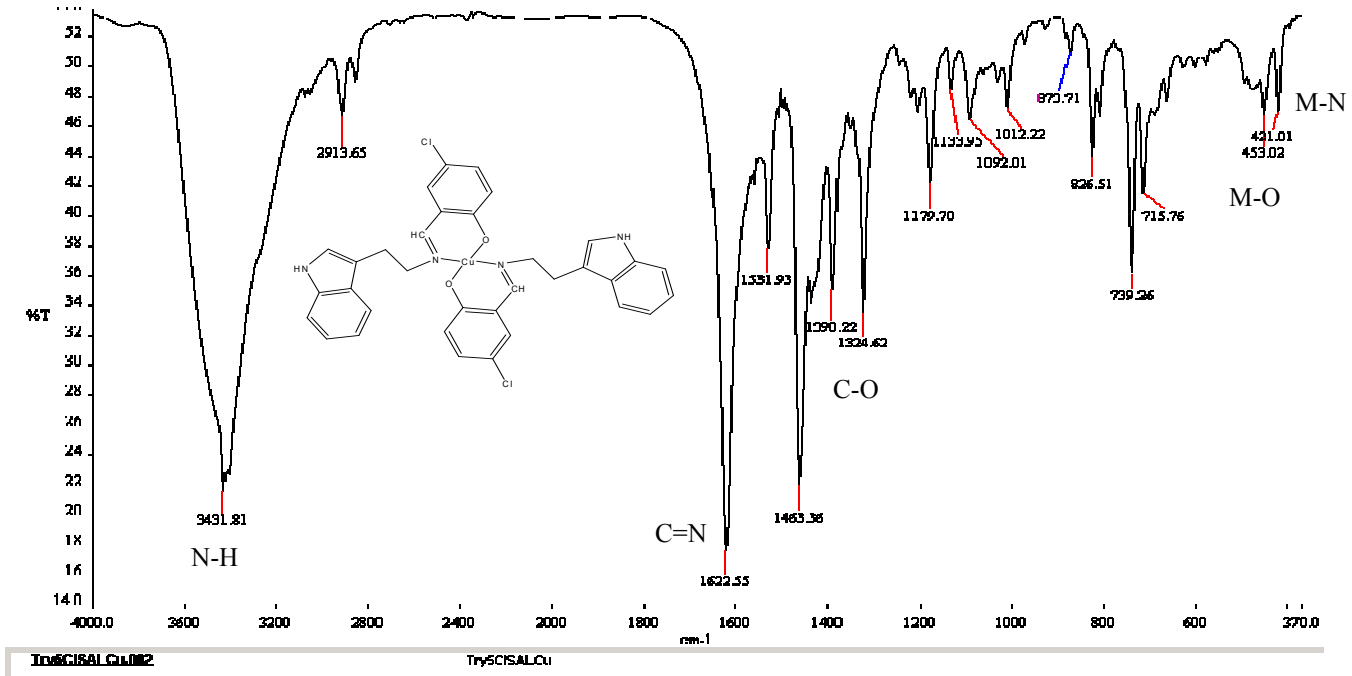

Fig 3.8: IR spectra of: Bis{4-chloro-2-[2-(1H-indol-3-yl)ethyliminomethyl]phenolato-κ2N,O}copper(II) $(TCS)_2Cu$

3.1.3 IR spectra of the ligand: 1H-Indole-3-ethylene-5-nitrosalicylaldimine (TNS) and its Zn, Ni, and Cu complexes:

The IR spectra of the ligand together with its complexes were shown in table (3.3) and figures 3.9, 3.10, 3.11 and 3.12.

Table (3.3):

IR spectra of the ligand TNS and its Zn, Ni, and Cu complexes:

Compound	N-H	O-H	C-H aliphatic	C=N	C-O	C-H Out of plane Ar	M-O	M-N
TNS	3360	-	2929	1647	1301	741	-	-
$(TNS)_2Zn$	3414	-	2925	1635	1316	739	518	425
$(TNS)_2Ni$	3414	-	2951	1603	1315	748	526	425
$(TNS)_2Cu$	3399	-	2913	1619	1301	739	553	446

From the table above it can be concluded that for the free ligand N-H indolic stretching frequency appears at 3360 cm^{-1}. The azomethine (–C=N) band in this case appears a little bit higher at 1647 cm^{-1} with respect to the previously described ligands. The band at 1301

cm^{-1} is assigned to the C-O stretching of the phenolic group and the band at 1545 cm^{-1} could be ascribed to the vibrations of the nitro group [60].

With regard to the zinc complex of this ligand, the –C=N band was shifted to 1635 cm^{-1} due to the withdrawal of electron density from the nitrogen atom owing to co-ordination to the Zn metal [62, 29]. Similar shift to higher frequency was observed for the C-O stretching band. Bands at 518 cm^{-1} and 425 cm^{-1} are due to Zn-O and Zn-N vibrations respectively.

In $(TNS)_2Ni$ complex, the C=N band appears at a more lower wave number 1603 cm^{-1} in comparison with the zinc complex of the same ligand. The band at 526 cm^{-1} was assignable to Ni-O bond, and Ni-N band is not clear in the spectra. Tentative assignments can be postulated for this bond either 425 cm^{-1} or 484 cm^{-1}.

The same description can be given to $(TNS)_2Cu$ complex. Similarities in the trends of IR bands were clearly observed suggesting similar structure to the zinc and nickel complexes. The bands between 588 – 420 cm^{-1} are assigned to vibrations that probably coupled Cu-N and Cu-O in accordance with the literature [21, 63, and 67].

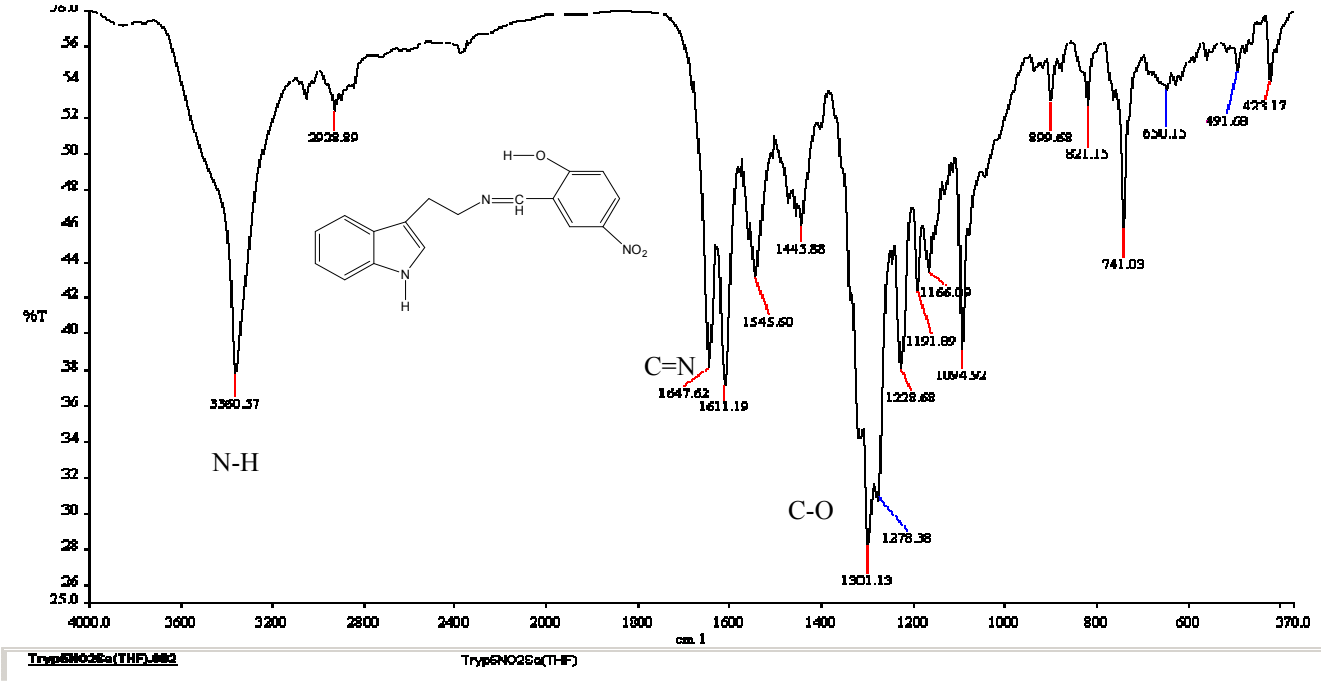

Fig 3.9: IR spectra of: 1H-Indole-3-ethylene-5-nitrosalicylaldimine (TNS)

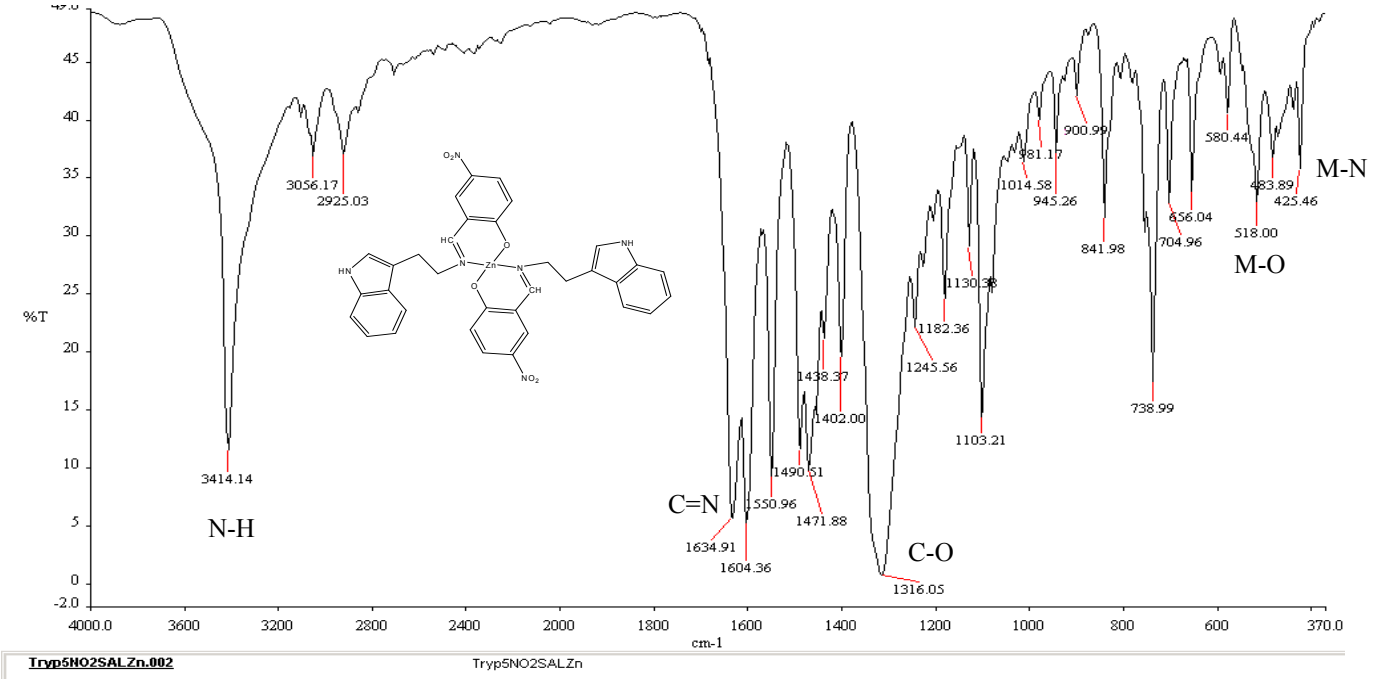

Fig 3.10: IR spectra of: Bis *{*4-nitro-2-[2-(1H-indol-3-yl) ethyliminomethyl]phenolato-*κ*2N,O*}*zinc(II) $(TNS)_2Zn$

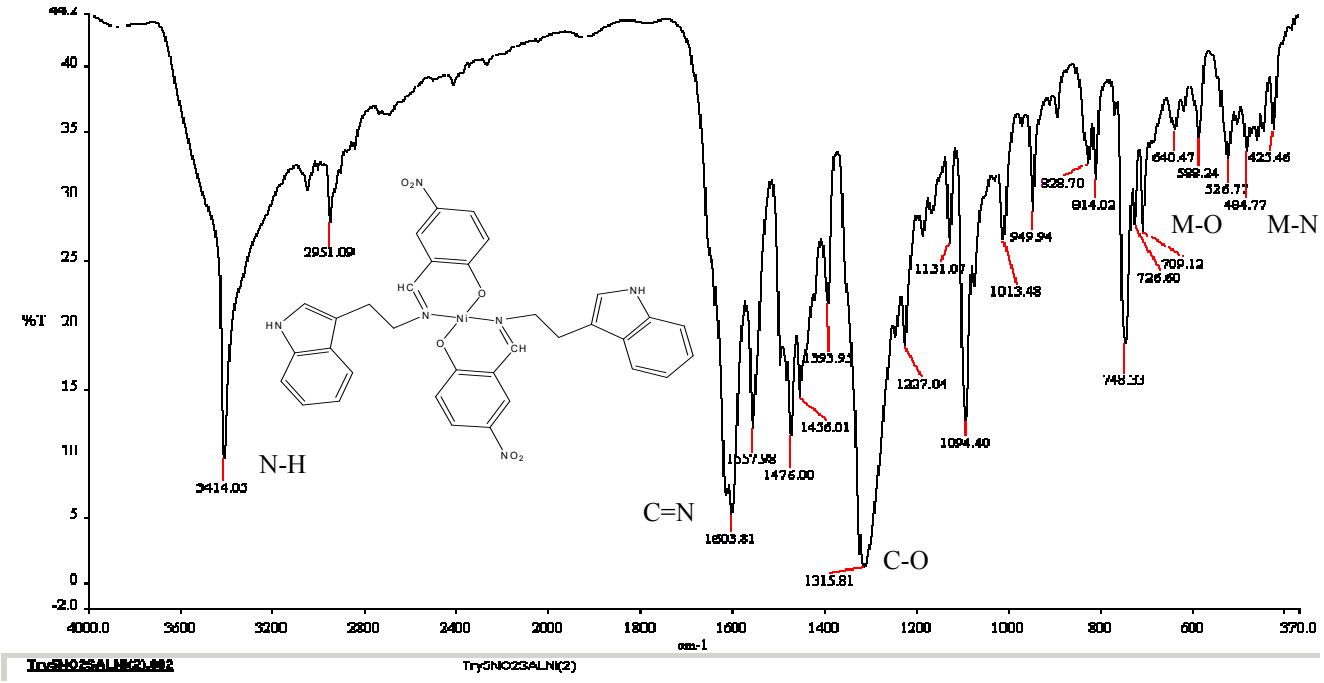

Fig 3.11: IR spectra of: Bis *{*4-nitro-2-[2-(1H-indol-3-yl) ethyliminomethyl]phenolato-*κ*2N,O*}*nickel(II) $(TNS)_2Ni$

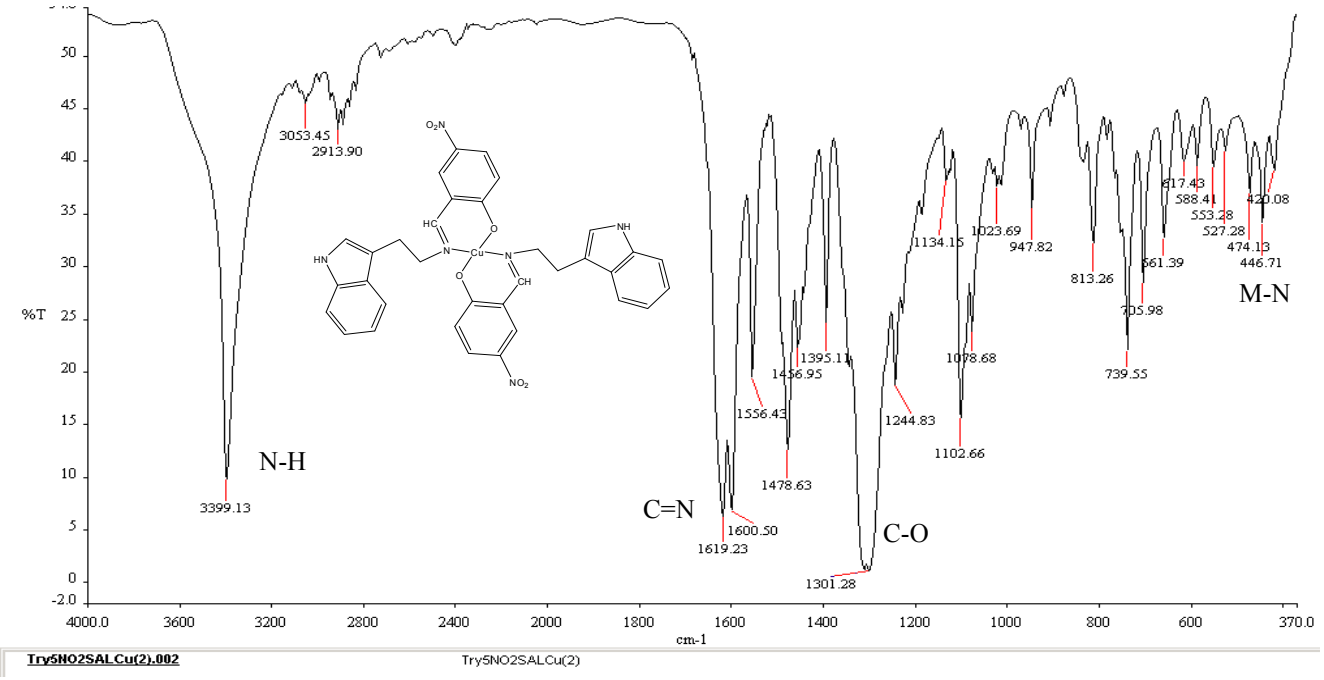

Fig 3.12: IR spectra of: Bis *{*4-nitro-2-[2-(1H-indol-3-yl) ethyliminomethyl] phenolato-*κ*2N, O*}* copper (II) $(TNS)_2Cu$

3.1.4 IR spectra of the ligand:

1H-Indole-3-ethylene-3-5-di-tertiarybutylsalicylaldimine (TTET) and its Zn, Ni, and Cu complexes:

Table (3.4):

IR spectra of the ligand TTET and its Zn, Ni, and Cu complexes:

Compound	N-H	O-H	C-H aliphatic	C=N	C-O	C-H Out of plane Ar	M-O	M-N
TTET	3400	overlap	2953	1631	1250	750	-	-
$(TTET)_2Zn$	3410	-	2956	1615	1254	744	540	488
$(TTET)_2Ni$	3404	-	2952	1613	1255	742	542	485
$(TTET)_2Cu$	3428	-	2954	1618	1257	745	539	476

IR spectra for the ligand and its complexes were shown in table (3.4) and figures 3.13, 3.14, 3.15, and 3.16

The stretching vibration of the indolic N-H group for the ligand was found at 3400 cm^{-1}, while the broad band associated with the hydroxyl group overlaps the C-H aliphatic band range. The azomethine stretching frequency lies within the normal range at 1631 cm^{-1},

C-O at 1250 cm^{-1} and the aromatic out-of-plane bending mode at 750 cm^{-1}.

For $(TTET)_2Zn$ complex the broad overlapping O-H vibration was disappeared indicating that, the deprotonation of the ligand was occurred upon complexation, and this fact was supported by the downward displacement of the azomethine –C=N band to 1615 cm^{-1}. The new band 540 cm^{-1} corresponds to Zn-O stretch and the band at 488 cm^{-1} corresponds to Zn-N stretch.

Similar correlations can be mentioned for Ni and Cu complexes, shifting to lower wave numbers was noted for the azomethine group due to co-ordination of the nitrogen atom to the metal center, thus for nickel complex this band shifts more further to 1613 cm^{-1}, and be more or less the same for the copper complex at 1618 cm^{-1} as its zinc congener. For the three complexes the phenolic C-O band shifts to higher frequency [64, 57]. The shift may be interpreted in terms of π-conjugation between the benzene ring and the chelate ring of the complex [36].

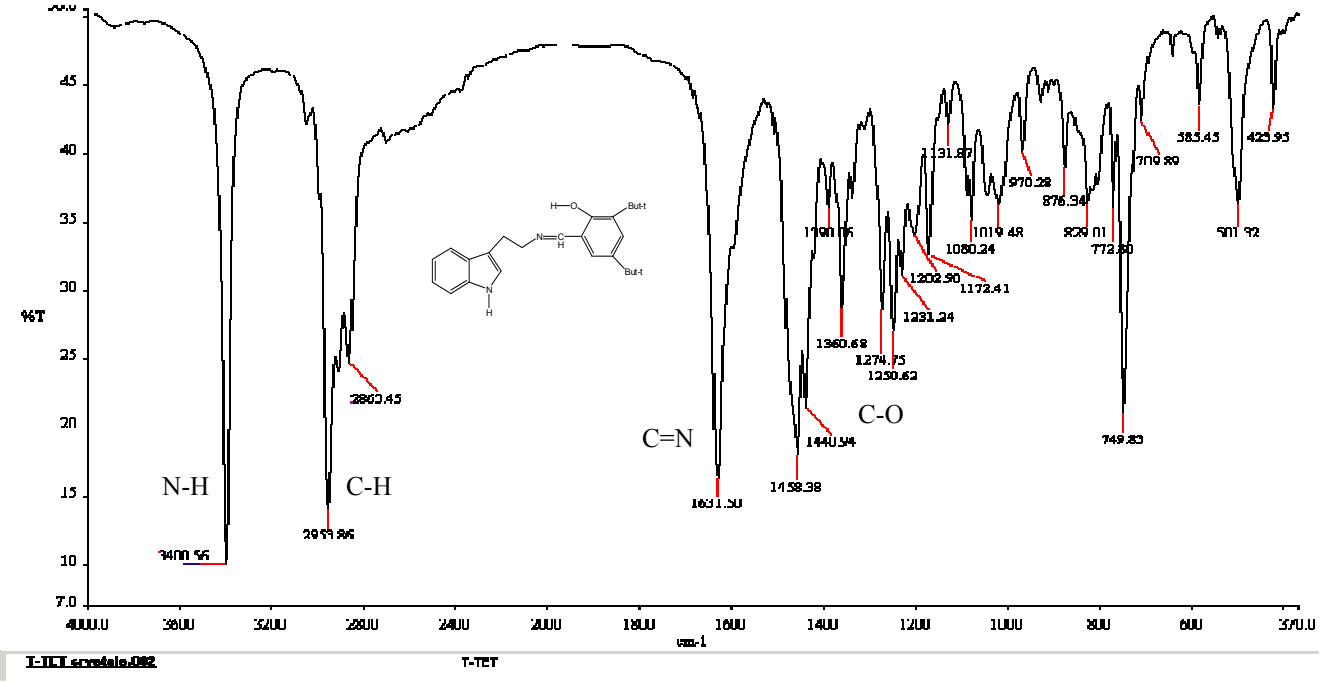

Fig 3.13: IR spectra of: 1H-Indole-3-ethylene-3-5-di-tertiarybutylsalicylaldimine (TTET)

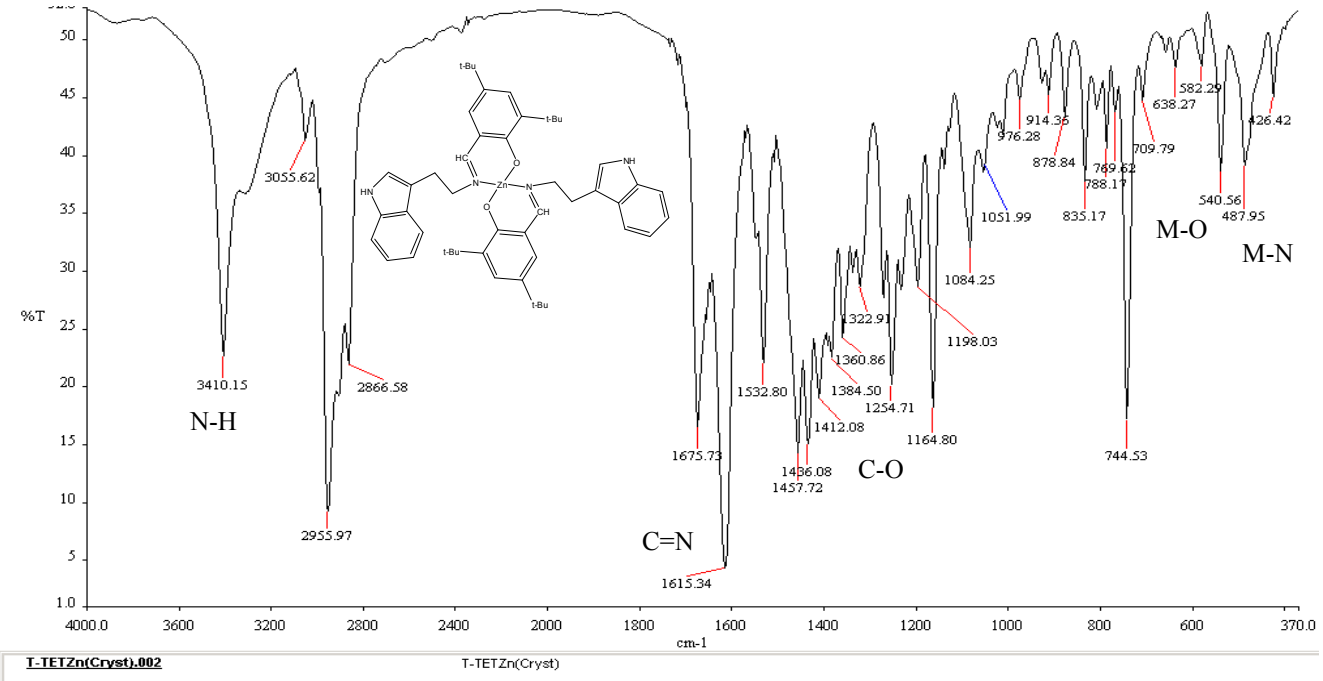

Fig 3.14: IR spectra of: Bis(1H-Indole-3-ethylene-3-5-di-tertiarybutylsalicylaldiminato-k^2N,O)Zn(II) $(TTET)_2Zn$

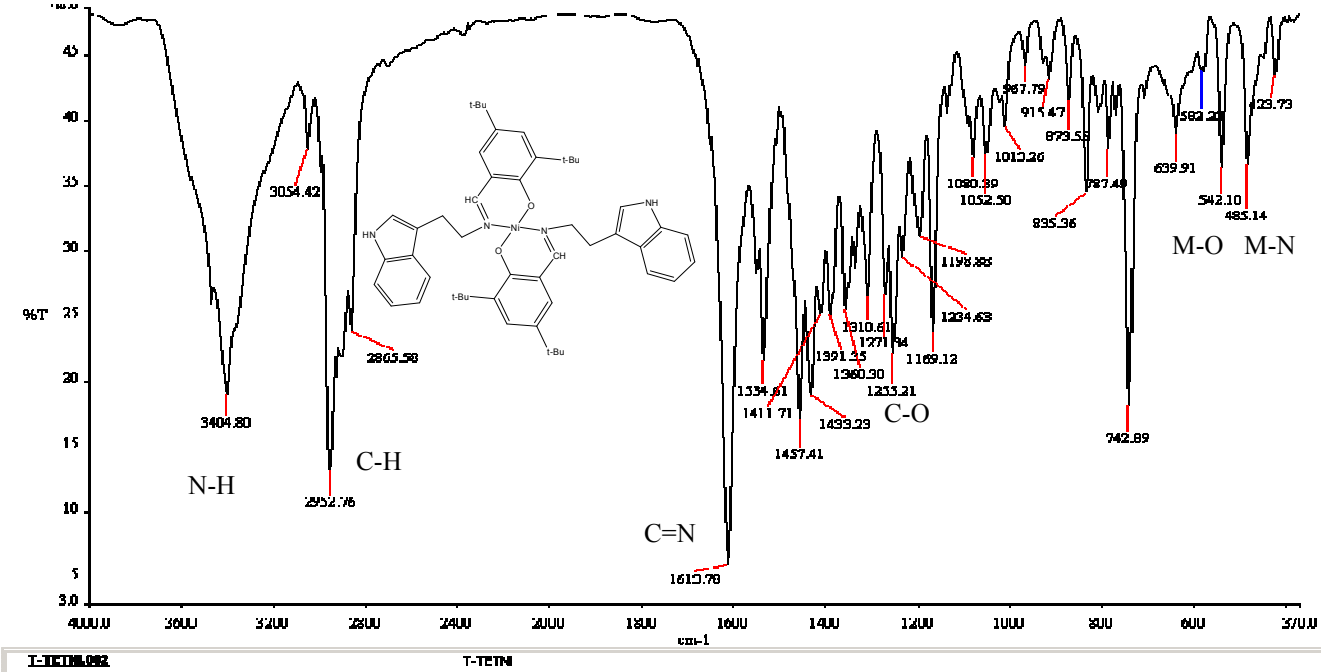

Fig 3.15: Bis (1H-Indole-3-ethylene-3-5-di-tertiarybutylsalicylaldiminato-k^{2}N,O)Ni(II) $(TTET)_2Ni$

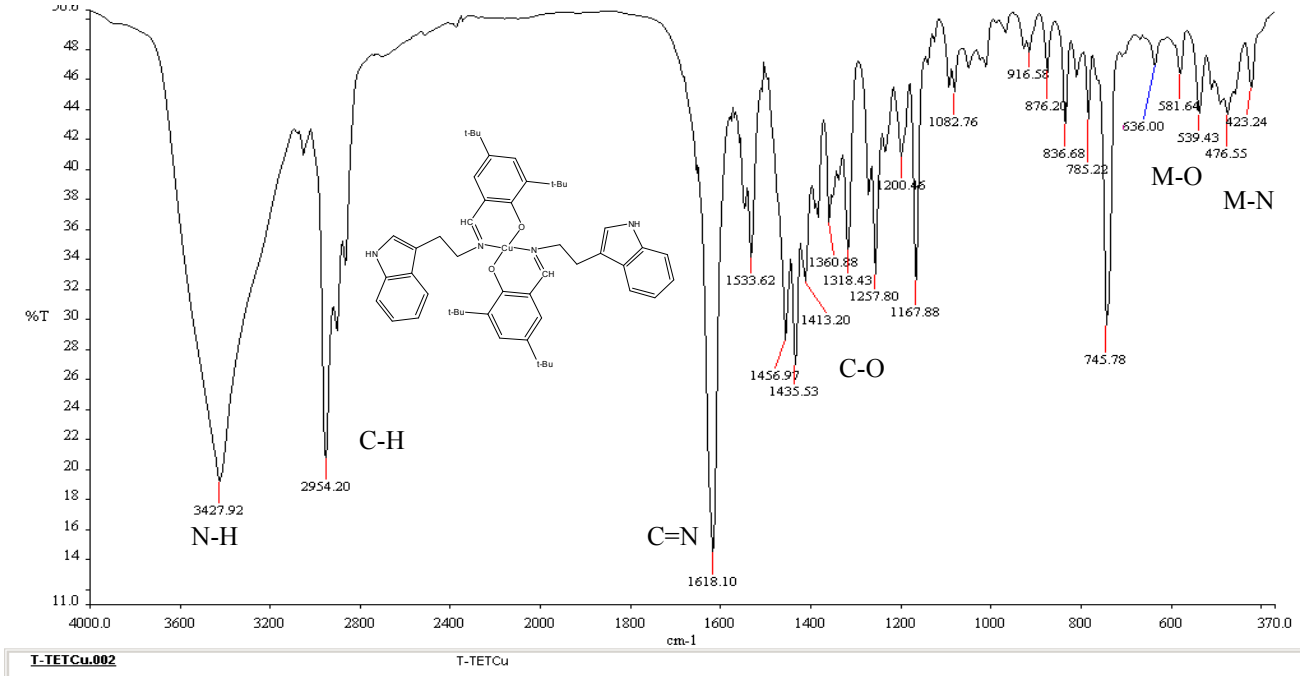

Fig 3.16: IR spectra of: Bis (1H-Indole-3-ethylene-3-5-di-tertiarybutylsalicylaldiminato-k^{2}N,O)Cu(II) $(TTET)_2Cu$

3.1.5 IR spectra of the ligand: 2-{1-[2-(1H-Indole-3-yl) ethylimino]-ethyl}phenol (THAP) and its Zn, Ni, and Cu complexes:

The IR spectra of the ligand and its complexes have been summarized in table (3.5) and presented in figures 3.17, 3.18, 3.19 and 3.20

Table (3.5): IR spectra of the ligand THAP and its Zn, Ni, and Cu complexes:

Compound	N-H	O-H	C-H Aliphatic	C=N	C-O	C-H Out of plane Ar.	M-O	M-N
THAP	3433	3142-2875Brd	2926	1609	1265	731	-	-
$(THAP)_2Zn$	3442	-	2872	1610	1261	750	581	-
$(THAP)_2Ni$	3409	-	2917	1611	1220	745	583	428
$(THAP)_2Cu$	3371	-	2940	1599	1237	738	525	429

The indolic N-H stretching frequency is not clearly shown in the spectra and may be embedded in the broad hydroxyl band in the range 3433 cm^{-1} – 2875 cm^{-1}, aliphatic C-H stretch appears at the wave number 2926 cm^{-1} and –C=N stretching frequency at 1609 cm^{-1} as expected. C-O phenolic stretching vibration wave number was 1265 cm^{-1} and the aromatic out-of-plane bending mode at 731 cm^{-1}[65].

In the zinc complex spectrum of the ligand, the indolic N-H vibration was clearly appeared at 3442 cm^{-1} owing to the disappearance of the broad O-H band upon complexation, indicating deprotonation of the ligand and the oxygen atom was

participated in bond formation with the metal center. The C-H aliphatic stretching frequency was shifted to 2872 cm^{-1}, and the wave number of the C=N stretching frequency appears at 1610 cm^{-1}. This band doesn't shift considerably, and may indicate that the azomethine nitrogen atom does not contribute in bond formation through the lone pair donation. This phenomenon was confirmed by the X-ray crystal structure and the ligand acts only as a unidentate ligand through the hydroxyl oxygen atom [66]. Further evidence for this is derived from the shifting of the C-O band and the creation of the new band at 581 cm^{-1} assignable to Zn-O stretch as well as the disappearance of the Zn-N band as compared to the previous zinc complexes of similar ligands.

For the nickel complex of the ligand, N-H stretching vibration appears at 3409 cm^{-1} upon disappearance of the broad O-H band, indicating co-ordination through O-H oxygen atom. Azomethine wave number appears at 1611 cm^{-1}, and the C-O vibration shifts to lower frequency 1220 cm^{-1}. New bands at 583 cm^{-1} and 428 cm^{-1} are assignable to M-O and M-N vibrations respectively [64].

In the case of copper complex of the ligand, as compared to the free ligand, the N-H indolic vibration was clearly shown at 3371 cm^{-1}, and the O-H band was vanished. This illustrate that, deprotonation of the ligand occurred through complex formation. The –C=N stretching vibration shifts to lower wave number and appears at 1599 cm^{-1} a feature indicates decreasing of the bond order upon complex formation due to the participation of the nitrogen lone pair on dative bond. The C-O phenolic band shifts to 1237 cm^{-1} as well. This also may confirm C-O → Cu donation. New bands appear in the spectrum at 525 cm^{-1} and 429 cm^{-1} ascribed to Cu-O and Cu-N vibrations respectively.

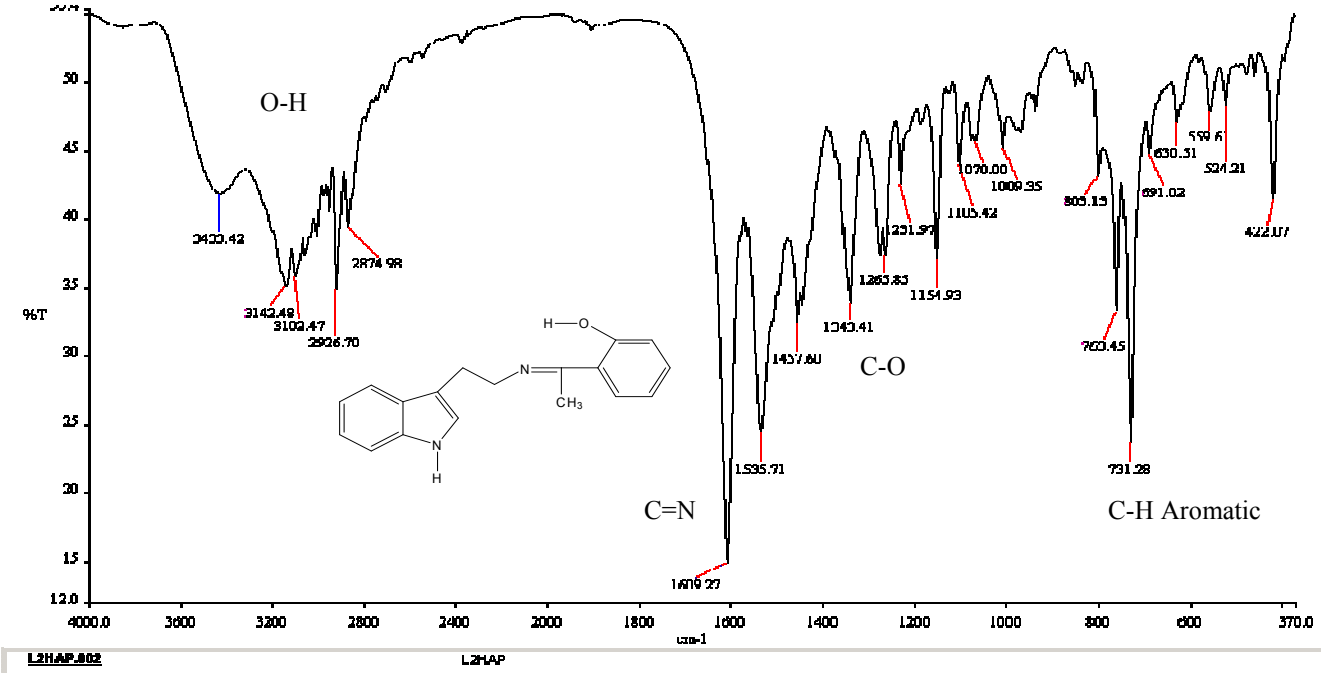

Fig 3.17: IR spectra of: 2-{1-[2-(1H-Indole-3-yl) ethylimino]-ethyl} phenol (THAP)

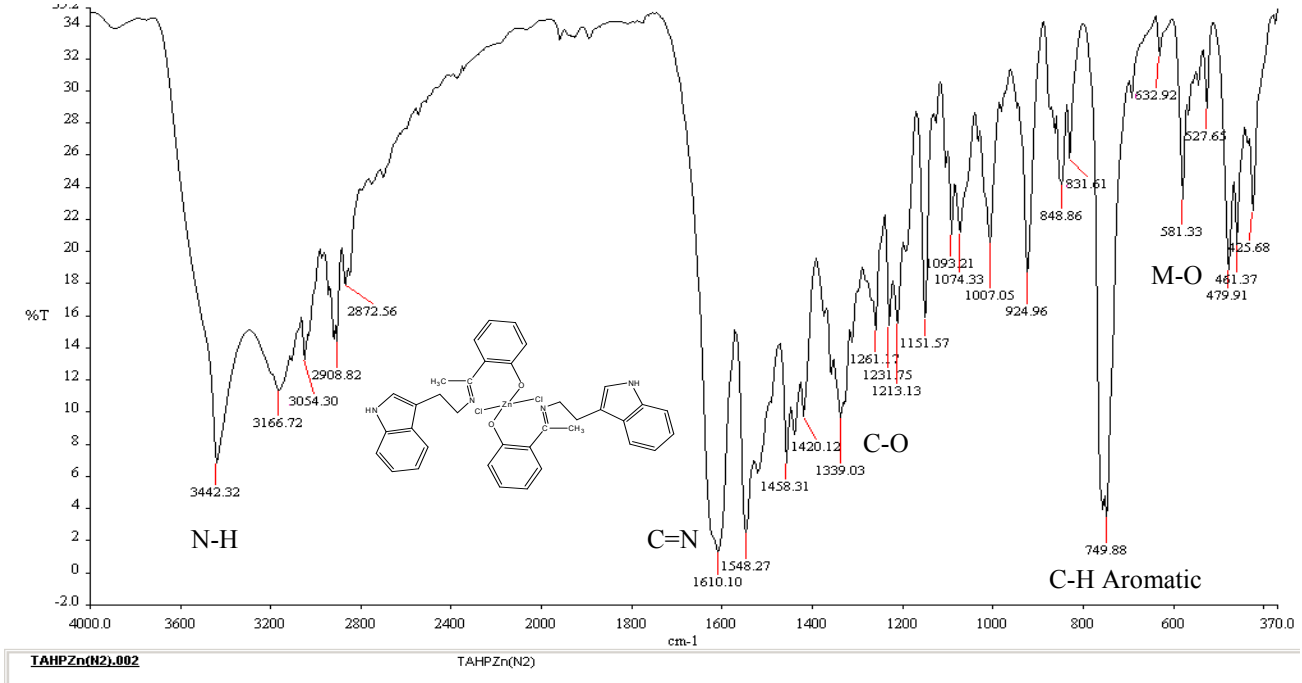

Fig 3.18: IR spectra of: Dichloridobis(2-{1-[2-(1H-indol-3-yl)-ethyliminio]ethyl}phenolate-*k*O)zinc(II) $(THAP)_2Zn$

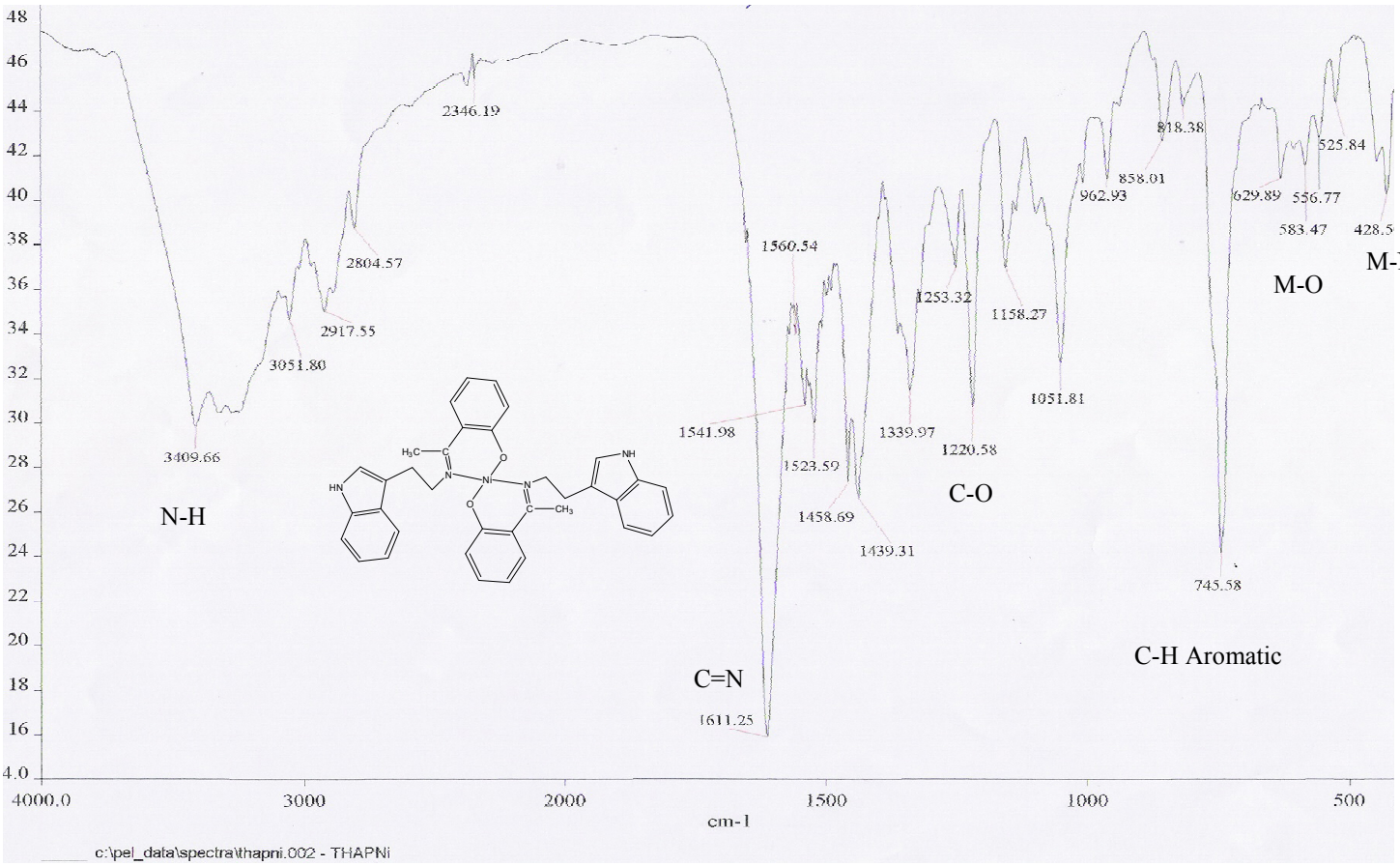

Fig 3.19 IR spectra of: bis(2-{1-[2-(1H-indol-3-yl)- ethyliminio]ethyl}phenolato-k^2N, O)Ni(II) $(THAP)_2Ni$

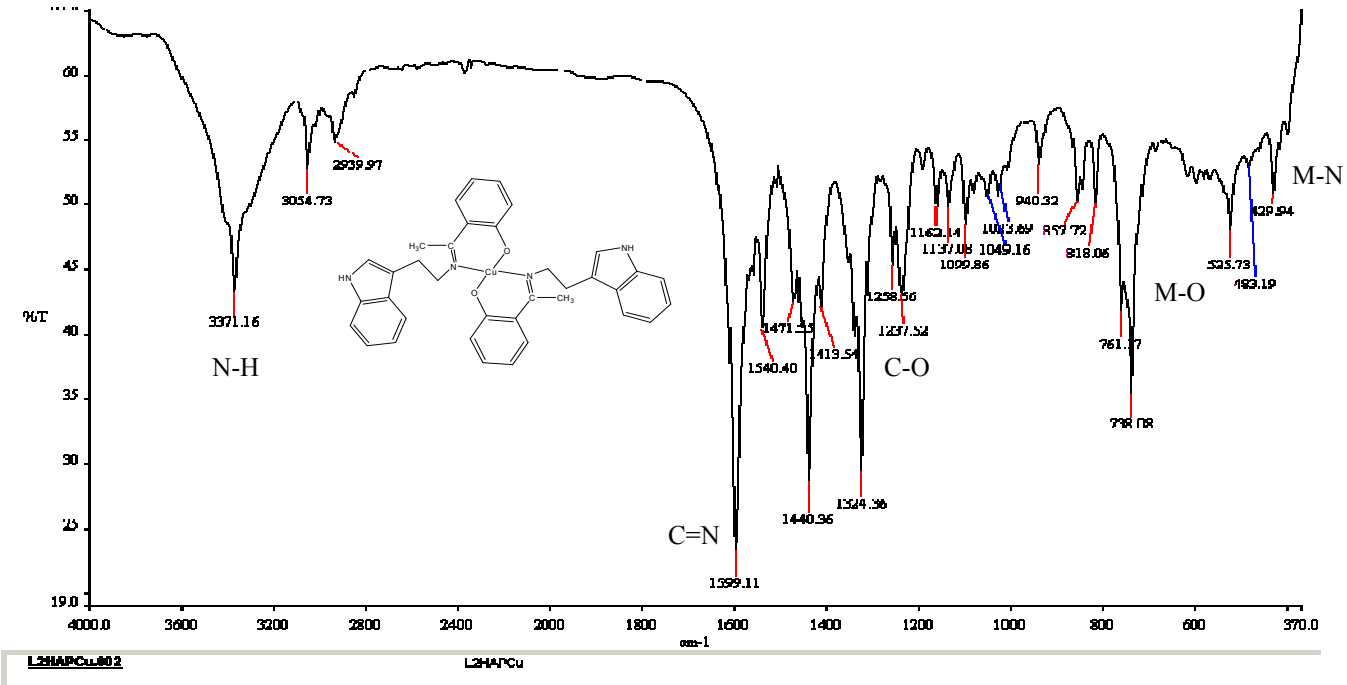

Fig 3.20: IR spectra of: Preparation of: Bis(2-{1-[2-(1H-indol-3-yl)-ethyliminio]ethyl}phenolato-k^2N, O)Cu(II) $(THAP)_2Cu$

3.1.6 IR spectra of the ligand: 2-{1-[2-(1H-Indole-3-yl)-ethylimino]-ethyl}-4-methyl phenol: (TMeHAP) and its Cu complex:

The summery for the spectral lines was given in table (3.6) and the spectra itself was shown in figures 3.21 and 3.22.

Table (3.6): IR spectra of TMeHAP and its Cu complex:

Compound	N-H	O-H	C-H Aliphatic	C=N	C-O	C-H Out of plane Ar.	M-O	M-N
TMeHAP	Superimposed	3167-2915	2915	1605	1280	753	-	-
$(TMeHAP)_2Cu$	3417	-	2918	1589	1315	740	509	424

Like the previous ligand, the sharp N-H vibration band was superimposed on the broad O-H phenolic hydroxyl band at the range 3167 – 2915 cm^{-1}. The strong band at 1605 cm^{-1} belongs to the –C=N stretching frequency and the C-O phenolic band appears at 1280 cm^{-1}. The strong sharp band at 753 cm^{-1} is due to aromatic out-of-plane bending mode.

In the copper complex of the ligand, the broad O-H stretching band was disappeared and in turn the embedded N-H band was appeared as a sharp band at the wave number 3417 cm^{-1}. The azomethine band shifts to 1589 cm^{-1} upon complexation confirming the previously mentioned information of nitrogen lone pair donation towards the metal ion. The C-O band appears at 1315 cm^{-1} and the sharp strong band at 740 cm^{-1} could be attributed to the out-of-plane aromatic bending mode. Once again new bands in the region 509 cm^{-1} – 424 cm^{-1} were appeared due to Cu-O and Cu-N vibrations.

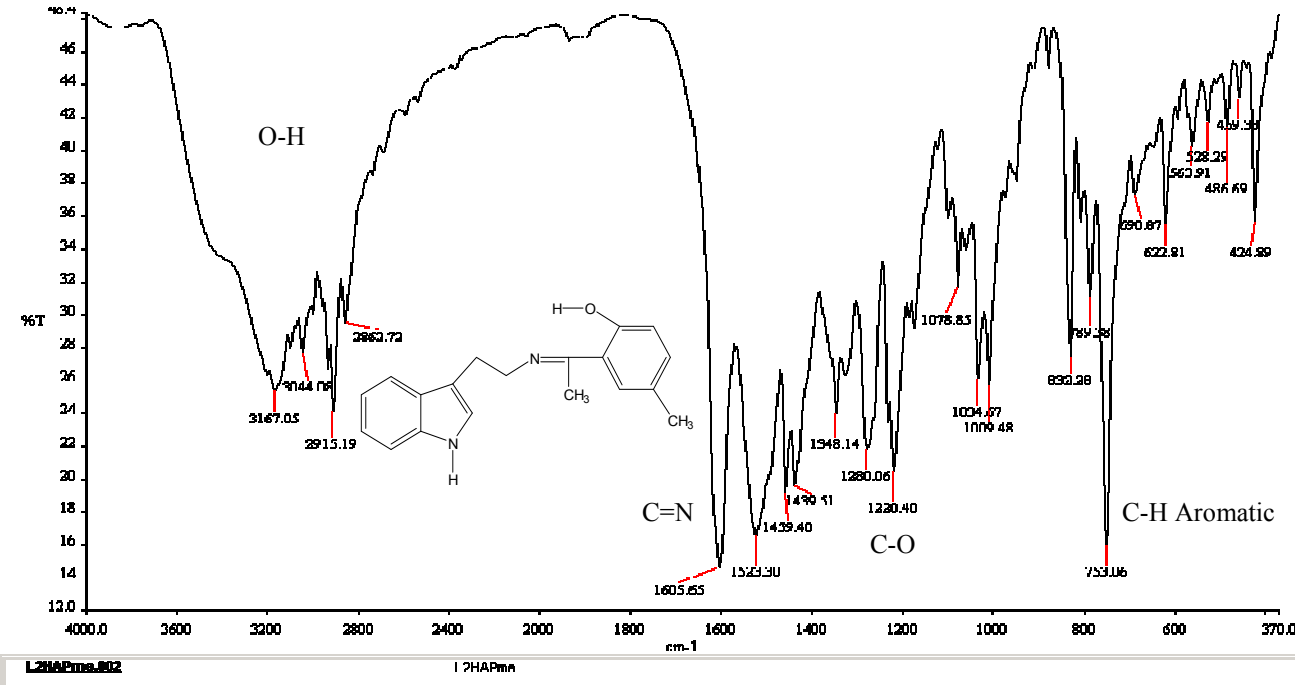

Fig 3.21: IR spectra of: 2-{1-[2-(1H-Indole-3-yl)-ethylimino]-ethyl}-4-methyl phenol (TMeHAP)

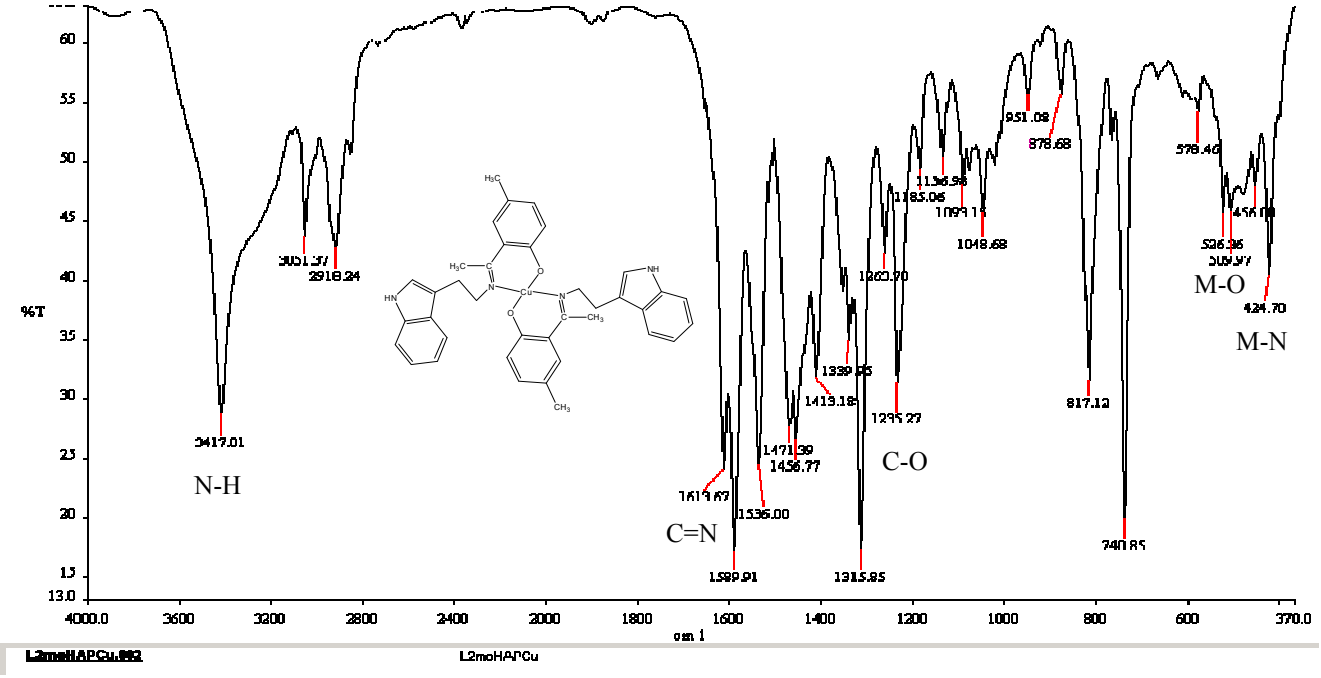

Fig 3.22: IR spectra of: Bis {2-{1-[2-(1H-Indole-3-yl)-ethylimino]-ethyl}-4-methyl phenolato-k^2N, O}Cu(II) $(TMeHAP)_2Cu$

3.1.7 IR spectra of the ligand: 2-{1-[2-(1H-Indole-3-yl)-ethylimino]-ethyl}-4-methoxy phenol (TOMeHAP) and its Ni, and Cu complexes:

The main bands of the spectra were summarized in table (3.7) and complete spectra was shown in figures 3.23, and 3.24

Table (3.7): IR spectra of the ligand TOMeHAP and its Ni, and Cu complexes

Compound	N-H	O-H	C-H Aliphatic	C=N	C-O	C-H Out of plane Ar.	M-O	M-N
TOMeHAP	-	3166	2913	1602	1222	757	-	-
$(TOMeHAP)_2Ni$	3331	-	2929	1599	1214	745	536	426
$(TOMeHAP)_2Cu$	3413	-	2930	1598	1213	745	531	421

It is shown from the table that, like the previously described ligand, the indolic N-H stretching frequency was overlapped by the broad O-H band at 3166 cm^{-1}. The azomethine (–C=N) functional group frequency appears in the normal range at 1602 cm^{-1}, and the band at 1222 cm^{-1} is due to the C-O phenolic stretching mode. The characteristic out-of-plane aromatic band displayed at 757 cm^{-1} in the spectra.

In the case of Ni complex of the ligand, the N-H stretching band appears as a medium intensity band at 3331 $cm^{-1}$and O-H phenolic band was not shown in the spectra. The C=N stretching band shifts a little bit to 1599 cm^{-1} as compared to the free ligand, and so the phenolic C-O band which shifts to 1214 cm^{-1}. This phenomenon explained the fact that co-ordination through both nitrogen and oxygen atom has occurred. This fact can be

supported by the appearance of new band 536 cm^{-1} ascribed to Ni-O and 426 cm^{-1}, may be due to Ni-N bond.

The same explanation can be described to the copper complex. The O-H stretching frequency was diminished, and the azomethine C=N frequency shifts to lower wave number at 1598 cm^{-1} proving co-ordination through the nitrogen lone pair towards the copper ion. Similarly low frequency shift was observed for the phenolic C-O band from 1222 cm^{-1} in the free ligand to 1213 cm^{-1} in the complex. A band at 531 cm^{-1} may be due to Cu-O bond and the Cu-N band appears as a weak band at 421 cm^{-1}.

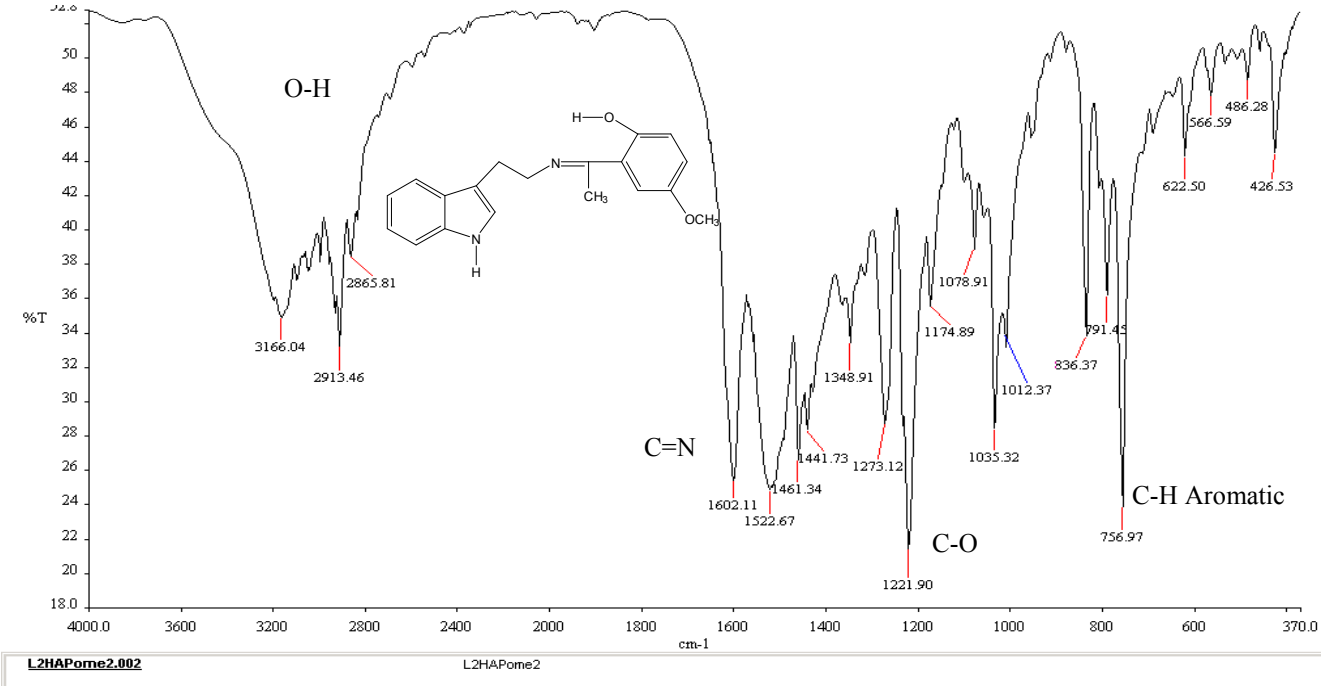

Fig 3.23: IR spectra of: 2-{1-[2-(1H-Indole-3-yl)-ethylimino]-ethyl}-4-methoxy phenol (TOMeHAP)

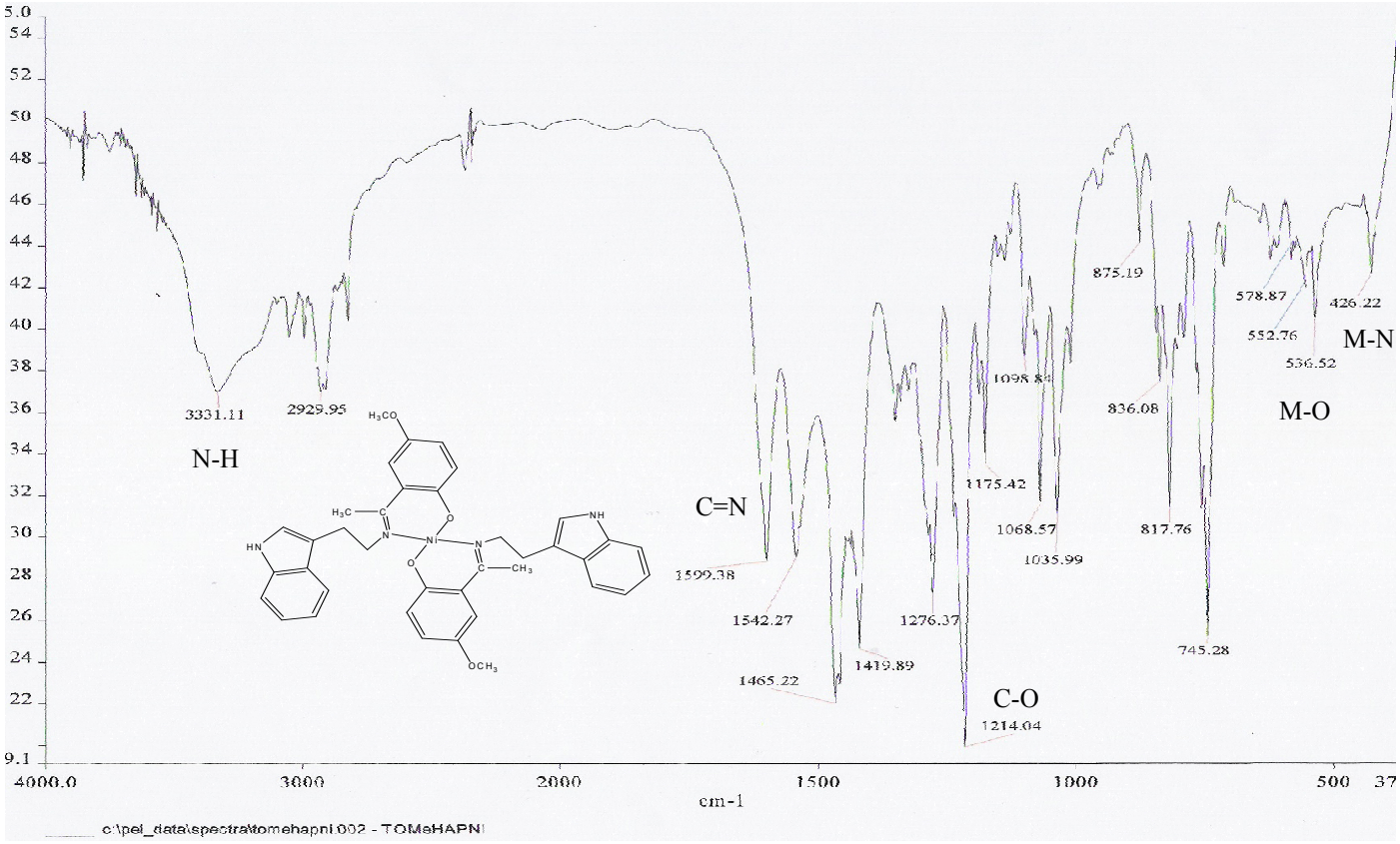

Fig 3.24: IR spectra of: bis{2-{1-[2-(1H-Indole-3-yl)-ethylimino]-ethyl}-4 methoxyphenolato-k^{2}N,O}Ni(II): $(TOMeHAP)_2Ni$

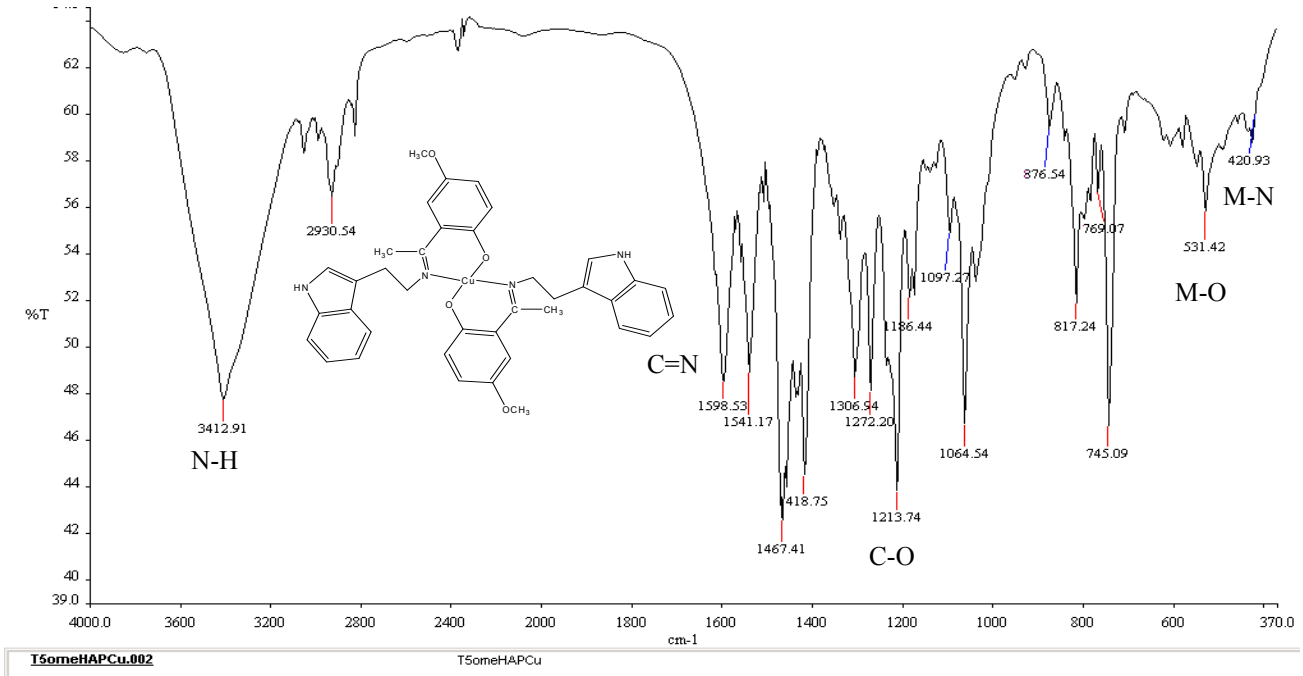

Fig 3.25: IR spectra of: Bis {2-{1-[2-(1H-Indole-3-yl)-ethylimino]-ethyl}-4-methoxy phenolato-k^{2}N,O}Cu(II) $(TOMeHAP)_2Cu$

3.1.8 IR spectra of the ligand: 2-{1-[2-(1H-Indole-3-yl)-ethylimino]-ethyl}-4-chloro phenol: (TClHAP) and its Ni and Cu complexes:

The main IR bands for the ligand and complexes are given in table (3.8) and figures 3.26, 3.27 and 3.28

Table (3.8): IR spectra of the ligand TClHAP and its Ni, and Cu complexes:

Compound	N-H	O-H	C-H Aliphatic	C=N	C-O	C-H Out of plane Ar.	M-O	M-N
TClHAP	3407	3055	2916	1614	1297	743	-	-
$(TClHAP)_2Ni$	3350	-	2932	1602	1306	743	517	450
$(TClHAP)_2Cu$	3419	-	2920	1594	1315	737	593	490

As it can be shown from the table, strong band at a wave number of 3407 cm^{-1} could be assigned to the N-H indolic stretching vibration; while the hydroxyl band can not be identified clearly in the spectra may be due to hydrogen bond. The band at 2916 cm^{-1} is due to C-H aliphatic stretching frequency. Schiff base formation can be proved by the appearance of the strong sharp band of azomethine –C=N group at 1614 cm^{-1} and the phenolic C-O band appears at 1297 cm^{-1} in the usual expected range. The strong sharp band at 743 cm^{-1} was attributable to aromatic out-of-plane C-H bending mode.

In comparing the spectra of the Ni complex to that of the free ligand, the most characteristic feature is the absence of the broad O-H band, probably due to deprotonation of the ligand upon complex formation. The azomethine -C=N stretching band shifts to lower wave number 1602 cm^{-1}, while the phenolic C-O stretching band shifts remarkably to higher frequency 1306 cm^{-1} as compared to the ligand. This shift suggests that co-ordination through the oxygen atom has occurred. The sharp aromatic out-of-plane band remains intact, and the new bands at the low wave numbed end of the spectra 517 cm^{-1} and 450 cm^{-1} could be assigned to Ni-O and Ni-N frequencies respectively.

The comparison of the IR spectra of the ligand and its copper complex illustrates, principally, coordination to the copper centre is in two ways. The band appearing at 1614 cm^{-1} due to the azomethine linkage in the ligand is shifted to lower frequency by 20 cm^{-1} in the complex. This proves azomethine nitrogen interaction with the metal ion. A broad band centered at 3055 cm^{-1} assigned to O-H in the Schiff base was no longer found in the spectra of the metal complex. Instead, appearance of strong band at 1315 cm^{-1} due to C-O stretching vibration was observed, indicating deprotonation and coordination of the hydroxyl oxygen to the copper ion. Further conclusive evidence of the coordination pattern was provided by the appearance of weak intensity bands at 593 cm^{-1} and 490 cm^{-1} assignable to Cu-O and Cu-N vibrations respectively.

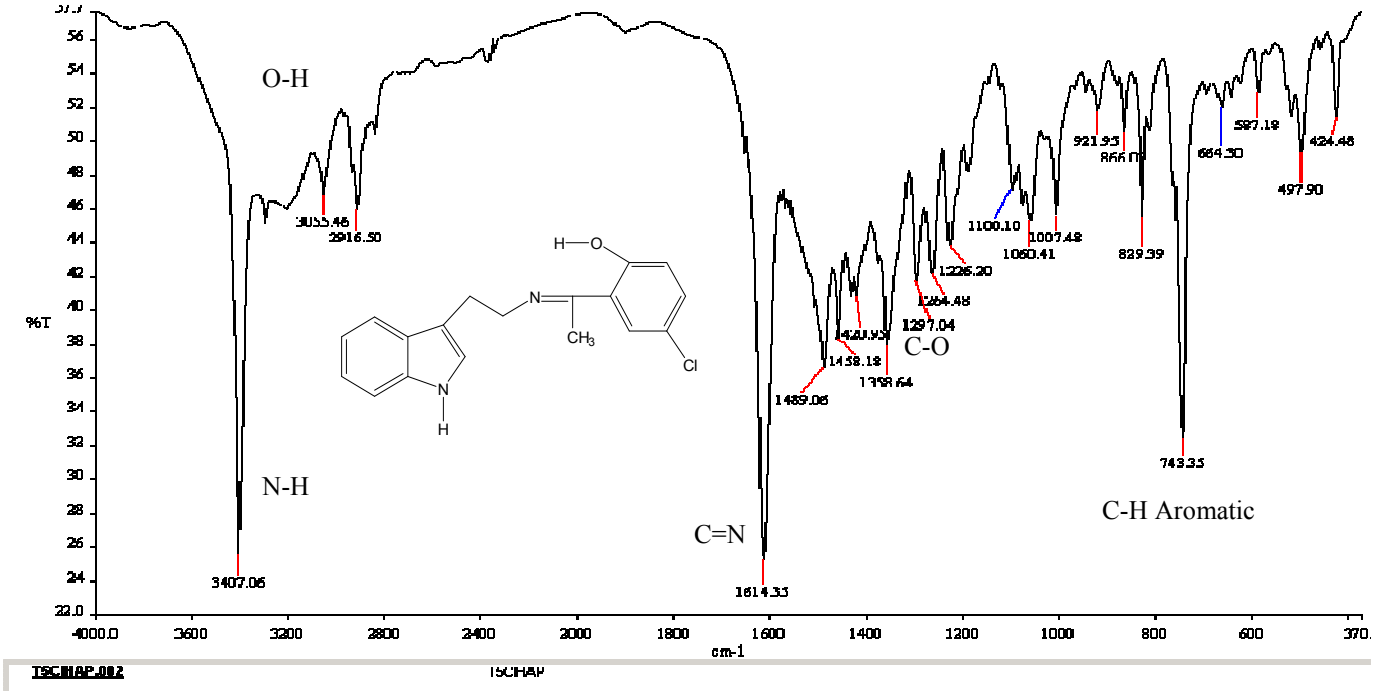

Fig 3.26: IR spectra of: 2-{1-[2-(1H-Indole-3-yl)-ethylimino]-ethyl}-4-chloro phenol (TClHAP)

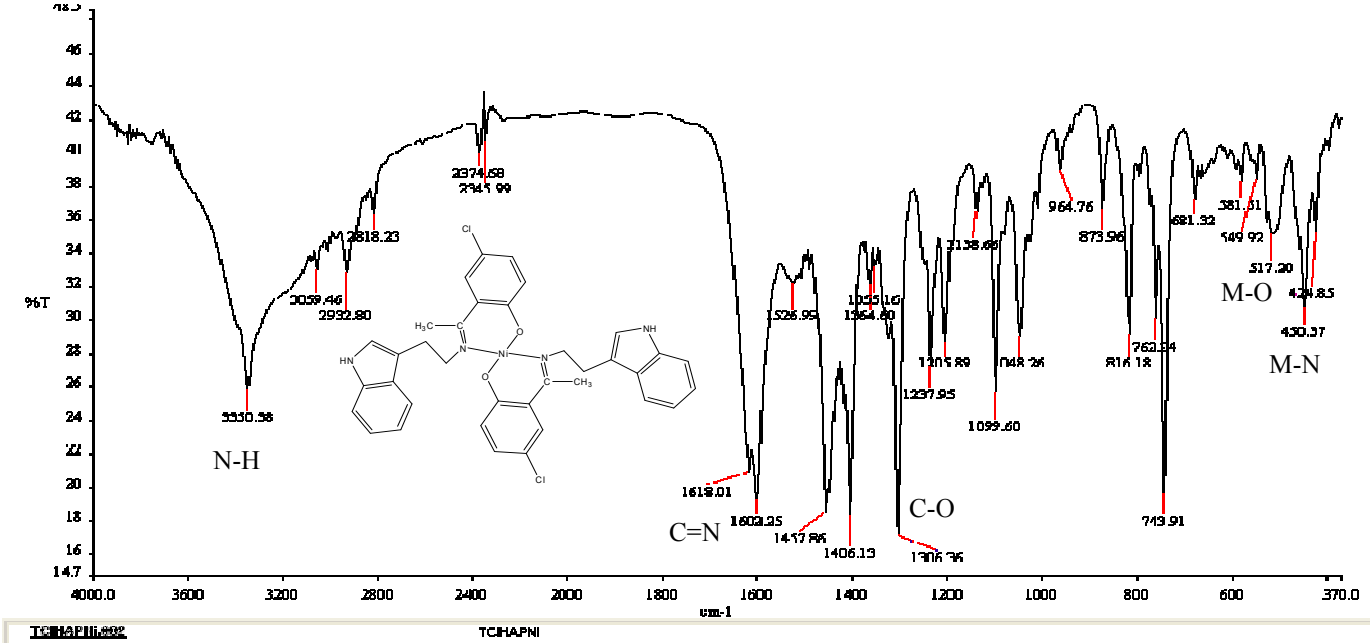

Fig 3.27: IR spectra of: bis{2-{1-[2-(1H-Indole-3-yl)-ethylimino]-ethyl}-4-chlorophenolato-k^2N,O}Ni(II): $(TClHAP)_2Ni$

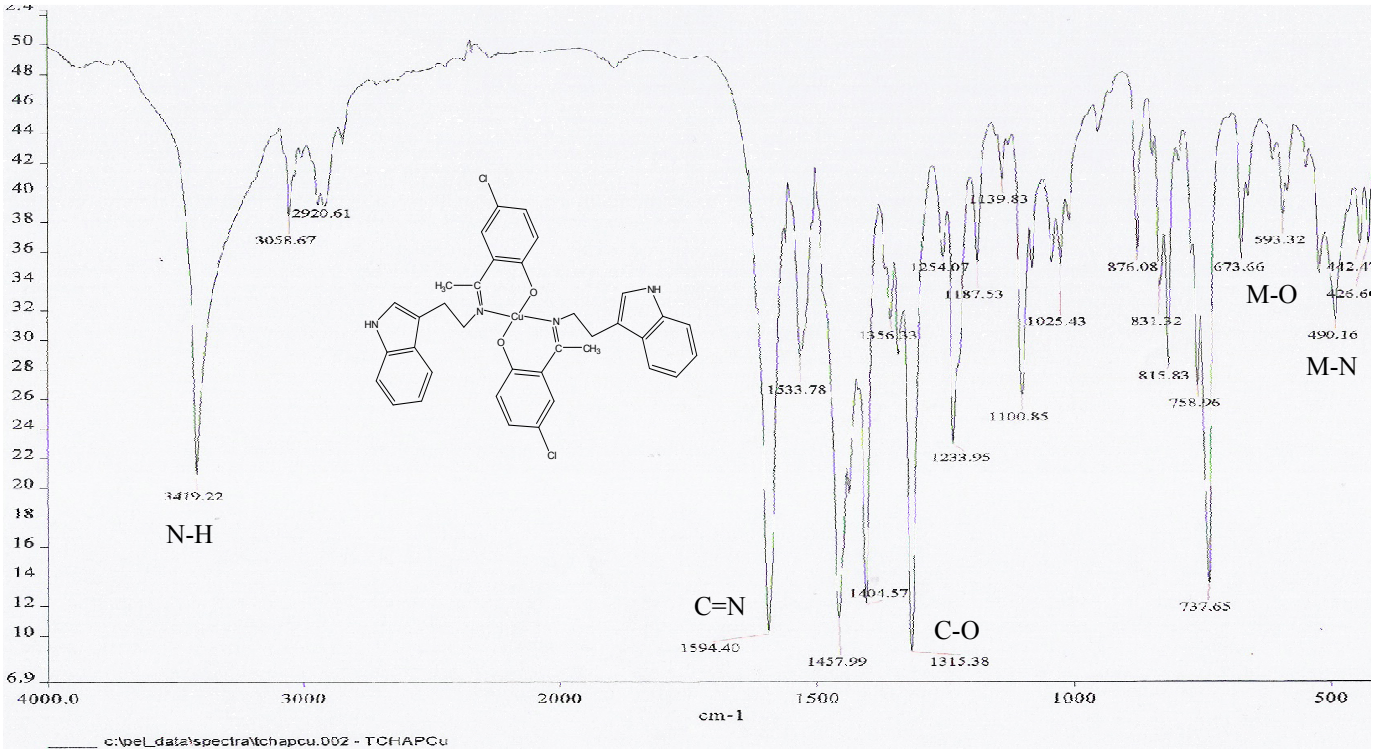

Fig 3.28: IR spectra of: bis{2-{1-[2-(1H-Indole-3-yl)-ethylimino]-ethyl}-4-chlorophenolato-k^{2}N,O}Cu(II): $(TClHAP)_2Cu$

3.1.9 IR spectra of the ligand: 4-Bromo-2-{1-[2-(1H-Indole-3-yl)-ethylimino]-ethyl}-phenol (TBrHAP) and its copper complex:

The main IR bands of the ligand and complexes are given in table (3.9) and figures 3.29 and 3.30

Table (3.9): IR spectra of the ligand TBrHAP and its copper complex:

Compound	N-H	O-H	C-H Aliphatic	C=N	C-O	C-H Out of plane Ar.	M-O	M-N
TBrHAP	3406	3054	2915	1618	1230	746	-	-
$(TBrHAP)_2Cu$	3414	-	2943	1592	1233	737	590	490

As for the previous chloro-substituted ligand, the indolic N-H stretching mode appears almost in the same frequency 3406 cm^{-1}, and the broad band centered at 3054 cm^{-1} belongs to the intra-molecular hydrogen bonded O-H group. The sharp band at 1618 cm^{-1} could clearly be assigned to –C=N vibration. C-O stretching mode appears at low frequency 1230 cm^{-1} as compared to the chloro-substituted ligand described earlier, and the sharp band at 746 cm^{-1} is the aromatic out-of-plane bending vibration.

In the spectra of the copper complex, there is a remarkable disappearance of the O-H band probably owing to deprotonation and co-ordination through the oxygen atom and the azomethine –C=N band shifts to lower wave number to be at 1592 cm^{-1}. This imposes further evidence to the participation of the azomethine nitrogen atom in a dative bond through its lone pair of electrons and the ligand acts as a bidentate ligand. New bands at the wave numbers 590 cm^{-1} and 490 cm^{-1} could be ascribed to metal-ligand vibrations Cu-O and Cu-N respectively.

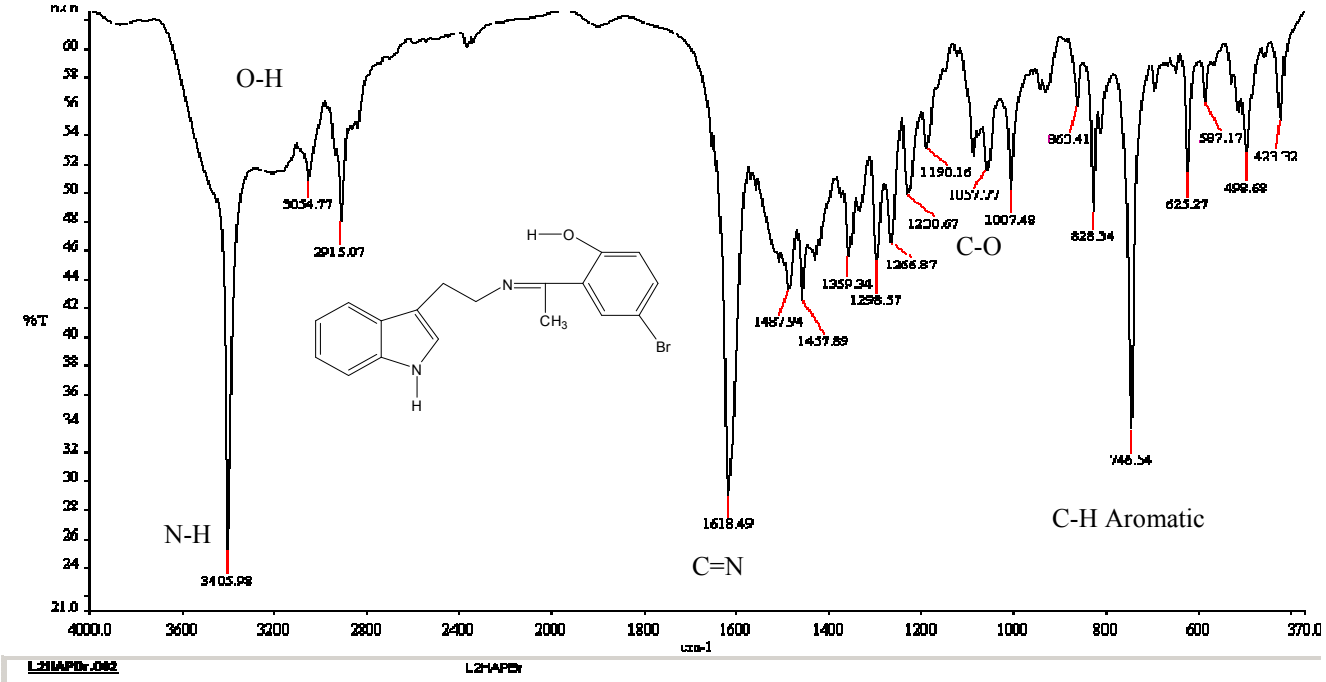

Fig 3.29: IR spectra of: 4-Bromo- 2-{1-[2-(1H-Indole-3-yl)-ethylimino]-ethyl}- phenol (TBrHAP)

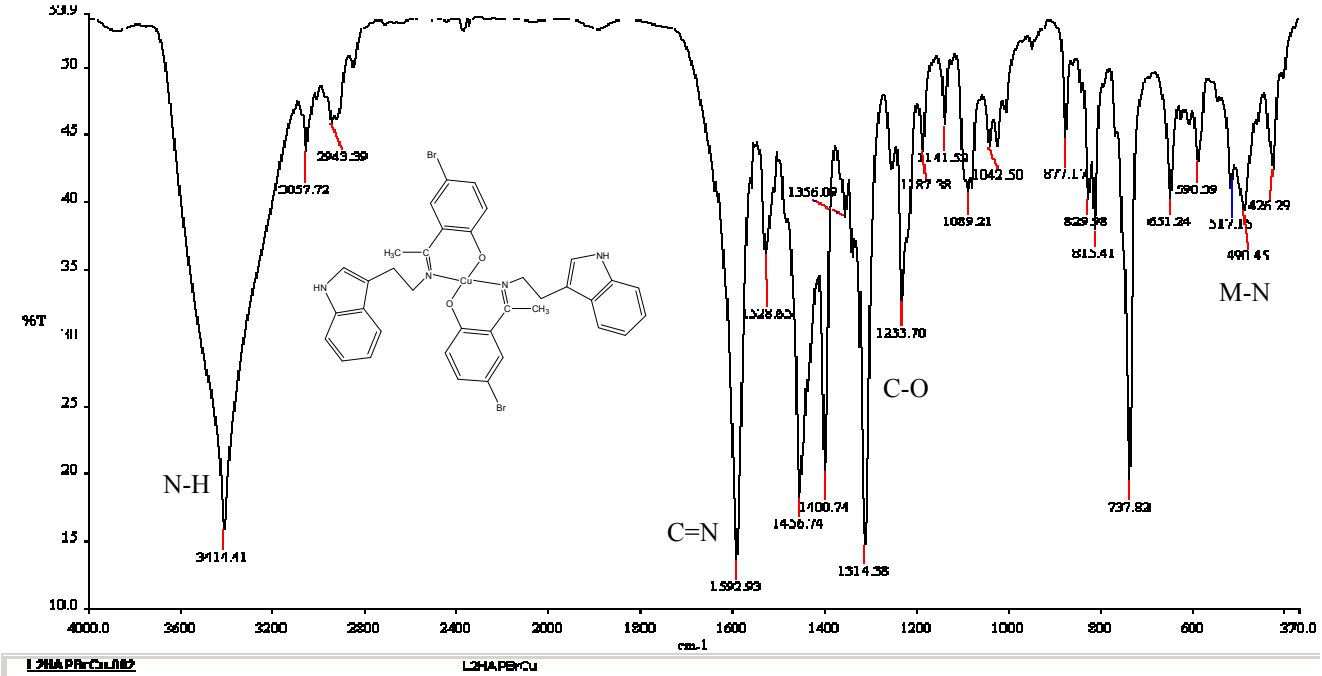

Fig 3.30: IR spectra of: Bis {2-{1-[2-(1H-Indole-3-yl)-ethylimino]-ethyl}-4-bromo phenolato-k^{2}N,O}Cu(II)

3.2 Proton NMR spectra of the ligands and complexes:

3.2.1 Proton NMR spectra of the ligand: 1H-Indole-3-ethylenesalicylaldimine (TS):

The ^{1}H NMR spectra of the ligand TS was recorded in d^{6}-DMSO with chemical shifts expressed in ppm using tetramethylsilane (TMS) as internal standard was given in table (3.10) and shown in figure 3.31

Table (3.10): ^{1}H NMR spectra of TS and its Zn, Ni, and Cu complexes

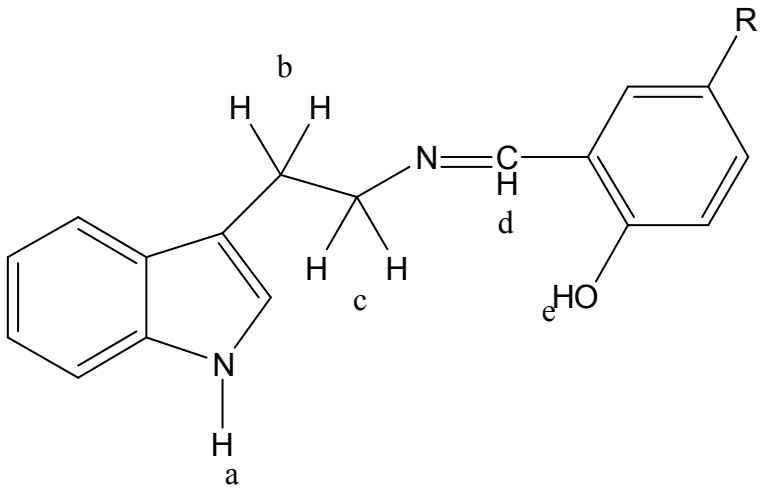

R = H , Cl , NO_2

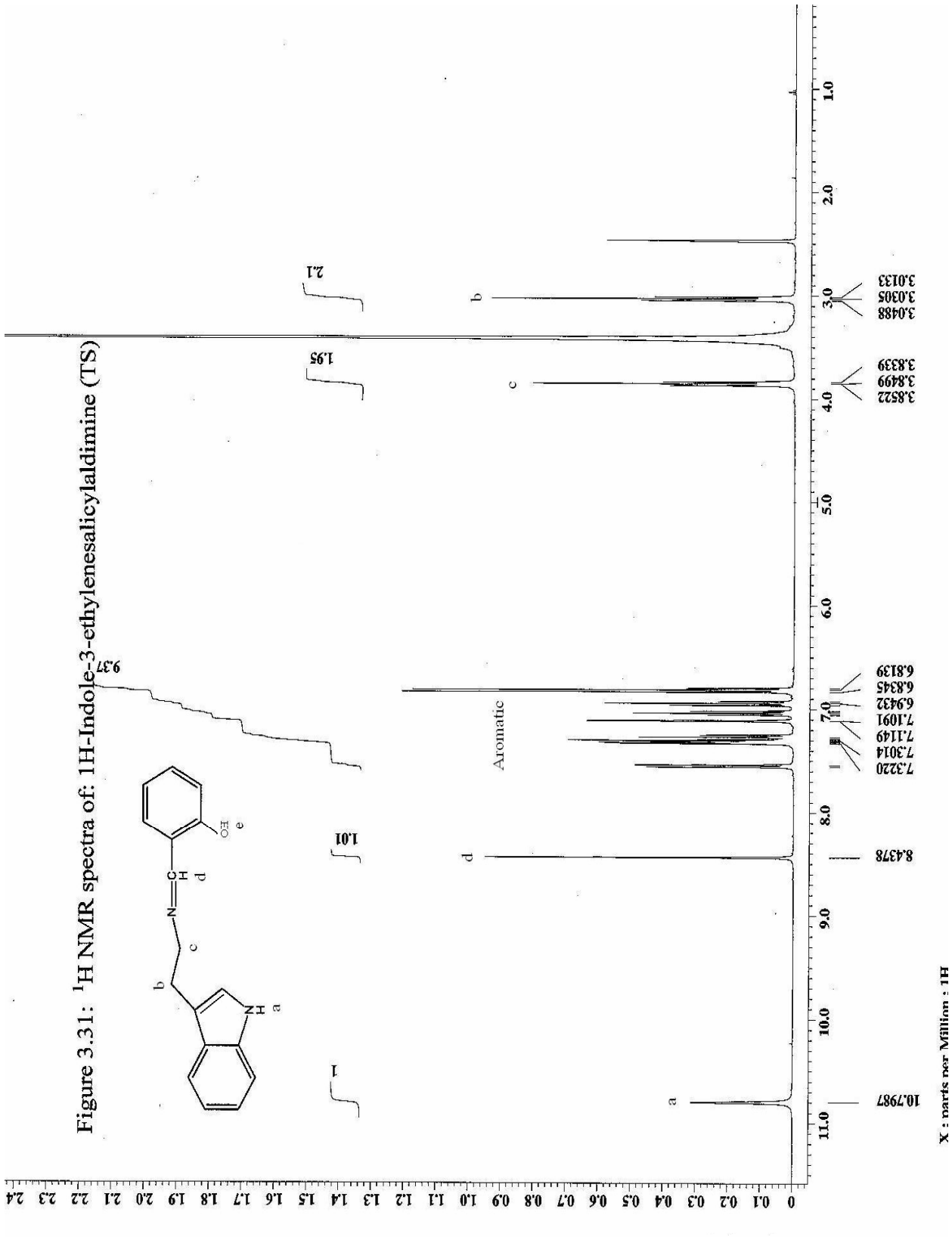
Figure 3.31: ^{1}H NMR spectra of: 1H-Indole-3-ethylenesalicylaldimine (TS)
Aromatic
X : parts per Million : 1H

Table 3.10: ^{1}H NMR Chemical shifts in ppm:

Compound	H_a	H_b	H_c	H_d	H_e	$H_{aromatic}$
TS	10.79(s)	3.03(t)	3.85(t)	8.43(s)	-	6.81-7.32(m)
$(TS)_2Zn$	10.76(s)	2.88(t)	3.71(t)	8.39(s)	-	6.56-7.30(m)
$(TS)_2Ni$	No clear spectra					
$(TS)_2Cu$	No clear spectra					

It can be concluded that the data shown in the table agrees well with the proposed structure shown above. The indolic proton H_a appears as a singlet at 10.79 ppm, integration due to one proton. This position may be overlapping with the hydroxyl O-H proton when deuterated chloroform were used as a solvent [21] due to the effect of intra-molecular hydrogen bonding with the azomethine nitrogen atom [63]. The aliphatic (-CH_2-) protons H_b resonate as a triplet at 3.03 ppm and the other (-CH_2-) protons of the tryptamine moiety H_c also resonate as a triplet at higher frequency 3.85 ppm. The aldehydic proton H_d resonates as a singlet down field at 8.43 ppm, and the aromatic protons appears in the range 6.81 – 7.32 ppm as a multiplet integration indicates 9 protons altogether. The peaks at 2.50 and ≈ 3.40 ppm are solvent peaks.

If we consider the zinc complex of the ligand, the spectra is somewhat similar to the ligand indicating a symmetrical arrangement of the ligand around the metal ion (See Fig 3.32). The O-H proton signal was disappeared as a result of proton substitution by a cation. H_b protons go to slightly lower chemical shift value 2.88 ppm and so H_c protons to 3.71 ppm. The aldehydic proton appears at 8.39 ppm as a singlet and the aromatic protons in the usual range 6.56 – 7.30 ppm as a multiplet.

No ^{1}H NMR spectra was detected for Ni and Cu complexes of the ligand because they are paramagnetic in solution.

3.2.2 Proton NMR spectra of the ligand: 1H-Indole-3-ethylene-5-chlorosalicylaldimine (TCS):

The NMR spectrum of the ligand was summarized in table (3.11) with chemical shifts expressed in ppm downfield tetrametyl silane as internal reference. The full spectrum was shown in Fig 3.33.

Table (3.11): ^{1}H NMR spectra of TCS and its Zn complex:

Compound	H_a	H_b	H_c	H_d	H_e	$H_{aromatic}$
TCS	10.80(s)	3.03(t)	3.85(t)	8.45(s)	-	6.82-7.42(m)
$(TCS)_2Zn$	10.79(s)	2.90(t)	3.74(t)	8.40(s)	-	6.74 –7.30(m)

The indolic N-H proton appears as a singlet at 10.80 ppm. Two triplets at 3.03 ppm and 3.85 ppm are due to the ethylene (-CH_2-) groups of the tryptamine H_b and H_c respectively. The aldehydic proton H_d observed as a singlet at 8.45 ppm, and the aromatic protons in the range 6.82 – 7.42 ppm as a multiplet. Integration line indicates 8 protons altogether due to the presence of chlorine substituent compared to the previous unsubstituted ligand.

For $(TCS)_2Zn$ complex, likewise the spectra appears to be closely similar to the ligand spectra (See Fig 3.34) and this phenomenon may be explained according to the

symmetrical arrangement of the ligand atoms around the central zinc ion. The only remarkable difference is the absence of the hydroxyl proton signal H_e as a result of complex formation besides a slight shift of the position of the aromatic protons chemical shift values in relation to the ligand.

No clear spectrum was recorded for the nickel and copper complexes of this ligand due to their paramagnetic nature in solution.

3.2.3 Proton NMR spectra of the ligand: 1H-Indole-3-ethylene-5-nitrosalicylaldimine (TNS):

The spectrum was shown in table (3.12) with chemical shifts in ppm downfield tetramethyl silane as refrence. Full spectrum was shown in Fig 3.35.

Table (3.12): ^{1}H NMR spectra of the ligand TNS and its complexes:

Compound	H_a	H_b	H_c	H_d	H_e	$H_{aromatic}$
TNS	10.89(s)	3.10(t)	3.90(t)	8.59(s)	-	6.52-7.98(m)
$(TNS)_2Zn$	10.77(s)	2.89(t)	3.82(t)	8.43(s)	-	6.68-8.22(m)
$(TNS)_2Ni$	No clear spectra					
$(TNS)_2Cu$	No clear spectra					

H_a proton in the structure proposed resonates as a singlet at 10.89 ppm and the aliphatic protons H_b and H_c resonate as triplets at 3.10 ppm and 3.90 ppm respectively. The aldehydic proton H_d appears as a singlet at 8.59 ppm and the aromatic protons in the range of 6.52 ppm to 7.98 ppm as multiplet. The integration line indicates that the signals are due to 8 protons as expected.

In the case of zinc complex of the ligand (See Fig 3.36), a slight displacement of chemical shift values has occurred. The indolic N-H proton labeled H_a appears at 10.77 ppm compared to10.89 ppm in the free ligand. The aromatic protons range extends to 8.22 ppm, reported data is recorded in table (3.12)

No clear spectrum was recorded for nickel and copper complexes because they are paramagnetic in solution.

3.2.4 Proton NMR spectra of the ligand:

1H-Indole-3-ethylene-3-5-di-tertiarybutylsalicylaldimine (TTET) and its Zn, Ni, and Cu complexes:

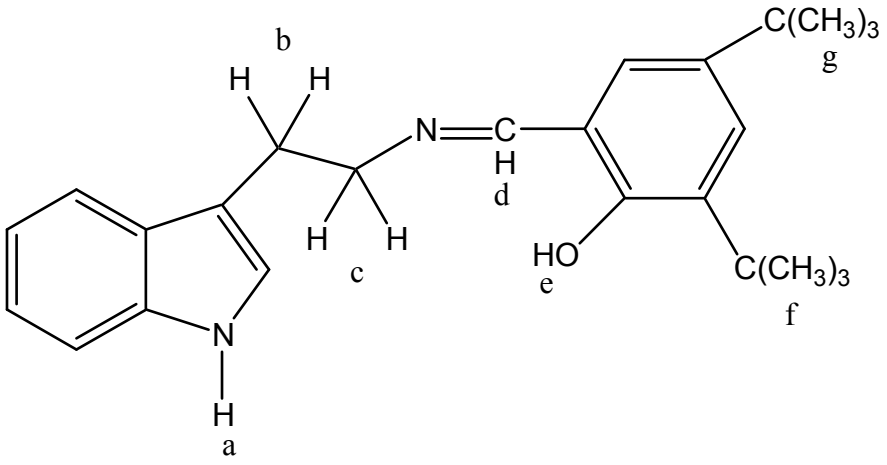

Table (3.13): ^{1}H NMR spectra of the ligand TTET and its complexes:

Compound	H_a	H_b	H_c	H_d	H_e	H_f	H_g	$H_{aromatic}$
TTET	10.72(s)	3.03(t)	3.81(t)	8.44(s)	9.90(s)	1.32(s)	1.24(s)	6.93-7.62(m)
$(TTET)_2Zn$	10.73(s)	3.02(t)	3.82(t)	8.44(s)	-	1.35(s)	1.23(s)	6.68-7.36(m)

$(TTET)_2Ni$	No spectra (paramagnetic)
$(TTET)_2Cu$	No spectra (paramagnetic)

The data was summarized in table (3.13) and the spectra was shown in figure (3.37)

It can be drawn from the table that, the indolic proton H_a resonates as a singlet at 10.72 ppm, the triplets appears in 3.03 ppm and 3.81 ppm are due to the protons H_b and H_c respectively. This can be supported by the integration line which reveals that the signal is due to two protons each. Further more there are singlets at 1.32 ppm and 1.24 ppm due to 9 protons each and this can be ascribed for the tertiary butyl protons H_f and H_g respectively. The aldehydic proton appears down field at 8.44 ppm and the aromatic protons appear as a multiplet in the range 6.93 – 7.62 ppm.

With respect to zinc complex of the ligand (Fig 3.38), the hydroxyl H_e proton signal was disappeared indicating deprotonation and participation of the phenolic oxygen atom in co-ordination to zinc ion as proved by the X-ray structure. The indolic N-H proton H_a shifts a little bit to 10.73 ppm. The ethyleneic protons H_b and H_c appear in the usual range of aliphatic protons at 3.02 and 3.82 ppm respectively. Integration line indicates two protons each. Also the singlets at 1.35 ppm and 1.23 ppm were due to the tertiary butyl protons H_f and H_g successively. The spectra look somewhat similar to the ligand spectra indicating that the ligands arranged symmetrically around the metal ion which seems to be in the centre of symmetry.

No spectra have been observed for Ni and Cu complexes due to paramagnetic effects in these compounds.

Figure 3.32: ^{1}H NMR spectra of: bis(1H-Indole-3-ethylenesalicylaldiminato-k^2N,O)Zn(II): $(TS)_2Zn$

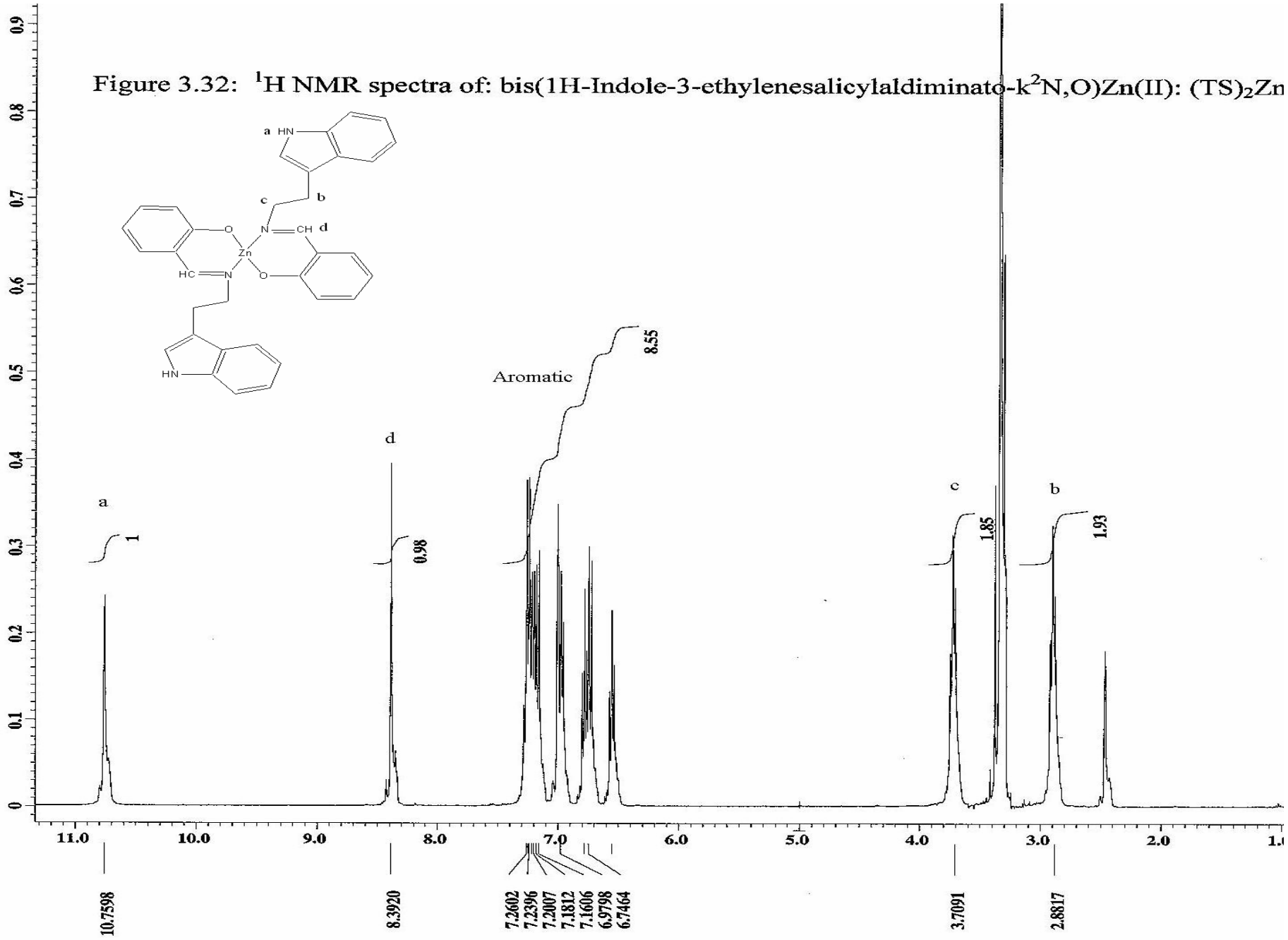

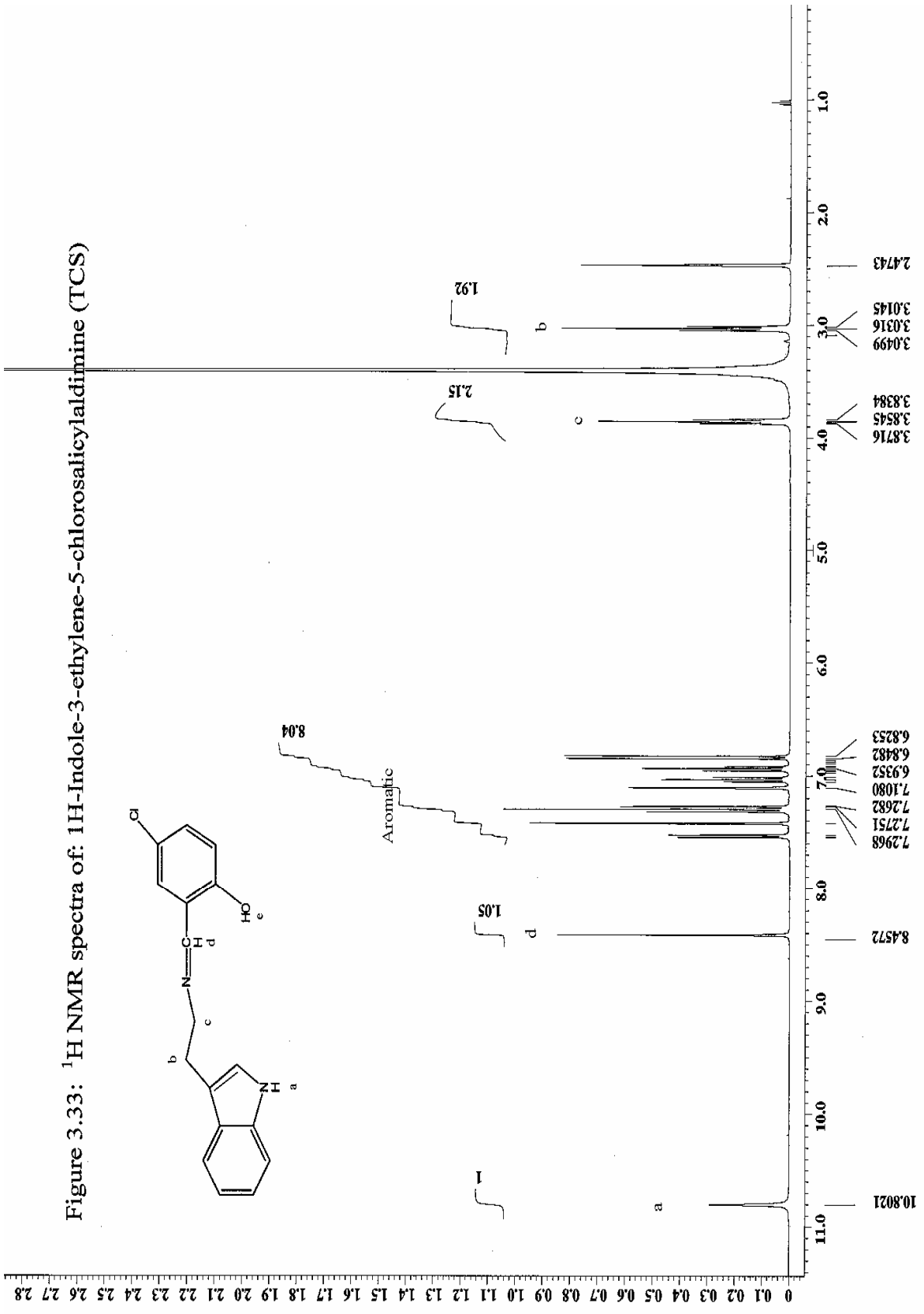

Figure 3.33: ^{1}H NMR spectra of: 1H-Indole-3-ethylene-5-chlorosalicylaldimine (TCS)

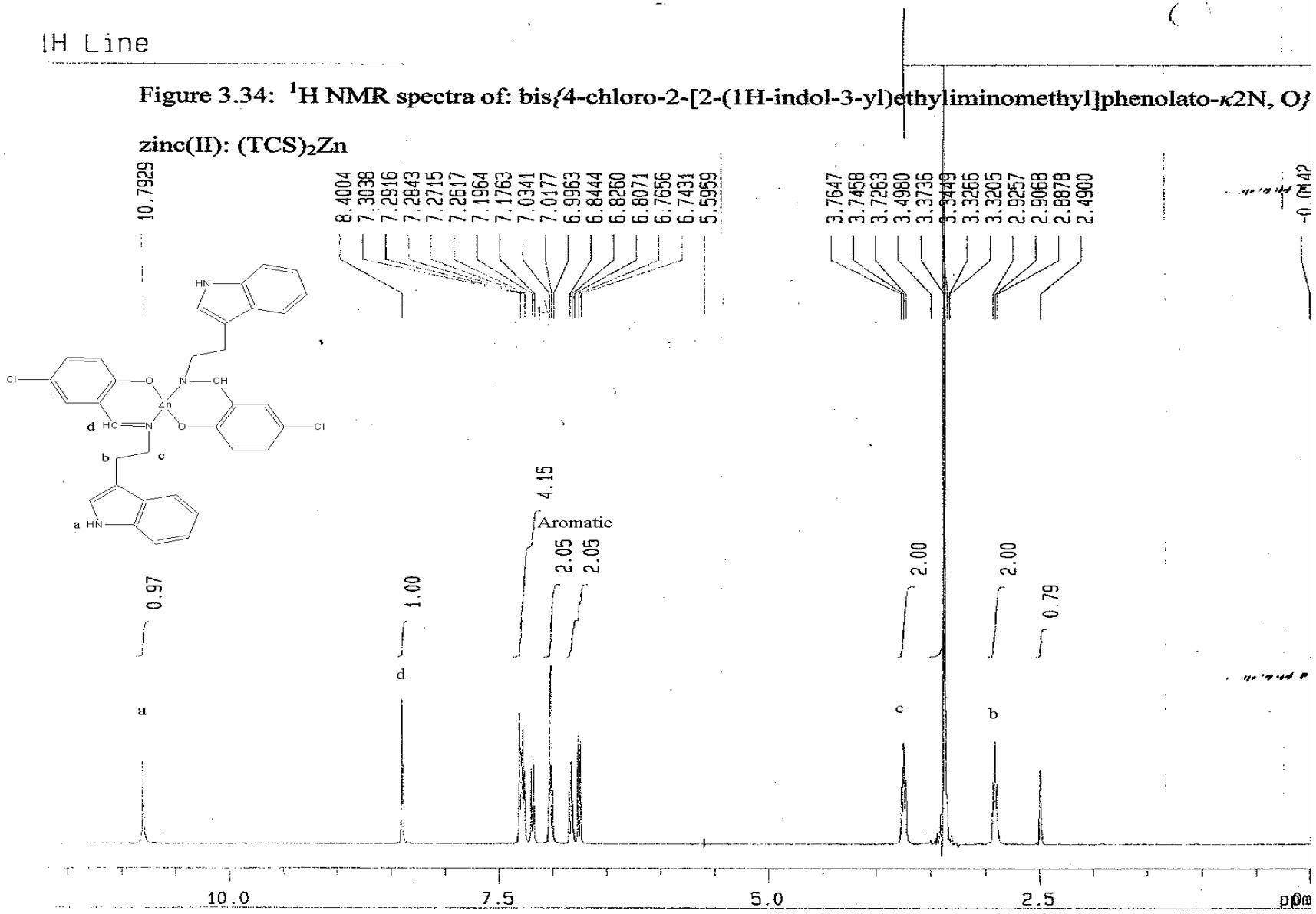

Figure 3.34: ^{1}H NMR spectra of: bis{4-chloro-2-[2-(1H-indol-3-yl)ethyliminomethyl]phenolato-κ2N, O} zinc(II): $(TCS)_2Zn$

Figure 3.35: ^{1}H NMR spectra of: 1H-Indole-3-ethylene-5-nitrosalicylaldimine (TNS)

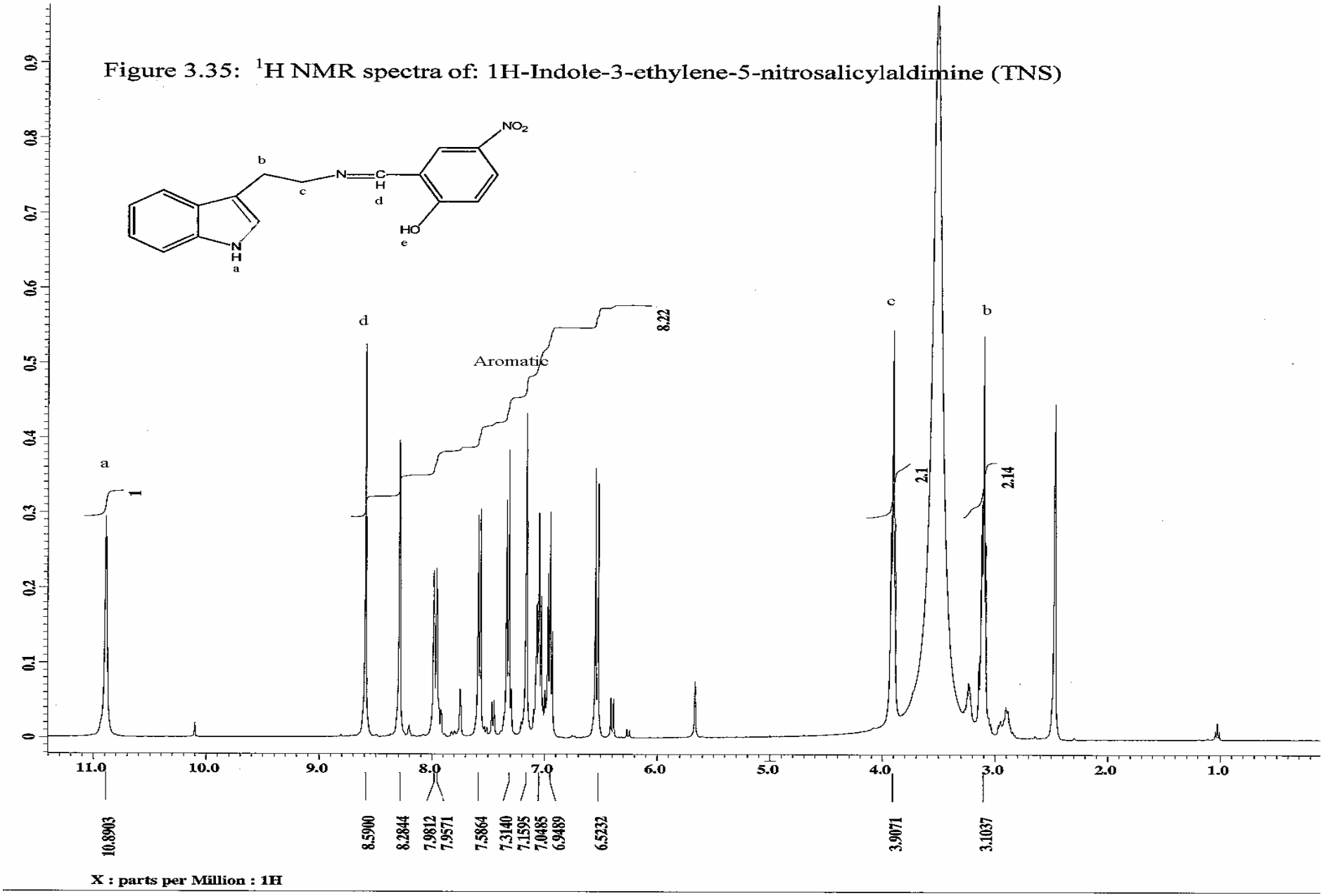

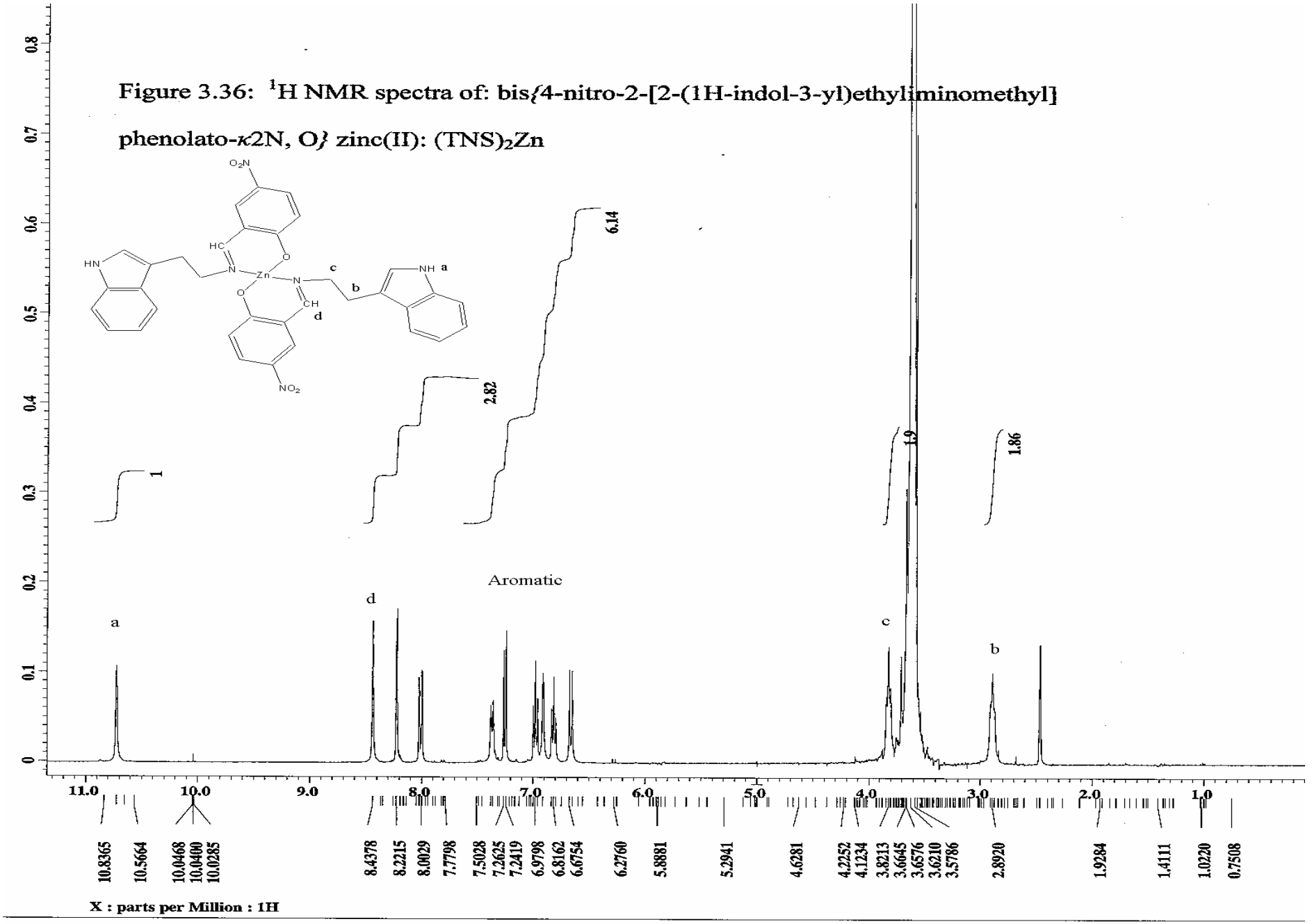
Figure 3.36: ^{1}H NMR spectra of: bis{4-nitro-2-[2-(1H-indol-3-yl)ethyliminomethyl] phenolato-κ2N, O} zinc(II): (TNS)$_2$Zn
O2N
HC
HN
N
Zn
O
N
c
NH a
b
CH
d
NO2
1
2.82
6.14
1.9
1.86
Aromatic
a
d
c
b
11.0
10.0
9.0
8.0
7.0
6.0
5.0
4.0
3.0
2.0
1.0
10.8365
10.5664
10.0468
10.0400
10.0285
8.4378
8.2215
8.0029
7.7798
7.5028
7.2625
7.2419
6.9798
6.8162
6.6754
6.2760
5.8881
5.2941
4.6281
4.2252
4.1234
3.8213
3.6645
3.6576
3.6210
3.5786
2.8920
1.9284
1.4111
1.0220
0.7508
X : parts per Million : 1H

Figure 3.37: ^{1}H NMR spectra of: 1H-Indole-3-ethylene-3-5-di-tertiarybutylsalicylaldimine (TTET)

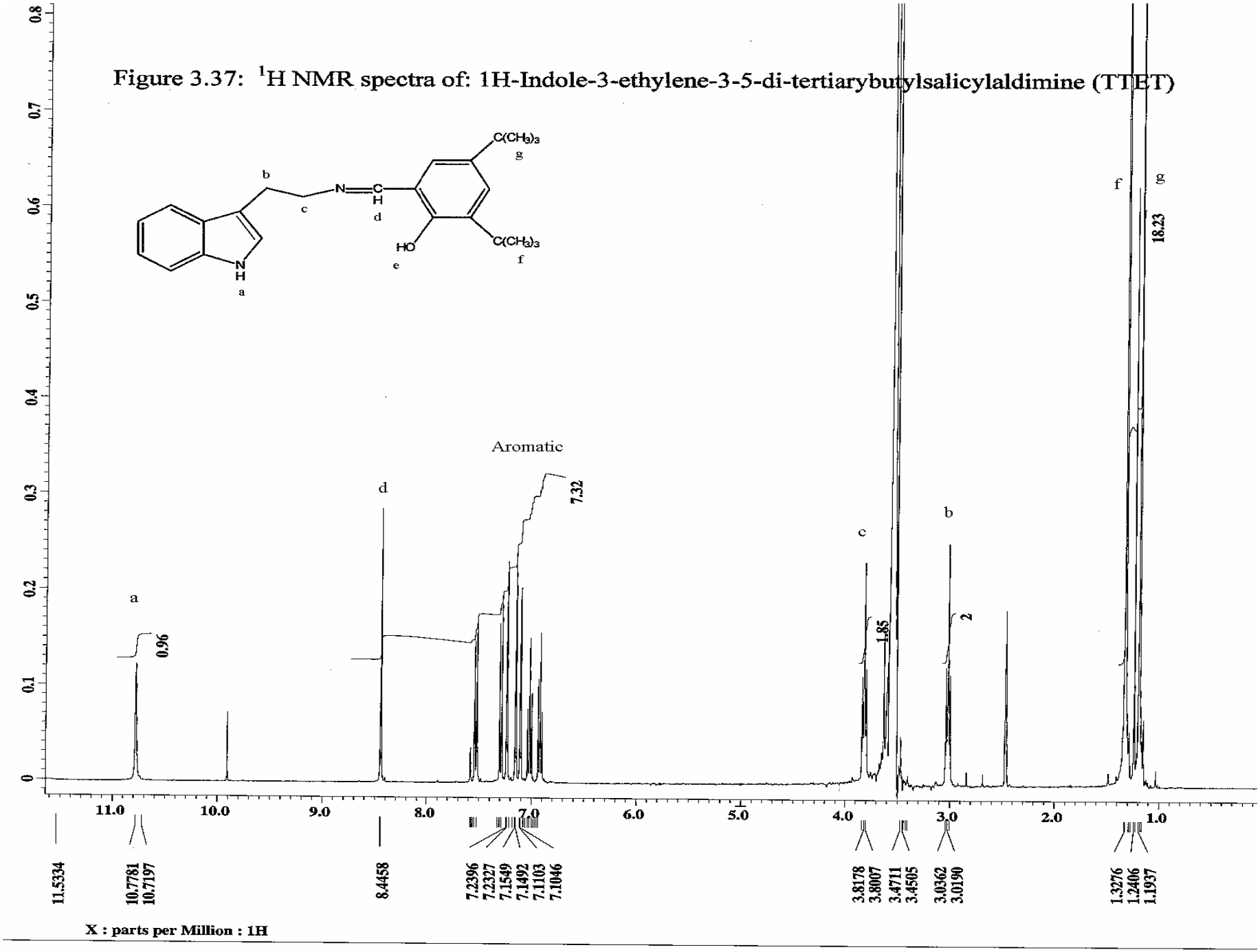

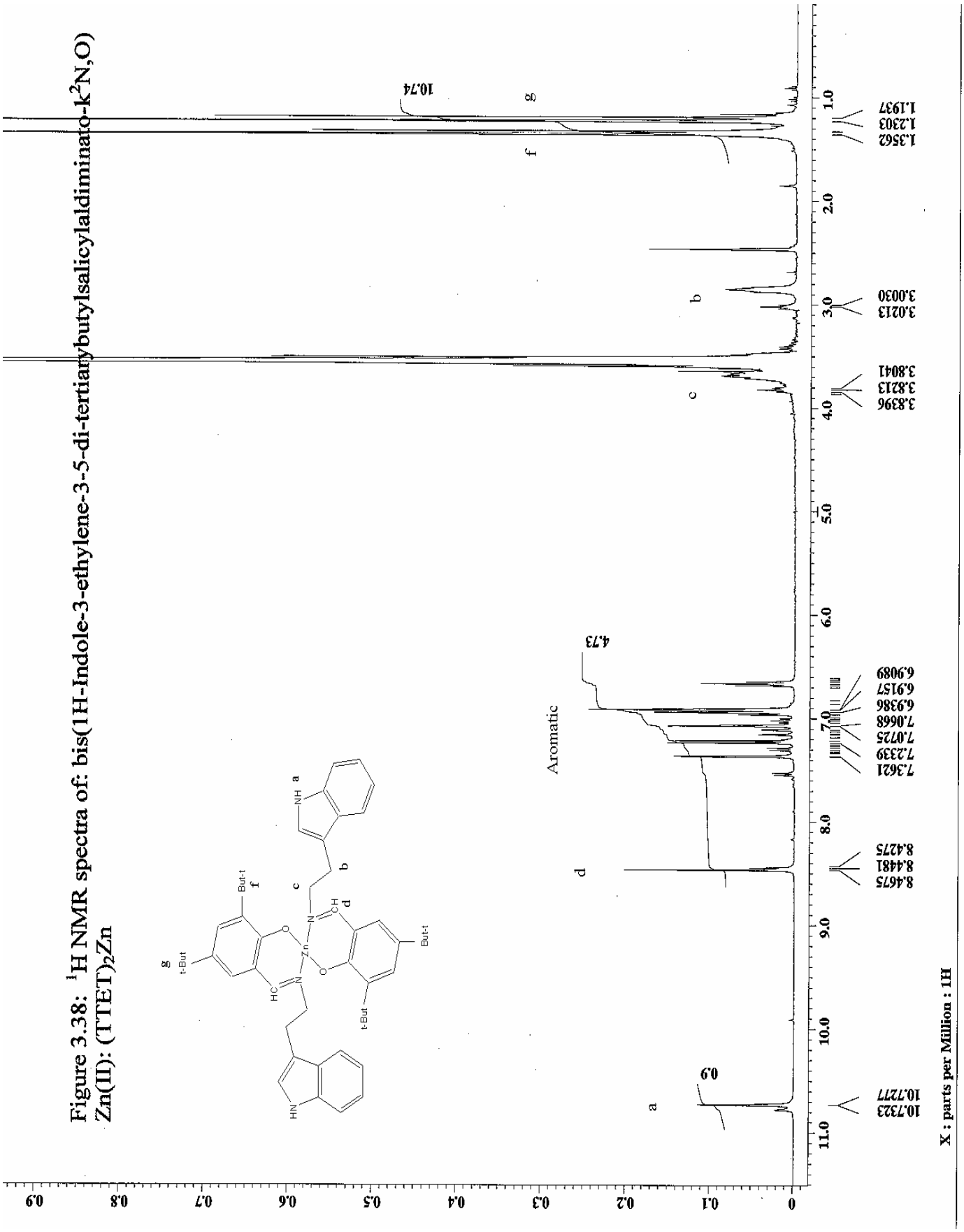
Figure 3.38: ^{1}H NMR spectra of: bis(1H-Indole-3-ethylene-3-5-di-tertiarybutylsalicylaldiminato-K^{2}N,O) Zn(II): (TTET)$_2$Zn
Aromatic
X : parts per Million : 1H

3.2.5 Proton NMR spectra of the ligand:

2-{1-[2-(1H-Indole-3-yl)ethylimino]-ethyl } phenol (THAP) and its complexes:

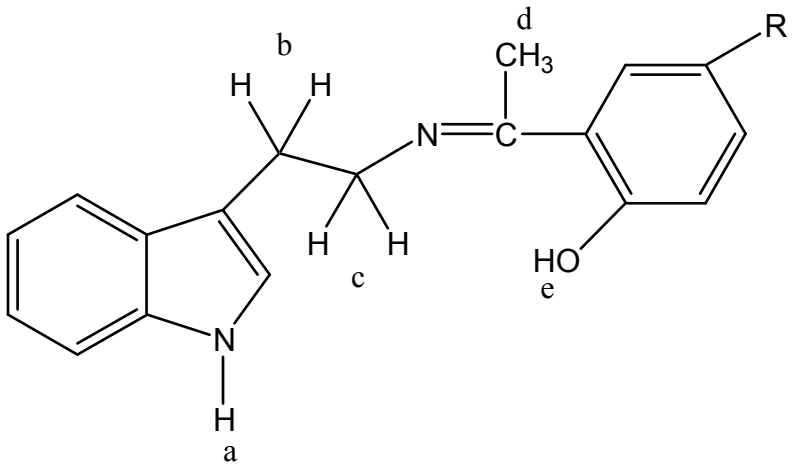

R = CH_3 , OCH_3 , Cl , Br

Table (3.14): 1H NMR spectra of the ligand THAP and its zinc complex

Compound	H_a	H_b	H_c	H_d	H_e	H_R	$H_{aromatic}$
THAP	10.82(s)	3.08(t)	3.84(t)	2.26(s)	-	-	6.66-7.57(m)
$(THAP)_2Zn$	10.83(s)	3.09(t)	3.86(t)	2.28(s)	-	-	6.67-7.59(m)

^{1}H NMR spectra of the ligand was summarized in table (3.14) with chemical shifts expressed in ppm down field tetra methylsilane as reference. The spectrum was shown in Fig. 3.39.

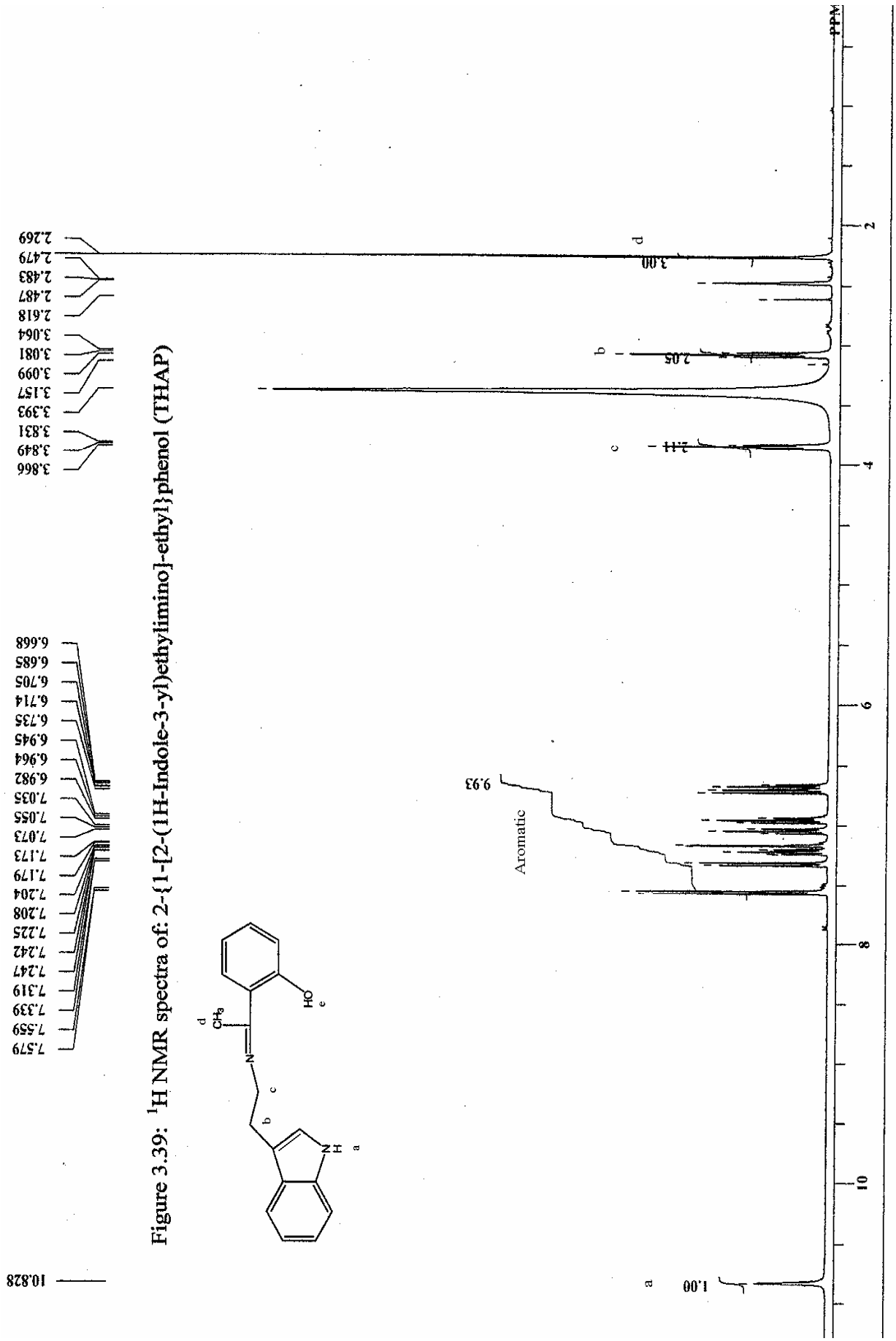

Figure 3.39: ^{1}H NMR spectra of: 2-{1-[2-(1H-Indole-3-yl)ethylimino]-ethyl}phenol (THAP)

It can be shown from the table that the singlet appears at 10.82 ppm can be attributed to the indolic N-H proton H_a in the diagram of the structure proposed. As for the previous ligands, the ethyleneic protons H_b and H_c resonates at 3.08 ppm and 3.84 ppm as triplets respectively. The methyl protons H_d resonates at 2.26 ppm as a singlet. Integration line confirms 3 protons in contrast to only one proton for the previously described ligands.

The signals between 6.66 ppm and 7.57 ppm are due to 9 aromatic protons as the integration implies.

The proton signal H_e was absent in the zinc complex spectra (Fig.3.40). The absence of salicylaldehyde OH signal is evidently due to the coordination of this oxygen to the metal ion after deprotonation [29].

3.2.6 Proton NMR spectra of the ligand: 2-{1-[2-(1H-Indole-3-yl)-ethylimino]-ethyl}-4-methyl phenol (TMeHAP):

Table (3.15): ^{1}H NMR spectra of the ligand: TMeHAP and its complexes:

Compound	H_a	H_b	H_c	H_d	H_e	H_R	$H_{aromatic}$
TMeHAP	10.82(s)	3.07(t)	3.83(t)	2.25(s)	-	2.20(s)	6.63-7.57(m)
$(TMeHAP)_2Cu$	No clear spectra						

The proton NMR spectra was displayed in figure (3.41) and summarized in table (3.15), chemical shifts are measured in ppm using d^6-DMSO as solvent.

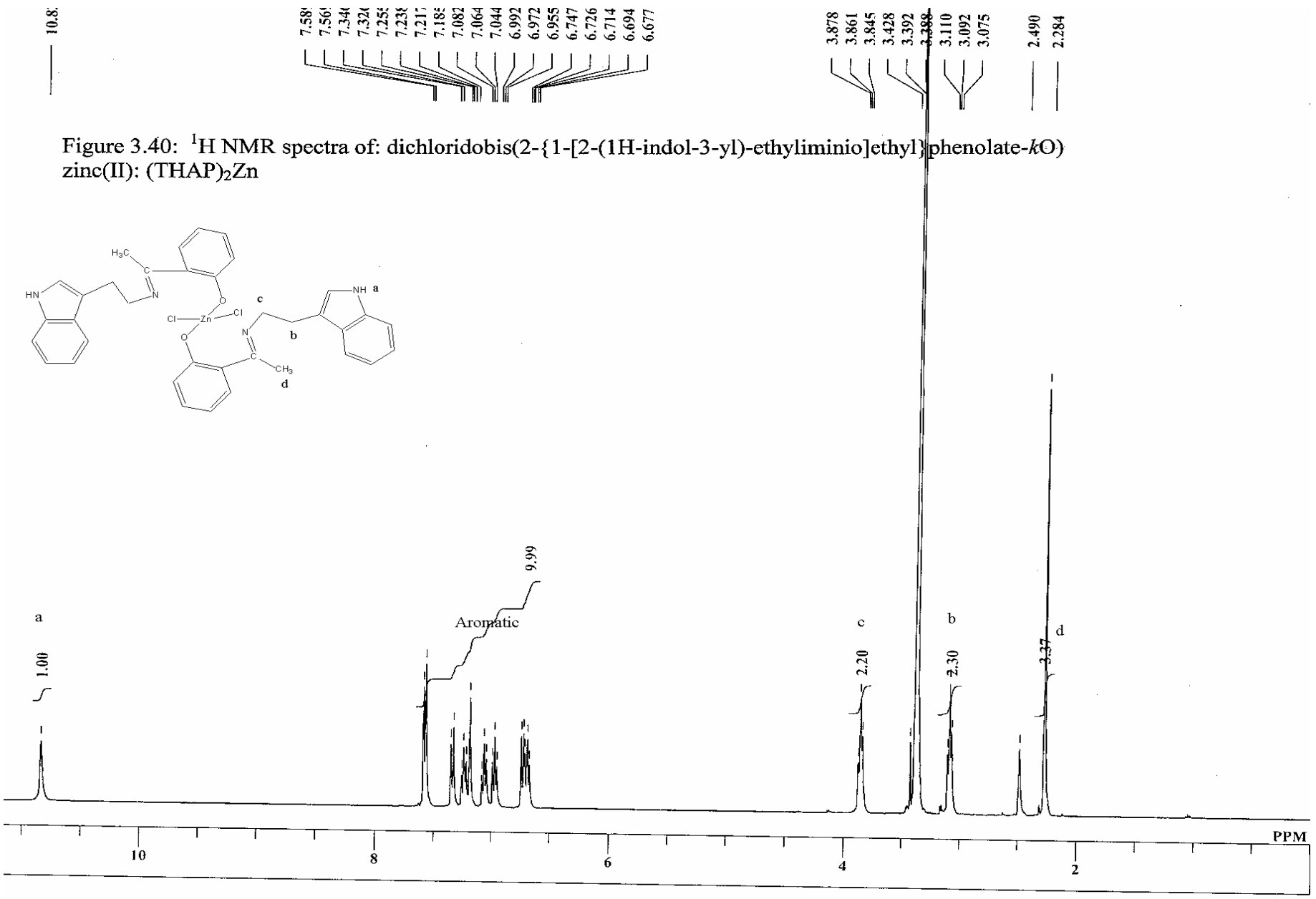

Figure 3.40: ^{1}H NMR spectra of: dichloridobis(2-{1-[2-(1H-indol-3-yl)-ethyliminio]ethyl}phenolate-*k*O) zinc(II): $(THAP)_2Zn$

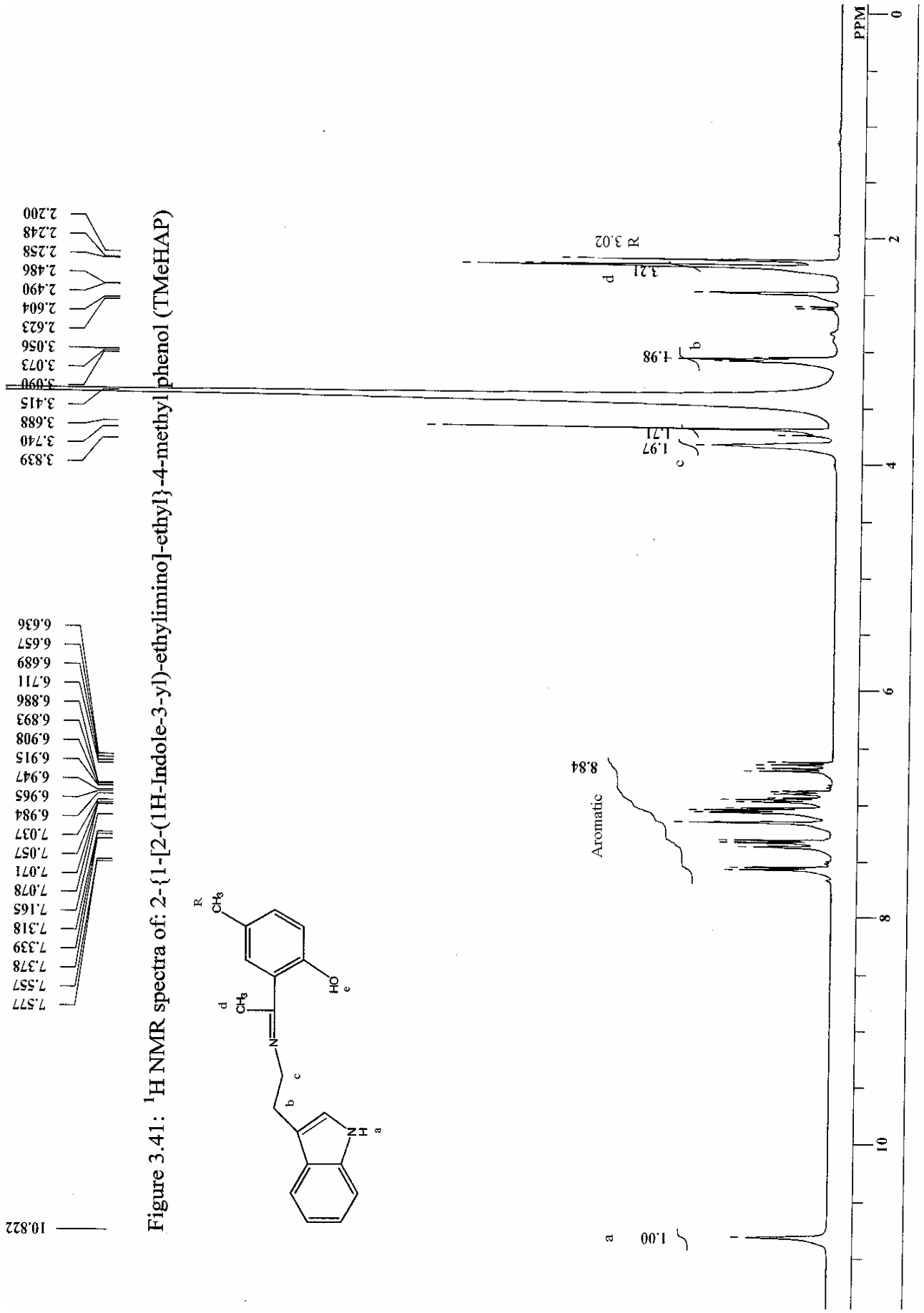

Figure 3.41: ^{1}H NMR spectra of: 2-{1-[2-(1H-Indole-3-yl)-ethylimino]-ethyl}-4-methyl phenol (TMeHAP)

The spectrum is very similar to the previously described ligand except that the singlet at 2.20 ppm is due to the methyl protons in the fifth position of the hydroxyaceophenone moiety. Further more, integration line indicates 8 protons in place of 9 protons in the case of THAP owing to the substitution of this proton by the methyl group. The copper complex spectrum was unclear.

3.2.7 Proton NMR spectra of the ligand:

2-{1-[2-(1H-Indole-3-yl)-ethylimino]-ethyl}-4-methoxy phenol (TOMeHAP):

^{1}H NMR spectra for the ligand was shown in figure (3.42) and summarized in table (3.16).

Table (3.16): ^{1}H NMR spectra of the ligand: TOMeHAP and its complexes:

Compound	H_a	H_b	H_c	H_d	H_e	H_R	$H_{aromatic}$
TOMeHAP	10.82(s)	3.07(t)	3.84(t)	2.26(s)	-	3.74(s)	6.69-7.58(m)
$(TOMeHAP)_2Cu$	No clear spectra						

It can be shown from the table that, the indolic N-H proton H_a appears at 10.82 ppm and the ethyleneic two ($-CH_2-$) groups of the tryptamine moiety H_b and H_c resonates at 3.07 ppm and 3.84 ppm as a triplets respectively. These are quite similar to the same protons in the ligand TMeHAP described above. In relation to the methoxy (OCH_3) protons, it is observed that these protons resonate further downfield at 3.74 ppm if compared to the

methyl protons of the previously described ligand. This is because of the effect exerted by the electronegative oxygen atom in the methoxy group. The aromatic protons are observed in the range 6.69 ppm to 7.58 ppm as a multiplet due to 8 protons.

No spectrum was reported for the copper complex of this ligand because it is paramagnetic in solution.

3.2.8 Proton NMR spectra of the ligand:

2-{1-[2-(1H-Indole-3-yl)-ethylimino]-ethyl}-4-chloro phenol (TClHAP):

Table (3.17): ^{1}H NMR spectra of the ligand TClHAP:

Compound	H_a	H_b	H_c	H_d	H_e	H_R	$H_{aromatic}$
TClHAP	10.83(s)	3.08(t)	3.87(t)	2.28(s)	-	-	6.72-7.57(m)

Proton NMR spectra of this ligand was shown in figure (3.43) and summarized in table (3.17)

It is clear that the signal at 10.83 ppm is due to the indolic N-H proton H_a in a similar manner as in the previously described ligands. Also the triplets due to ethylene groups in the tryptamine moiety which appears at 3.08 ppm and 3.87 ppm for the protons labeled (b) and (c) successively. The methyl protons (d) resonate as a singlet at 2.28 ppm, and the aromatic protons in the range of 6.72 – 7.57 ppm as a multiplet of 8 protons.

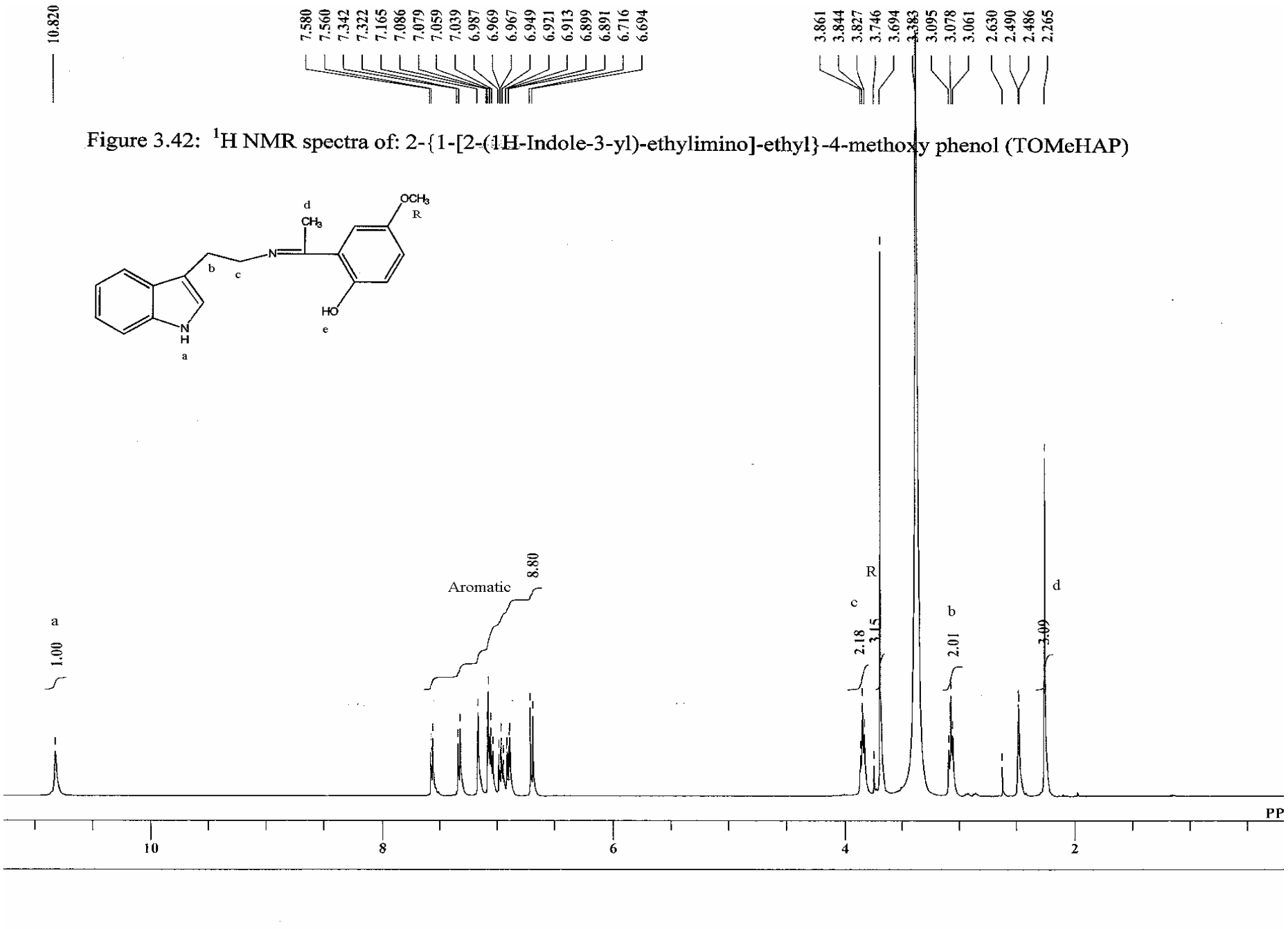

Figure 3.42: ^{1}H NMR spectra of: 2-{1-[2-(1H-Indole-3-yl)-ethylimino]-ethyl}-4-methoxy phenol (TOMeHAP)

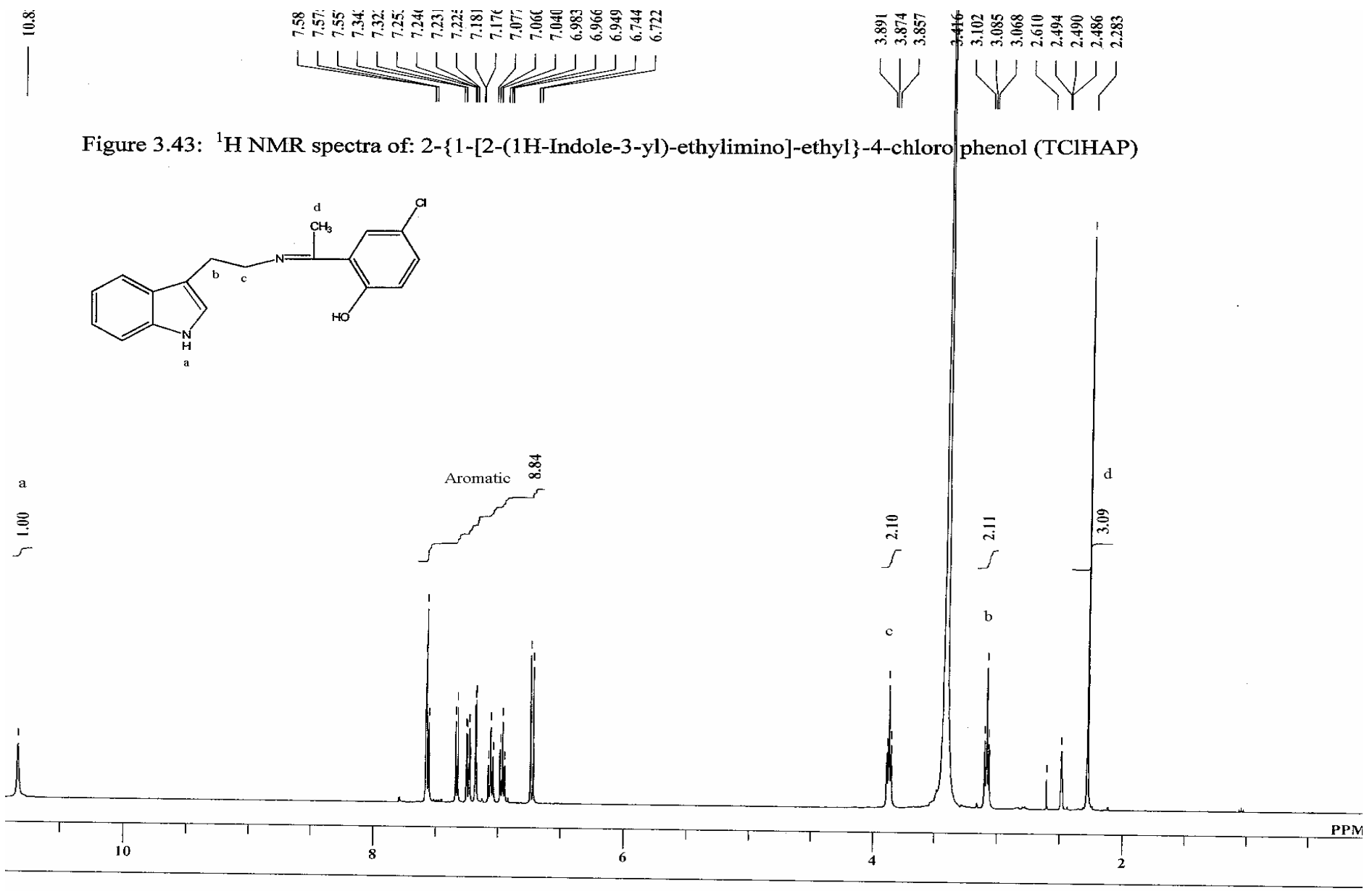

Figure 3.43: ^{1}H NMR spectra of: 2-{1-[2-(1H-Indole-3-yl)-ethylimino]-ethyl}-4-chloro phenol (TClHAP)

3.2.9 Proton NMR spectra of the ligand:

2-{1-[2-(1H-Indole-3-yl)-ethylimino]-ethyl}-4-bromo phenol (TBrHAP):

Table (3.18): ^{1}H NMR spectra of the ligand TBrHAP:

Compound	H_a	H_b	H_c	H_d	H_e	H_R	$H_{aromatic}$
TBrHAP	10.84(s)	3.08(t)	3.85(t)	2.28(s)	-	-	6.66-7.68(m)

^{1}H NMR spectra of the ligand with a summery of the main signals was reported in table (3.18), and shown in figure (3.44). It can be depicted that the general features of the spectra is closely similar to the chlorosubstituted ligand described above, and the same explanation can be drawn from the table as indicated.

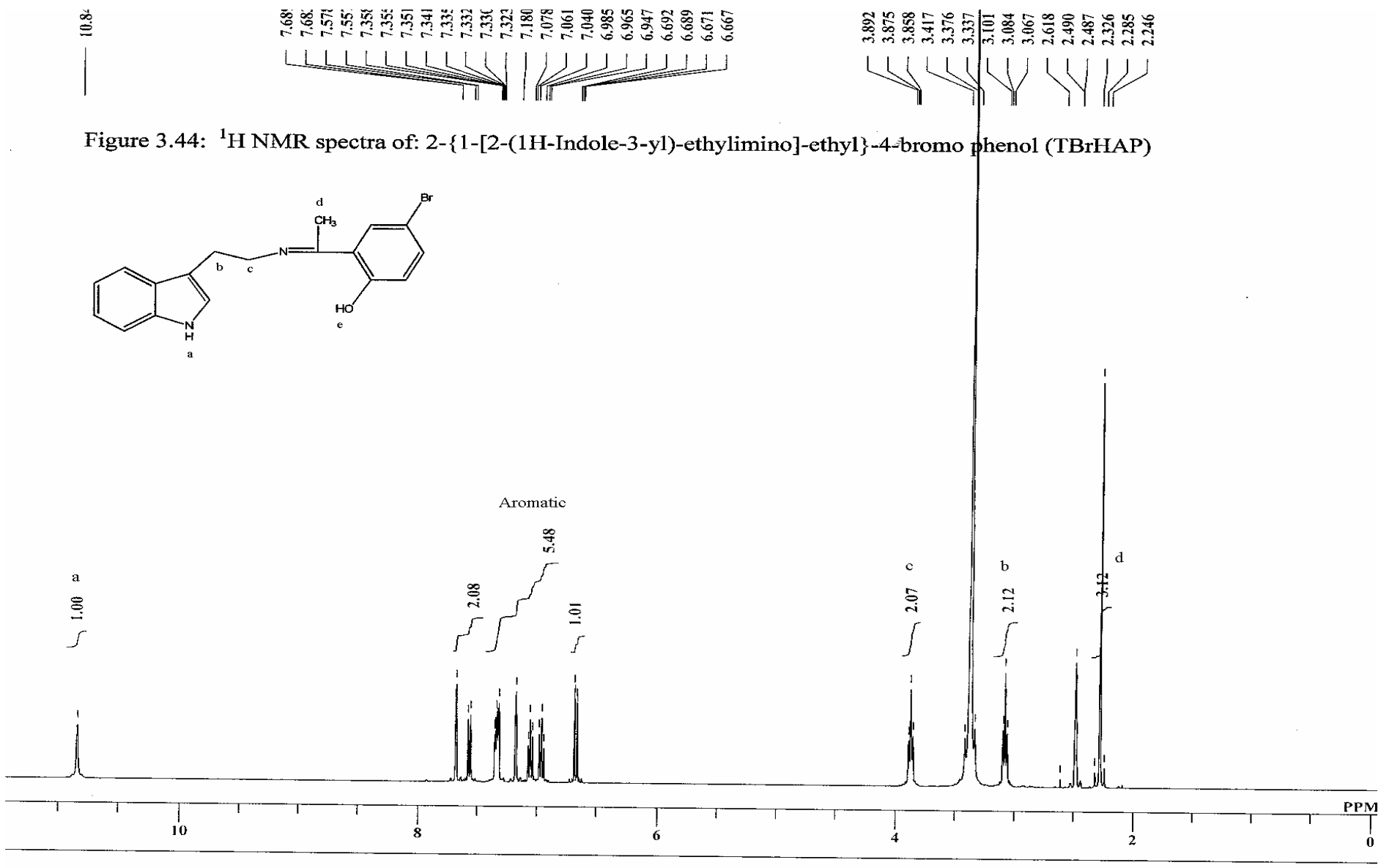

Figure 3.44: ^{1}H NMR spectra of: 2-{1-[2-(1H-Indole-3-yl)-ethylimino]-ethyl}-4-bromo phenol (TBrHAP)

3.3 ^{13}Carbon NMR spectra of the ligands and complexes:

3.3.1 $^{13}C\{^{1}H\}$ NMR spectra of the ligand: 1H-Indole-3-ethylenesalicylaldimine (TS) and its complexes:

The ^{13}C spectrum was recorded in d^{6}-DMSO as solvent, chemical shifts expressed in ppm from tetra methylsilane. The spectra was summarized in table (3.19) and displayed in figure (3.45).

Table (3.19): ^{13}C NMR spectra of TS and its complexes:

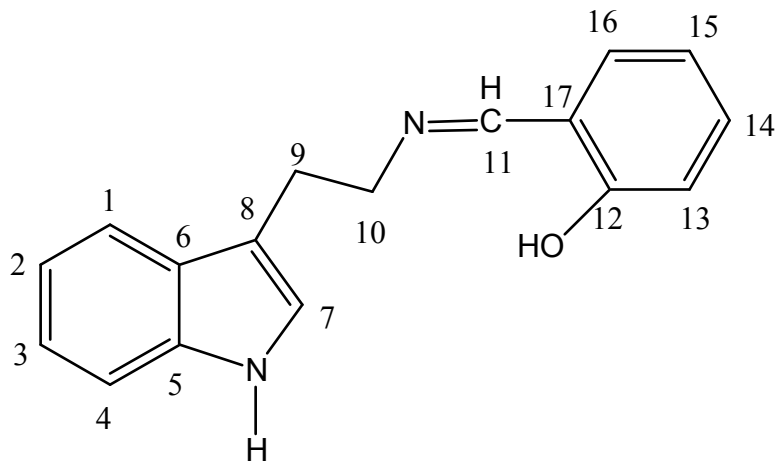

Chemical shift values in ppm:

Compound	$C_{aromatic}$	C_9	C_{10}	C_{11}	C_{12}
TS	111.92-166.26	27.09	59.34	161.53	166.26

Table 3.19 continued

Compound	$C_{aromatic}$	C_9	C_{10}	C_{11}	C_{12}
$(TS)_2Zn$	111.01-172.35	26.67	60.88	170.48	172.35
$(TS)_2Ni$	No clear spectra was obtained (paramagnetic)				
$(TS)_2Cu$	No clear spectra was obtained (paramagnetic)				

The peaks at low frequencies 27.09 and 59.34 ppm were characteristic of sp^3 carbon atoms and can be assigned to the ethylenic carbons C_9 and C_{10} labeled in the proposed structure above. Further support to the structure also comes from the appearance of two single peaks at high chemical shift values 161 ppm and 166 ppm which can be ascribed for the azomethine carbon C_{11} and the phenolic carbon C_{12} respectively. The aromatic carbons C_1 to C_8, and C_{13} to C_{17} appeared in the region 111.9 – 166.2 ppm within the normal range of aromatic carbons (100 –175 ppm) in general [67], and the total number of peaks agrees well with the expected peaks for the structure.

^{13}C spectrum of $(TS)_2Zn$ complex was shown in figure (3.46). The spectra showed that the azomethine carbon atom C_{11} shifts to higher frequency 170.48 ppm in comparison with 161.53 ppm in the free ligand. This result together with what have been reported in the IR spectra indicates that the ligand coordinated to the metal center through azomethine nitrogen atom. Further more, the phenolate carbon atom C_{12} found in the free ligand at 166.26 ppm was shifted to 172.35 ppm in the complex, indicating that the ligand coordinated to the metal center through deprotonated enolic form as shown in the complex sketch drawn above (See experimental part). All these facts have been supported by the X-ray structure analysis of the complex which will be discussed later.

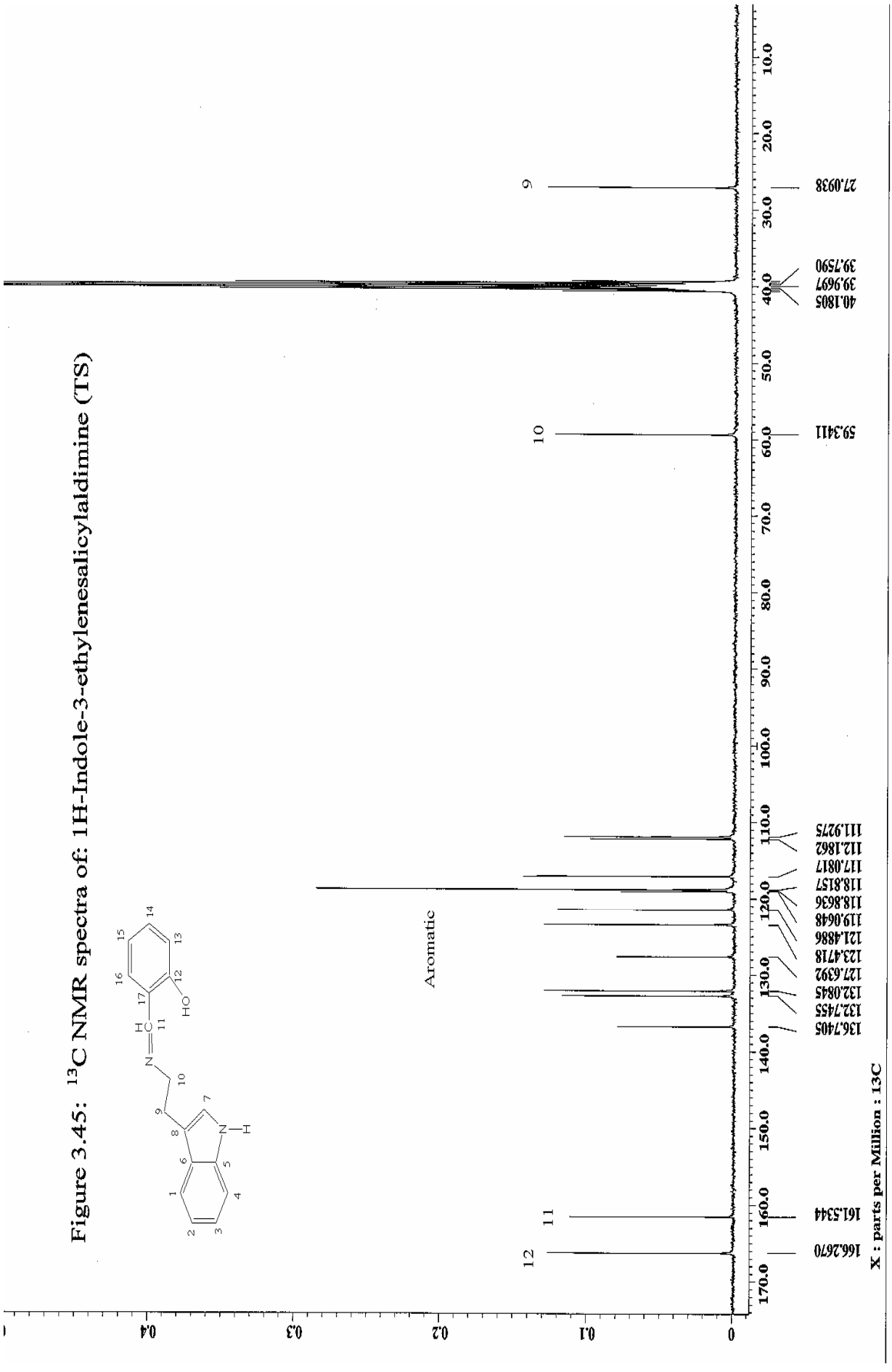
Figure 3.45: ^{13}C NMR spectra of: 1H-Indole-3-ethylenesalicylaldimine (TS)
Aromatic
166.2670
161.5344
136.7405
132.7455
132.0845
127.6392
123.4718
121.4886
119.0648
118.8636
118.8157
117.0817
112.1862
111.9275
59.3411
40.1805
39.9697
39.7590
27.0938
X : parts per Million : 13C

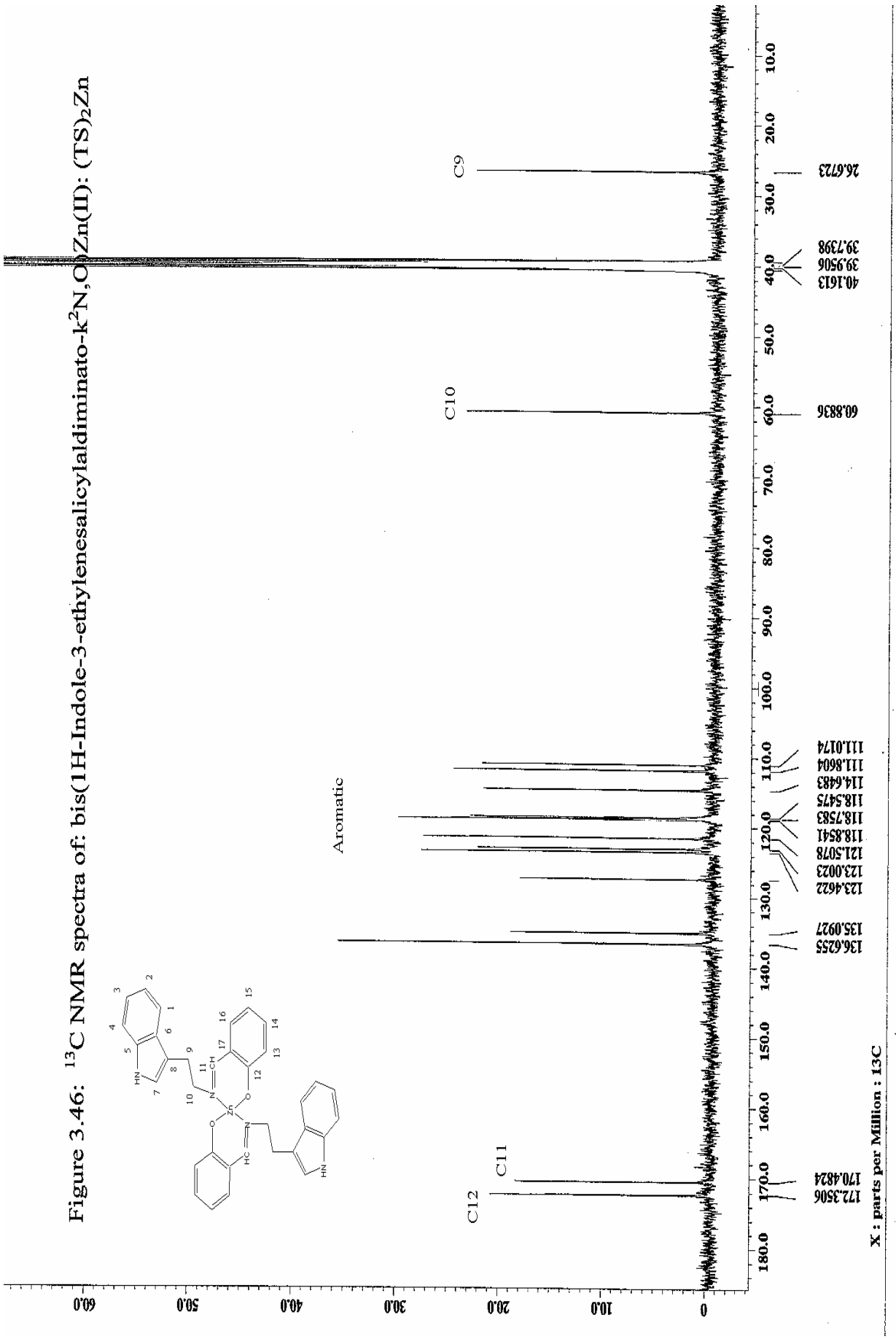

Figure 3.46: ^{13}C NMR spectra of: bis(1H-Indole-3-ethylenesalicylaldiminato-k^2N,O)Zn(II): $(TS)_2Zn$

3.3.2 ^{13}C {^{1}H} NMR spectra of the ligand: 1H-Indole-3-ethylene-5-chlorosalicylaldimine (TCS) and its zinc complex:

The ^{13}C NMR spectra was summarized in table (3.20) and shown in figure (3.47), chemical shifts expressed in ppm and d^6-DMSO was used as a solvent.

Table (3.20): ^{13}C NMR spectra of the ligand TCS and its Zn complex:

Compound	$C_{aromatic}$	C_9	C_{10}	C_{11}	C_{12}
TCS	111.93-165.20	26.90	59.03	160.89	165.20
$(TCS)_2Zn$	110.91-171.44	26.68	60.97	169.13	171.44

The proposed structure can also be verified from ^{13}C spectral data. The greatest downfield peaks at 165.20 ppm attributed to a carbon atom directly attached to the electronegative oxygen atom. The second most down field peak at 160.89 ppm can be assigned to the azomethine carbon C_{11}. The aliphatic carbons observed upfield at 26.90 ppm for C_9 and 59.03 ppm for C_{10}. The rest of the peaks lie on the aromatic region of the spectra and hence can be attributed to 11 carbon atoms.

^{13}C spectrum for the zinc complex was shown in figure (3.48). In this spectra it is worthwhile to note here that the -C=N carbon was shifted further down field by 8.24 ppm proving the azomethine nitrogen engagement in bond formation with the zinc ion. Evidence of phenolic oxygen coordination can also be emphasized by the shift of the free ligand ^{13}C signal (C_{12}) from 165.20 ppm in the free ligand to 171.44 ppm in the complex.

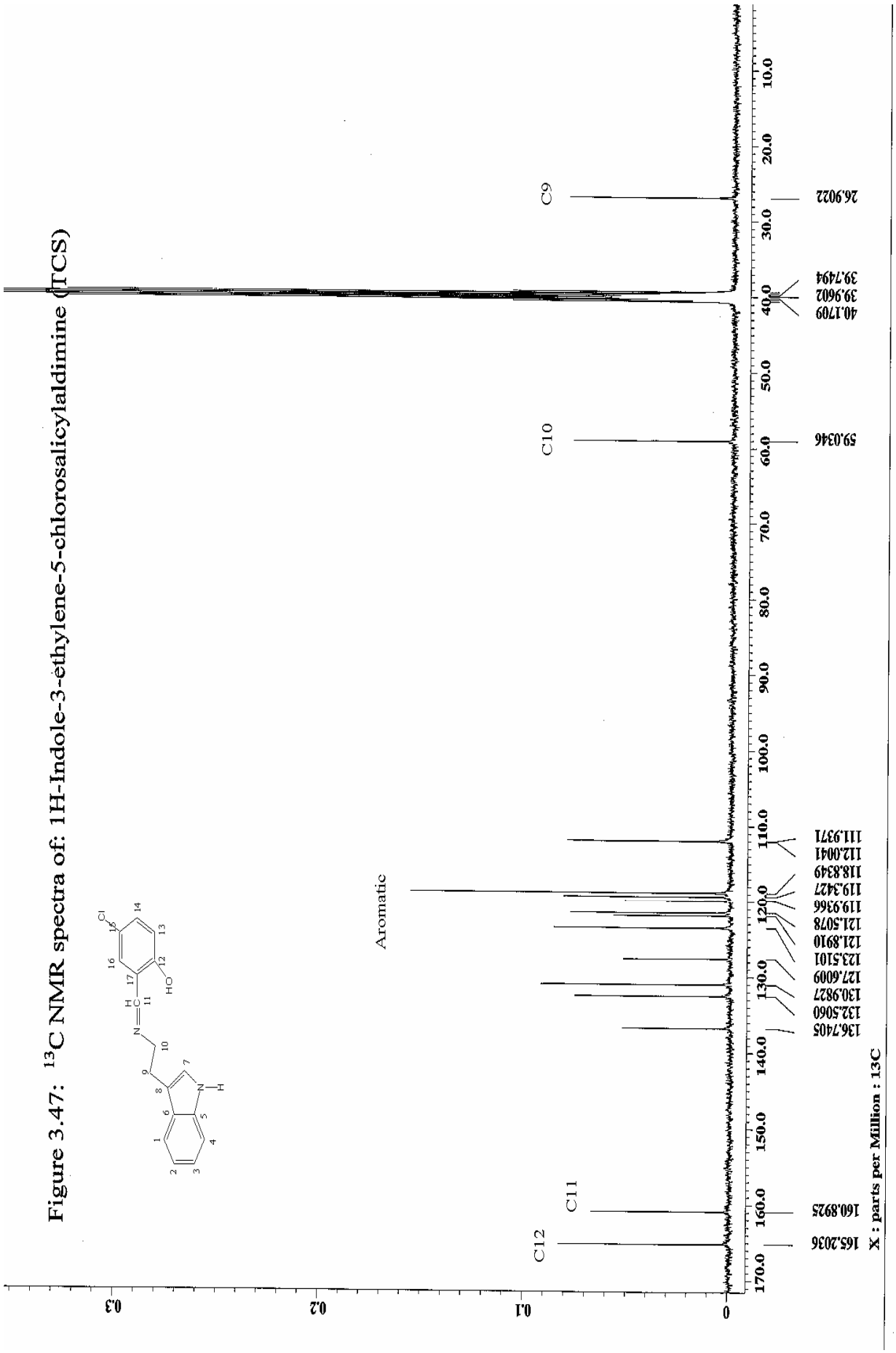
Figure 3.47: ^{13}C NMR spectra of: 1H-Indole-3-ethylene-5-chlorosalicylaldimine (TCS)
C9
C10
C11
C12
Aromatic
26.9022
39.7494
39.9602
40.1709
59.0346
111.9371
112.0041
118.8349
119.3427
119.9366
121.5078
121.8910
123.5101
127.6009
130.9827
132.5060
136.7405
160.8925
165.2036
X : parts per Million : 13C

Figure 3.48: ^{13}C NMR spectra of: bis{4-chloro-2-[2-(1H-indol-3-yl)ethyliminomethyl] phenolato-κ2N, O} zinc(II): $(TCS)_2Zn$

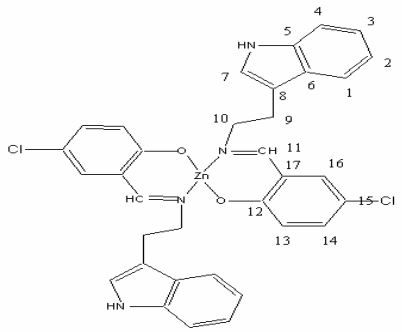

Other ^{13}C signals look almost the same with minor change observed in the position of C_{10} chemical shift.

3.3.3 ^{13}C {^{1}H} NMR spectra of the ligand: 1H-Indole-3-ethylene-5-nitrosalicylaldimine (TNS) and its zinc complex:

Table (3.21): ^{13}C NMR spectra of the ligand TNS and its Zn complex:

Compound	$C_{aromatic}$	C_9	C_{10}	C_{11}	C_{12}
TNS	110.50-178.70	25.93	52.95	167.50	178.70
$(TNS)_2Zn$	111.41-176.58	27.51	61.49	171.17	176.58

The spectrum of the ligand was shown in Fig. 3.49.

The ^{13}C NMR spectral data of the ligand in d^6-DMSO exhibited 17 signals as expected. In comparison to the previous ligand the most downfield peak appears at 178.7 ppm and could be attributed to a carbon atom attached to electronegative atom C_{12} in the diagram. The azomethine carbon C_{11} was observed in the normal region 167.5 ppm in comparison to the previous ligand. The upfield signals 25.9 ppm and 52.9 ppm are likely to arise from the aliphatic C_9 and C_{10} respectively. The rest of the signals in the range 110.5 to 178.7 ppm are due to the aromatic carbons.

The spectrum of zinc complex of the ligand was shown in figure (3.50) and summarized in table (3.21) above. Adequate support for the proposed structure was provided by ^{13}C NMR spectrum where the azomethine –C=N carbon appears more downfield at 171.17

ppm suggesting coordination to the zinc ion via the attached nitrogen atom. Also the shift observed for C_{12} carbon signal implies participation of the phenolic oxygen atom in chelate formation with the metal center. Other bands such as C_9 and C_{10} shifts slightly to higher chemical shift values as it can be seen in the table above.

3.3.4 $^{13}C\{^1H\}$ NMR spectra of the ligand:

1H-Indole-3-ethylene-3-5-di-tertiarybutylsalicylaldimine (TTET):

The spectra was summarized in table (3.22) and displayed in figure (3.51).

Table (3.22): ^{13}C NMR spectra of the ligand TTET and its Zn complex:

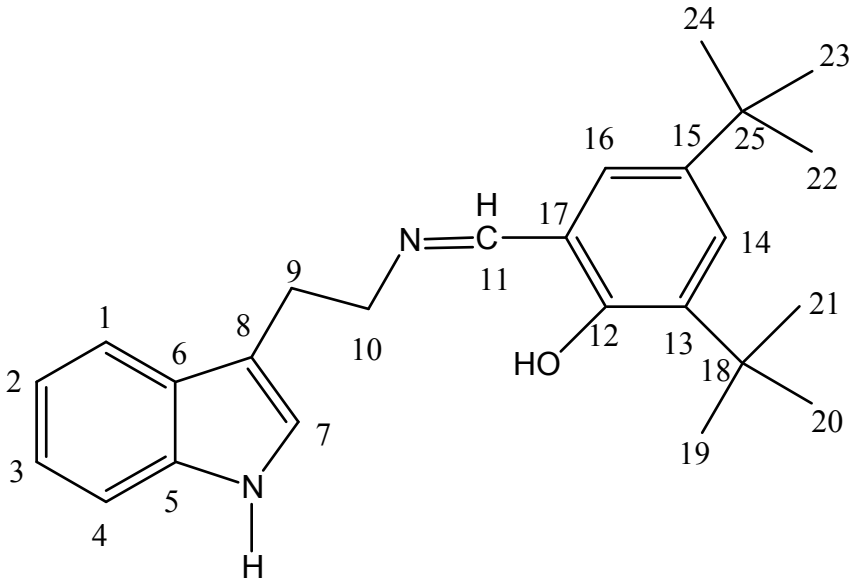

Table 3.22: Chemical shift values imp pm:

Compound	C (Aromatic)	C9	C10	C11	C12	C18	C19,20,21	C22,23,24	C25
T-TET	111.8-167.4	34.34	59.46	158.45	167.43	27.22	31.83	29.77	35.09
$(TTET)_2Zn$	111.11-173.14	34.08	61.11	168.01	173.14	26.97	31.88	29.85	35.70

It is worthwhile to mention here that, there are more peaks in this spectra compared to the previous ones due to the presence of two tertiary butyl groups in position 3 and 5 of the salicylaldehyde moiety. Carbons C_{19}, C_{20}, and C_{21} are equivalent and gives rise to only one peak at 31.83 ppm, while C_{22}, C_{23} and C_{24} are equivalent and gives rise to a single peak at 29.77 ppm. The quaternary carbon atoms C_{18} and C_{25} resonate at 27.22 and 35.09 ppm respectively. The ethylenic carbons appear in the usual range 34.34 ppm and 59.46 ppm for C_9 and C_{10} respectively. The down field signals at 158.45 ppm and 167.43 ppm could be assigned to C_{11} and C_{12} successively. Those positions are due to the effects exerted by the azomethine nitrogen and phenolic oxygen atoms directly attached. The rest of the signals at the range 111.8 ppm – 167.4 ppm are due to aromatic carbons.

The ^{13}C spectrum of zinc complex of this ligand was shown in figure (3.52). From the spectra it was clearly shown that the significant shift observed on the azomethine –C=N carbon to lower field 168.01 ppm compared to the ligand implies strong participation of the azomethine nitrogen atom in chelate formation to the metal center through its lone pair. Moreover, the phenolic carbon C_{12} chemical shift value shifts to 173.14 ppm than 167.43 ppm in the ligand. This also can be considered as adequate evidence for the

involvement of the phenolic oxygen tom in bond formation to the zinc ion after deprotonation. These facts have been supported by the X-ray diffraction structure for the complex, and it will be discussed later in this thesis. Other signals display almost the same chemical shift values with little variations and can be assigned accordingly.

3.3.5 ^{13}C {^{1}H} NMR spectra of the ligand:

2-{1-[2-(1H-Indole-3-yl)ethylimino]-ethyl } phenol (THAP):

The spectra was summarized in table (3.23) and shown in figure (3.53)

Table (3.23): ^{13}C NMR spectra of the ligand: THAP

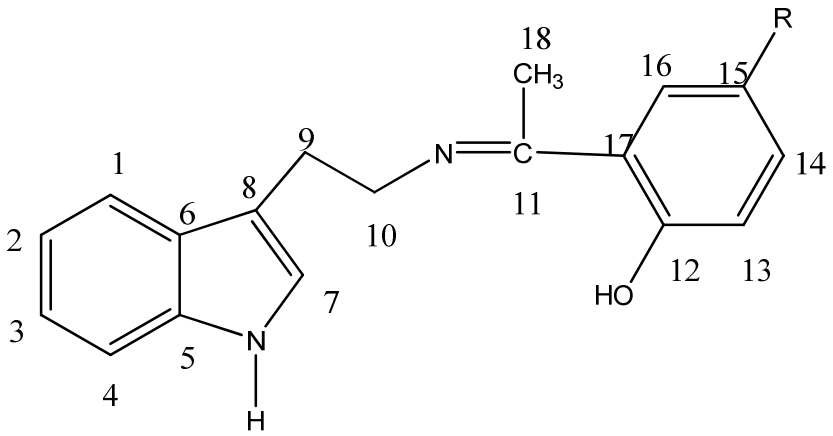

R = H , Cl , Br , Me , OMe

Table 3.23: Chemical shifts in ppm

Compound	C (Aromatic)	C9	C10	C11	C12	C18	C(Me,OMe)
THAP	111.40-136.26	25.92	49.00	164.43	172.42	14.27	-
$(THAP)_2Zn$	111.92-136.77	26.42	49.48	165.00	172.99	14.81	-

It can be shown that, ^{13}C spectra of this ligand provides further support to the proposed structure shown. There are 18 peaks representing all the existing carbon atoms as expected. The most down field peak at 172.42 ppm could be assigned to the phenolic carbon C-OH labeled C_{12}. This position is because of the deshielding effect of the electro negatively oxygen atom directly attached, while the peak at 164.43 ppm can be assigned to the azomethine carbon atom C_{11}. 13 peaks in the region 111.40 – 136.26 arose as a result of the aromatic carbon atoms and the up field peaks at 25.92 ppm and the 49.00 ppm were attributed to the carbons labeled C_9 and C_{10} respectively.

The spectrum of the zinc complex is shown in Fig. 3.54.

It is clear from the spectra that the azomethine carbon atom C_{11} does not shift considerably like the affected carbon atoms of similar zinc complexes described previously in this thesis (at least 3.37 ppm in $(TNS)_2Zn$). This implies that this carbon atom does not participate in bond formation with the zinc ion, a phenomenon that was confirmed by X-ray structure analysis. Also, slight shift was noted for the phenolic carbon C_{12} chemical shift value (ca 0.57 ppm) in comparison to the ligand, though X-ray study reveals that the oxygen atom is coordinated to the zinc ion.

Figure 3.49: ^{13}C NMR spectra of: 1H-Indole-3-ethylene-5-nitrosalicylaldimine (TN$)

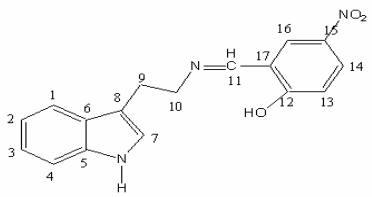

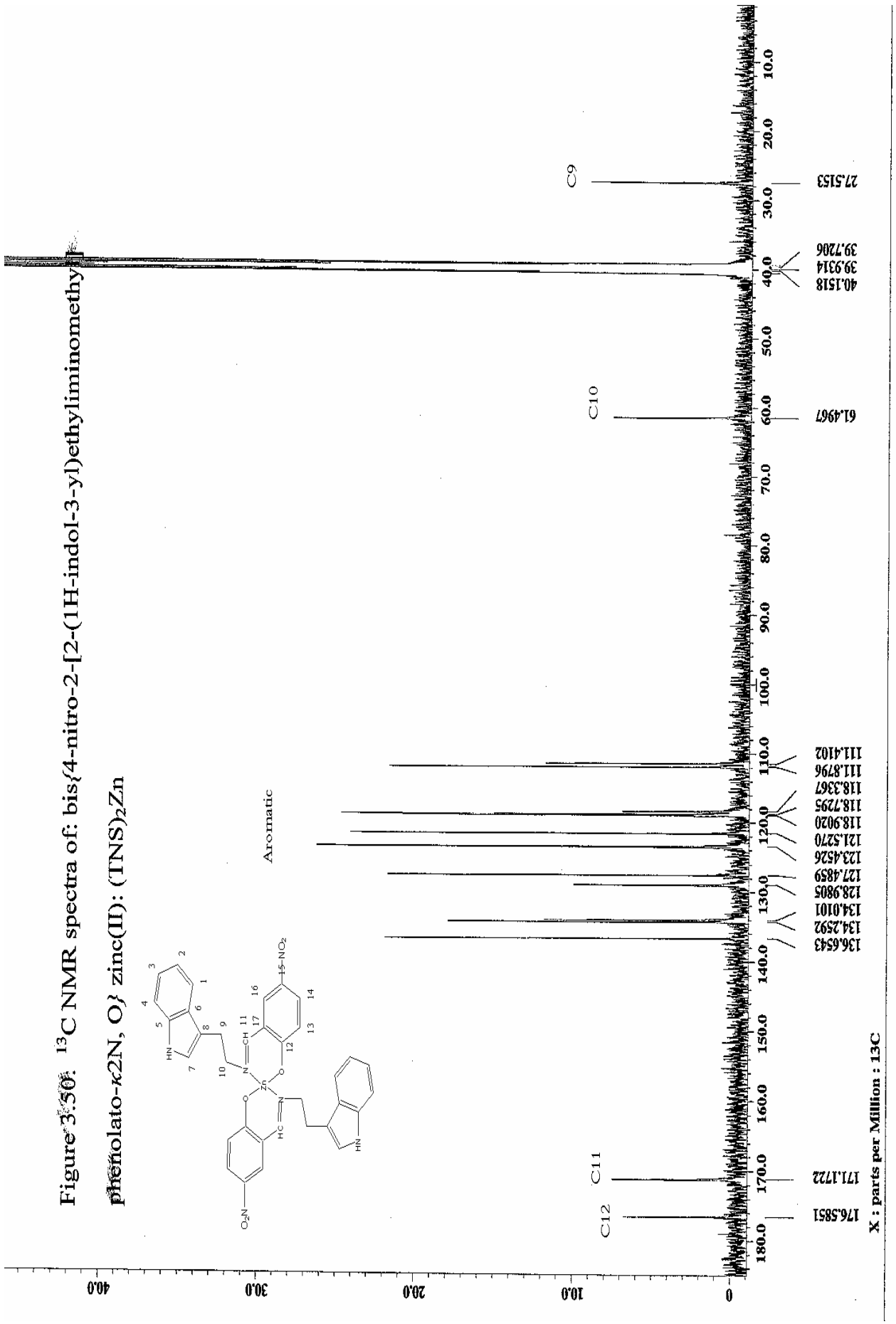

Figure 3.56: ^{13}C NMR spectra of: bis{4-nitro-2-[2-(1H-indol-3-yl)ethyliminomethyl] phenolato-κ2N, O} zinc(II): $(TNS)_2Zn$

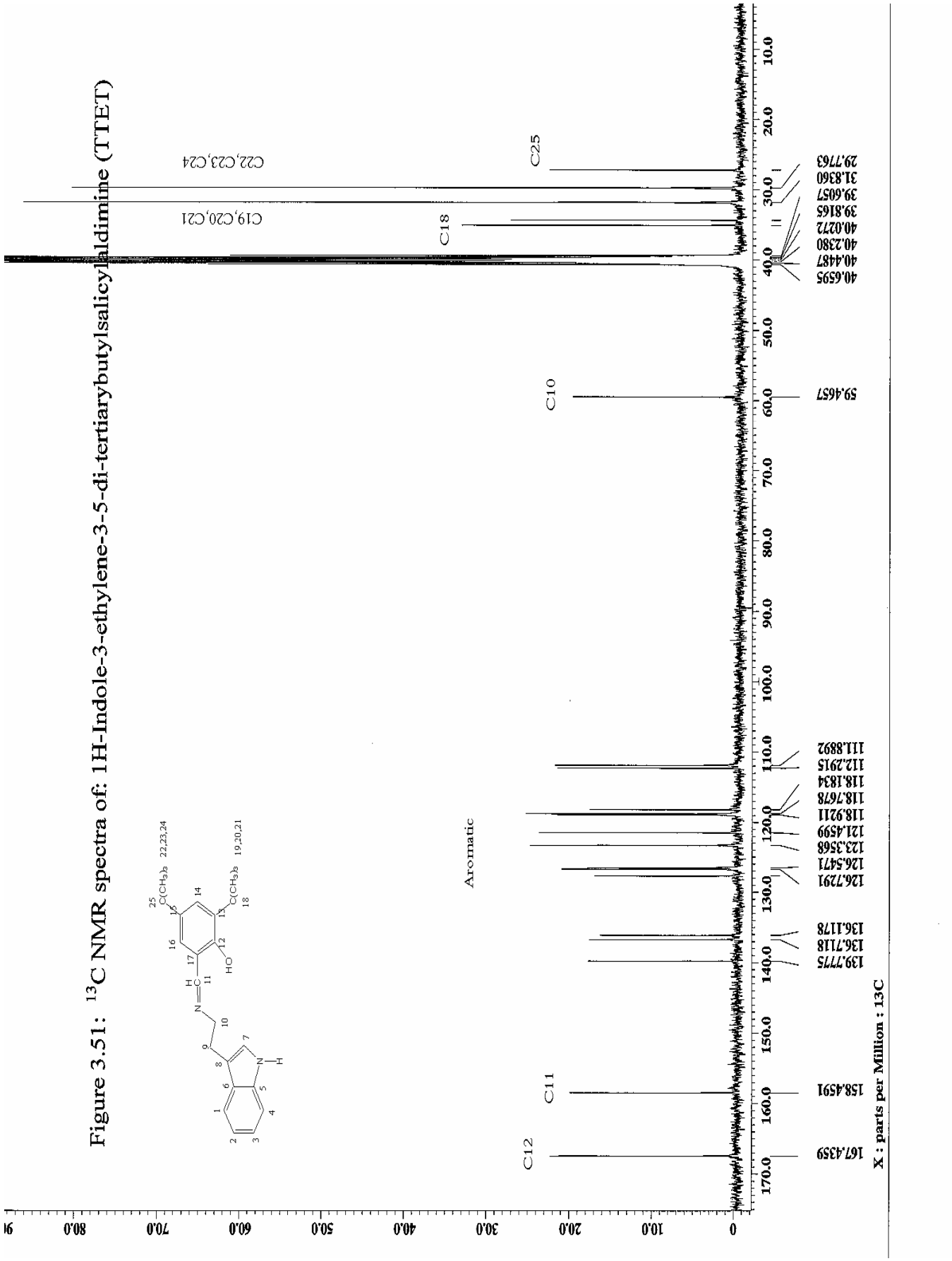

Figure 3.51: ^{13}C NMR spectra of: 1H-Indole-3-ethylene-3-5-di-tertiarybutylsalicylaldimine (TTET)

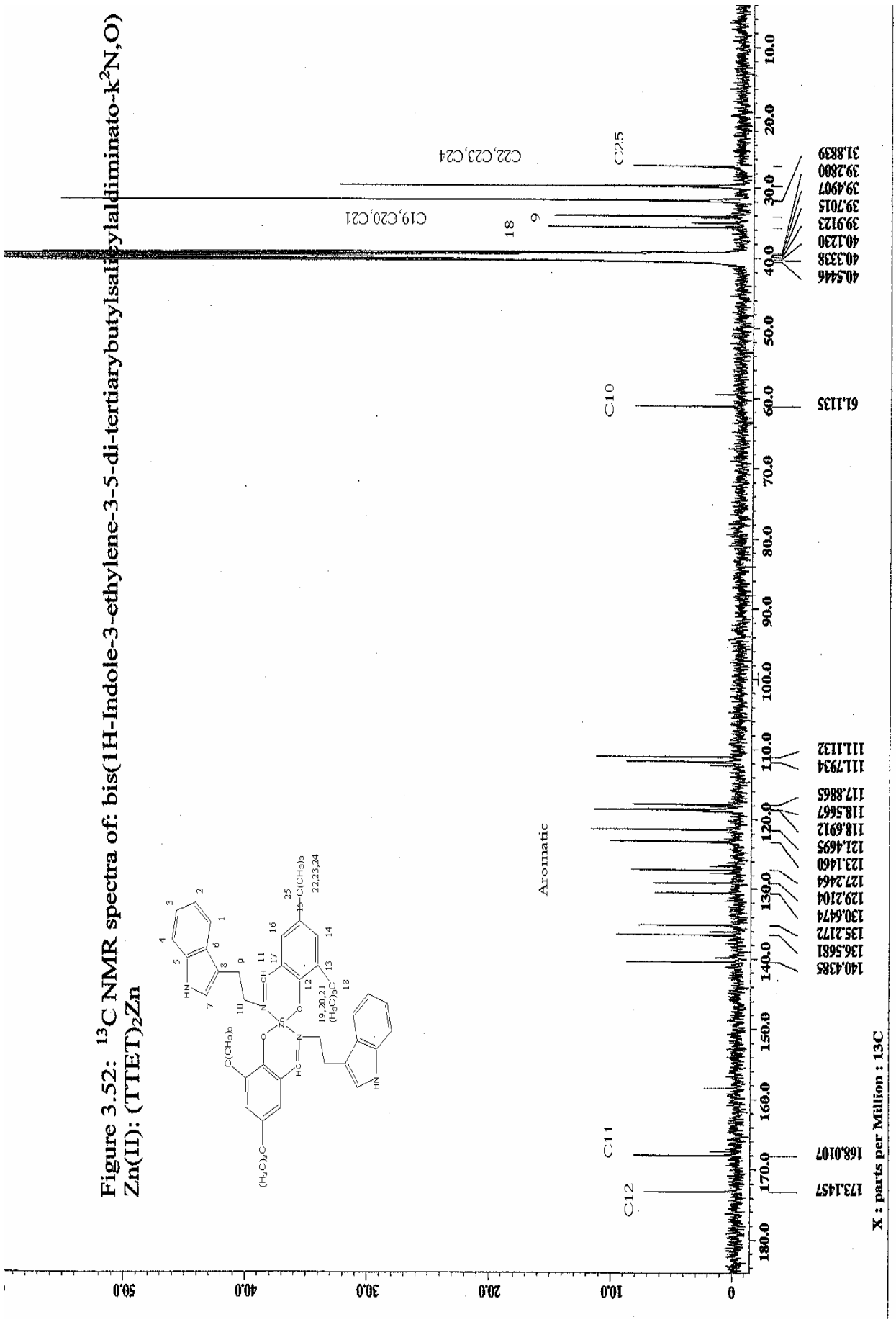
Figure 3.52: ^{13}C NMR spectra of: bis(1H-Indole-3-ethylene-3-5-di-tertiarybutylsalicylaldiminato-k^{2}N,O) Zn(II): (TTET)$_2$Zn
C19,C20,C21
C22,C23,C24
C25
C10
C11
C12
Aromatic
X : parts per Million : 13C

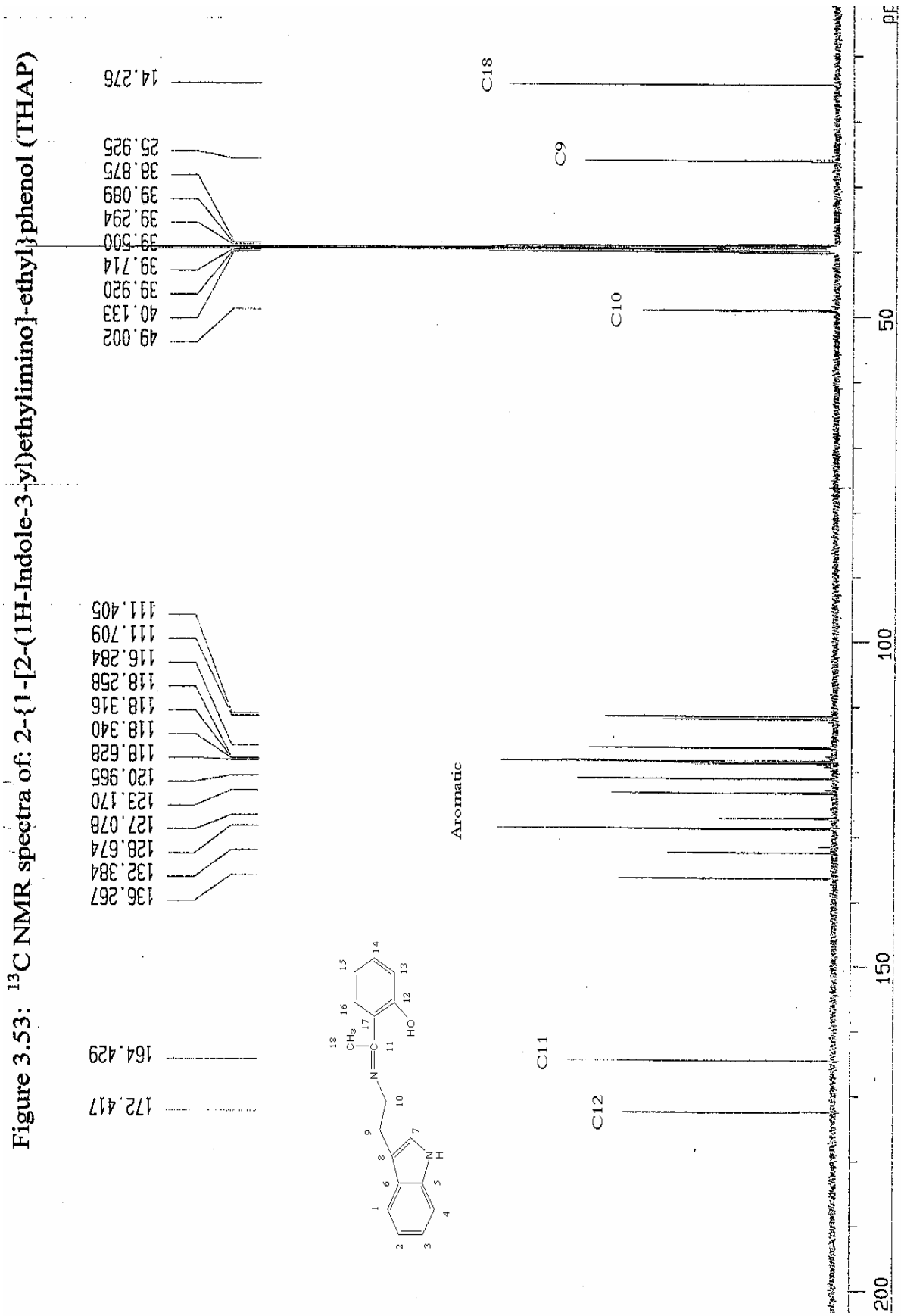

Figure 3.53: ^{13}C NMR spectra of: 2-{1-[2-(1H-Indole-3-yl)ethylimino]-ethyl}phenol (THAP)

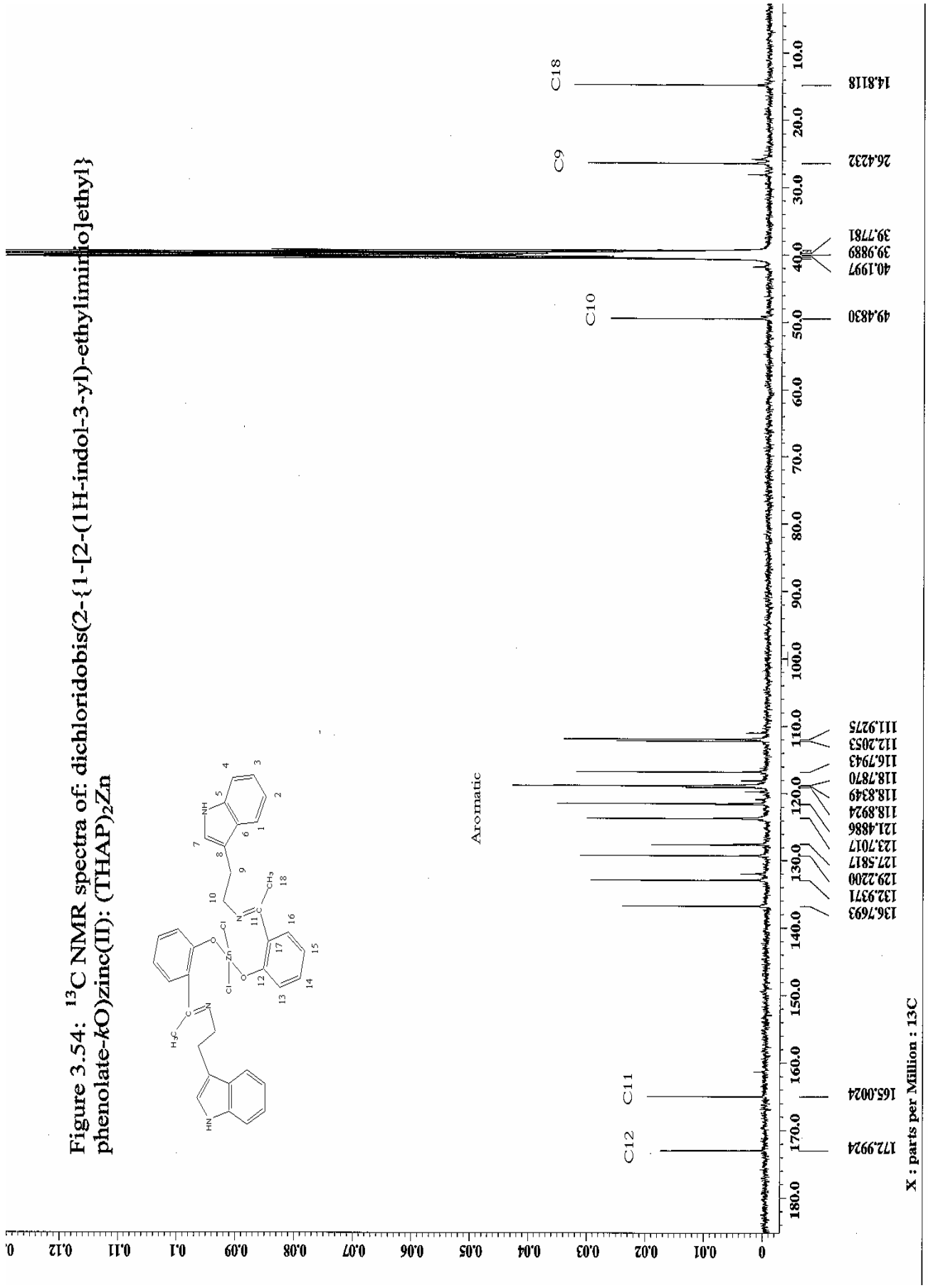

Figure 3.54: ^{13}C NMR spectra of: dichloridobis(2-{1-[2-(1H-indol-3-yl)-ethylimino]ethyl} phenolate-*k*O)zinc(II): $(THAP)_2Zn$

3.3.6 $^{13}C\ \{^{1}H\}$ NMR spectra of the ligand:

2-{1-[2-(1H-Indole-3-yl)-ethylimino]-ethyl}-4-methyl phenol (TMeHAP):

The ^{13}C spectra of this ligand is shown in table (3.24) and figure (3.55)

Table (3.24): ^{13}C NMR spectra of the ligand TMeHAP:

Compound	C Aromatic	C9	C10	C11	C12	C18	C(Me,OMe)
TMeHAP	111.44-172.11	26.06	49.28	161.57	172.11	14.31	20.27

Compared to the previously discussed ligand, the spectra of this ligand reveals one more additional peak in the up field region associated to the methyl group carbon on position 5 of the hydroxyacetophenone moiety. Aromatic carbons exist in the region between 111.44 ppm to 172.11 ppm. The down field peaks at 161.57 ppm and 172.11 were ascribed to the carbons C_{11} and C_{12} respectively. The peak at 14.31 ppm is due to the methyl carbon C_{18} and the ethylenic carbons appear in their expected positions 26.06 ppm for C_9 and 49.28 ppm for C_{10} as compared to the previous ligand.

No clear spectrum was shown for the Cu complex of this ligand due to paramagnetic effects.

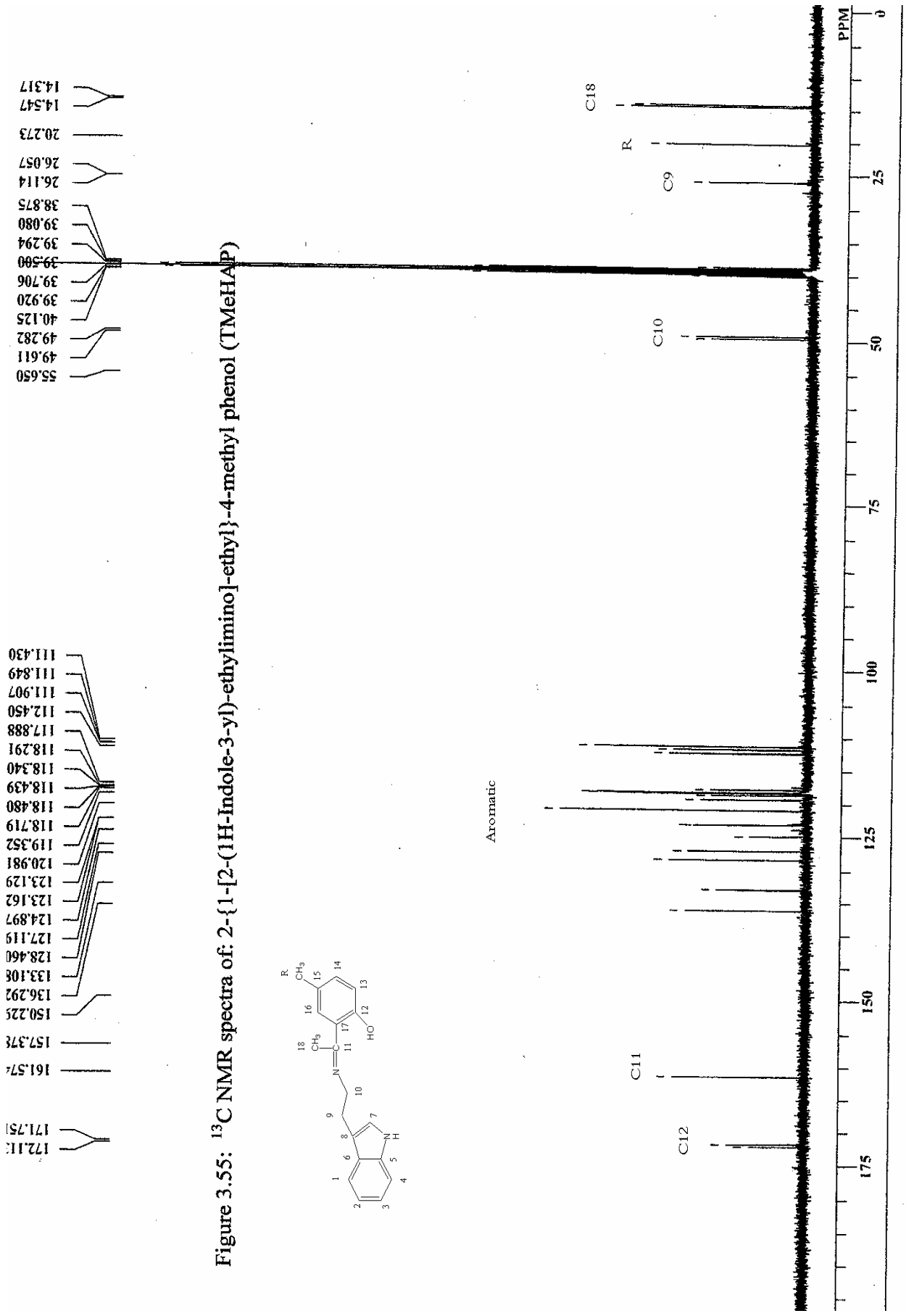

Figure 3.55: ^{13}C NMR spectra of: 2-{1-[2-(1H-Indole-3-yl)-ethylimino]-ethyl}-4-methyl phenol (TMeHAP)

3.3.7 $^{13}C\ \{^{1}H\}$ spectra of the ligand:

2-{1-[2-(1H-Indole-3-yl)-ethylimino]-ethyl}-4-methoxy phenol (TOMeHAP):

The spectra was also summarized in table (3.25) and shown in figure (3.56)

Table (3.25): ^{13}C NMR spectra of the ligand TOMeHAP:

Compound	C (Aromatic)	C9	C10	C11	C12	C18	C(Me,OMe)
TOMeHAP	111.41-171.7	26.09	49.61	157.32	171.73	14.53	55.70

The remarkable difference between the spectra of this ligand and the previously mentioned methyl substituted one lies in the position of the chemical shift of the methoxy carbon atom which lie at 55.70 ppm compared to 20.27 ppm for the previous ligand. This is because of the effect exerted by the electronegative oxygen atom. The rest of the spectra look somewhat similar to the previous one with some variations in the positions of chemical shift values.

3.3.8 $^{13}C\ \{^{1}H\}$ NMR spectra of the the ligand:

4-choloro- 2-{1-[2-(1H-Indole-3-yl)-ethylimino]-ethyl}- phenol (TClHAP):

The spectrum was shown in table (3.26) with the most important chemical shift values for different carbon atoms, and figure (3.57).

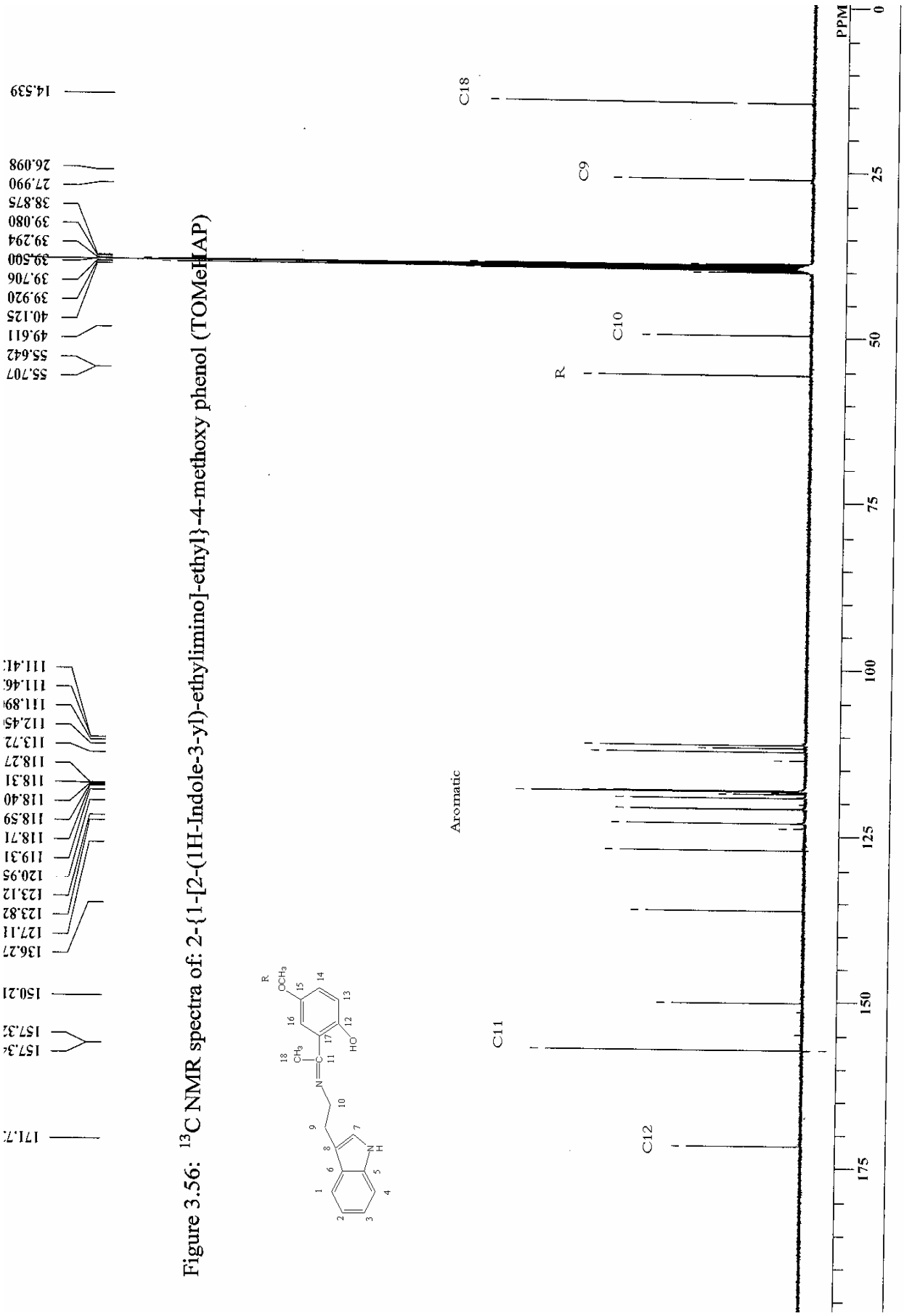

Figure 3.56: ^{13}C NMR spectra of: 2-{1-[2-(1H-Indole-3-yl)-ethylimino]-ethyl}-4-methoxy phenol (TOMeHAP)

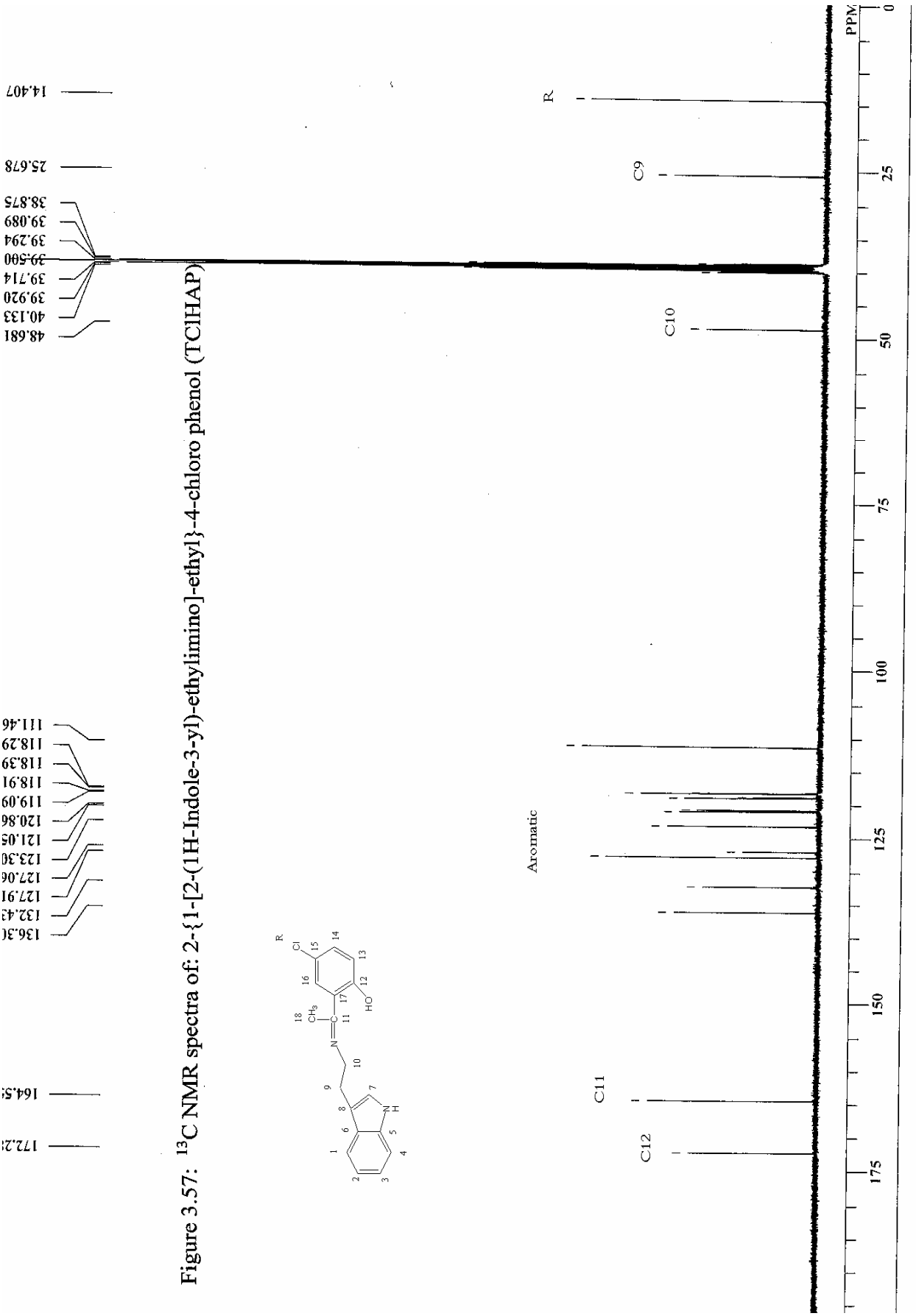

Figure 3.57: ^{13}C NMR spectra of: 2-{1-[2-(1H-Indole-3-yl)-ethylimino]-ethyl}-4-chloro phenol (TClHAP)

Table (3.26): ^{13}C NMR spectra of the ligand TClHAP:

Compound	C (Aromatic)	C9	C10	C11	C12	C18	C(Me,OMe)
TClHAP	111.46-172.28	25.67	48.68	164.55	172.28	14.40	-

18 peaks were shown in the spectra as expected in which 15 of them are in the range of aromatic carbons, while the rest lies up field at 14.40 ppm, 25.67 ppm, and 48.68 ppm assignable to C_{18}, C_9 and C_{10} labeled in the proposed structure above. The most down field peaks at 172.28 ppm and 164.55 ppm could be attributed to the phenolic C_{12} and azomethine carbon atom C_{11} respectively.

3.3.9 ^{13}C {^{1}H} NMR spectra of the the ligand:

4-bromo- 2-{1-[2-(1H-Indole-3-yl)-ethylimino]-ethyl}- phenol (TBrHAP):

The spectrum was summarized in table (3.27) with the most important chemical shift values for different carbon atoms, and shown in figure (3.58).

Table (3.27): ^{13}C NMR spectra of the ligand TBrHAP:

Compound	C (Aromatic)	C9	C10	C11	C12	C18	C(Me,OMe)
TBrHAP	106.8-172.77	26.13	49.08	165.55	172.77	14.88	-

Also 18 peaks were shown in the spectra as expected in which 15 of them are in the range of aromatic carbons, while the rest lies up field at 14.88 ppm, 26.13 ppm, and 49.08 ppm assignable to C_{18}, C_9, and C_{10} labeled in the proposed structure above. The most down field peaks at 172.77 ppm and 165.55 ppm could be attributed to the phenolic C_{12} and azomethine carbon atom C_{11} respectively.

Figure 3.58: ^{13}C NMR spectra of: 4-Bromo-2-{1-[2-(1H-Indole-3-yl)-ethylimino]-ethyl}-phenol (TBrHAP

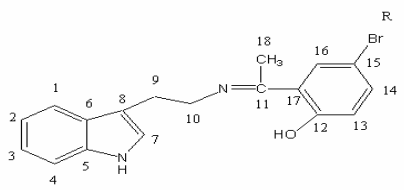

3.4 UV-Visible Spectra of the ligands and complexes:

3.4.1 UV-Vis spectra of the ligand: 1H-Indole-3-ethylenesalicylaldimine (TS) and its Zn, Ni, and Cu complexes:

The electronic spectra of the ligand TS and its zinc, nickel and copper complexes with their tentative assignments are given in table (3.28) and figures (3.59, 3.60, 3.61 and 3.62)

Table (3.28): UV-Vis spectra of TS and its Zn, Ni, and Cu complexes:

Compound	Conc (mol/L)	ε ($mol^{-1}Lcm^{-1}$)	λ max (nm)	Assignment
TS	2.84×10^{-4}	5.32×10^{3}	314	n - π^*
		8.75×10^{3}	291	$\pi - \pi^*$ chelate ring
		9.13×10^{3}	283	$\pi - \pi^*$ chelate ring
		9.41×10^{3}	267	$\pi - \pi^*$ indole group
$(TS)_2Zn$	1.26×10^{-4}	8.67×10^{3}	364.5	CT
		1.77×10^{4}	275	$\pi - \pi^*$ ligand
		2.50×10^{3}	244	$\pi - \pi^*$ ligand

Table 3.28 continued

Compound	Conc (mol/L)	ε ($mol^{-1}Lcm^{-1}$)	λ max (nm)	Assignment
$(TS)_2Ni$	2.56×10^{-4}	222.4	605	d-d transition
	1.28×10^{-4}	5.74×10^{3}	377	n - π^*
		7.36×10^{3}	323	CT
		2.68×10^{3}	278	$\pi - \pi^*$ ligand
		3.00×10^{3}	216	$\pi - \pi^*$ ligand
$(TS)_2Cu$		1.22×10^{4}	364.5	CT , n - π^*
		2.44×10^{4}	283	$\pi - \pi^*$
		2.61×10^{4}	275	$\pi - \pi^*$

The spectra were measured in dimethyl sulphoxide (DMSO) as a solvent. For the ligand the intense double band in the region 283 nm to 291 nm is characteristic for $\pi - \pi^*$ transitions of hydrogen-bonded conjugated chelate rings [22]. This phenomenon seems to arise from the two tautomeric forms (keto-enol) possible for each hydrogen-bonded ring of the ligand [24]. The band at 267 nm is associated with $\pi - \pi^*$ transition of the indole group, where as the weak band at 404 nm is assignable to transition of the chelate ring.

In the case of metal complexes, the absorption band assigned to n - π^* looks quite different from those of the ligand. Instead of the simple double or triple bands, the metal chelates have complicated systems of bands of different intensities. This provides further evidence for complex formation. $(TS)_2Zn$ complex exhibits two absorption maxima. The band at 364 nm is due to charge transfer probably from metal to ligand. The intensity and

position of this band seems to indicate the presence of a tetrahedral environment around the zinc ion [68]. The bands at 275 nm and 244 nm could be attributed to the ligand.

With respect to the nickel complex $(TS)_2Ni$, three absorption maxima was observed as well as a weak band at 605 nm when more concentrated solution was used. The band at 377 nm may be due to n - π^* transition, where as the more intense band at 323 nm was attributed to charge transfer from ligand to metal or vise versa. The band at 605 nm is typical of ligand field transition (d-d transition) [21]. The position of this band could never be obtained with any accuracy because of the more intense higher energy ligand bands, and even the existence of the lower energy band can only be postulated on the basis of comparison with other compounds of similar structure [58]. This is why this band disappears from the spectra of dilute solution of the complex. This band could be attributed to $^1A_{1g} - {}^1B_{1g}$ transition [26] suggesting a trans-planar arrangement for the NiN_2O_2 chromophore.

Regarding the copper complex, 3 bands can be identified. The band at 364 nm is in part due to an internal n – π^* transition of the ligand and also to a charge transference probably from the metal to the ligand [21]. The fine-structured bands at 283 nm and 275 nm could be a composite of different types of individual transitions [58].

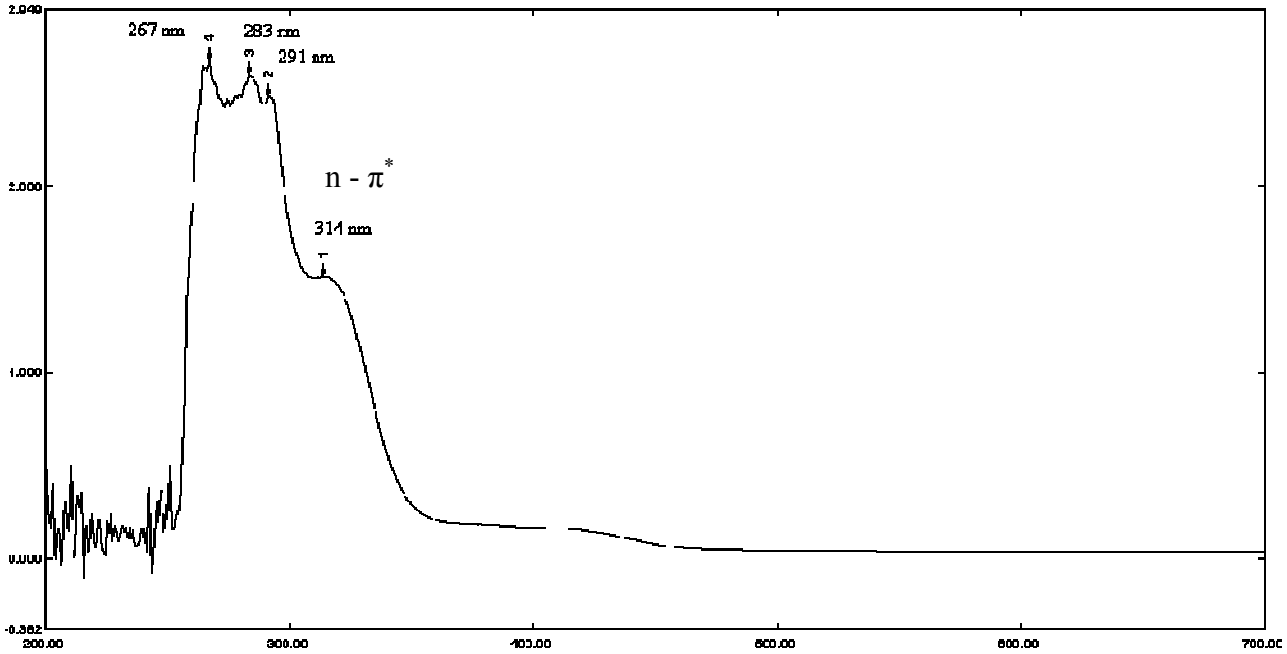

Fig 3.59: UV spectra of: 1H-Indole-3-ethylenesalicylaldimine (TS)

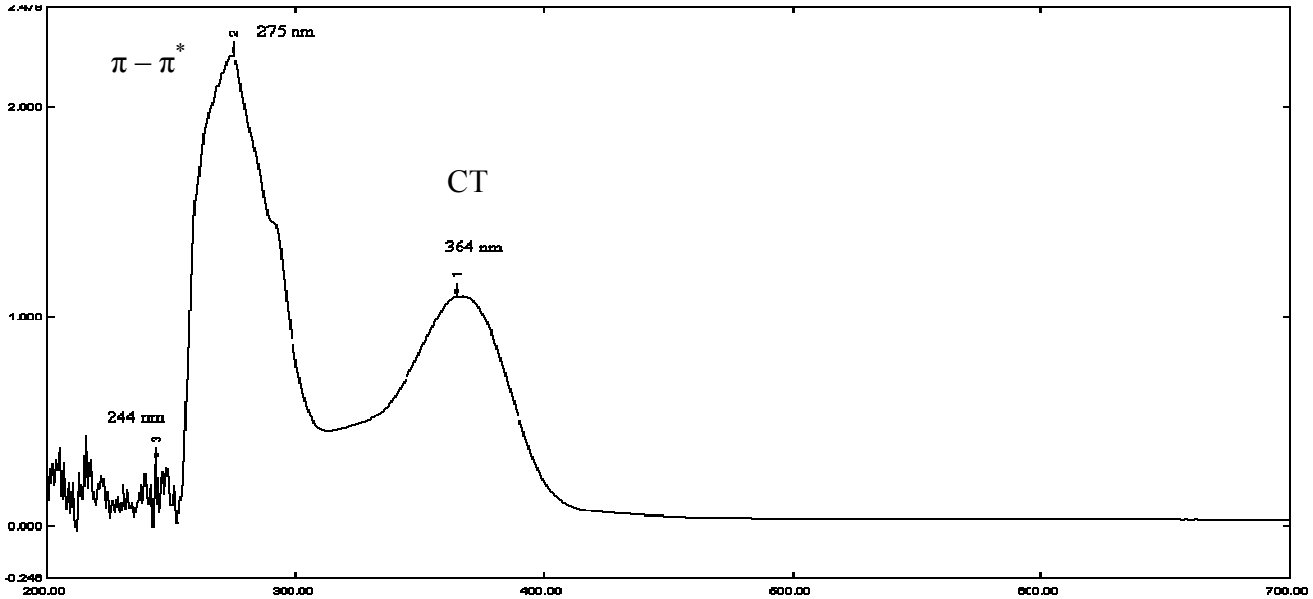

Fig 3.60: UV spectra of: bis (1H-Indole-3-ethylenesalicylaldiminato-k^{2}N, O)Zn(II): $(TS)_2Zn$

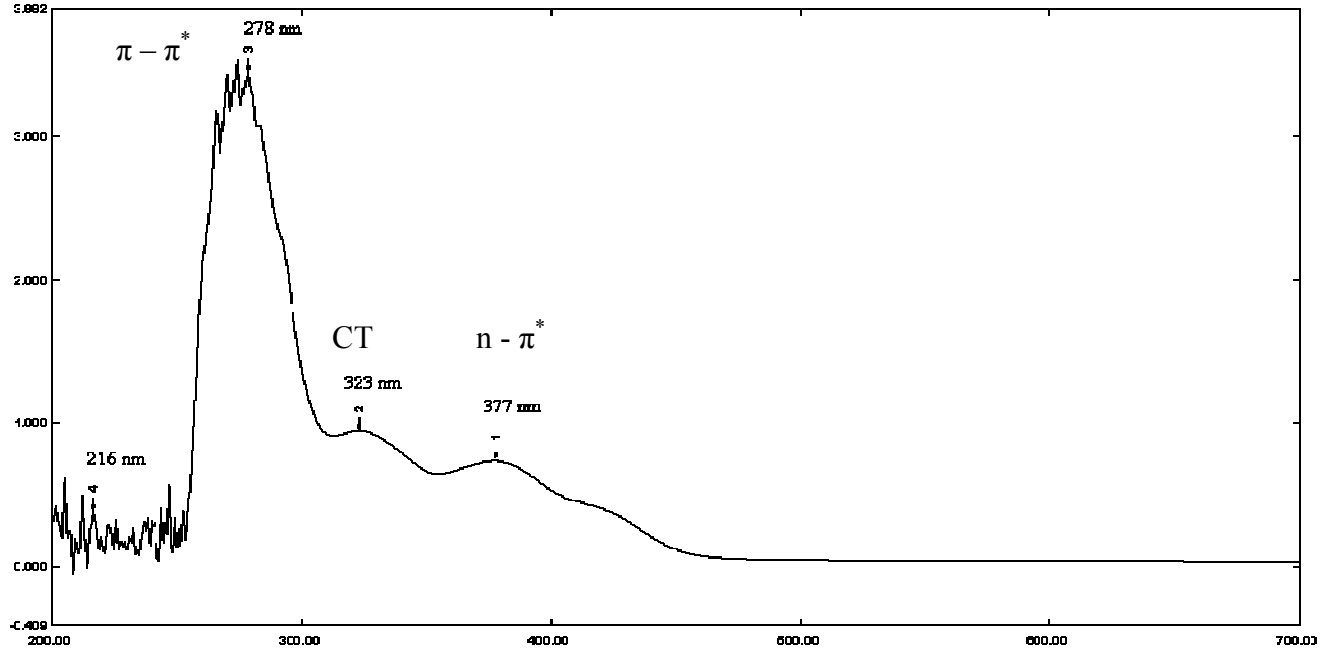

Fig 3.61: UV spectra of: bis (1H-Indole-3-ethylenesalicylaldiminato-k^{2}N,O)Ni(II): $(TS)_2Ni$

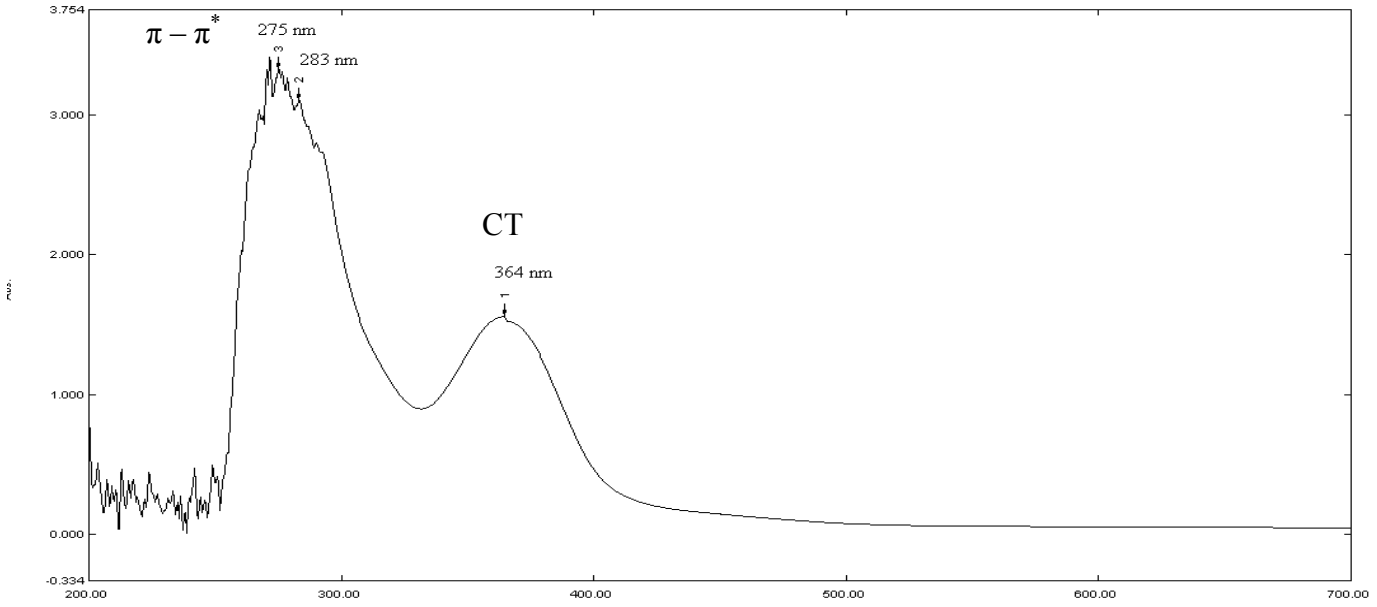

Fig 3.62: UV spectra of: bis (1H-Indole-3-ethylenesalicylaldiminato-k^{2}N,O)Cu(II): $(TS)_2Cu$

3.4.2 UV-Vis spectra of the ligand: 1H-Indole-3-ethylene-5-chlorosalicylaldimine (TCS) and its Zn, Ni and Cu complexes:

The UV-Vis spectra of the ligand together with its zinc, nickel, and copper complexes were shown in table (3. 29) and figure (3.63, 3.64, 3.65 and 3.66).

Table (3.29): UV-Vis. spectra of TCS and its Zn, Ni and Cu complexes:

Compound	Conc (mol/L)	ε ($mol^{-1}Lcm^{-1}$)	λ max (nm)	Assignment
TCS	4.01×10^{-4}	684.7	419.5	n - π^*
		4.11×10^{3}	326	π – π^* indole group
		8.0×10^{3}	284	π – π^* chelate ring
		7.72×10^{3}	265	π – π^* chelate ring
$(TCS)_2Zn$	1.26×10^{-4}	1.34×10^{4}	375.5	CT , n - π^*
		2.07×10^{4}	272	π – π^* ligand
$(TCS)_2Ni$	4.20×10^{-5}	1.06×10^{4}	384.5	CT
		2.83×10^{4}	273.5	π – π^* ligand
		-	226.5	π – π^* ligand
$(TCS)_2Cu$	4.17×10^{-5}	9.73×10^{3}	373	CT , n - π^*
		1.76×10^{4}	291	π – π^* ligand
		2.23×10^{4}	260	π – π^* ligand

The UV-Vis spectra of the ligand look closely similar to the spectra of TS with some shifts in the position of the bands. The peak at 419 nm could be related to n - π^* (ε = 684.7 $mol^{-1}Lcm^{-1}$). The double band in the region 250 nm – 300 nm is characteristic of a hydrogen-bonded $\pi - \pi^*$ transitions indicating an equilibrium between keto and enol forms. The band at 326 nm could be attributed to $\pi - \pi^*$ transition of indole group. This band shifts to longer wave length may be due to the effect of the chlorine substituent in the salicylaldehyde moiety with respect to the unsubstituted ligand.

The complexes spectra generally show the characteristic bands of the free ligand with some changes both in wave lengths and intensity. Spectra of the zinc complex of the ligand exhibit two distinctive bands. The band at 375 nm with molar absorptivity of 1.3×10^4 $mol^{-1}Lcm^{-1}$ could be ascribed to a combination of charge transfer and n - π^* transitions. The position of this band is consistent with a tetrahedral geometry around the zinc ion [55]. The other band at 272 nm was associated with the ligand.

For Ni complex, the charge transfer band at 384.5 nm is more intense with respect to the same band in $(TS)_2Ni$ complex, with a bathochromic shift of 61.5 nm may be due to the effect of the chlorine substituent. The rest of the bands at 273 nm and 226 nm were associated with the $\pi - \pi^*$ transitions of the ligand.

In the copper complex of the ligand, the band at 373 nm is associated with a combination of charge transfer and n - π^* transition, whereas bands between 260-291 nm were ligand $\pi - \pi^*$ transitions.

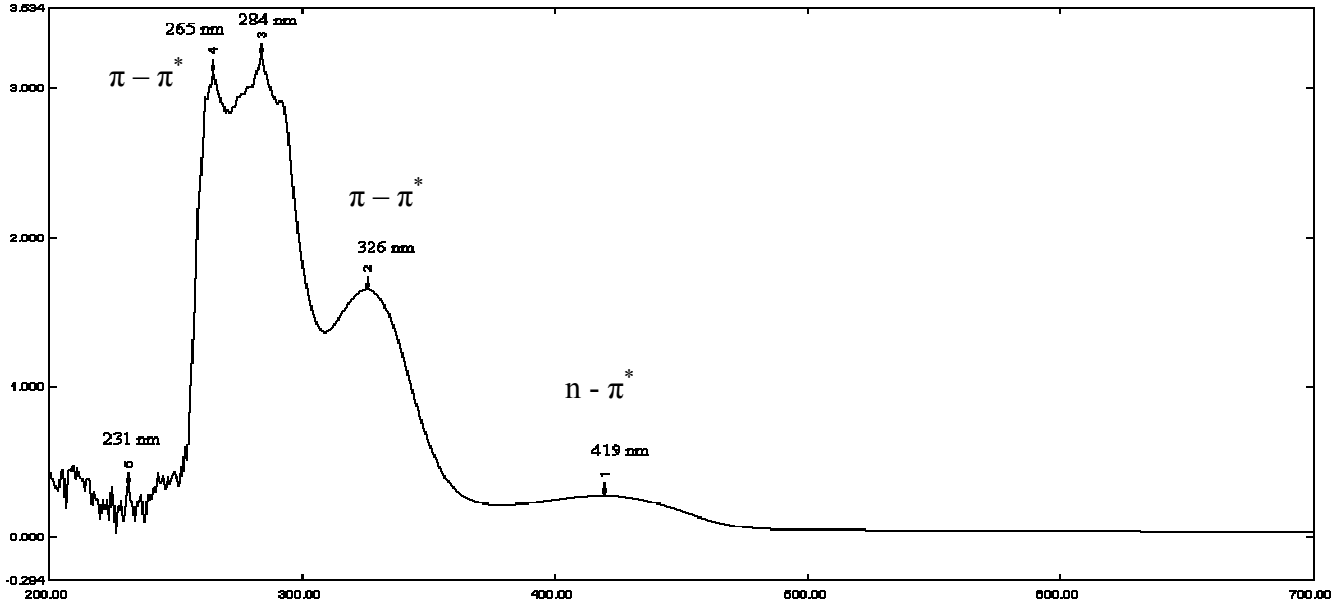

Fig 3.63: UV spectra of: 1H-Indole-3-ethylene-5-chlorosalicylaldimine (TCS)

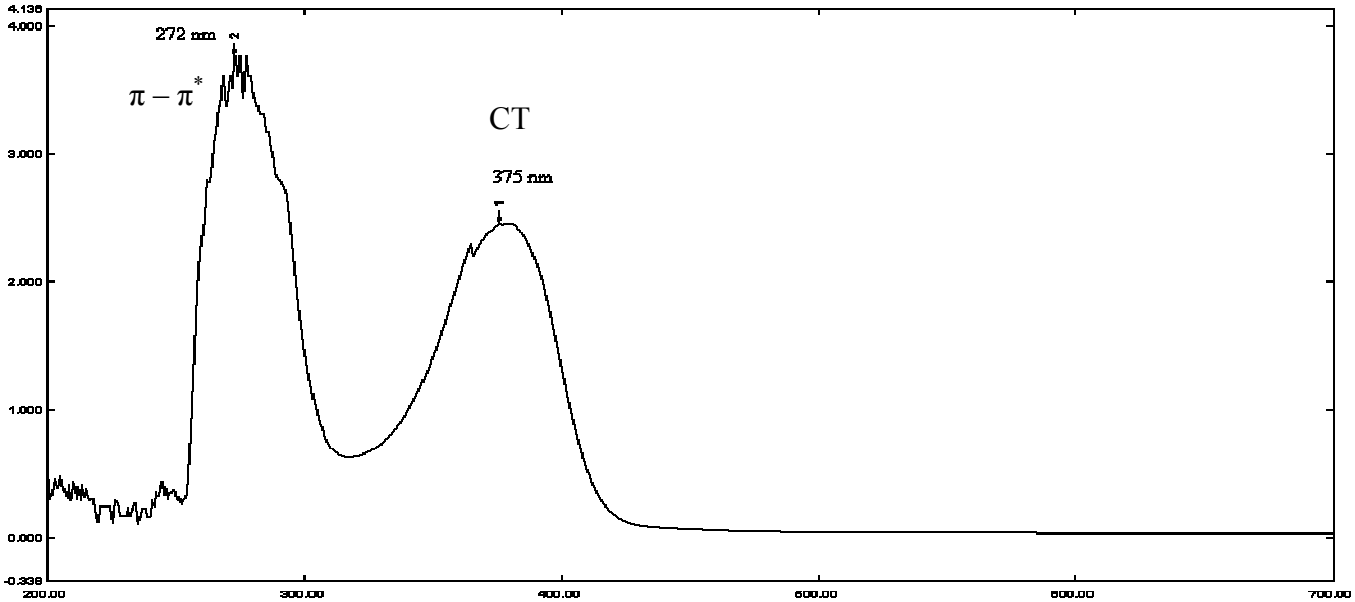

Fig 3.64: UV spectra of: bis {4-chloro-2-[2-(1H-indol-3-yl)ethyliminomethyl]phenolato-κ^2N, O} zinc(II): $(TCS)_2Zn$

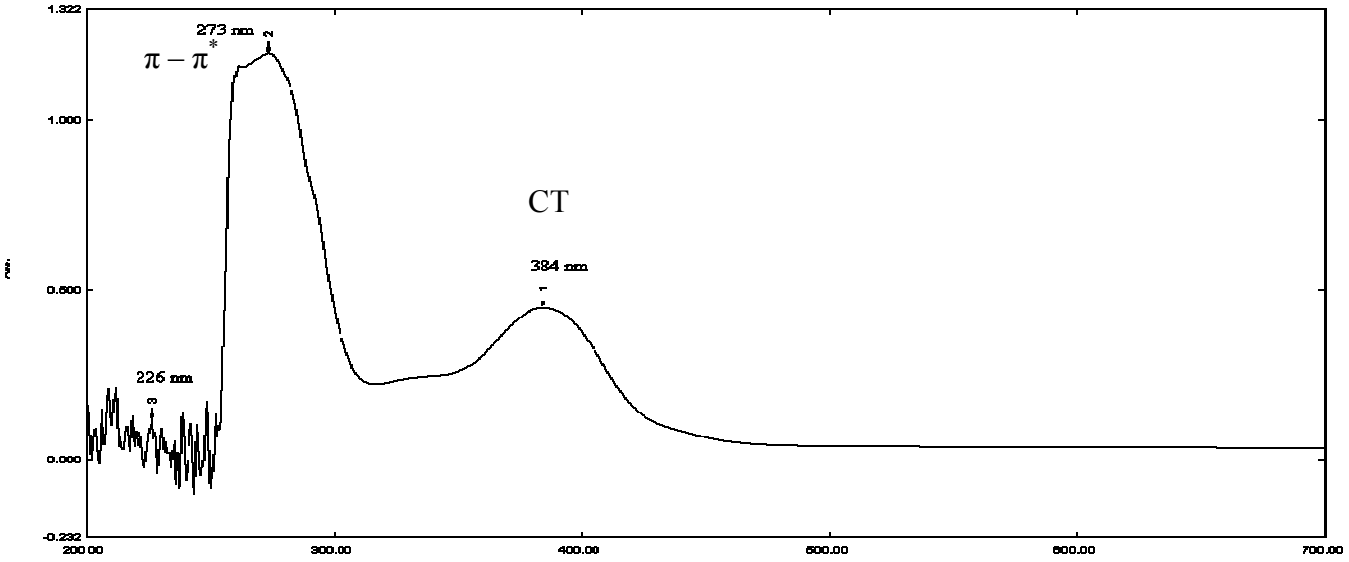

Fig 3.65: UV spectra of: bis {4-chloro-2-[2-(1H-indol-3-yl)ethyliminomethyl]phenolato-κ^2N, O} nickel(II): $(TCS)_2Ni$

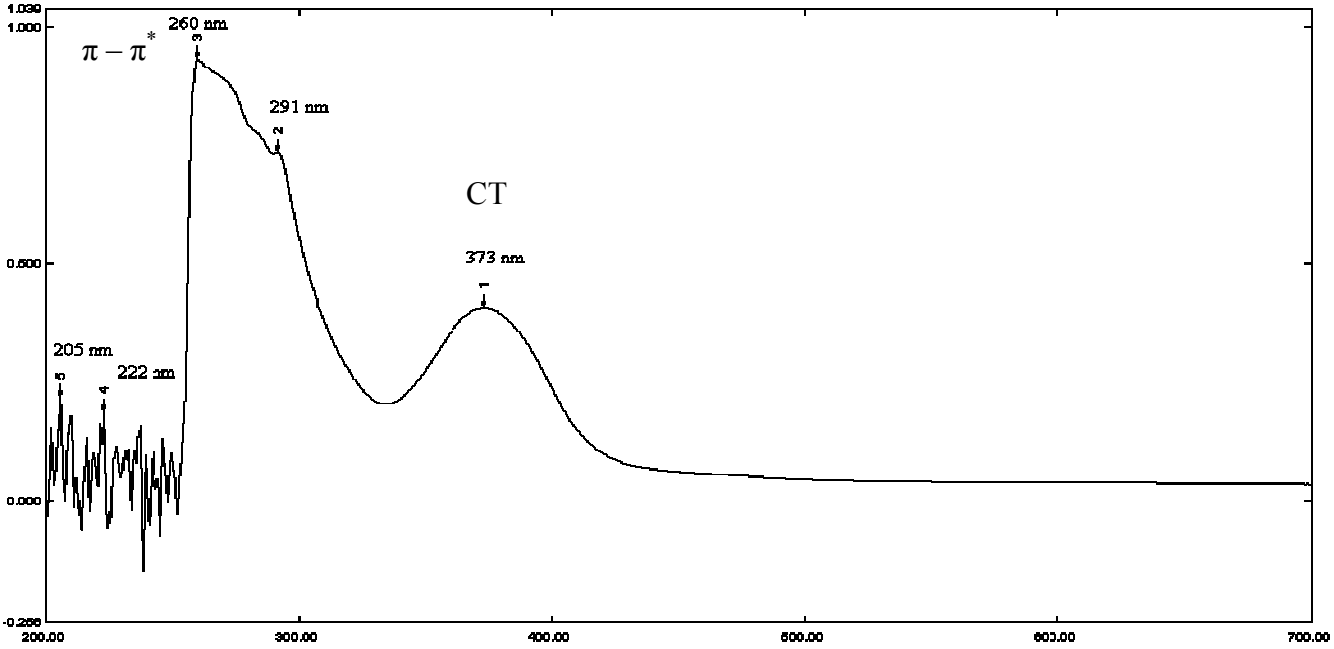

Fig 3.66: UV spectra of: bis{4-chloro-2-[2-(1H-indol-3-yl)ethyliminomethyl]phenolato-κ^2N, O} copper(II): $(TCS)_2Cu$

3.4.3 UV-Vis spectra of the ligand: 1H-Indole-3-ethylene-5-nitrosalicylaldimine (TNS) and its Zn, Ni, and Cu complexes:

The UV-Vis spectra of the ligand and complexes was carried out in DMSO as a solvent and represented in table (3.30) and figures (3.67, 3.68, 3.69, and 3.70) together with their tentative assignments.

Table (3.30): UV-Vis spectra of TNS and its Zn, Ni, and Cu complexes:

Compound	Conc (mol/L)	ε ($mol^{-1}Lcm^{-1}$)	λ max (nm)	Assignment
TNS	9.70×10^{-5}	1.40×10^{4}	420	n - π^*
		1.18×10^{4}	368	π – π^* chelate ring
		1.20×10^{4}	260	π – π^* chelate ring
$(TNS)_2Zn$	5.50×10^{-5}	3.01×10^{4}	377.5	CT , n - π^*
		2.22×10^{4}	260	π – π^* indole group
$(TNS)_2Ni$	3.70×10^{-5}	5.87×10^{4}	410	CT
		2.84×10^{4}	283	π – π^* ligand
		2.68×10^{4}	259	π – π^* ligand
$(TNS)_2Cu$	3.67×10^{-5}	4.25×10^{4}	383	CT , n - π^*
		4.03×10^{4}	261	π – π^* ligand

The spectra of the ligand show 3 absorption maxima. The intense band at 420 nm could be attributed to n - π^*. The intensity of this band have been increased because of the additive effect of the two isolated chromophores (–CH=N-) and the nitro group in the fifth position of the benzene ring [69]. The band at 368 nm is due to $\pi - \pi^*$ transition of the chelate ring. A bathochromic shift of this band in relation to the 314 nm band of TS ligand is due to the increased ketonic character of the phenolic C-O bond caused by the effect of electron withdrawal of the nitro group. The band at 260 nm could be assigned to $\pi - \pi^*$ transition associated with the indole group.

In case of zinc complex of this ligand, likewise two bands arose. The intense band at 377 nm may be assigned to both n - π^* transition and charge transfer from metal to the ligand. The band at 260 nm exhibit shoulder and may be associated with transitions $\pi - \pi^*$ of the indole group of the ligand.

Similarly the nickel complex spectra exhibit three main absorption bands. The band at 410 nm was assignable to charge transfer as indicated for the zinc complex mentioned above. The other bands could be assigned to the ligand $\pi - \pi^*$ transitions. The ligand field transition was not shown in the spectra, may be due to the use of very dilute solution, in addition to the relatively low molar extinction coefficient (ε) for this type of transition.

The copper complex electronic spectra in DMSO shows bands at 383 nm ($\varepsilon = 4.25\times10^4$ $mol^{-1}Lcm^{-1}$), 261 nm ($\varepsilon = 4.0\times10^4$ $mol^{-1}Lcm^{-1}$) and a weak band at 249 nm ($\varepsilon = 1.1\times10^4$ $mol^{-1}Lcm^{-1}$). The band at 383 nm is ascribed to the charge transfer between the metal and the ligand, while the band at 261 nm can be attributed to $\pi - \pi^*$ transition of the ligand. Also the ligand field d-d transition is not seen in the spectra, perhaps due to comparatively low molar absorptivity coefficient associated with this transition.

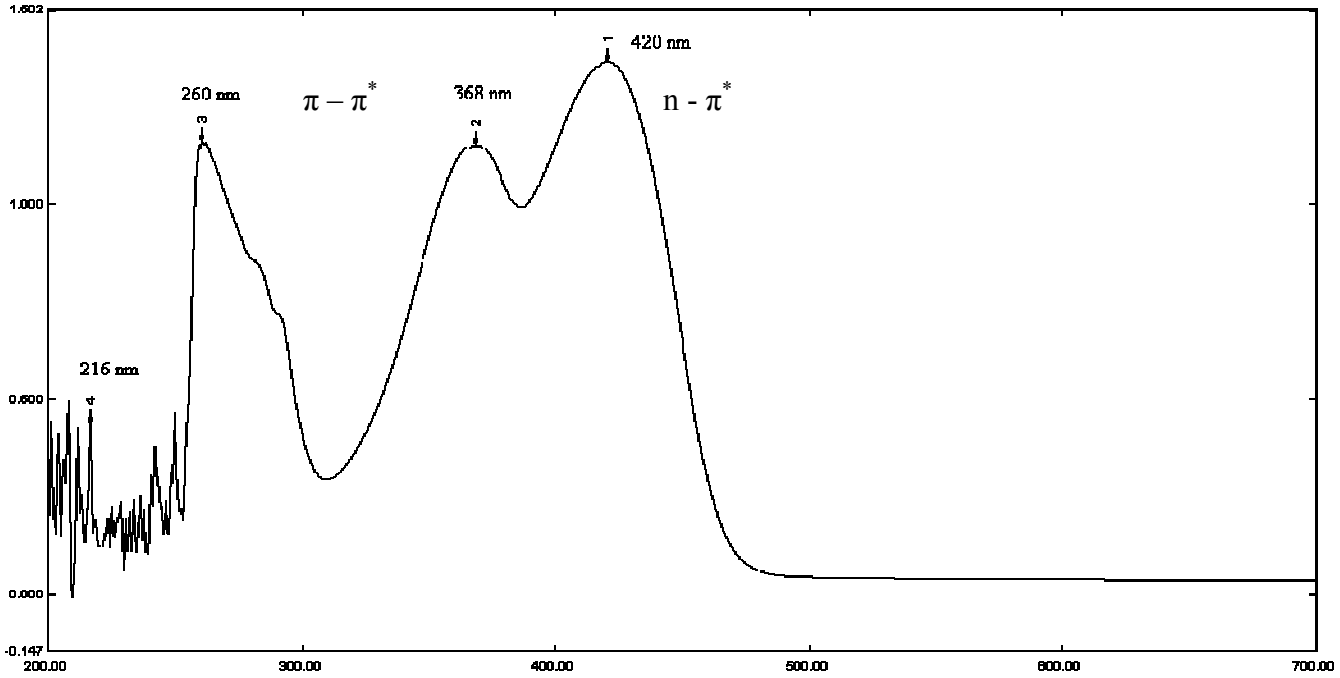

Fig 3.67: UV spectra of: 1H-Indole-3-ethylene-5-nitrosalicylaldimine (TNS)

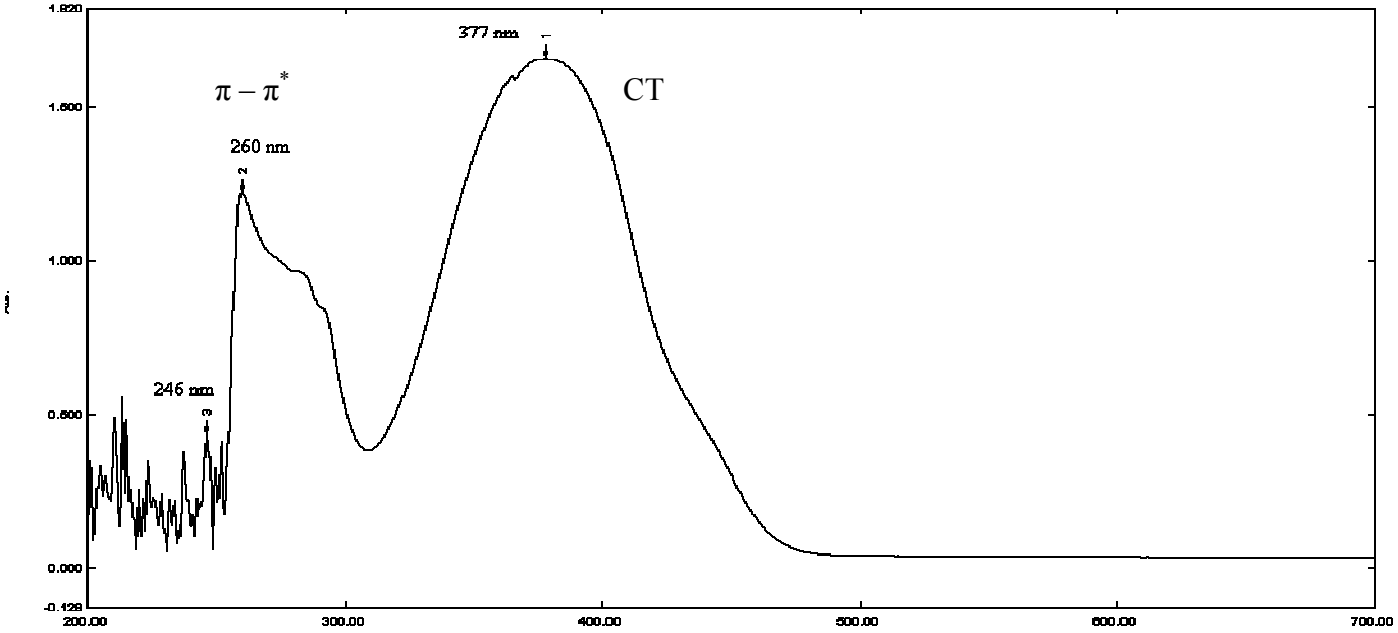

Fig 3.68: UV spectra of: bis {4-nitro-2-[2-(1H-indol-3-yl)ethyliminomethyl]phenolato-κ^2N, O} zinc(II): $(TNS)_2Zn$

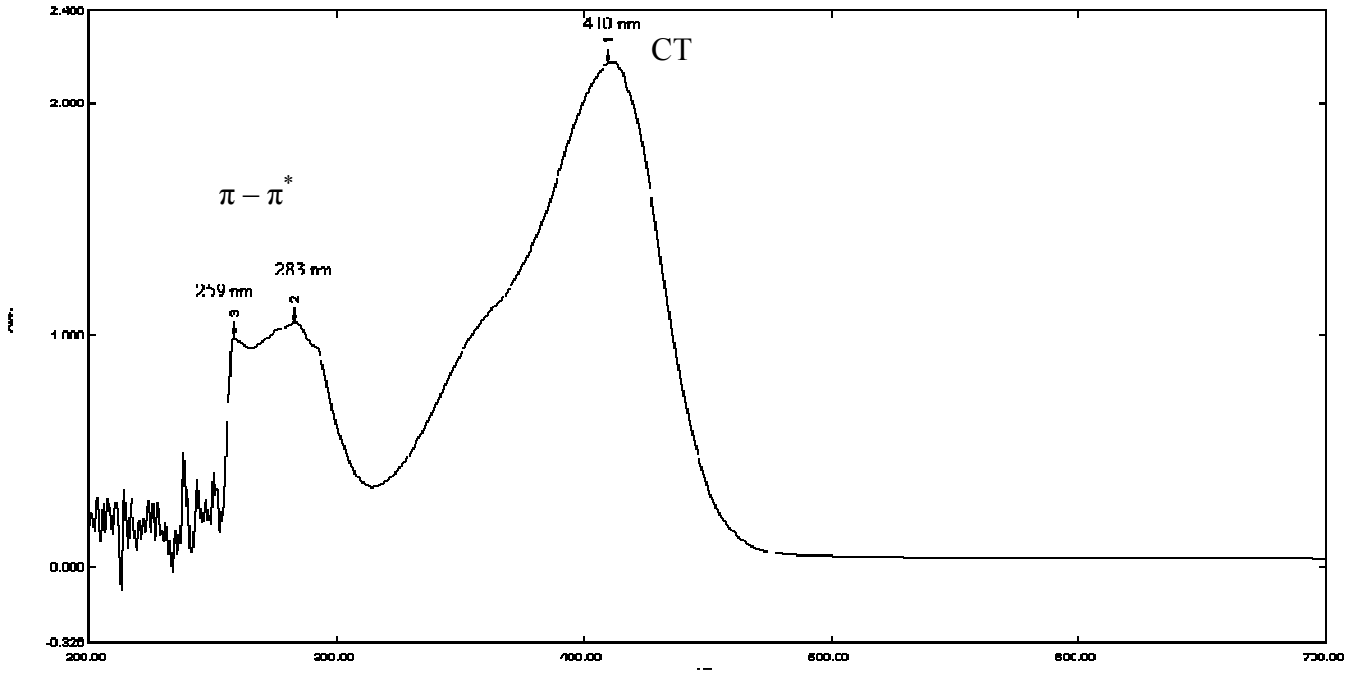

Fig 3.69: UV spectra of: bis {4-nitro-2-[2-(1H-indol-3-yl)ethyliminomethyl]phenolato-κ^2N, O} nickel(II): $(TNS)_2Ni$

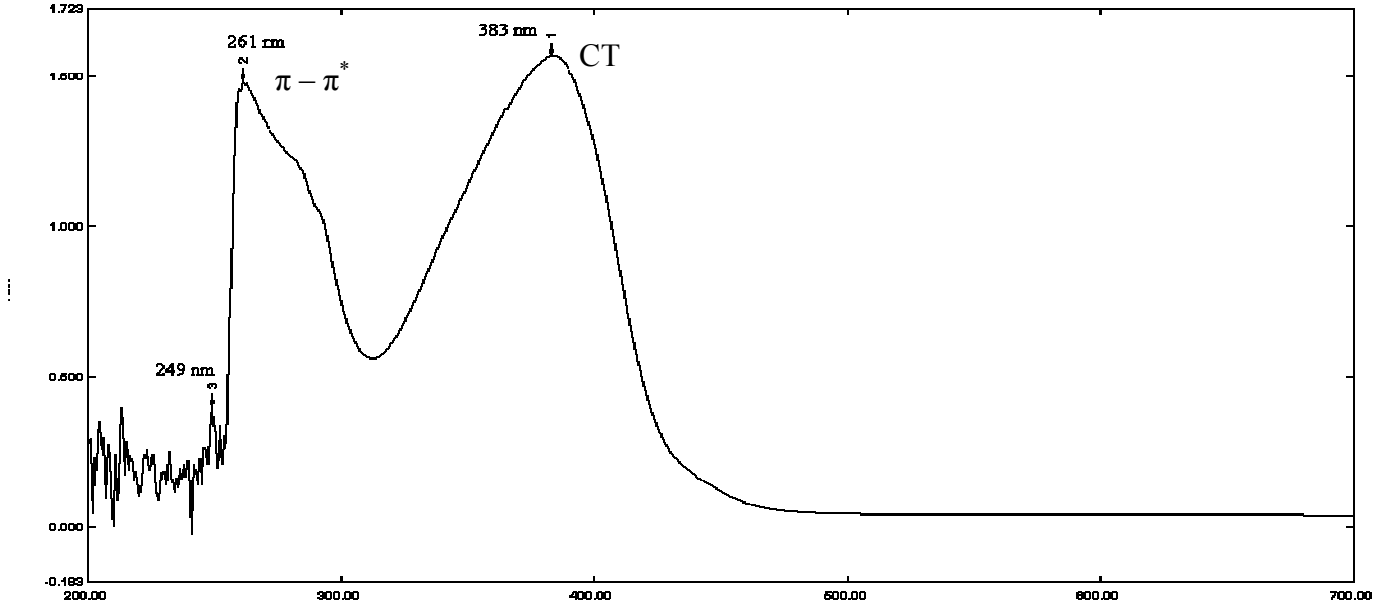

Fig 3.70: UV spectra of: bis{4-nitro-2-[2-(1H-indol-3-yl)ethyliminomethyl]phenolato-κ^2N, O} copper(II): $(TNS)_2Cu$

3.4.4 UV-Vis spectra of the ligand:

1H-Indole-3-ethylene-3-5-di-tertiarybutylsalicylaldimine (TTET) and its Zn, Ni, and Cu complexes:

The UV-Vis spectra of the ligand in DMSO together with its zinc, nickel, and copper complexes were shown in table (3.31) and figures (3.71, 3.72, 3.73 and 3.74).

Table (3.31): UV-Vis spectra of the ligand TTET and its Zn, Ni, and Cu complexes.

Compound	Conc (mol/L)	ε ($mol^{-1}Lcm^{-1}$)	λ max (nm)	Assignment
TTET	3.45×10^{-4}	376.5	417	n - π^*
		3.53×10^{3}	327	π – π^* chelate ring
		9.77×10^{3}	267	π – π^* indole group
$(TTET)_2Zn$	1.60×10^{-4}	9.32×10^{4}	381.5	CT , n - π^*
		1.93×10^{4}	283	π – π^* ligand
$(TTET)_2Ni$	1.50×10^{-4}	7.65×10^{3}	385	CT
		2.67×10^{4}	281	π – π^* ligand
		1.50×10^{4}	248	π – π^* ligand
$(TTET)_2Cu$	1.60×10^{-4}	1.09×10^{4}	377	CT , n - π^*
		1.07×10^{4}	325	π – π^* ligand
		2.48×10^{4}	282	π – π^* ligand

The spectra of the ligand composed of 3 main absorption maxima. n - π^* transition appears as a low intensity band at 417 nm (ε = 376.5 $mol^{-1}cm^{-1}$). This band considerably shifts to longer wave length as compared to the previous ligand may be due to the effect of two tertiary butyl substituents in position 3 and 5 in the salicylaldehyde moiety. The band at 327 nm with intermediate intensity could be assigned to $\pi - \pi^*$ transition of hydrogen-bonded chelate ring, where as the band at 267 nm is attributed to $\pi - \pi^*$ transitions of indole group.

As for the previous ligands, the zinc complex of this ligand also reveals two absorption maxima. The intense charge transfer band at 381 nm which is characteristic of a tetrahedrally co-ordinated zinc ion, and a band at 283 nm which can be assigned for ligand transitions.

For Ni complex of the ligand, the band at 385 nm is assigned to the phenolate to nickel charge transfer while the band at 281 nm, 248 nm were associated with $\pi - \pi^*$ transitions of the ligand.

With respect to the copper complex spectra of this ligand, if compared with the free ligand, the band at 377 nm is more intense than the corresponding band 417 nm of the ligand and this band can be assigned to a mixed charge transfer and n - π^* transition. This band was also revealed a hyperchromic (blue) shift upon complexation. The other bands at 325 nm and 282 nm are associated with the ligand.

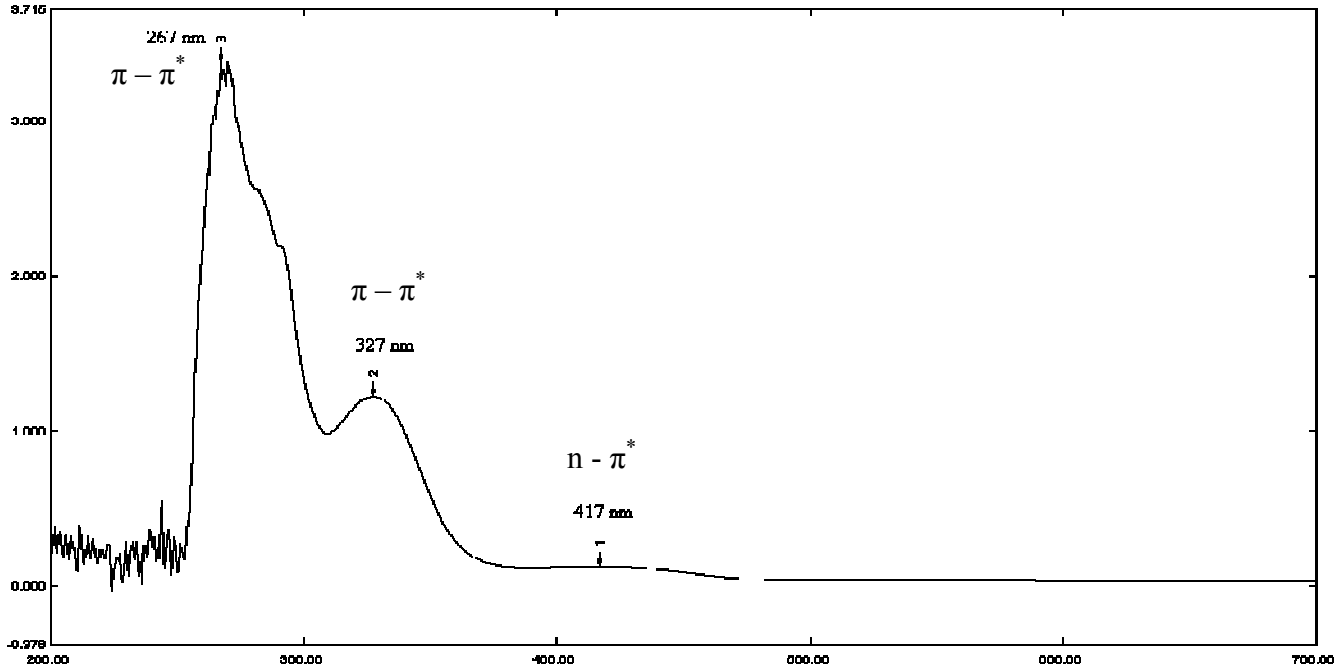

Fig 3.71: UV spectra of: 1H-Indole-3-ethylene-3-5-di-tertiarybutylsalicylaldimine (TTET)

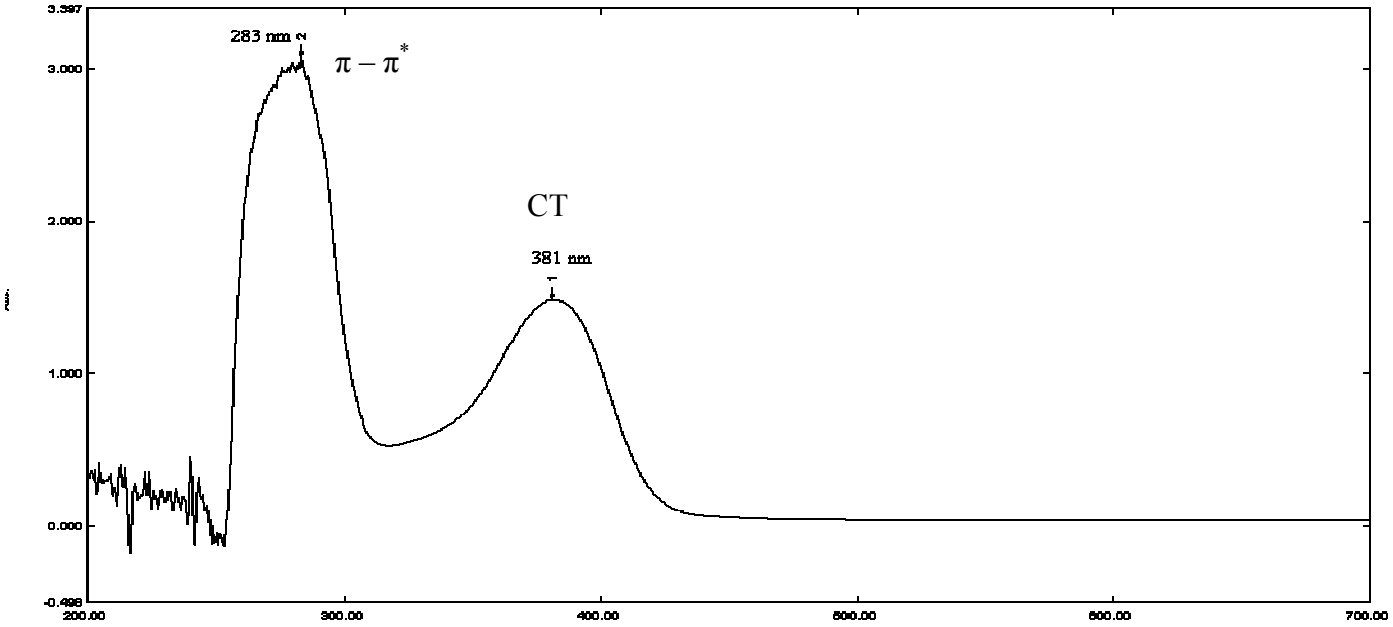

Fig 3.72: UV spectra of: bis(1H-Indole-3-ethylene-3-5-di-tertiarybutylsalicylaldiminato-k^2N,O)Zn(II): $(TTET)_2Zn$

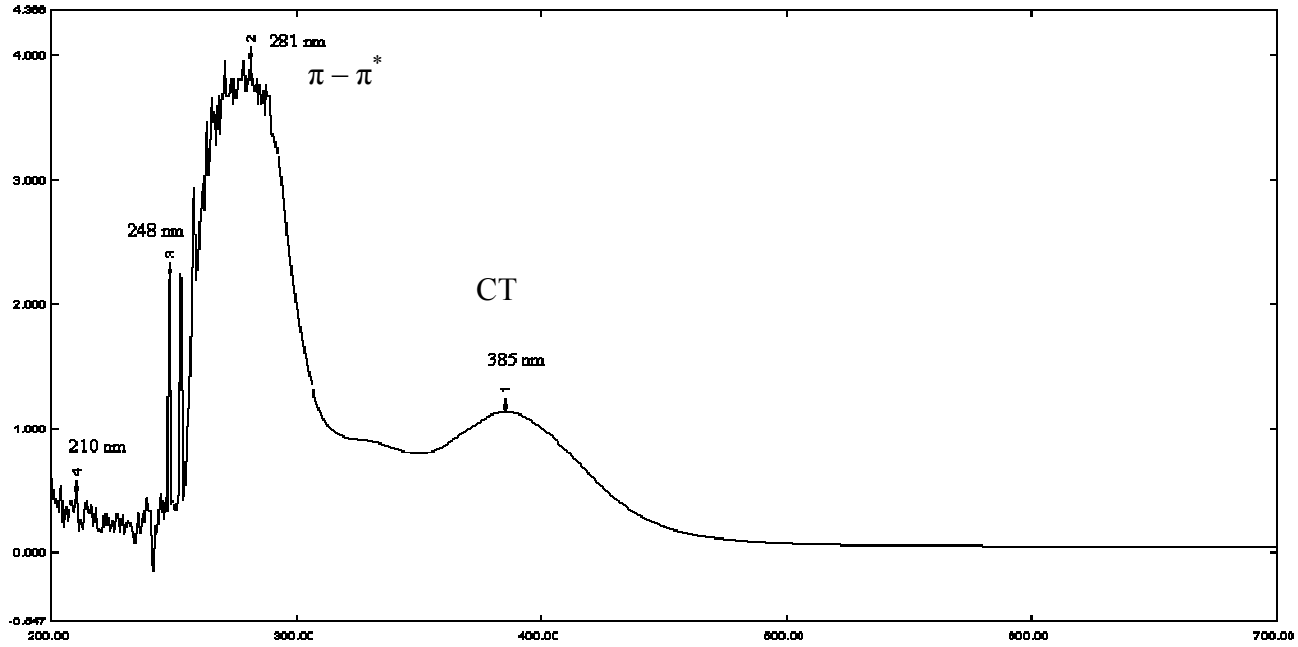

Fig 3.73: UV spectra of: bis (1H-Indole-3-ethylene-3-5-di-tertiarybutylsalicylaldiminato-k^2N,O)Ni(II): $(TTET)_2Ni$

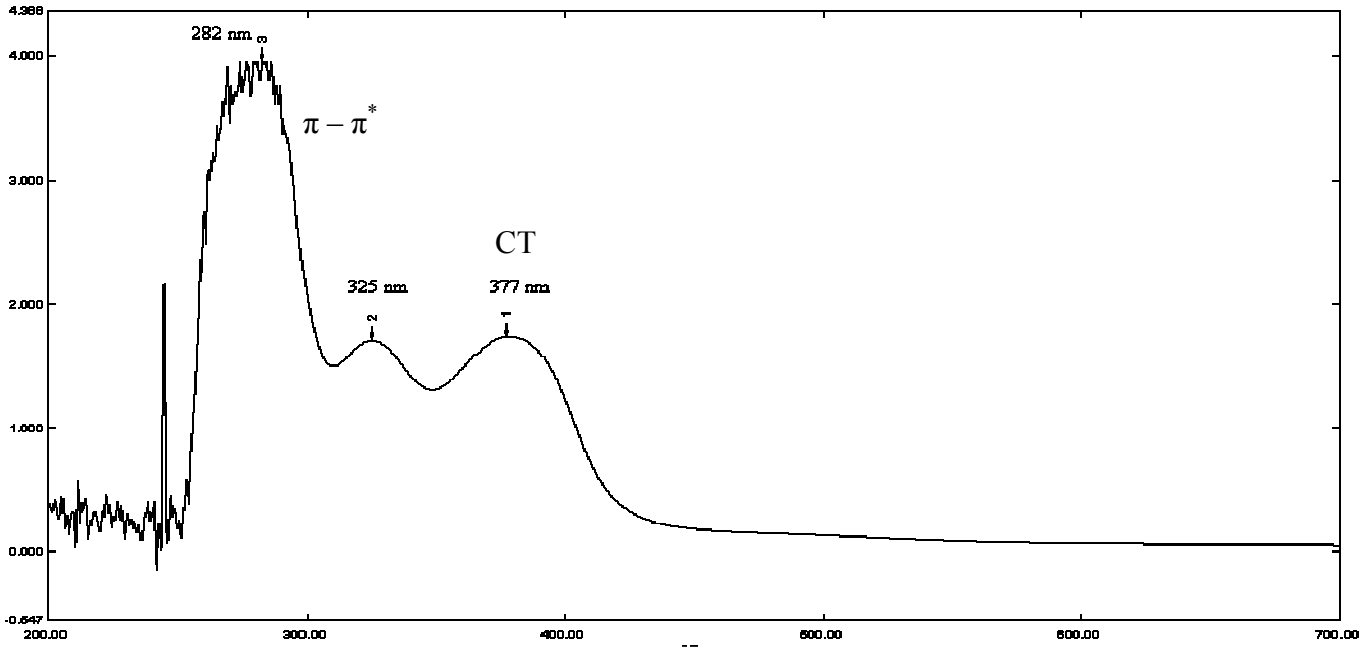

Fig 3.74: UV spectra of: bis (1H-Indole-3-ethylene-3-5-di-tertiarybutylsalicylaldiminato-k^2N,O)Cu(II): $(TTET)_2Cu$

3.4.5 UV-Vis spectra of the ligand:

2-{1-[2-(1H-Indole-3-yl)ethylimino]-ethyl } phenol (THAP) and its complexes:

The UV-Vis spectra of the ligand was carried out in DMSO as solvent, and shown in table (3.32) and figures (3.75, 3.76, 3.77 and 3.78).

Table (3.32): UV-Vis spectra of THAP and its zinc, nickel and copper complexes:

Compound	Conc (mol/L)	ε ($mol^{-1}Lcm^{-1}$)	λ max (nm)	Assignment
THAP	9.88×10^{-5}	1.56×10^{3}	395	n - π^*
		3.67×10^{3}	317	$\pi - \pi^*$ chelate ring
		6.94×10^{3}	291	-
		7.74×10^{3}	282	-
		7.78×10^{3}	276	$\pi - \pi^*$ indole group
		9.42×10^{3}	260	$\pi - \pi^*$ indole group
$(THAP)_2Zn$	1.08×10^{-4}	3.63×10^{3}	394	n - π^*
		9.93×10^{3}	316	$\pi - \pi^*$ chelate ring
		2.20×10^{4}	275	$\pi - \pi^*$ indole group
		2.36×10^{4}	262	$\pi - \pi^*$ indole group

Table 3.32 continued

Compound	Conc (mol/L)	ε ($mol^{-1}Lcm^{-1}$)	λ max (nm)	Assignment
$(THAP)_2Ni$	7.33×10^{-5}	-	572	d-d transition
		5.06×10^{3}	388	CT, n - π^*
		2.34×10^{4}	263	π – π^* indole group
$(THAP)_2Cu$	6.47×10^{-5}	7.86×10^{3}	358	CT , n - π^*
		2.13×10^{4}	273	π – π^* ligand

The spectra exhibit bands at 395 nm, 317 nm, 291 nm and 276 nm which are well consistent with what have been reported by Perdo Martin *et al* with same ligand in chloroform [25]. The band at 395 nm could be assigned to n - π^* transition of chelate ring in the same way as in the ligand TS. Further more the band at 317 nm was assigned to π – π^* transition of chelate ring. This band has been shifted slightly to longer wave length in comparison to TS described earlier. The bands at 276 nm and 260 nm were associated with π – π^* transitions of the indole group.

If we compare the spectra of the zinc complex with that of the free ligand, it was observable that there is no remarkable difference between the two. Since the azomethine group does not participate in coordination with the zinc atom, the n - π^* transition remains the same and has not been affected. No charge transfer bands were observed due to the stable d^{10} configuration in the zinc ion.

For nickel complex, the n - π^* transition has shifted to lower wave length indicating coordination of the azomethine nitrogen atom to the metal centre. The band at 263 nm is

due to $\pi - \pi^*$ transition of the ligand. A low intensity band at 572 nm is due to d-d transition.

For copper complex of the ligand, two bands can be distinguished in the spectra. The band at 358 nm is in part due to n - π^* transition, and also to charge transference probably from ligand to the metal. It has been reported that, the diffuse reflectance spectra of copper complexes of this type of ligands exhibit bands at 700-800 nm consistent with a distorted pseudotetrahedral disposition around the copper ion [25, 73]. The band at 273 nm is due to $\pi - \pi^*$ transition of the ligand.

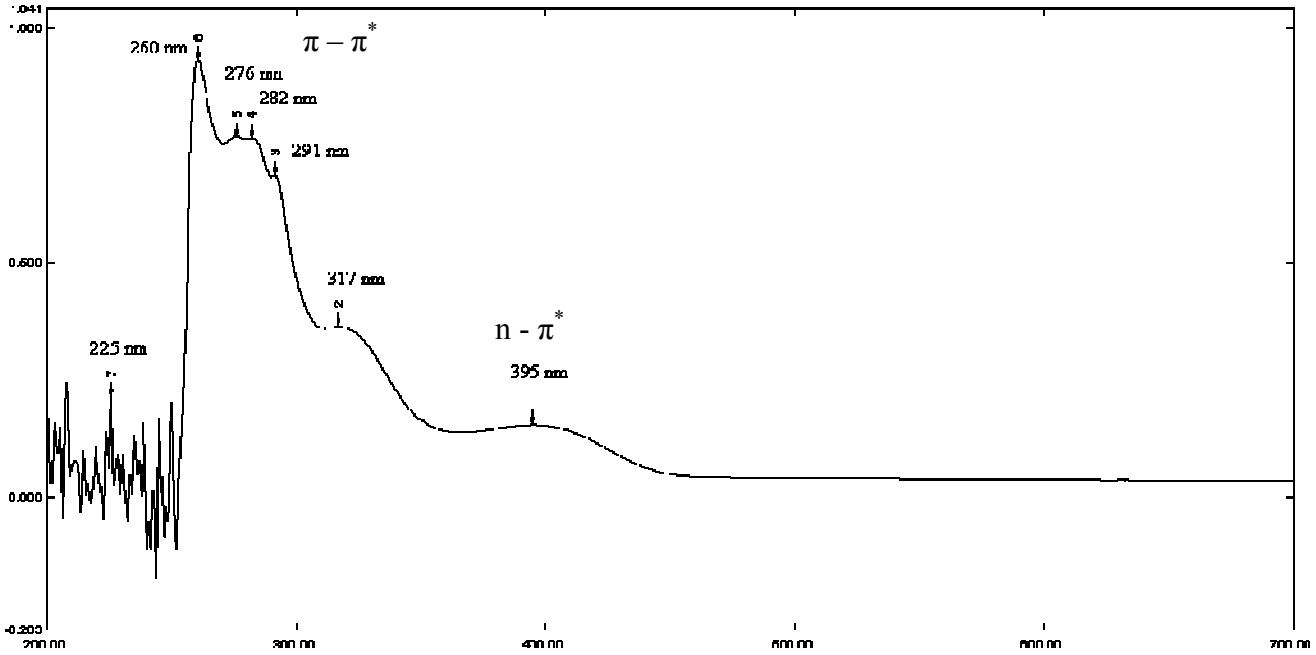

Fig 3.75: UV spectra of: 2-{1-[2-(1H-Indole-3-yl)ethylimino]-ethyl}phenol (THAP)

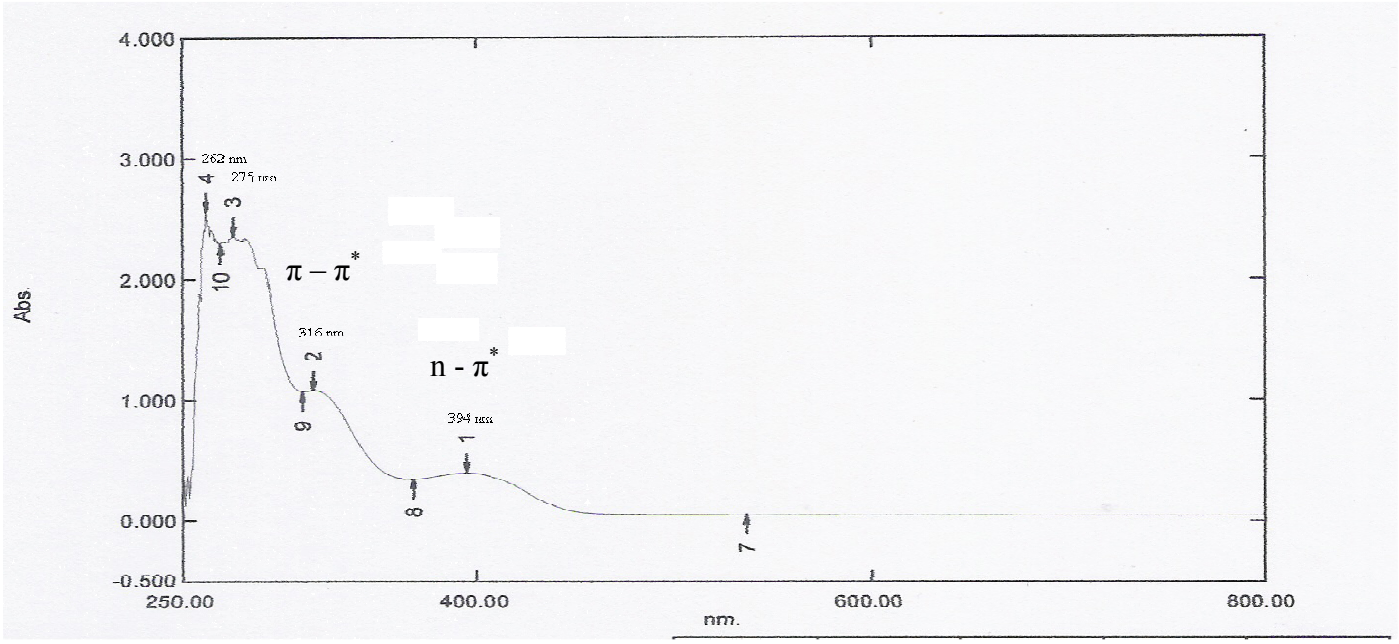

Fig 3.76: UV spectra of: dichloridobis(2-{1-[2-(1H-indol-3-yl) ethyliminio]ethyl}phenolate-*k*O)zinc(II) $(THAP)_2Zn$

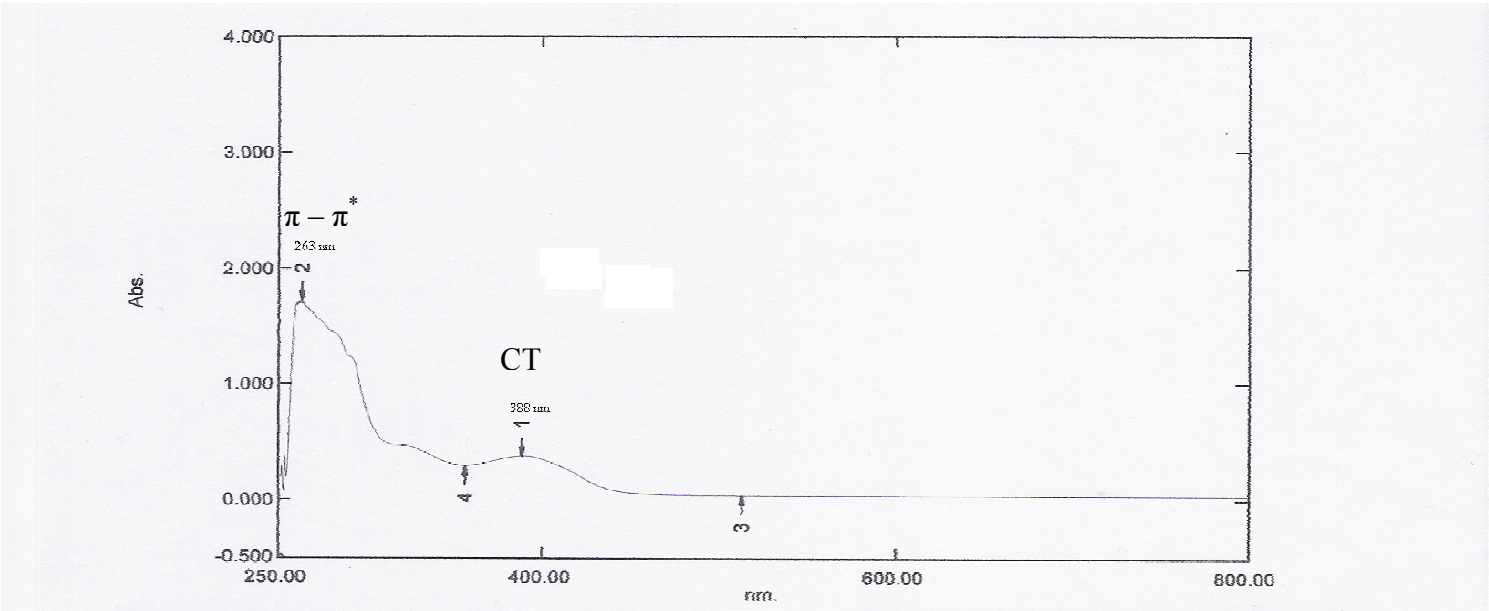

Fig 3.77: UV spectra of: bis(2-{1-[2-(1H-indol-3-yl)- ethyliminio]ethyl}phenolato-k^2N, O)Ni(II): $(THAP)_2Ni$

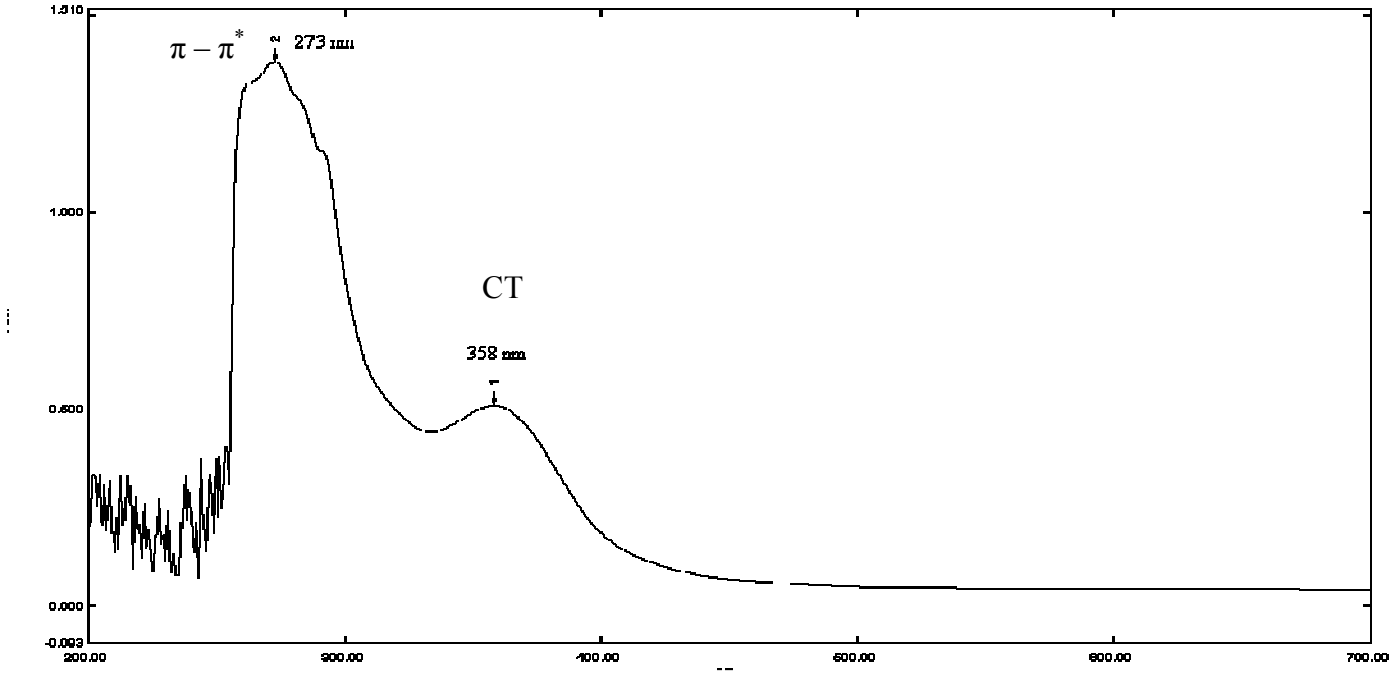

Fig 3.78: UV spectra of: bis (2-{1-[2-(1H-indol-3-yl)-ethyliminio]ethyl}phenolato-k^2N, O)Cu(II): $(THAP)_2Cu$

3.4.6 UV-Vis spectra of the ligand: 2-{1-[2-(1H-Indole-3-yl)-ethylimino]-ethyl}-4-methyl phenol (TMeHAP) and its copper complex:

The UV-Vis spectra of the ligand and its complex together with the corresponding tentative assignments are given in table (3.33) and figure (3.79 and 3.80).

Table (3.33): UV-Vis spectra of TMeHAP and its copper complex:

Compound	Conc (mol/L)	ε ($mol^{-1}Lcm^{-1}$)	λ max (nm)	Assignment
TMeHAP	1.54×10^{-4}	3.77×10^{3}	338	$\pi - \pi^*$ chelate ring
		8.08×10^{3}	282	$\pi - \pi^*$ indole group
		8.02×10^{3}	275	$\pi - \pi^*$ indole group
		1.03×10^{4}	260	$\pi - \pi^*$ indole group
$(TMeHAP)_2Cu$	6.57×10^{-5}	9.71×10^{3}	358	CT , n - π^*
		2.40×10^{4}	272	$\pi - \pi^*$ ligand

It is clearly observed that the spectrum of this ligand is closely similar to the spectra of THAP mentioned above with the bands red shifted. The band at 338 nm compared to 317 nm in THAP ligand is related to $\pi - \pi^*$ transition of chelate ring, while the double bands at 282 nm, 275 nm and 260 nm were associated with $\pi - \pi^*$ transitions of indole group.

With regard to the copper complex of the ligand, two bands have been identified. The band at 358 nm could be assigned to a mixed n - π^* transition of the ligand and charge transfer from ligand to the metal. As it has been reported by Perdo Martin *et al* [25], the copper ion have been slightly distorted from trans planar N_2O_2 arrangement to

pseudotetrahedral geometry probably due to the substitution of the hydrogen atom on the

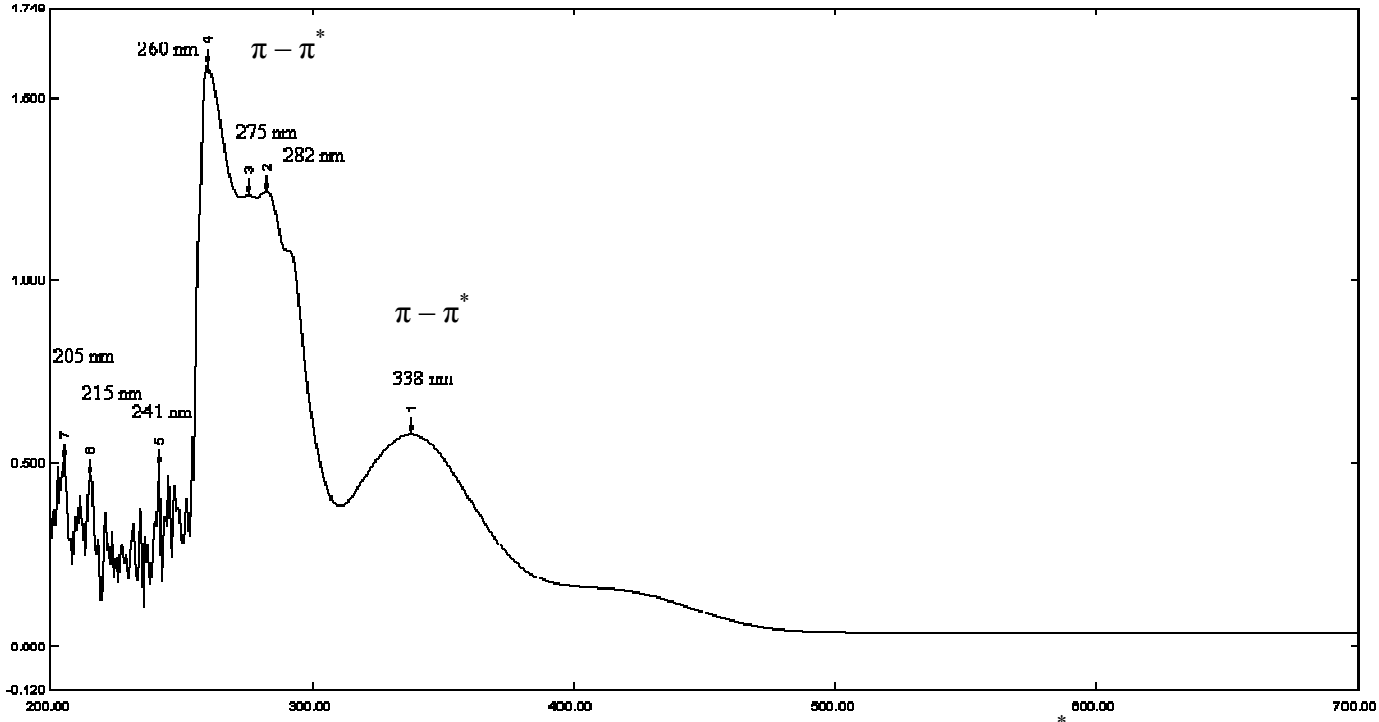

iminic carbon by methyl group. The band at 272 nm is assigned to $\pi - \pi^*$ of the ligand.

Fig 3.79: UV spectra of: 2-{1-[2-(1H-Indole-3-yl)-ethylimino]-ethyl}-4-methyl phenol (TMeHAP)

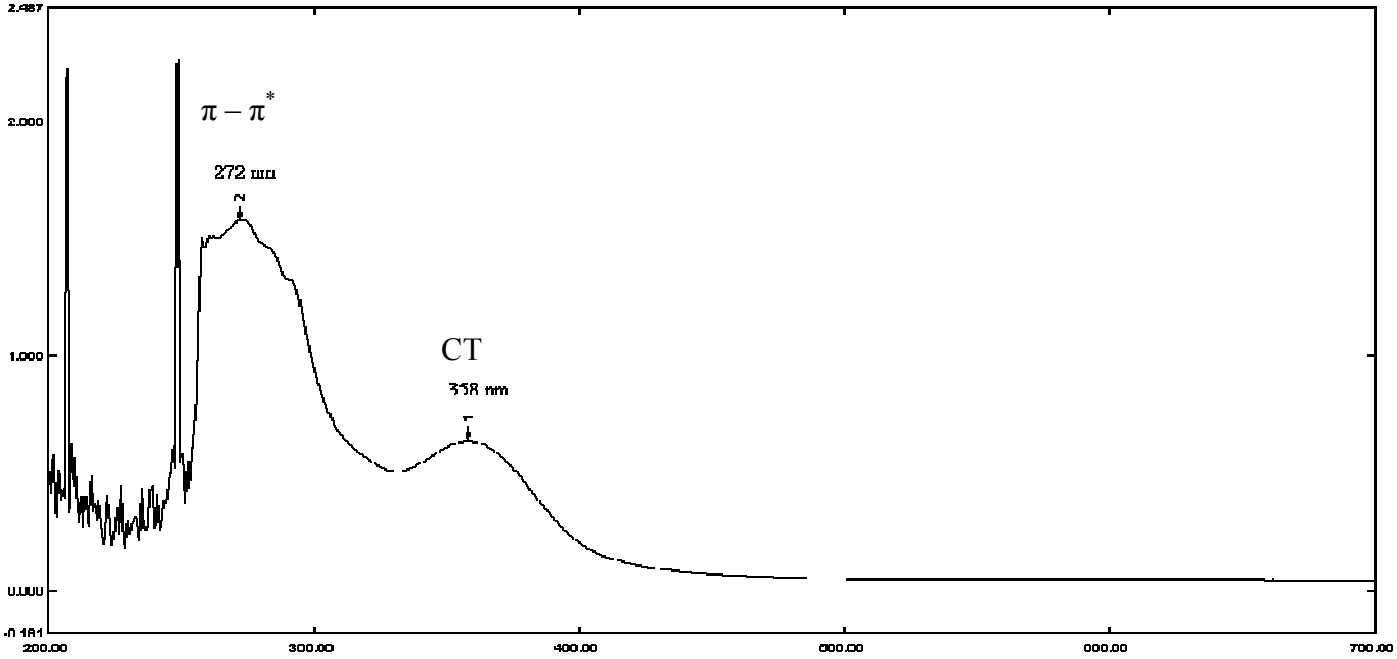

Fig 3.80: UV spectra of: bis{2-{1-[2-(1H-Indole-3-yl)-ethylimino]-ethyl}-4-methylphenolato-k^2N,O}Cu(II): $(TMeHAP)_2Cu$

3.4.7 UV-Vis spectra of the ligand:

2-{1-[2-(1H-Indole-3-yl)-ethylimino]-ethyl}-4-methoxy phenol (TOMeHAP) and its nickel and copper complexes:

The spectra of the ligand have been summarized with relevant assignments in table (3.34) and shown in figures (3.81, 3.82 and 3.83)

Table (3.34): UV-Vis spectra of the ligand TOMeHAP and its nickel and copper complexes:

Compound	Conc (mol/L)	ε ($mol^{-1}Lcm^{-1}$)	λ max (nm)	Assignment
TOMeHAP	1.13×10^{-4}	3.98×10^{3}	346	$\pi - \pi^*$ chelate ring
		7.94×10^{3}	281	$\pi - \pi^*$ indole group
		9.40×10^{3}	261	$\pi - \pi^*$ indole group
$(TOMeHAP)_2Ni$	1.48×10^{-4}	364.86	572	d-d transition
		4.03×10^{3}	412	CT, n-π^* transition
		7.97×10^{3}	344	$\pi - \pi^*$ chelate ring
		2.48×10^{4}	273	$\pi - \pi^*$ indole group
$(TOMeHAP)_2Cu$	1.91×10^{-4}	6.45×10^{3}	386	CT , n - π^*
		1.80×10^{4}	268	$\pi - \pi^*$ ligand

Three main bands can be distinguished in this case. The band at 346 nm is due to $\pi - \pi^*$ transition of the chelate ring. This band is red shifted in comparison to the same band in THAP ca 317 nm. This shift indicates that the ketonic character of the C-O bond have

been increased as a result of the deactivation effect exerted in the ortho and para position of the phenyl ring by the methoxy group [24]. The bands at 281 nm and 261 nm were well consistent with those found by P.Gili *et al* in similar ligands and can be assigned to $\pi - \pi^*$ transitions of the indole group [24].

With regard to the nickel complex, the band at 572 nm could be assigned to $^1A_{1g}$-$^1B_{1g}$ transition which is consistent with a square planar geometry around the nickel ion [71]. The band at 412 nm is probably a mixed n - π^* and charge transfer. There is a slight hypsochromic shift of the $\pi - \pi^*$ band upon coordination [60, 72]. The strong absorption at 273 nm is assigned to $\pi - \pi^*$ of benzene ring.

For copper complex of the ligand, the spectra reveal two main bands. The band at 386 nm is bathochromically shifted in comparison to the same band at 358 nm of the previous copper complex of the ligand TMeHAP and can be assigned to a mixed n - π^* transition and charge transference. The band at 268 nm is associated with $\pi - \pi^*$ transition of the ligand.

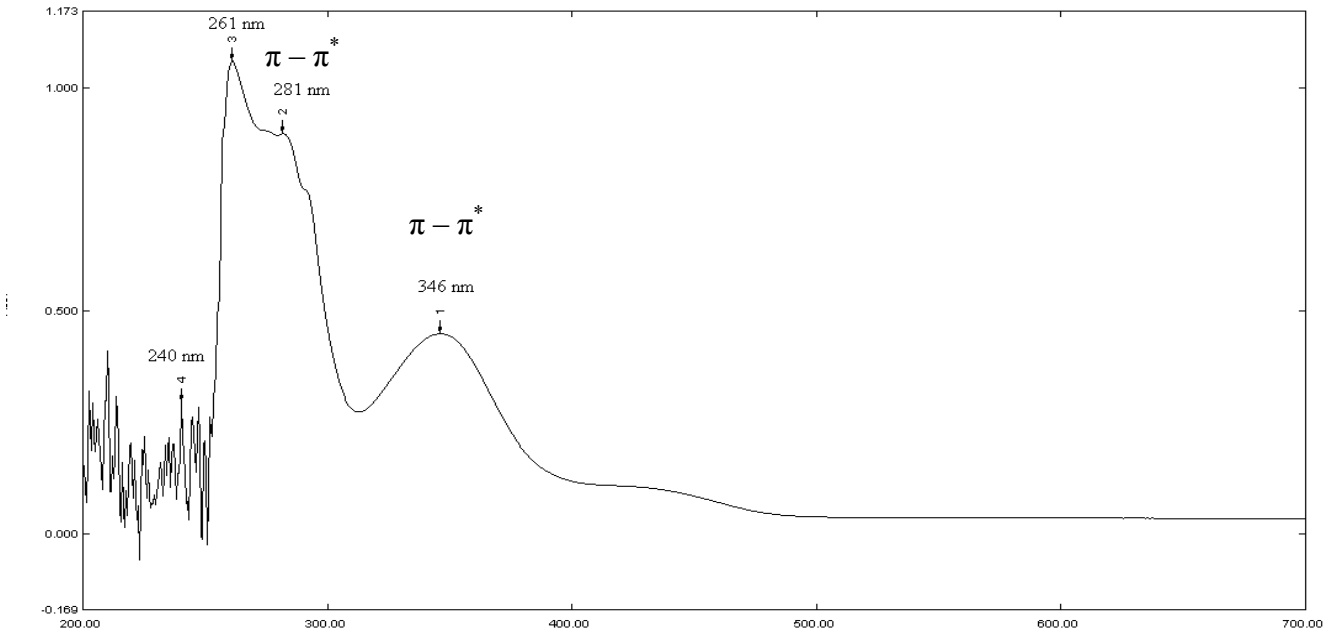

Fig 3.81: UV spectra of: 2-{1-[2-(1H-Indole-3-yl)-ethylimino]-ethyl}-4-methoxy phenol (TOMeHAP)

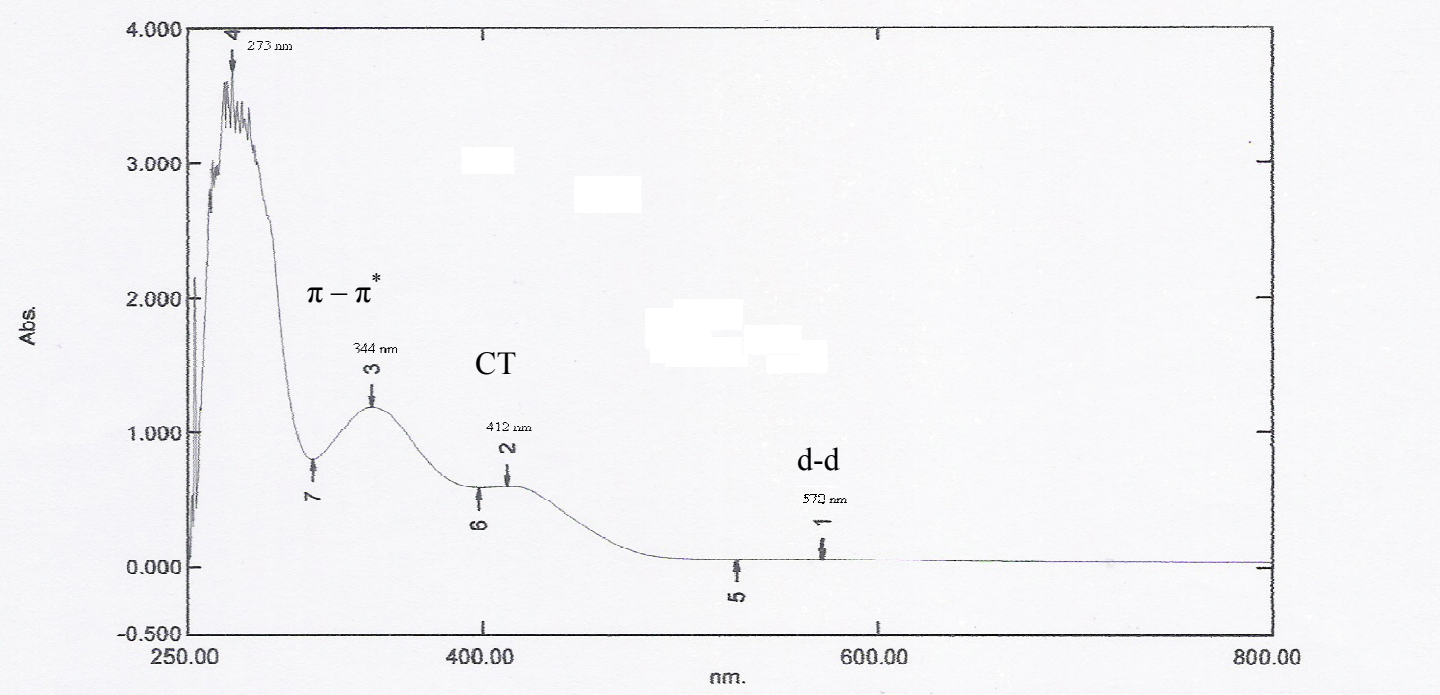

Fig 3.82: UV spectra of: bis{2-{1-[2-(1H-Indole-3-yl)-ethylimino]-ethyl}-4-methoxyphenolato-k^2N,O}Ni(II): $(TOMeHAP)_2Ni$

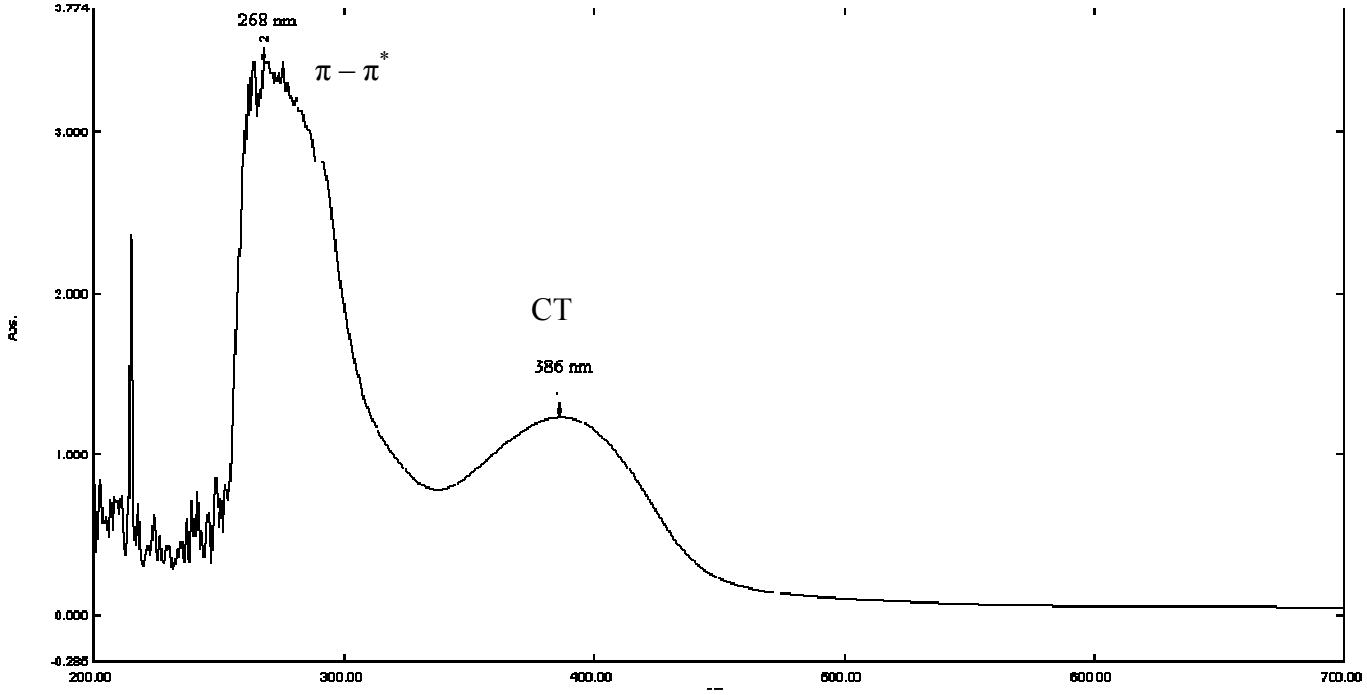

Fig 3.83: UV spectra of: bis{2-{1-[2-(1H-Indole-3-yl)-ethylimino]-ethyl}-4-methoxyphenolato-k^2N,O}Cu(II): $(TOMeHAP)_2Cu$

3.4.8 UV-Vis Spectra of the ligand:

4-choloro- 2-{1-[2-(1H-Indole-3-yl)-ethylimino]-ethyl}- phenol (TClHAP) and its nickel and copper complexes:

Table (3.35) summarizes the main spectral bands of the compounds with their tentative assignments. Full spectra were provided in figures (3.84, 3.85 and 3.86)

Table 3.35:

UV-Vis Spectra of the ligand: 4-choloro- 2-{1-[2-(1H-Indole-3-yl)-ethylimino]-ethyl}-phenol (TClHAP) and its nickel and copper complexes:

Compound	Conc (mol/L)	ε ($mol^{-1}Lcm^{-1}$)	λ max (nm)	Assignment
TClHAP	1.51×10^{-4}	1.87×10^{3}	405	n- π^*
		3.20×10^{3}	329	$\pi-\pi^*$ ligand
		7.45×10^{3}	275	$\pi-\pi^*$ ligand
		8.21×10^{3}	260	-
$(TClHAP)_2Ni$		179.45	557	d-d transition
		7.01×10^{3}	392	CT
		6.14×10^{3}	333	$\pi-\pi^*$
		2.47×10^{4}	270	$\pi-\pi^*$ benzene ring
$(TClHAP)_2Cu$	3.0×10^{-3}	229.14	615	d-d transition
		1.22×10^{4}	368	CT
		2.60×10^{4}	283	$\pi-\pi^*$ ligand
		2.75×10^{4}	260	$\pi-\pi^*$ ligand

The ligand spectrum reveals four main bands. The band at 405 nm is related to n- π^* transition, whereas the band at 329 nm is assigned to $\pi-\pi^*$ which involves molecular orbitals essentially localized on the C=N group and the benzene ring. The strong absorptions at 275 nm and 260 nm were assigned to $\pi-\pi^*$ transitions of the benzene ring [60].

Differences are observed in the UV-Vis. Spectra of the nickel complex when compared with that of the corresponding free ligand. The n- π^* transition of the ligand was obscured by the strong charge transfer band at 392 nm. The $\pi - \pi^*$ type of transition due to –C=N chromophore shifts to 333 nm on coordination. There is a weak intensity band at 557 nm which is related to d-d transitions.

The copper complex spectra show four main bands. The band at 615 nm is related to a d-d transition expected for pseudotetrahedral geometry [70]. The strong band at 368 nm could be assigned to LMCT, whereas the bands at 283 nm and 260 nm were assigned to $\pi - \pi^*$ transitions of the ligand.

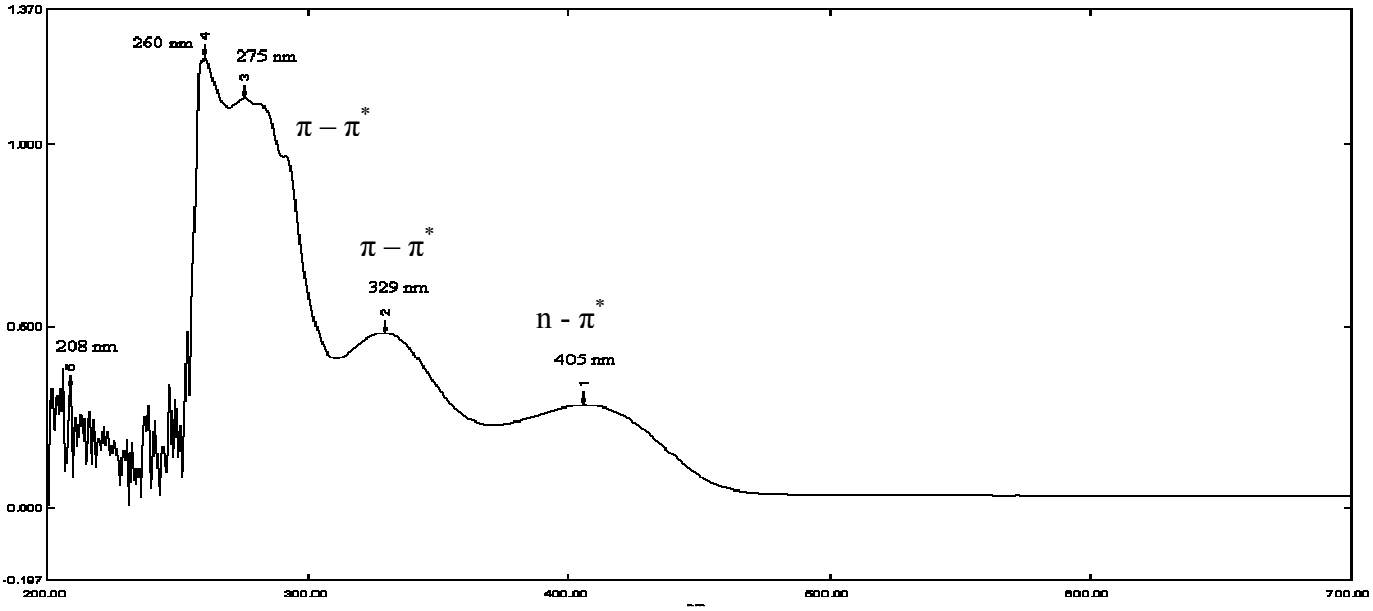

Fig 3.84: UV spectra of: 2-{1-[2-(1H-Indole-3-yl)-ethylimino]-ethyl}-4-chloro phenol (TClHAP)

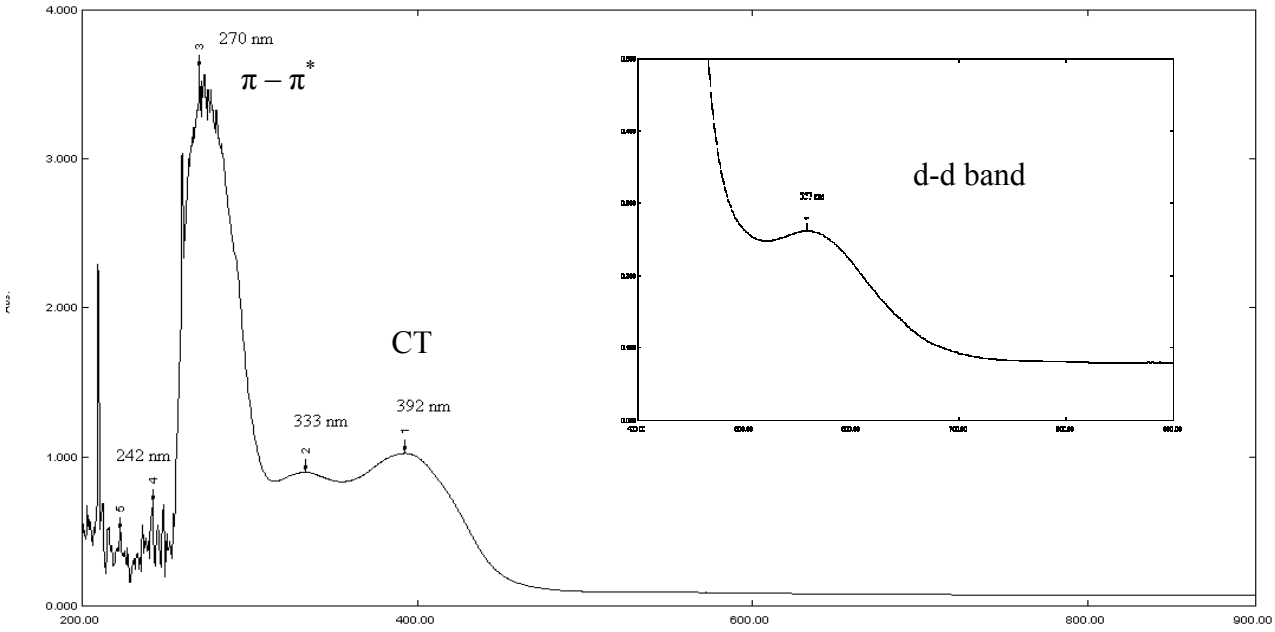

Fig 3.85: UV-Vis spectra of: bis{2-{1-[2-(1H-Indole-3-yl)-ethylimino]-ethyl}-4-chlorophenolato-k^{2}N,O}Ni(II): $(TClHAP)_2Ni$

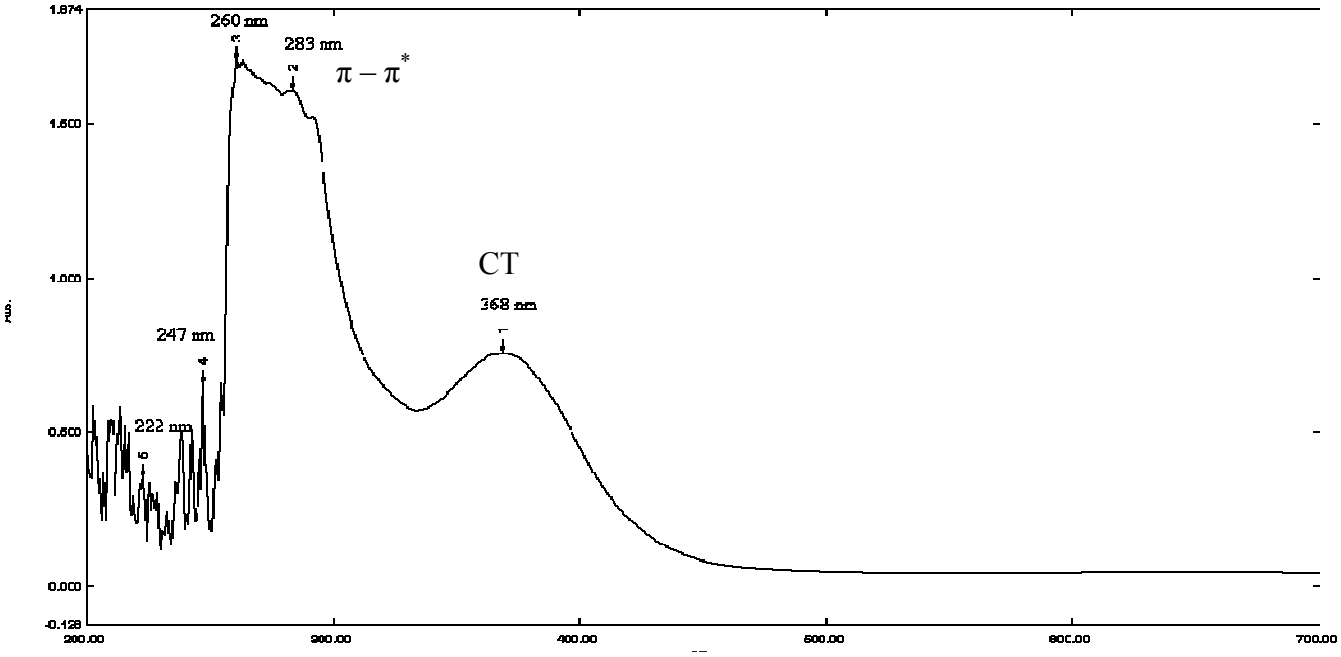

Fig 3.86: UV-Vis spectra of: bis{2-{1-[2-(1H-Indole-3-yl)-ethylimino]-ethyl}-4-chlorophenolato-k^{2}N,O}Cu(II): $(TClHAP)_2Cu$

3.4.9 UV-Vis Spectra of the ligand:

4-bromo- 2-{1-[2-(1H-Indole-3-yl)-ethylimino]-ethyl}- phenol (TBrHAP) and its copper complex:

The main spectral bands were summarized in table (3.36), and the complete spectra were shown in figures (3.87 and 3.88).

Table 3.36:

UV-Vis Spectra of: 4-bromo- 2-{1-[2-(1H-Indole-3-yl)-ethylimino]-ethyl}- phenol (TBrHAP) and its copper complex:

Compound	Conc (mol/L)	ε ($mol^{-1}Lcm^{-1}$)	λ max (nm)	Assignment
TBrHAP	3.35×10^{-4}	823.8	405	$n - \pi^*$
		1.16×10^{3}	330	$\pi - \pi^*$ imino group
		2.81×10^{3}	275	$\pi - \pi^*$ ligand
		3.33×10^{3}	259	$\pi - \pi^*$ ligand
$(TBrHAP)_2Cu$	1.5410^{-4}	7.86×10^{3}	364	CT
		2.54×10^{4}	270	$\pi - \pi^*$

In the spectra of the ligand, the bands between 259-275 nm were attributed to benzene $\pi - \pi^*$ transitions [56, 76]. The band at 405 nm is assigned to $n - \pi^*$ transition, associated with the azomethine chromophore, whereas the band at 330 nm could be related to the imino $\pi - \pi^*$ transition.

In the copper complex, the n – π^* band of the ligand, was obscured or disappeared, probably because of the ligand imino-nitrogen coordination to the copper ion. The intense band at 364 nm was associated with a charge transfer between the metal and the ligand. The imino $\pi - \pi^*$ transitions in the complex were also shifted to some extent confirming the ligand bonding to the copper ion through the imino nitrogen atom. The d-d bands were not observed due to the low concentration of the complex solution.

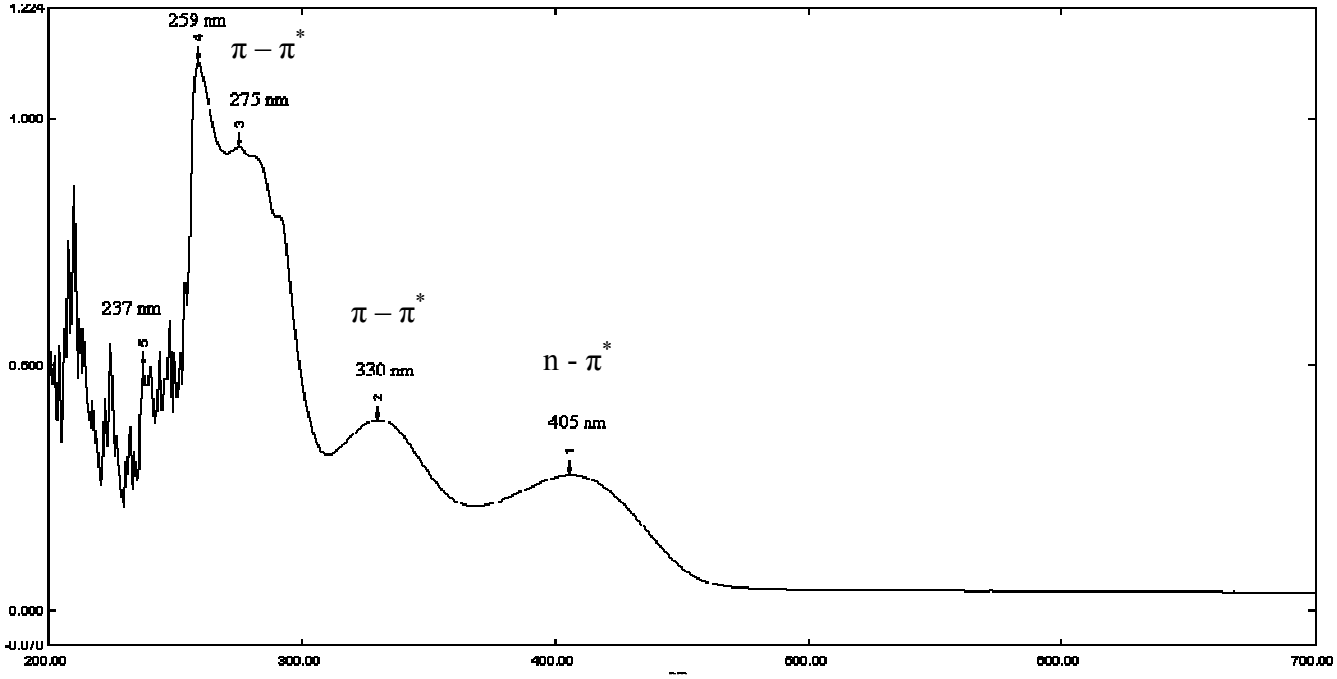

Fig 3.87: UV spectra of: 4-Bromo-2-{1-[2-(1H-Indole-3-yl)-ethylimino]-ethyl}-phenol (TBrHAP)

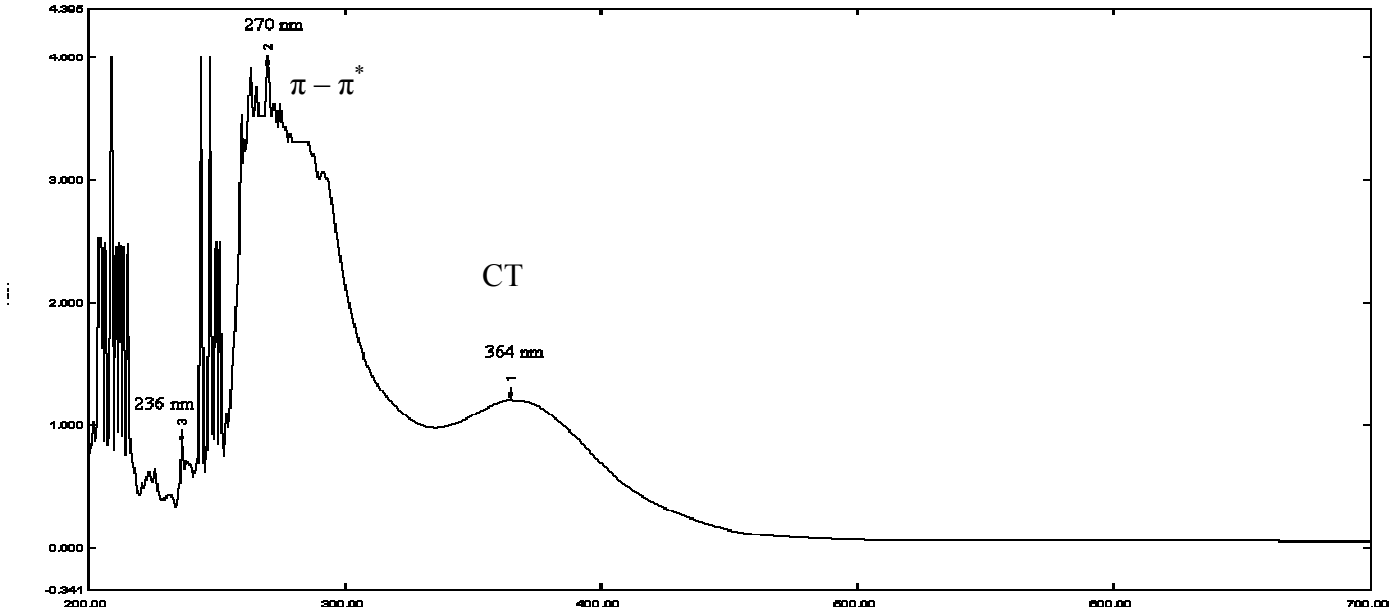

Fig 3.88: UV spectra of: bis{2-{1-[2-(1H-Indole-3-yl)-ethylimino]-ethyl}-4-bromophenolato-k^2N,O}Cu(II): $(TBrHAP)_2Cu$

3.5. X-ray structures of the ligands and complexes:

Only the successful attempts to re-crystallize the compounds were described here.

3.5.1 Crystal structure of the ligand: 1H-Indole-3-ethylene-5-nitrosalicylaldimine (TNS):

Crystal data and structure refinement for the ligand were summarized in table (3.37), and bond lengths and bond angles are given in tables (3.38, 3.39)

Table 3.37:

Crystal data and structure refinement for TNS:

Identification code	TNS
Empirical formula	C17H15N3O3
Formula weight	309.32
Temperature	139 (2) K
Wavelength	0.71073 A
Crystal system, space group	Monoclinic, C2/c
Unit cell dimensions	a = 14.5990 (7) A alpha = 90 deg.
	b = 9.5027 (5) A beta = 95.712 (2) deg.
	c = 21.5373 (10) A gamma = 90 deg.
Volume	2973.0 (3) A^3
Z, Calculated density	8, 1.382 Mg/m^3
Absorption coefficient	0.10 mm^{-1}
F(000)	1296
Crystal size	0.51 × 0.30 × 0.19 mm
Theta range for data collection	5.1–59.5 deg.
Limiting indices	$h = -14 \rightarrow 18$, $k = -12 \rightarrow 9$, $l = -27 \rightarrow 26$
Reflections collected / unique	6383 / 3312 [R(int) = 0.023]
Completeness to theta = 25.00	100.0 %
Absorption correction	none
Refinement method	Full-matrix least-squares on F^2
Data / restraints / parameters	3312 / 2 / 216

Goodness-of-fit on F^2	1.06
Final R indices [I>2sigma(I)]	R1 = 0.049, wR2 = 0.161
Largest diff. peak and hole	1.18 and -0.27 e.A^-3

Table 3.38:

Bond lengths (Å) for TNS:

O1—C1	1.264 (2)	C7—H7	0.9500
O2—N1	1.231 (2)	C8—C9	1.527 (3)
O3—N1	1.237 (2)	C8—H8A	0.9900
N1—C4	1.433 (2)	C8—H8B	0.9900
N2—C7	1.292 (2)	C9—C10	1.498 (2)
N2—C8	1.454 (2)	C9—H9A	0.9900
N2—H2N	0.883 (10)	C9—H9B	0.9900
N3—C12	1.363 (3)	C10—C11	1.359 (3)
N3—C11	1.371 (2)	C10—C17	1.430 (2)
N3—H3N	0.879 (10)	C11—H11	0.9500
C1—C2	1.439 (2)	C12—C13	1.396 (3)
C1—C6	1.446 (3)	C12—C17	1.407 (2)
C2—C3	1.355 (3)	C13—C14	1.375 (3)
C2—H2	0.9500	C13—H13	0.9500
C3—C4	1.402 (3)	C14—C15	1.389 (4)
C3—H3	0.9500	C14—H14	0.9500

C4—C5	1.375 (2)	C15—C16	1.375 (3)
C5—C6	1.393 (3)	C15—H15	0.9500
C5—H5	0.9500	C16—C17	1.394 (3)
C6—C7	1.421 (2)	C16—H16	0.9500

Table (3.39): Bond angles (Deg) for TNS:

O2—N1—O3	121.71 (18)	N2—C8—H8B	109.5
O2—N1—C4	118.51 (17)	C9—C8—H8B	109.5
O3—N1—C4	119.78 (16)	H8A—C8—H8B	108.1
C7—N2—C8	125.09 (16)	C10—C9—C8	111.78 (14)
C7—N2—H2N	114.5 (16)	C10—C9—H9A	109.3
C8—N2—H2N	120.4 (16)	C8—C9—H9A	109.3
C12—N3—C11	108.79 (15)	C10—C9—H9B	109.3
C12—N3—H3N	127.4 (16)	C8—C9—H9B	109.3
C11—N3—H3N	123.3 (16)	H9A—C9—H9B	107.9
O1—C1—C2	121.60 (16)	C11—C10—C17	106.10 (15)
O1—C1—C6	122.27 (16)	C11—C10—C9	127.56 (17)
C2—C1—C6	116.12 (16)	C17—C10—C9	126.29 (17)
C3—C2—C1	122.05 (17)	C10—C11—N3	110.38 (16)
C3—C2—H2	119.0	C10—C11—H11	124.8
C1—C2—H2	119.0	N3—C11—H11	124.8

C2—C3—C4	119.64 (16)	N3—C12—C13	130.60 (18)
C2—C3—H3	120.2	N3—C12—C17	107.60 (15)
C4—C3—H3	120.2	C13—C12—C17	121.76 (19)
C5—C4—C3	121.81 (17)	C14—C13—C12	117.22 (19)
C5—C4—N1	119.53 (17)	C14—C13—H13	121.4
C3—C4—N1	118.65 (16)	C12—C13—H13	121.4
C4—C5—C6	119.41 (17)	C13—C14—C15	121.91 (19)
C4—C5—H5	120.3	C13—C14—H14	119.0
C6—C5—H5	120.3	C15—C14—H14	119.0
C5—C6—C7	119.05 (16)	C16—C15—C14	120.9 (2)
C5—C6—C1	120.95 (16)	C16—C15—H15	119.6
C7—C6—C1	119.97 (16)	C14—C15—H15	119.6
N2—C7—C6	123.14 (17)	C15—C16—C17	119.08 (19)
N2—C7—H7	118.4	C15—C16—H16	120.5
C6—C7—H7	118.4	C17—C16—H16	120.5
N2—C8—C9	110.52 (14)	C16—C17—C12	119.15 (17)
N2—C8—H8A	109.5	C16—C17—C10	133.65 (16)
C9—C8—H8A	109.5	C12—C17—C10	107.12 (16)

Hydrogen bond geometry:

D—H……A	D—H	H……..A	D……A	D—H…..A
N2—H2n….O1	0.88 (1)	1.87 (2)	2.602 (2)	139 (2)
N3—H3n…O2i	0.88 (1)	2.36 (2)	3.027 (2)	133 (2)
N3—H3n…O3i	0.88 (1)	2.23 (1)	3.100 (2)	171 (2)

Symmetry code: (i) x - 1; y; z.

The carbon-bound H atoms were placed at calculated positions (C–H 0.95 Å), and were included in the refinement in the riding model approximation with *U*(H) set to 1.2*U*eq(C). The amino hydrogen atom was located in a difference fourier map, and was refined with a distance restraint of N–H 0.88±0.01 Å [74].

The final difference fourier map had a large peak at 1.5 Å from O1 and H2*n*. This peak is not near the nitro group even though this group has larger thermal parameters than the rest of the molecule. All e.s.d.'s (except the e.s.d. in the dihedral angle between two l.s. planes) are estimated using the full covariance matrix. The cell e.s.d.'s are taken into account individually in the estimation of e.s.d.'s in distances, angles and torsion angles; correlations between e.s.d.'s in cell parameters are only used when they are defined by crystal symmetry. An approximate (isotropic) treatment of cell e.s.d.'s is used for estimating e.s.d.'s involving l.s. planes.

As it can be seen from the X-ray perspective attached (Figure (3.89)) the ligand exists in the zwitterionic form with the phenol H atom transferred to the imine group. Adjacent zwitterions are linked into a linear chain running along the axis by an indole–hydroxy N—H···O hydrogen bond [3.100 (2) A°]. The C10-C11 bond length in the indolic group

is 1.36 Å slightly shorter than a normal aromatic C-C bond (1.39 Å) as it has been reported for the ligand TS described earlier [75], and the phenomena also has been described in a radiation protector tryptamine hydrochloride [76].

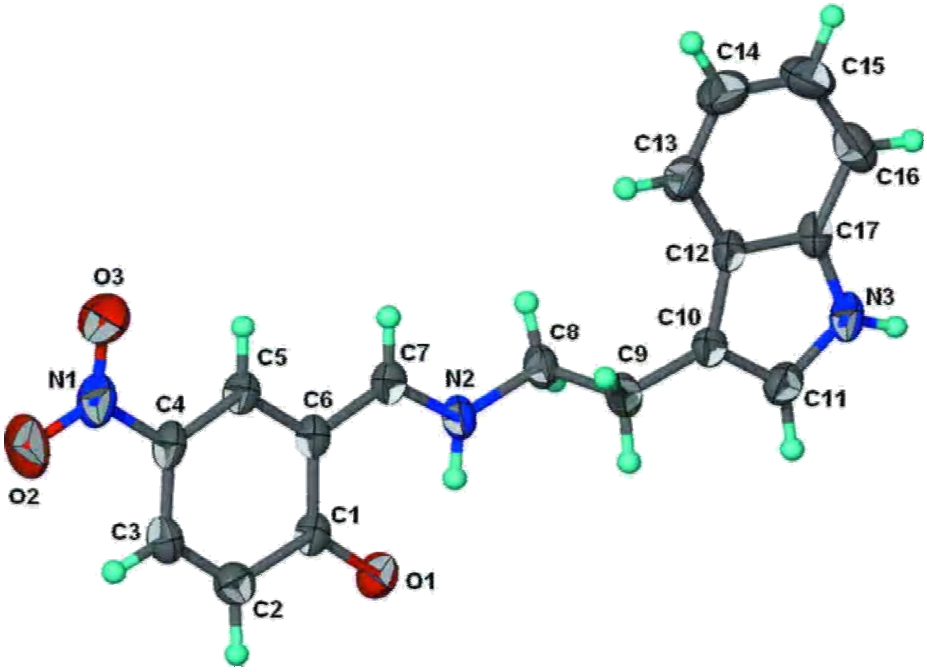

Fig 3.89: X-ray perspective of: 1H-Indole-3-ethylene-5-nitrosalicylaldimine (TNS)

3.5.2 Crystal structure of the complex: Bis(1H-Indole-3-ethylenesalicylaldiminato-k^2N,O)Ni(II) $(TS)_2Ni$:

The crystal data and structure refinement for the complex were shown in table (3.40), and bond lengths and bond angles were summarized in tables (3.41 and 3.42). Thermal ellipsoid plot for the complex was given in figure (3.90).

Table 3.40:

Crystal data and structure refinement for $(TS)_2Ni$:

Identification code	$(TS)_2Ni$
Empirical formula	[Ni(C17H15N2O)2]_2C3H7NO
Formula weight	731.52
Temperature	103 (2) K
Wavelength	0.71073A
Crystal system, space group	Monoclinic, C2/c
Unit cell dimensions	a = 38.927 (2)A alpha = 90 deg.
	b = 5.6999 (3)A beta = 98.489 (2)deg.
	c = 15.7560 (8)A gamma = 90 deg.
Volume	3457.6 (3)A^3
Z, Calculated density	4, 1.405 Mg/m^3
Absorption coefficient	0.61 mm^{-1}
F(000)	1544
Crystal size	0.70 × 0.32 × 0.07mm
Theta range for data collection	2.6–28.5 deg.
Limiting indices	$h = -48 \rightarrow 50$, $k = -7 \rightarrow 5$, $l = -19 \rightarrow 20$
Reflections collected / unique	3875 / 2900 [R(int) = 0.030]
Completeness to theta = 25.00	100.0 %
Absorption correction	multi-scan (SADABS; Sheldrick, 1996)
Max. and min. transmission	0.958 and 0.673
Refinement method	Full-matrix least-squares on F^2

Data / restraints / parameters	3875 / 0 / 234
Goodness-of-fit on F^2	1.03
Final R indices [I>2sigma(I)]	R1 = 0.048, wR2 = 0.133
Largest diff. peak and hole	0.82and −0.48 e.A^-3

Table 3.41:

Bond lengths (Å) for $(TS)_2Ni$:

Ni1—O1	1.829 (2)	C8—H8A	0.9900
Ni1—N1	1.922 (2)	C8—H8B	0.9900
O1—C1	1.310 (3)	C9—C11	1.490 (4)
O2—C18	1.184 (5)	C9—H9A	0.9900
N1—C7	1.297 (3)	C9—H9B	0.9900
N1—C8	1.479 (3)	C10—C11	1.368 (4)
N3—C17	1.363 (4)	C10—H10	0.9500
N3—C10	1.373 (4)	C11—C12	1.433 (4)
N3—H3N	0.8800	C12—C13	1.397 (4)
N4—C18	1.320 (4)	C12—C17	1.423 (4)
N4—C19	1.431 (4)	C13—C14	1.375 (4)
N4—C20	1.445 (4)	C13—H13	0.9500
C1—C2	1.408 (4)	C14—C15	1.412 (5)
C1—C6	1.410 (4)	C14—H14	0.9500
C2—C3	1.383 (4)	C15—C16	1.373 (5)
C2—H2	0.9500	C15—H15	0.9500

C3—C4	1.394 (4)	C16—C17	1.393 (4)
C3—H3	0.9500	C16—H16	0.9500
C4—C5	1.372 (4)	C18—H18	0.9500
C4—H4	0.9500	C19—H19A	0.9800
C5—C6	1.405 (4)	C19—H19B	0.9800
C5—H5	0.9500	C19—H19C	0.9800
C6—C7	1.432 (4)	C20—H20A	0.9800
C7—H7	0.9500	C20—H20B	0.9800
C8—C9	1.524 (4)	C20—H20C	0.9800

Table 3.42:

Bond angles for $(TS)_2Ni$:

O1i—Ni1—O1	180.00 (10)	H9A—C9—H9B	108.1
O1i—Ni1—N1i	92.81 (9)	C11—C10—N3	110.8 (3)
O1—Ni1—N1i	87.19 (9)	C11—C10—H10	124.6
O1i—Ni1—N1	87.19 (9)	N3—C10—H10	124.6
O1—Ni1—N1	92.81 (9)	C10—C11—C12	105.9 (2)
N1i—Ni1—N1	180.000 (1)	C10—C11—C9	127.1 (3)
C1—O1—Ni1	127.41 (19)	C12—C11—C9	127.0 (2)
C7—N1—C8	114.6 (2)	C13—C12—C17	118.4 (3)
C7—N1—Ni1	124.0 (2)	C13—C12—C11	134.6 (3)
C8—N1—Ni1	121.26 (17)	C17—C12—C11	107.0 (2)
C17—N3—C10	108.6 (2)	C14—C13—C12	119.3 (3)

C17—N3—H3N	125.7	C14—C13—H13	120.3
C10—N3—H3N	125.7	C12—C13—H13	120.3
C18—N4—C19	120.9 (3)	C13—C14—C15	121.3 (3)
C18—N4—C20	121.4 (3)	C13—C14—H14	119.3
C19—N4—C20	117.6 (3)	C15—C14—H14	119.3
O1—C1—C2	118.5 (3)	C16—C15—C14	120.9 (3)
O1—C1—C6	123.2 (2)	C16—C15—H15	119.6
C2—C1—C6	118.3 (3)	C14—C15—H15	119.6
C3—C2—C1	120.4 (3)	C15—C16—C17	117.9 (3)
C3—C2—H2	119.8	C15—C16—H16	121.1
C1—C2—H2	119.8	C17—C16—H16	121.1
C2—C3—C4	120.9 (3)	N3—C17—C16	130.1 (3)
C2—C3—H3	119.5	N3—C17—C12	107.7 (3)
C4—C3—H3	119.5	C16—C17—C12	122.2 (3)
C5—C4—C3	119.5 (3)	O2—C18—N4	127.9 (4)
C5—C4—H4	120.2	O2—C18—H18	116.1
C3—C4—H4	120.2	N4—C18—H18	116.1
C4—C5—C6	120.7 (3)	N4—C19—H19A	109.5
C4—C5—H5	119.6	N4—C19—H19B	109.5
C6—C5—H5	119.6	H19A—C19—H19B	109.5
C5—C6—C1	120.0 (3)	N4—C19—H19C	109.5
C5—C6—C7	119.2 (3)	H19A—C19—H19C	109.5
C1—C6—C7	120.8 (2)	H19B—C19—H19C	109.5

N1—C7—C6	126.2 (3)	N4—C20—H20A	109.5
N1—C7—H7	116.9	N4—C20—H20B	109.5
C6—C7—H7	116.9	H20A—C20—H20B	109.5
N1—C8—C9	113.5 (2)	N4—C20—H20C	109.5
N1—C8—H8A	108.9	H20A—C20—H20C	109.5
C9—C8—H8A	108.9	H20B—C20—H20C	109.5
N1—C8—H8B	108.9	H9A—C9—H9B	108.1
C9—C8—H8B	108.9	C11—C10—N3	110.8 (3)
H8A—C8—H8B	107.7	C11—C10—H10	124.6
C11—C9—C8	110.4 (2)	N3—C10—H10	124.6
C11—C9—H9A	109.6	C10—C11—C12	105.9 (2)
C8—C9—H9A	109.6	C10—C11—C9	127.1 (3)
C11—C9—H9B	109.6	C12—C11—C9	127.0 (2)
C8—C9—H9B	109.6	C13—C12—C17	118.4 (3)

Symmetry codes: (i) −*x*+1/2, −*y*+3/2, −*z*+1.

The carbon-bound H atoms were placed at calculated positions (C—H = 0.95–0.98 Å) and were included in the refinement in the riding-model approximation, with *U*(H) set to 1.2–1.5*U*eq(C). The amino H atom also similarly generated [N—H = 0.88Å and *U*(H) = 1.2*U*eq(N)].

The nickel atom lies on a centre of inversion. It is N,O-chelated by the deprotonated Schiff base 2-[2-(1H-indol-3-yl)ethyliminomethyl] phenolate ligand in a square-planar coordination environment. The molecule is linked to a solvent molecule by an indole–

dimethylformamide N—H·····O hydrogen bond. Deviations in the planarity of the trans NiN_2O_2 group has occurred. The Ni – O distance is 1.83 Å and the Ni – N distance is 1.92 Å, hence the planar coordination around the nickel atom is rhombically distorted with the longer axis along N – Ni – N and shorter along O –Ni – O, with N1-Ni-O1 angle of 92.81 degrees analogous to other planar complexes found in the literature [66, 80, 81]. Upon complexation, the C1-O1 bond distance goes from 1.34 Å in the ligand to 1.31 Å in the complex as a consequence of deprotonation at O1 and formation of the complex. Also as expected the angles in the salicylaldehyde moiety undergo modifications on coordination, for example, the angle O1-C1-C6 in the ligand which was found to be 120.7 ^{o} in the ligand goes to 123.2^{o} as a result of complex formation [58, 82].

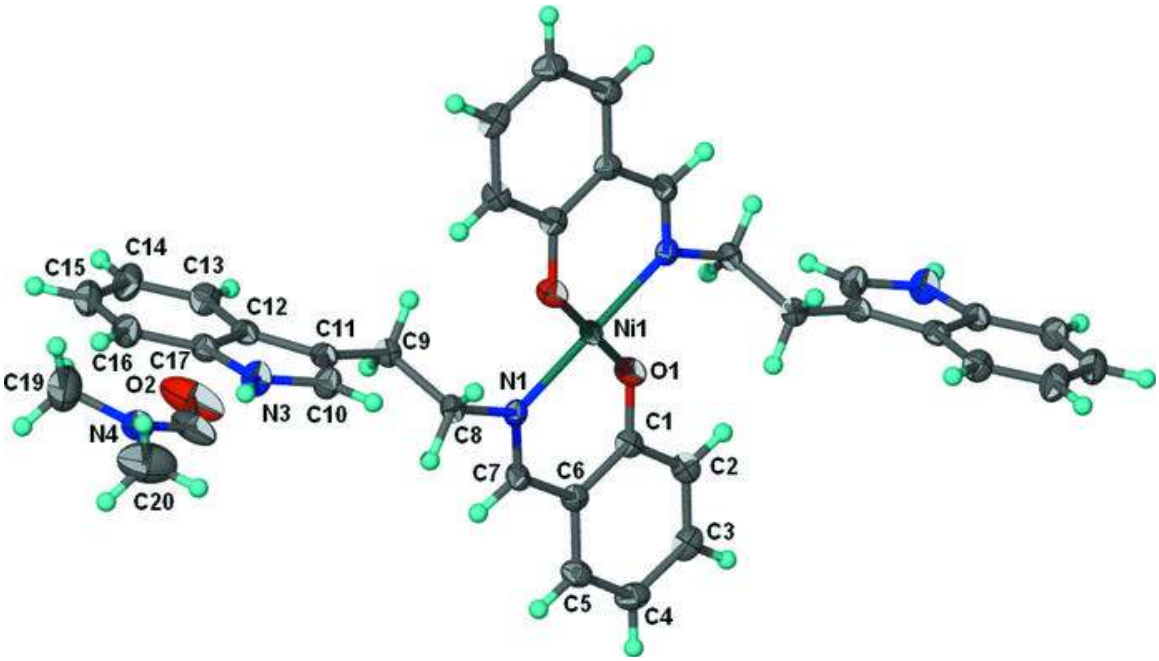

Fig 3.90: Thermal ellipsoid plot of Ni(C17H14N2O)2.2DMF; displacement ellipsoids are drawn at the 70% probability level, and H atoms are shown as spheres of arbitrary radii.

3.5.3 X-ray crystal structure for the complex: Bis{4-chloro-2-[2-(1H-indol-3-yl)ethyliminomethyl] phenolato-κ2N,O}zinc(II): $(TCS)_2Zn$:

Crystal data and structure refinement for the complex were shown in table (3.43), and bond lengths and bond angles were summarized in tables (3.44 and 3.45). Thermal ellipsoid plot for the complex was given in figure (3.91).

Table 3.43:

Crystal data and structure refinement for $(TCS)_2Zn$:

Identification code	$(TCS)_2Zn$
Empirical formula	Zn(C17H14ClN2O)2
Formula weight	660.87
Temperature	128 (2) K
Wavelength	0.71073 A
Crystal system, space group	Monoclinic, C2/c
Unit cell dimensions	a = 25.8989(3) A alpha = 90 deg.
	b = 5.4960(1)A beta = 91.801 (1) deg.
	c = 20.6138(3)A gamma = 90 deg.
Volume	2932.73 (8)A^3
Z, Calculated density	4 , 1.497Mg/m^3
Absorption coefficient	1.06 mm^-1
F(000)	1360
Crystal size	0.50 x 0.30 x 0.17 mm
Theta range for data collection	2.5 —31.2° deg.

Limiting indices	-33<=h<=33 , -6<=k<=7 , -26<=l<=26
Reflections collected / unique	17664 / 3352 [R(int) = 0.025]
Completeness to theta = 25.00	100.0 %
Absorption correction	Multi-scan
Max. and min. transmission	0.840 and 0.714
Refinement method	Full-matrix least-squares on F^2
Data / restraints / parameters	3352 / 14 / 251
Goodness-of-fit on F^2	1.21
Final R indices [I>2sigma(I)]	R1 = 0.025 , wR2 = 0.100
Largest diff. peak and hole	0.55 and - 0.56 e.A^-3

Table 3.44:

Bond lengths (Å) for: $(TCS)_2Zn$

Zn1-O2	1.907(1)	C7-H7	0.994(9)
Zn1-O1	1.907(1)	C8-C9	1.523(2)
Zn1-N1	2.016(1)	C8-H81	0.989(9)
Zn1-N3	2.016(1)	C8-H82	0.994(10)
Cl1-C4	1.745(2)	C9-C10	1.502(2)
O1-C1	1.312(2)	C9-H91	0.998(10)
N1-C7	1.282(2)	C9-H92	1.004(10)
N1-C8	1.469(2)	C10-C11	1.366(3)
C1-C2	1.419(2)	C10-C12	1.439(3)
C1-C6	1.427(2)	C11-H11	0.990(10)

N2-C17	1.374(2)	C12-C13	1.402(3)
N2-C10	1.383(2)	C19-C18	1.415(2)
N2-H2N	0.870(10)	C13-C14	1.379(3)
C2-C3	1.374(2)	C13-H13	0.998(10)
C2-H2	0.994(10)	C15-C16	1.405(3)
C3-C4	1.391(3)	C15-H15	0.990(10)
C3-H3	1.001(10)	C16-C17	1.382(3)
C4-C5	1.370(2)	C16-H16	0.992(10)
C5-C6	1.410(2)	C17-C12	1.398(2)
C5-H5	0.999(10)	C17-H17	0.996(10)
C6-C7	1.453(2)		

Table 3.45:

Bond angles for $(TCS)_2Zn$

O1-Zn1-O2	116.62(8)	N1-C8-H81	108.7(12)
O1-Zn1-N1	95.57(5)	C9-C8-H81	109.5(12)
O1-Zn1-N3	125.55(6)	N1-C8-H82	109.4(14)
O2-Zn1-N1	125.55(6)	C9-C8-H82	110.3(13)
O2-Zn1-N3	95.57(5)	H81-C8-H82	107.8(18)
N1-Zn1-N3	99.56(8)	C10-C9-C8	110.87(15)
C1-O1-Zn1	124.38(11)	C10-C9-H91	109.5(17)
C7-N1-C8	118.25(14)	C8-C9-H91	109.0(16)
C7-N1-Zn1	120.68(11)	C10-C9-H92	110.3(16)

C8-N1-Zn1	119.96(10)	C8-C9-H92	110.3(15)
O1-C1-C2	118.25(15)	H91-C9-H92	107(2)
O1-C1-C6	124.63(15)	C11-C10-C12	106.68(16)
C2-C1-C6	117.12(14)	C11-C10-C9	127.04(19)
C17-N2-C10	109.06(15)	C12-C10-C9	126.20(17)
C17-N2-H2N	125.3(18)	C11-C10-N2	109.81(16)
C10-N2-H2N	125.7(18)	C13-C12-C17	118.94(17)
C3-C2-C1	122.28(16)	C13-C12-C11	134.06(17)
C3-C2-H2	118.2(14)	C17-C12-C11	106.99(15)
C1-C2-H2	119.6(14)	C14-C13-C12	118.76(19)
C2-C3-C4	119.47(15)	C14-C13-H13	120.0(14)
C2-C3-H3	119.0(14)	C12-C13-H13	121.2(14)
C4-C3-H3	121.5(14)	C14-C15-C16	121.4(19)
C5-C4-C3	120.68(16)	C14-C15-H15	118.7(15)
C5-C4-C11	119.65(14)	C16-C15-H15	119.8(15)
C3-C4-C11	119.66(13)	C17-C16-C15	121.4(2)
C4-C5-C6	120.98(16)	C17-C16-H16	120.4(16)
C4-C5-H5	118.2(14)	C15-C16-H16	118.2(16)
C6-C5-H5	120.8(14)	C16-C17-C18	117.02(18)
C5-C6-C1	119.38(14)	C16-C17-H17	121.9(15)
C5-C6-C7	115.93(14)	C16-C17-H17	121.1(15)
C1-C6-C7	124.69(14)	N2-C17-C16	130.10(17)
N1-C7-C6	126.44(15)	N2-C17-C12	107.45(15)

N1-C7-H7	118.8(12)
C6-C7-H7	114.6(12)
N1-C8-C9	111.15(14)

Symmetry codes: (i) –x+1, y ,-z+3/2.

All hydrogen atoms were located in a difference fourier map and were refined with distance restraints of C-H 1.00 Å and N-H 0.88 Å; their temperature factors were freely refined. The Zn atom in the title compound, [Zn(C17H14ClN2O)2], is N,O-chelated by two deprotonated Schiff base monoanionic ligands in a tetrahedral coordination geometry. The Zn atom lies on a special position of site symmetry 2. The chlorine substituent does not lead to significant changes to the bond dimensions of the central metal.O1-Zn1-N1 bond angle was 95.57^{o} considerably different from the normal tetrahedral angle 109^{o} , while the angle O1-Zn1-N3 125.55^{o} more wider than the normal tetrahedral angle. This implies a distorted tetrahedral environment around the zinc atom. Moreover, the Zn1-O bond distance is 1.90 Å while Zn1-N distance is 2.01 Å [80].

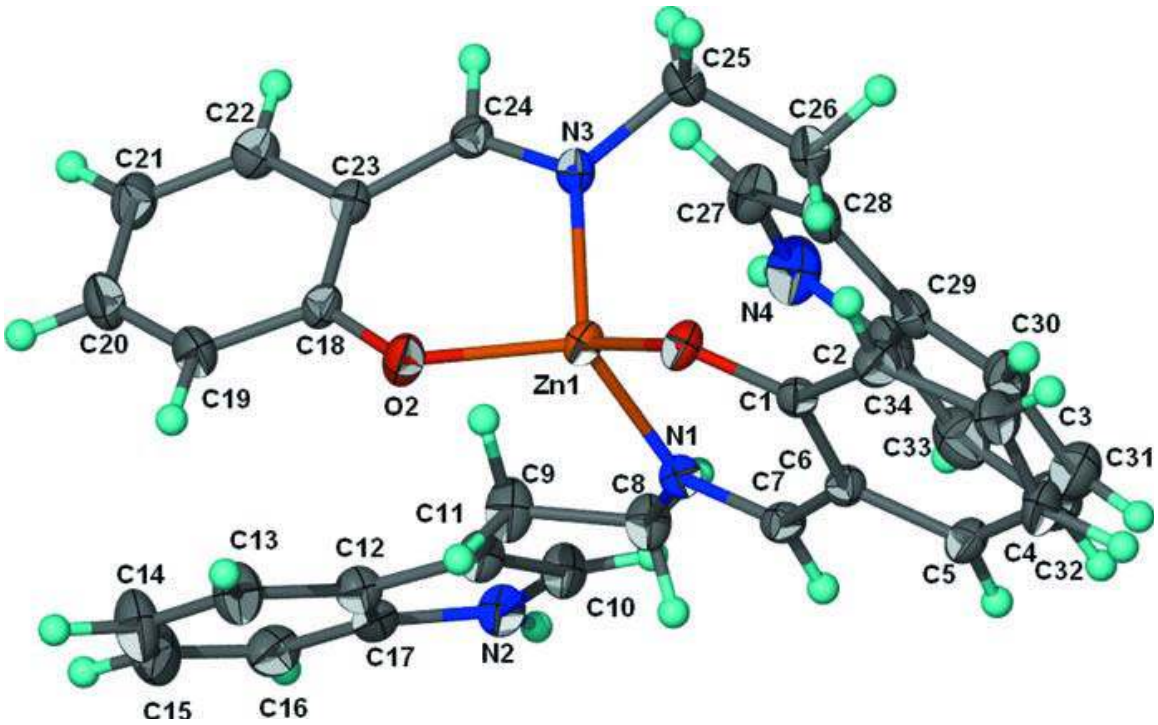

Fig 3.91: Thermal ellipsoid plot of Zn(C17H14ClN2O), displacement ellipsoids are drawn at 50% probability level, and hydrogen atoms are shown as spheres of arbitrary radii.

3.5.4 X-ray crystal structure for the complex:

Bis(1H-Indole-3-ethylene-3-5-di-tertiarybutylsalicylaldiminato-k^{2}N,O)Zn(II) (TTET)$_2$Zn:

Crystal data and structure refinement for the complex were shown in table (3.46), and bond lengths and bond angles were summarized in tables (3.47 and 3.38). Thermal ellipsoid plot for the complex was given in figure (3.92).

Table: 3.46:

Crystal data and structure refinement for: $(TTET)_2Zn$ complex:

Identification code	$(TTET)_2Zn$
Empirical formula	C27 H37 N2 O2 S Zn0.50
Formula weight	486.33
Temperature	100(2) K
Wavelength	0.71073 A
Crystal system, space group	Orthorhombic, Pbcn
Unit cell dimensions	a = 19.9694(4) A alpha = 90 deg.
	b = 8.1019(2) A beta = 90 deg.
	c = 32.7530(6) A gamma = 90 deg.
Volume	5299.11(19) A^3
Z, Calculated density	8, 1.219 Mg/m^3
Absorption coefficient	0.589 mm^-1
F(000)	2080
Crystal size	0.40 x 0.07 x 0.03 mm
Theta range for data collection	2.04 to 30.51 deg.
Limiting indices	-26<=h<=27, -11<=k<=11, -46<=l<=46
Reflections collected / unique	55274 / 7854 [R(int) = 0.0793]
Completeness to theta = 25.00	100.0 %
Absorption correction	Semi-empirical from equivalents
Max. and min. transmission	0.9826 and 0.7986

Refinement method	Full-matrix least-squares on F^2
Data / restraints / parameters	7854 / 78 / 336
Goodness-of-fit on F^2	1.019
Final R indices [I>2sigma(I)]	R1 = 0.0560, wR2 = 0.1271
R indices (all data)	R1 = 0.0996, wR2 = 0.1485
Largest diff. peak and hole	0.803 and -0.606 e.A^-3

Table 3.47:

Bond lengths (Å) for $(TTET)_2Zn$ complex:

Zn-O(1)	1.9121(15)	C(13)-H(13)	0.9500
Zn-N(1)	1.993(2)	C(14)-C(15)	1.399(5)
N(1)-C(7)	1.281(3)	C(14)-H(14)	0.9500
N(1)-C(8)	1.468(3)	C(15)-C(16)	1.369(5)
O(1)-C(1)	1.315(3)	C(15)-H(15)	0.9500
C(1)-C(6)	1.427(3)	C(16)-C(17)	1.395(4)
C(1)-C(2)	1.433(3)	C(16)-H(16)	0.9500
C(2)-C(3)	1.385(3)	C(20)-C(22)	1.526(4)
C(2)-C(20)	1.540(3)	C(20)-C(23)	1.528(4)
C(3)-C(4)	1.409(3)	C(20)-C(21)	1.538(4)
C(3)-H(3)	0.9500	C(21)-H(21A)	0.9800
C(4)-C(5)	1.371(3)	C(21)-H(21B)	0.9800
C(4)-C(40)	1.528(3)	C(21)-H(21C)	0.9800
C(5)-C(6)	1.412(3)	C(22)-H(22A)	0.9800

C(5)-H(5)	0.9500	C(22)-H(22B)	0.9800
C(6)-C(7)	1.443(3)	C(22)-H(22C)	0.9800
C(7)-H(7)	0.9500	C(23)-H(23A)	0.9800
C(8)-C(9)	1.493(4)	C(23)-H(23B)	0.9800
C(8)-H(8A)	0.9900	C(23)-H(23C)	0.9800
C(8)-H(8B)	0.9900	C(40)-C(41)	1.492(7)
C(9)-C(11)	1.501(3)	C(40)-C(43)	1.515(7)
C(9)-H(9A)	0.9900	C(40)-C(42)	1.610(8)
C(9)-H(9B)	0.9900	C(41)-H(41A)	0.9800
N(2)-C(17)	1.370(3)	C(41)-H(41B)	0.9800
N(2)-C(10)	1.371(3)	C(41)-H(41C)	0.9800
N(2)-H(2)	0.8800	C(42)-H(42A)	0.9800
C(10)-C(11)	1.367(4)	C(42)-H(42B)	0.9800
C(10)-H(10)	0.9500	C(42)-H(42C)	0.9800
C(11)-C(12)	1.435(4)	C(43)-H(43A)	0.9800
C(12)-C(13)	1.402(4)	C(43)-H(43B)	0.9800
C(12)-C(17)	1.410(3)	C(43)-H(43C)	0.9800
C(13)-C(14)	1.381(4)	C(13)-H(13)	0.9500

Table 3.48:

Bond angles (Deg.) for $(TTET)_2Zn$ complex:

O(1)-Zn-O(1′)	116.04(10)	C(13)-C(12)-C(11)	133.9(2)
O(1)-Zn-N(1)	95.89(7)	C(17)-C(12)-C(11)	107.0(2)
O(1)#1-Zn-N(1)	122.39(8)	C(14)-C(13)-C(12)	118.1(3)
N(1)-Zn-N(1)#1	105.87(12)	C(14)-C(13)-H(13)	121.0
C(7)-N(1)-C(8)	117.5(2)	C(12)-C(13)-H(13)	121.0
C(7)-N(1)-Zn	120.34(16)	C(13)-C(14)-C(15)	121.7(3)
C(8)-N(1)-Zn	122.07(16)	C(13)-C(14)-H(14)	119.2
C(1)-O(1)-Zn	125.73(14)	C(15)-C(14)-H(14)	119.2
O(1)-C(1)-C(6)	122.7(2)	C(16)-C(15)-C(14)	121.6(3)
O(1)-C(1)-C(2)	119.7(2)	C(16)-C(15)-H(15)	119.2
C(6)-C(1)-C(2)	117.6(2)	C(14)-C(15)-H(15)	119.2
C(3)-C(2)-C(1)	118.5(2)	C(15)-C(16)-C(17)	117.0(3)
C(3)-C(2)-C(20)	120.8(2)	C(15)-C(16)-H(16)	121.5
C(1)-C(2)-C(20)	120.7(2)	C(17)-C(16)-H(16)	121.5
C(2)-C(3)-C(4)	124.7(2)	N(2)-C(17)-C(16)	129.9(2)
C(2)-C(3)-H(3)	117.7	N(2)-C(17)-C(12)	107.6(2)
C(4)-C(3)-H(3)	117.7	C(16)-C(17)-C(12)	122.5(3)
C(5)-C(4)-C(3)	116.2(2)	C(22)-C(20)-C(23)	107.7(2)
C(5)-C(4)-C(40)	122.7(2)	C(22)-C(20)-C(21)	107.1(2)
C(3)-C(4)-C(40)	121.2(2)	C(23)-C(20)-C(21)	110.1(2)
C(4)-C(5)-C(6)	122.7(2)	C(22)-C(20)-C(2)	112.0(2)

C(4)-C(5)-H(5)	118.6	C(23)-C(20)-C(2)	109.9(2)
C(6)-C(5)-H(5)	118.6	C(21)-C(20)-C(2)	110.0(2)
C(5)-C(6)-C(1)	120.3(2)	C(20)-C(21)-H(21A)	109.5
C(5)-C(6)-C(7)	114.7(2)	C(20)-C(21)-H(21B)	109.5
C(1)-C(6)-C(7)	125.0(2)	H(21A)-C(21)-H(21B)	109.5
N(1)-C(7)-C(6)	127.9(2)	C(20)-C(21)-H(21C)	109.5
N(1)-C(7)-H(7)	116.0	H(21A)-C(21)-H(21C)	109.5
C(6)-C(7)-H(7)	116.0	H(21B)-C(21)-H(21C)	109.5
N(1)-C(8)-C(9)	110.3(2)	C(20)-C(22)-H(22A)	109.5
N(1)-C(8)-H(8A)	109.6	C(20)-C(22)-H(22B)	109.5
C(9)-C(8)-H(8A)	109.6	H(22A)-C(22)-H(22B)	109.5
N(1)-C(8)-H(8B)	109.6	C(20)-C(22)-H(22C)	109.5
C(9)-C(8)-H(8B)	109.6	H(22A)-C(22)-H(22C)	109.5
H(8A)-C(8)-H(8B)	108.1	H(22B)-C(22)-H(22C)	109.5
C(8)-C(9)-C(11)	114.2(2)	C(20)-C(23)-H(23A)	109.5
C(8)-C(9)-H(9A)	108.7	C(20)-C(23)-H(23B)	109.5
C(11)-C(9)-H(9A)	108.7	H(23A)-C(23)-H(23B)	109.5
C(8)-C(9)-H(9B)	108.7	C(20)-C(23)-H(23C)	109.5
C(11)-C(9)-H(9B)	108.7	H(23A)-C(23)-H(23C)	109.5
H(9A)-C(9)-H(9B)	107.6	H(23B)-C(23)-H(23C)	109.5
C(17)-N(2)-C(10)	109.0(2)	C(41)-C(40)-C(43)	108.1(4)
C(17)-N(2)-H(2)	125.5	C(41)-C(40)-C(4)	113.0(3)
C(10)-N(2)-H(2)	125.5	C(43)-C(40)-C(4)	114.9(3)

C(11)-C(10)-N(2)	110.1(2)	C(41)-C(40)-C(42)	108.5(4)
C(11)-C(10)-H(10)	125.0	C(43)-C(40)-C(42)	104.8(4)
N(2)-C(10)-H(10)	125.0	C(4)-C(40)-C(42)	107.0(3)
C(10)-C(11)-C(12)	106.3(2)	C(40)-C(41)-H(41A)	109.5
C(10)-C(11)-C(9)	128.3(2)	C(40)-C(41)-H(41B)	109.5
C(12)-C(11)-C(9)	125.4(2)	C(40)-C(41)-H(41C)	109.5
C(13)-C(12)-C(17)	119.1(2)	C(40)-C(42)-H(42A)	109.5
		C(40)-C(42)-H(42B)	109.5

Because the zinc atom lies on a crystallographic 2-fold rotational axis of symmetry, it must be coordinated to two Schiff base ligand molecules. Bonding is through the deprotonated phenolate oxygen atom O1 and the azomethine nitrogen atom N1. Zinc coordination is only approximately tetrahedral, since the angles O1-Zn-O1$^{/}$ (116.04(10)), O1-Zn-N1 (95.89(7)) and N1-Zn-N1$^{/}$ (105.87(12)) differ significantly from the normal tetrahedral angle. The tertiary butyl group, connected to C4 of the salicylaldehyde moiety, is rotationally disordered around C4-C40 bond. Both this molecule and one solvate DMSO molecule are disordered in the crystal structure. The DMSO disorder is complex, but both are adequately modeled. In a similar compound [80], the angle N1-Zn-N1$^{/}$ which is 105.87(12) Å here, is larger than the corresponding angle (99.56(8)) in bis*{*4-chloro-2-[2-(1H-indol-3-yl)ethyliminomethyl] phenolato-*κ*2N, O*}* zinc(II). This may be due to the steric effects exerted by the bulky tertiary butyl groups in the salicylaldehyde moiety.

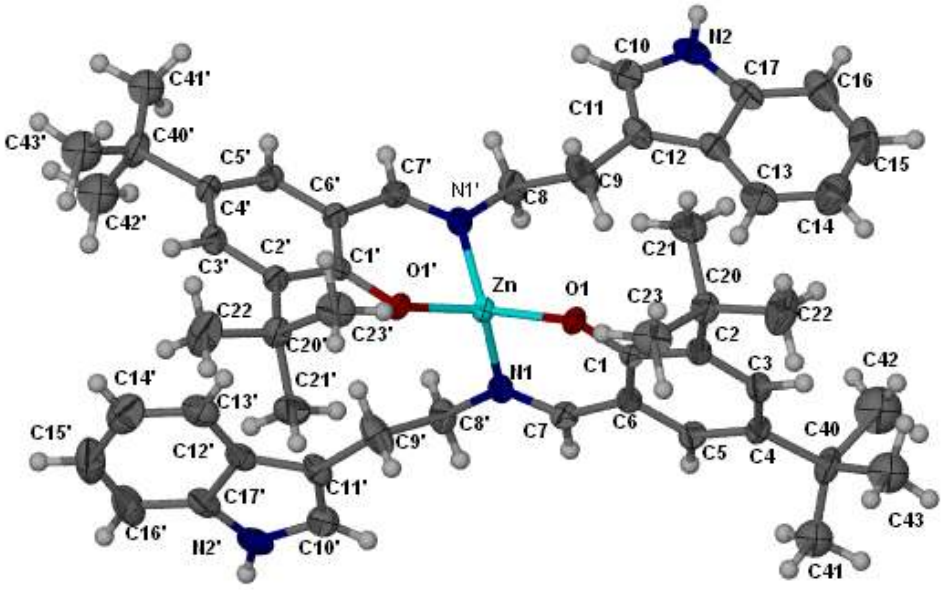

Fig 3.92: Thermal ellipsoid plot of $(TTET)_2Zn$ drawn at the 50% probability level. Hydrogen atoms are shown as spheres of arbitrary radii.

3.5.5 X-ray crystal structure of the complex:

Dichloridobis(2-{1-[2-(1H-indol-3-yl)-ethyliminio]ethyl}phenolate-kO)zinc(II)

$(THAP)_2Zn$:

Crystal data and structure refinement for the complex were shown in table (3.49), and bond lengths and bond angles were summarized in tables (3.50 and 3.51). X-ray molecular structure diagram was shown in figure (3.93).

Table 3.49:

Crystal data and structure refinement for: $(THAP)_2Zn$

Identification code	$(THAP)_2Zn$
Empirical formula	[ZnCl2(C18H18N2O)2]_2C18H18N2O
Formula weight	1249.65
Temperature	295 (2) K
Wavelength	0.71073A
Crystal system, space group	Monoclinic, C2
Unit cell dimensions	a = 25.8073 (4)A alpha = 90 deg.
	b = 9.1754 (1)A beta = 112.566 (1) deg.
	c = 14.3265 (2) A gamma = 90 deg.
Volume	3132.67 (7)A^3
Z, Calculated density	2 Mg/m^3
Absorption coefficient	0.54 mm^{-1}
F(000)	1312
Crystal size	0.10 × 0.06 × 0.05mm
Theta range for data collection	2.4–23.8 deg.
Limiting indices	$h = -33 \rightarrow 32$, $k = -11 \rightarrow 11$, $l = -18 \rightarrow 18$
Reflections collected / unique	36333 / 7190 [R(int) = 0.039]
Completeness to theta = 25.00	100.0 %
Absorption correction	multi-scan
Max. and min. transmission	0.974 and 0.866

Refinement method	Full-matrix least-squares on F^2
Data / restraints / parameters	7190 / 10 / 413
Goodness-of-fit on F^2	1.00
Final R indices [I>2sigma(I)]	R1 = 0.037, wR2 = 0.091
Largest diff. peak and hole	0.36 and −0.30e.A^-3

Table 3.50:

Bond lengths (Å) for: $(THAP)_2Zn$:

Zn1—O1i	1.987 (2)	C14—H14	0.9300
Zn1—O1	1.987 (2)	C15—C16	1.383 (5)
Zn1—Cl1i	2.2260 (6)	C15—H15	0.9300
Zn1—Cl1	2.2260 (6)	C16—C17	1.377 (5)
O1—C1	1.323 (3)	C16—H16	0.9300
O2—C19	1.298 (4)	C17—C18	1.391 (3)
N1—C7	1.290 (3)	C17—H17	0.9300
N1—C9	1.464 (3)	C19—C24	1.414 (4)
N1—H1N	0.86 (1)	C19—C20	1.416 (4)
N2—C12	1.363 (4)	C20—C21	1.365 (6)
N2—C18	1.367 (3)	C20—H20	0.9300
N2—H2N	0.86 (1)	C21—C22	1.358 (6)
N3—C25	1.273 (4)	C21—H21	0.9300
N3—C27	1.500 (7)	C22—C23	1.367 (5)
N3—C27'	1.502 (7)	C22—H22	0.9300

N3—H3N	0.87 (1)	C23—C24	1.413 (4)
N4—C30	1.364 (4)	C23—H23	0.9300
N4—C36	1.373 (4)	C24—C25	1.438 (4)
N4—H4N	0.86 (1)	C25—C26	1.489 (5)
C1—C2	1.401 (3)	C26—H26A	0.9600
C1—C6	1.421 (3)	C26—H26B	0.9600
C2—C3	1.374 (4)	C26—H26C	0.9600
C2—H2	0.9300	C27—C28	1.491 (9)
C3—C4	1.386 (4)	C27—H27A	0.9700
C3—H3	0.9300	C27—H27B	0.9700
C4—C5	1.372 (3)	C28—C29	1.506 (8)
C4—H4	0.9300	C28—H28A	0.9700
C5—C6	1.406 (3)	C28—H28B	0.9700
C5—H5	0.9300	C27'—C28'	1.485 (9)
C6—C7	1.449 (3)	C27'—H27C	0.9700
C7—C8	1.492 (3)	C27'—H27D	0.9700
C8—H8A	0.9600	C28'—C29	1.502 (8)
C8—H8B	0.9600	C28'—H28C	0.9700
C8—H8C	0.9600	C28'—H28D	0.9700
C9—C10	1.520 (4)	C29—C30	1.355 (4)
C9—H9A	0.9700	C29—C31	1.428 (4)
C9—H9B	0.9700	C30—H30	0.9300
C10—C11	1.500 (4)	C31—C32	1.392 (4)

C10—H10A	0.9700	C31—C36	1.406 (3)
C10—H10B	0.9700	C32—C33	1.375 (4)
C11—C12	1.358 (3)	C32—H32	0.9300
C11—C13	1.420 (4)	C33—C34	1.386 (4)
C12—H12	0.9300	C33—H33	0.9300
C13—C14	1.398 (3)	C34—C35	1.365 (5)
C13—C18	1.418 (4)	C34—H34	0.9300
C14—C15	1.374 (4)	C35—C36	1.386 (4)
		C35—H35	0.9300

Table 3.51:

Bond angles for $(THAP)_2Zn$:

O1—Zn1—O1i	99.84 (9)	N2—C18—C17	130.8 (3)
O1—Zn1—Cl1	110.51 (5)	N2—C18—C13	107.3 (2)
O1i—Zn1—Cl1i	110.51 (5)	C17—C18—C13	122.0 (3)
O1—Zn1—Cl1i	110.14 (5)	O2—C19—C24	121.6 (3)
O1i—Zn1—Cl1	110.14 (5)	O2—C19—C20	121.2 (3)
Cl1—Zn1—Cl1i	114.72 (3)	C24—C19—C20	117.2 (3)
C1—O1—Zn1	120.01 (14)	C21—C20—C19	121.5 (4)
C7—N1—C9	127.5 (2)	C21—C20—H20	119.3
C7—N1—H1N	114 (2)	C19—C20—H20	119.3
C9—N1—H1N	118 (2)	C20—C21—C22	121.4 (3)
C12—N2—C18	108.7 (2)	C20—C21—H21	119.3

C12—N2—H2N	125 (2)	C22—C21—H21	119.3
C18—N2—H2N	126 (2)	C21—C22—C23	119.5 (4)
C25—N3—C27	130.9 (9)	C21—C22—H22	120.3
C25—N3—C27'	119.5 (9)	C23—C22—H22	120.3
C27—N3—C27'	25.6 (9)	C22—C23—C24	121.6 (3)
C25—N3—H3N	120 (3)	C22—C23—H23	119.2
C27—N3—H3N	102 (3)	C24—C23—H23	119.2
C27'—N3—H3N	121 (3)	C19—C24—C23	118.8 (3)
C30—N4—C36	109.6 (3)	C19—C24—C25	121.3 (3)
C30—N4—H4N	130 (2)	C23—C24—C25	119.9 (3)
C36—N4—H4N	120 (2)	N3—C25—C24	117.8 (3)
O1—C1—C2	120.9 (2)	N3—C25—C26	120.5 (3)
O1—C1—C6	121.4 (2)	C24—C25—C26	121.7 (3)
C2—C1—C6	117.8 (2)	C25—C26—H26A	109.5
C3—C2—C1	121.8 (2)	C25—C26—H26B	109.5
C3—C2—H2	119.1	H26A—C26—H26B	109.5
C1—C2—H2	119.1	C25—C26—H26C	109.5
C2—C3—C4	120.5 (2)	H26A—C26—H26C	109.5
C2—C3—H3	119.8	H26B—C26—H26C	109.5
C4—C3—H3	119.8	C28—C27—N3	107.4 (8)
C5—C4—C3	119.2 (3)	C28—C27—H27A	110.2
C5—C4—H4	120.4	N3—C27—H27A	110.2
C3—C4—H4	120.4	C28—C27—H27B	110.2

C4—C5—C6	121.9 (3)	N3—C27—H27B	110.2
C4—C5—H5	119.1	H27A—C27—H27B	108.5
C6—C5—H5	119.1	C27—C28—C29	110.8 (10)
C5—C6—C1	118.8 (2)	C27—C28—H28A	109.5
C5—C6—C7	119.9 (2)	C29—C28—H28A	109.5
C1—C6—C7	121.3 (2)	C27—C28—H28B	109.5
N1—C7—C6	119.6 (2)	C29—C28—H28B	109.5
N1—C7—C8	119.2 (2)	H28A—C28—H28B	108.1
C6—C7—C8	121.2 (2)	C28'—C27'—N3	107.8 (10)
C7—C8—H8A	109.5	C28'—C27'—H27C	110.2
C7—C8—H8B	109.5	N3—C27'—H27C	110.2
H8A—C8—H8B	109.5	C28'—C27'—H27D	110.2
C7—C8—H8C	109.5	N3—C27'—H27D	110.2
H8A—C8—H8C	109.5	H27C—C27'—H27D	108.5
H8B—C8—H8C	109.5	C27'—C28'—C29	111.4 (11)
N1—C9—C10	109.8 (2)	C27'—C28'—H28C	109.3
N1—C9—H9A	109.7	C29—C28'—H28C	109.3
C10—C9—H9A	109.7	C27'—C28'—H28D	109.3
N1—C9—H9B	109.7	C29—C28'—H28D	109.3
C10—C9—H9B	109.7	H28C—C28'—H28D	108.0
H9A—C9—H9B	108.2	C30—C29—C31	106.5 (3)
C11—C10—C9	112.9 (2)	C30—C29—C28	132.3 (8)
C11—C10—H10A	109.0	C31—C29—C28	121.1 (8)

C9—C10—H10A	109.0	C30—C29—C28'	119.6 (8)
C11—C10—H10B	109.0	C31—C29—C28'	133.9 (8)
C9—C10—H10B	109.0	C28—C29—C28'	12.8 (15)
H10A—C10—H10B	107.8	C29—C30—N4	109.8 (3)
C12—C11—C13	106.5 (2)	C29—C30—H30	125.1
C12—C11—C10	127.6 (3)	N4—C30—H30	125.1
C13—C11—C10	125.8 (2)	C32—C31—C36	118.1 (3)
C11—C12—N2	110.6 (2)	C32—C31—C29	134.4 (2)
C11—C12—H12	124.7	C36—C31—C29	107.5 (3)
N2—C12—H12	124.7	C33—C32—C31	119.4 (3)
C14—C13—C18	118.0 (2)	C33—C32—H32	120.3
C14—C13—C11	135.1 (2)	C31—C32—H32	120.3
C18—C13—C11	106.9 (2)	C32—C33—C34	121.1 (3)
C15—C14—C13	119.9 (3)	C32—C33—H33	119.5
C15—C14—H14	120.0	C34—C33—H33	119.5
C13—C14—H14	120.0	C35—C34—C33	121.3 (3)
C14—C15—C16	120.8 (3)	C35—C34—H34	119.3
C14—C15—H15	119.6	C33—C34—H34	119.3
C16—C15—H15	119.6	C34—C35—C36	117.6 (3)
C17—C16—C15	121.6 (3)	C34—C35—H35	121.2
C17—C16—H16	119.2	C36—C35—H35	121.2
C15—C16—H16	119.2	N4—C36—C35	131.0 (3)
C16—C17—C18	117.7 (3)	N4—C36—C31	106.5 (2)

C16—C17—H17	121.2	C35—C36—C31	122.5 (3)
C18—C17—H17	121.2		

Symmetry codes: (i) −*x*+1, *y*, −*z*.

The ethylene linkage in the free Schiff base is disordered over two positions; these were arbitrarily assigned 0.5 site occupancies; the temperature factors of the primed atoms were set to those of the unprimed atoms. The N3–C27 and N3–C27' were restrained to within 0.01 Å of each other; the four C–C bonds were restrained to 1.50±0.01 Å.

Carbon-bound H-atoms were placed in calculated positions (C—H 0.93 to 0.98 Å) and were included in the refinement in the riding model approximation, with *U*(H) set to 1.2 to 1.5*U*(C). The amino H-atoms were located in a difference Fourier map, and were refined with an N–H distance restraint of 0.86±0.01 Å; their temperature factors were freely refined.

The compound crystallizes as a cocrystal coordinated and free zwitterions with an intramolecular N···O hydrogen bond.

In the mononuclear complex molecule the Zn atom, which lies on a twofold rotation axis, is coordinated by phenolate O atoms in tetrahedral coordination geometry. The coordinated Schiff base uses its indole NH donor site to form a hydrogen bond to the negatively charged phenolate O atom of the uncoordinated zwitterionic Schiff base. There is an intramolecular N—H···O hydrogen bond in the coordinated and uncoordinated Schiff bases. The indole NH site of the uncoordinated Schiff base does not engage in a hydrogen bond interaction. The CH2—CH2 group in the uncoordinated Schiff base is disordered equally over two positions. The Zn1—O1 bond distance is 1.98

Å while the Zn1—Cl1 bond length is 2.22 Å, O1—Zn1—Cl1 angle 110.51^{o} (5) deviates some what from the normal tetrahedral angle, and so do the Cl1—Zn1—Cl1i bond angle [81].

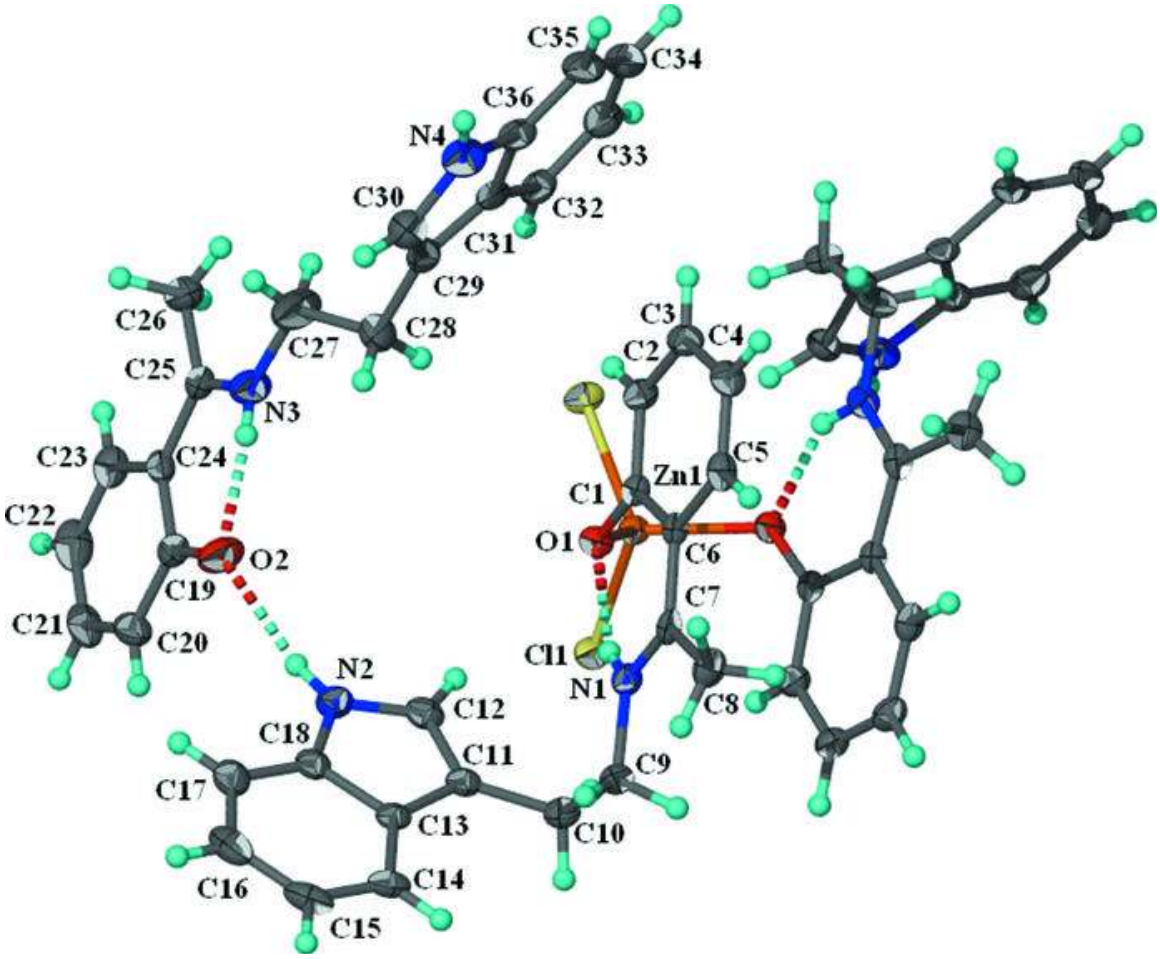

Fig 3.93: Thermal ellipsoid plot of ZnCl2(C18H18N2O)2.2C18H18N2O at the 70% probability level; hydrogen atoms are drawn as spheres of arbitrary radii. The symmetry-related zwitterionic Schiff base is not shown. Dashed lines denote hydrogen bonds. The mononuclear molecule lies on a twofold rotation axis.

CHAPTER FOUR

BIOLOGICAL ACTIVITIES

4. Biological activities

4.1 The anti-ulcerogenic activity of the Schiff bases and complexes (general aspects):

The anti-ulcer activity of a number of the Schiff base ligands and their metal complexes were evaluated against ethanol-induced gastric ulcer in rats. Experimental groups were orally pre-treated with low (30 mg/kg body weight) and high (60 mg/kg body weight) doses of the test compounds in 10% Tween-20 suspension. The ulcer control groups were pre-treated with vehicle 10% Tween-20. The reference group was orally pre-treated with 50 mg/kg Cimetidine.

Gastric ulcer was induced by intragstric application of absolute ethanol (5 ml/kg) according to the method described by Robert *et al* [82] with slight modification in adult male rats.

Peptic ulcers are caused when the natural balances between the aggressive factors of acid and pepsin and defensive mechanisms of mucus, bicarbonate, mucosal turnover and blood supply (mucosal barrier) are disturbed [83]. Baron *et al*, [84] have suggested that acid and pepsin are relatively less important as causative agents and that a defect in the defensive mechanism of gastric mucosa is the first step toward ulcer formation. Although in most cases the etiology of ulcer is unknown, it is generally accepted that it is the result of an imbalance between aggressive factors and maintenance of the mucosal integrity through the endogenous defense mechanism [83].

Ethanol is commonly used for inducing ulcer in experimental rats and lead to intense gastric mucosal damage. Ethanol shows its harmful effects either through direct generation of reactive metabolites, including free radical species that react with most of

the cell components, changing their structures and functions, or promote enhanced oxidative damage [85, 86]. Ethanol damage to the gastrointestinal mucosa starts with microvascular injury, namely disruption of the vascular endothelium resulting in increased vascular permeability, edema formation and epithelial lifting [87]. Ethanol produces necrotic lesions in the gastric mucosa by its direct toxic effect, reducing the secretion of bicarbonates and production of mucus [88]. Exposure to ethanol increases the extension of cellular damage in a dose-dependent way [89]. Ethanol is metabolized in the body and release superoxide anion and hydroperoxyl free radicals which are involved in the mechanism of acute and chronic ulceration in the gastric mucosa. Furthermore, disturbances in gastric secretion, damage to the gastric mucosa, alterations in permeability, gastric mucus depletion and free—radical production are observed after the administration of ethanol [90].

4.2 Animal Experiments:

4.2.1 Anti-ulcer experiment:

Adult male Sprague-Dawley rats were fasted for 48 hours before the experiment [91], but were allowed free access to drinking water till two hours before the experiment. During the fasting period, the rats were placed in four cages, with wide-mesh wire bottoms to prevent coprophagia, each cage contains six randomly selected rats.

Gastric ulcer was induced according to the method described by Robert *et al*. [82] with some modification in adult male Sprague-Dawley rats. Group 1 rats were negative controls that received 10 ml/kg of 10% Tween-20 orally by orogastric intubations; whereas Group 2 rats received oral doses of 50 mg/kg Cimetidine (10 ml/kg) as positive controls. Group 3 and 4 rats received oral high dose (60 mg/kg) and low dose (30 mg/kg)

of different synthesized Schiff bases and complexes, respectively. One hour after this pre-treatment, rats were gavaged with absolute ethanol (5 ml/kg) in order to induce gastric ulcers. The rats were euthanized 60 minutes later [92] by overdoses of diethyl ether and their stomachs were immediately excised. Each stomach was opened along the greater curvature, washed with distilled water and fixed in 10% buffered formalin for 15 minutes.

The stomachs were removed and the gastric juice was obtained from each stomach. The surface area (mm^2) covered by each lesion was measured [93], and the sum of erosion areas per rat stomach was estimated by using a microscope at magnification ×1.8. Percentage ulcerated surface (US), was calculated as: US(mm^2)=(total area covered by ulcers ÷total corpus mucosal surface) ×100.The ulcer index (UI) for each animal was then calculated as the mean ulcer score. Percentage inhibition (%I) was determined as [(UI in control – UI in test group) ÷ UI in control group] ×100 [94].

After the stomach contents were collected, they were centrifuged and gastric juice was separated from the mucus. The mucus content was weighed and expressed in terms of grams [95] and the pH of the stomach juice was recorded.

4.2.2 Acute toxicity test LD_{50}:

Adult male and female ICR mice (8 weeks old) were obtained from the Animal House, Faculty of Medicine, University of Malaya. The mice weighed between 30 -40 g. The animals were given standard rat pellets and tap water ad libitum. The acute toxicity study was used to determine a safe dose for the compounds. Thirty six ICR mice (18 males and 18 females) were assigned equally into 3 groups labeled as vehicle 10% Tween-20 (5 ml/kg); 2 g/kg and 5 g/kg for each of the compounds in 10% Tween-20 preparation.

These animals were subjected to overnight fasting (food but not water) prior to dosing. Food was withheld for a further 3 to 4 hours after dosing. The animals were observed for 30 min and 1, 2, 3 and 24 h after the administration for the onset of clinical or toxicological symptoms. Mortality, if any was observed over a period of 2 weeks. The acute toxicity LD_{50} was calculated as the geometric mean of the dose that resulted in 100% lethality and that which caused no lethality at all. The animals were sacrificed on the 15^{th} day. Histology, hematological and serum biochemical parameters were determined following standard methods [96, 97]. The study was approved by the ethics committee for animal experimentation, Faculty of Medicine, University of Malaya. All animals received human care according to the criteria outlined in the "Guide for the Care and Use of laboratory Animals" prepared by the National Academy of Sciences and published by the national Institute of health.

Results were shown in table (4.4).

4.3 Statistical analysis:

All values were reported as mean $\pm$ S.E.M. The statistical significance of differences between groups was assessed using one-way ANOVA. A value of $p<0.05$ was considered significant. (See appendix B)

4.4 The anti-ulcerogenic activity of: 1H-Indole-3-ethylenesalicylaldimine (TS) and its zinc, nickel and copper complexes:

The anti-ulcer results of TS and its Zn(II), Ni(II) and Cu(II) complexes were shown in table (4.1), and presented diagrammatically in figures (4.1, 4.2 and 4.3)

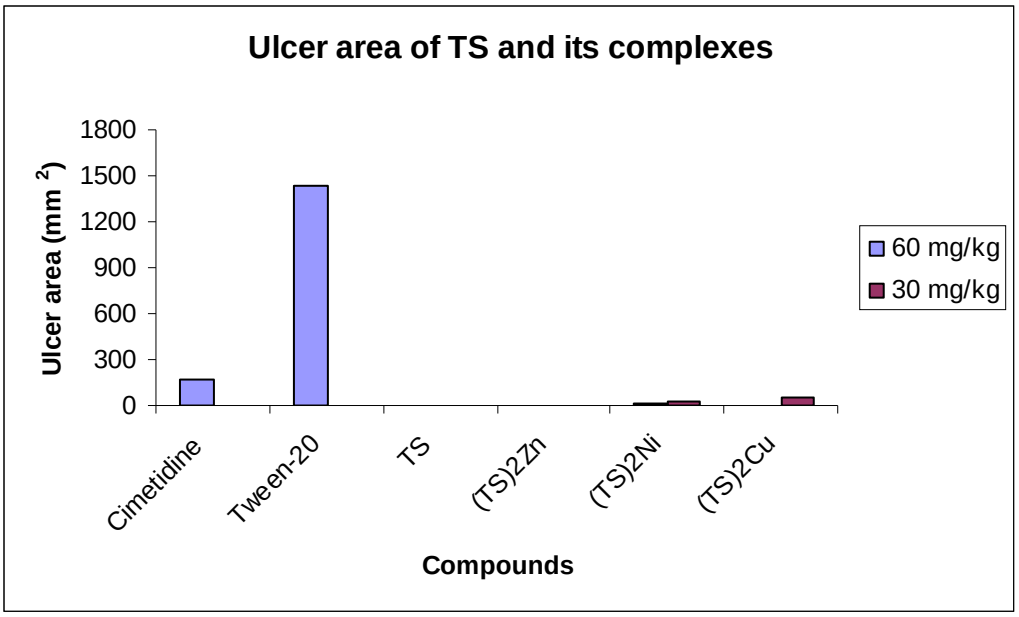

Figure 4.1: Ulcer area (mm^2) of TS and its Zn, Ni and Cu complexes:

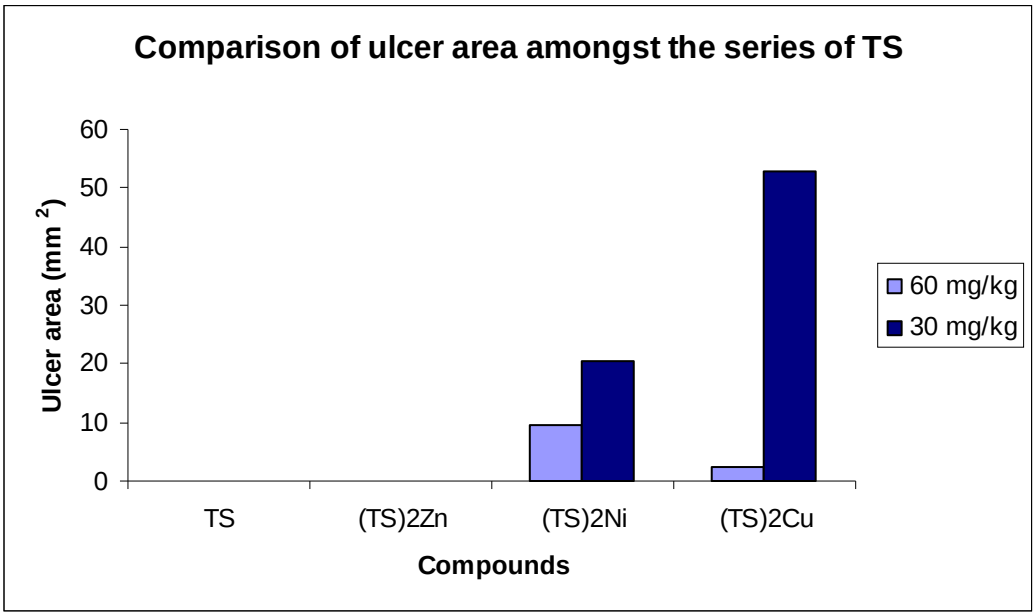

Figure 4.2: Comparison of ulcer areas (mm^2) among TS and its complexes.

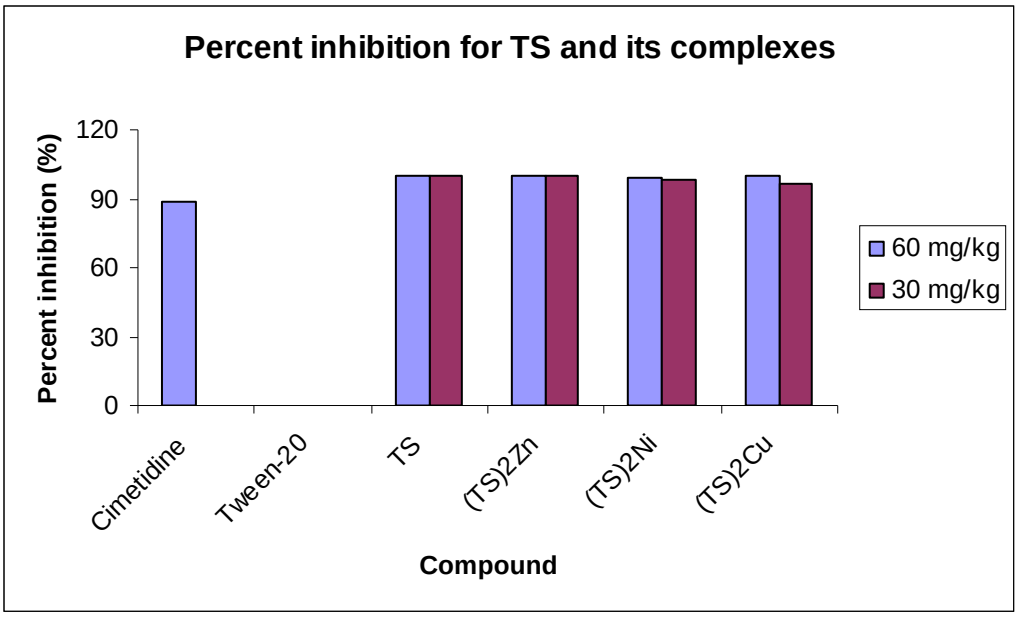

Figure 4.3: Percent inhibition for TS and its Zn, Ni and Cu complexes

Fig (4.1) shows the ulcer area (mm^2) in rat stomachs for the ligand and its complexes together with the positive and negative controls. It is clearly evident that TS and its complexes significantly reduced the ulcer area compared to Cimetidine when applied as high or low dose. Complexation of zinc metal to the ligand doesn't manifest any difference in lesions inhibition compared to the uncomplexed ligand, but still can be considered as potent anti-ulcer drug. Reduction of ulcer areas in the case of complexes probably have been achieved by stimulating the production of more mucus as it was shown in table (4.1).

It could be also concluded from figures (4.2) and (4.3) that, among the series, TS and its zinc complex reveals the greatest inhibition percentage, and the oral administration of the ligand or its zinc complex before ethanol administration significantly prevent ulceration up to 100%. Copper complex, when applied as a high dose, appears to have stronger effect in reducing the ulcer area than the nickel complex. Since copper complexes seem

to have superoxide dismutating activity, it is reasonable to suggest that the inactivation of superoxide anions protects the stomach wall. The radical scavenging property of the copper complex together with an increase of PGs may help to explain the gastroprotective effect of the compound [98].

Flattening of the folds was also observed (See Appendix C, a-c), which suggests that gastroprotective effect of the compounds might be due to a decrease in gastric motility. It is reported that the changes in the gastric motility may play a role in the development and prevention of experimental gastric lesions [99, 100]. Relaxation of circular muscles may protect the gastric mucosa through flattening of the folds. This will increase the mucosal area exposed to necrotizing agents and reduce the volume of the gastric irritants on rugal crest [101]. Ethanol produces a marked contraction of the circular muscles of rat fundic strip, and such a contraction can lead to mucosal compression at the site of the greatest mechanical stress, at the crests of mucosal folds leading to necrosis and ulceration [102].

4.5 The anti-ulcerogenic activity of: 1H-Indole-3-ethylene-5-chlorosalicylaldimine (TCS) and its zinc, nickel and copper complexes:

The anti-ulcer activity of TCS and its Zn(II), Ni(II) and Cu(II) complexes were summarized in table (4.2), and presented in figures (4.4, 4.5 and 4.6)

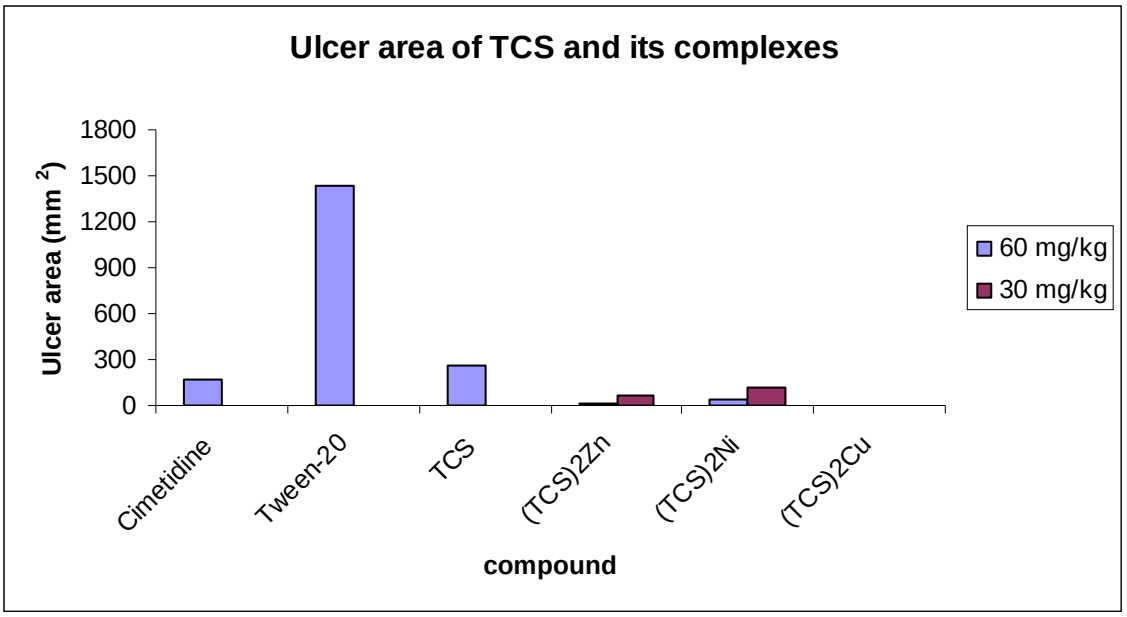

Figure 4.4: Ulcer area (mm^2) of TCS and its Zn, Ni and Cu complexes

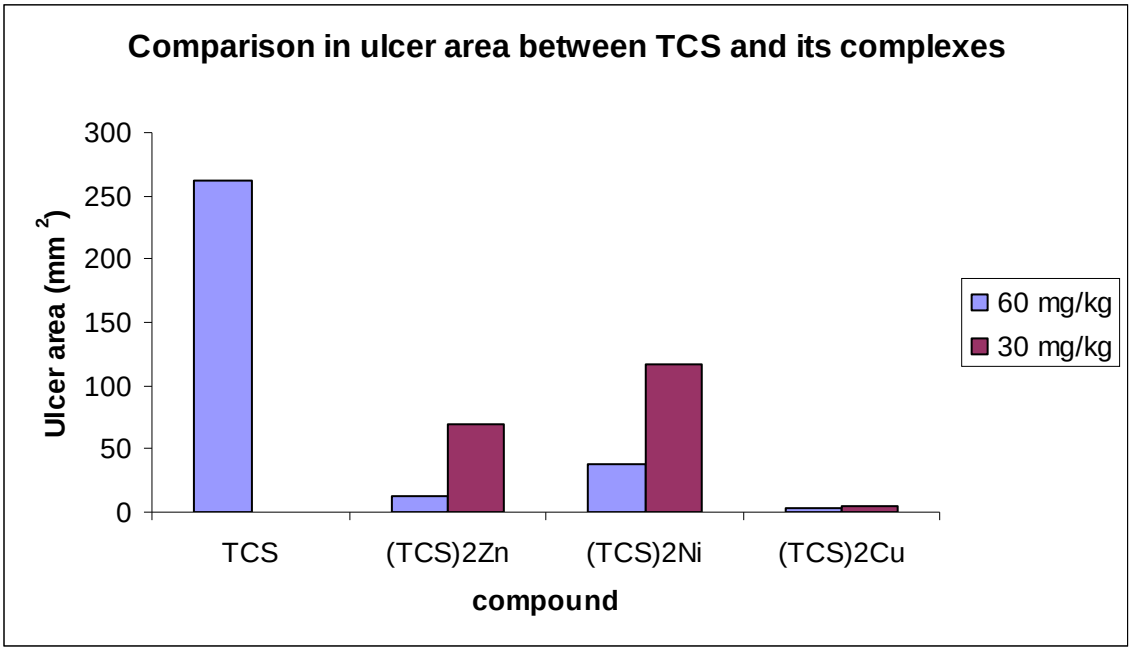

Figure 4.5: Comparison of ulcer areas (mm^2) among TCS and its complexes.

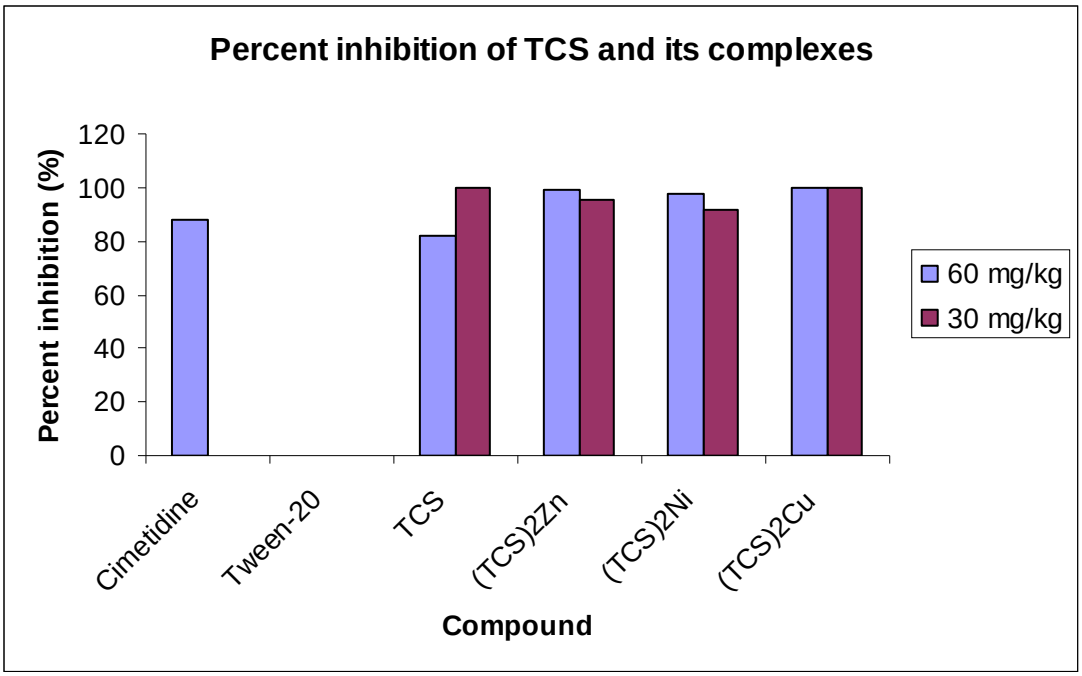

Figure 4.6: Percent inhibition for TCS and its Zn, Ni and Cu complexes.

TCS complexes are more effective as ulcer inhibitors than the free ligand, and reveal enhanced prevention when applied as high dose compared to Cimetidine, a standard drug used for curing gastric ulcer. Likewise, $(TCS)_2Cu$ complex was also considered as a more effective compound in reducing ulcer area among this series. This can be explained on the basis of stimulating the stomach to produce more mucus (2.8g compared to about 1.5g in the case of Ni and Zn complexes). Copper complexes have been shown to be concerned with the synthesis of procollagen, proelastin, or mucoplysaccharide, which are necessary for healing following tissue damage [48].

In the case of nickel complex, both the high and low doses brought about significant reduction of ulcer area compared to Cimetidine, and no significant difference were noted between the two doses. It is also noted here that, $(TCS)_2Zn$, in general, causes lesion damage resistance by approximately double the efficiency of $(TCS)_2Ni$ counterpart (Fig 4.5).

The unusual high ulcer damage observed upon application of high dose of the free ligand prior to ethanol administration can be understood on the basis of overdosing which brings about adverse effects and causes alterations in permeability and tissue functional disturbances.

4.6 The anti-ulcerogenic activity of: 1H-Indole-3-ethylene-5-nitrosalicylaldimine (TNS) and its Zn(II), Ni(II) and Cu(II) complexes:

The anti-ulcer activity of TNS and its Zn(II), Ni(II) and Cu(II) complexes were summarized in table (4.3), and presented in figures (4.7, 4.8 and 4.9)

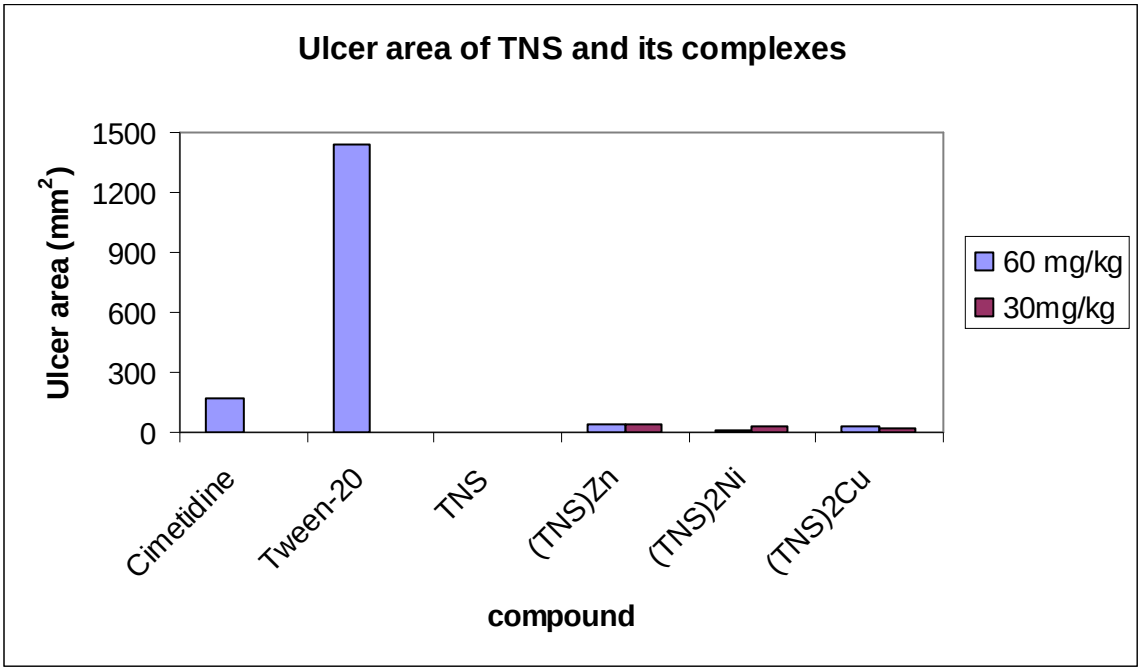

Figure 4.7: Ulcer area (mm^2) of TNS and its Zn, Ni and Cu complexes

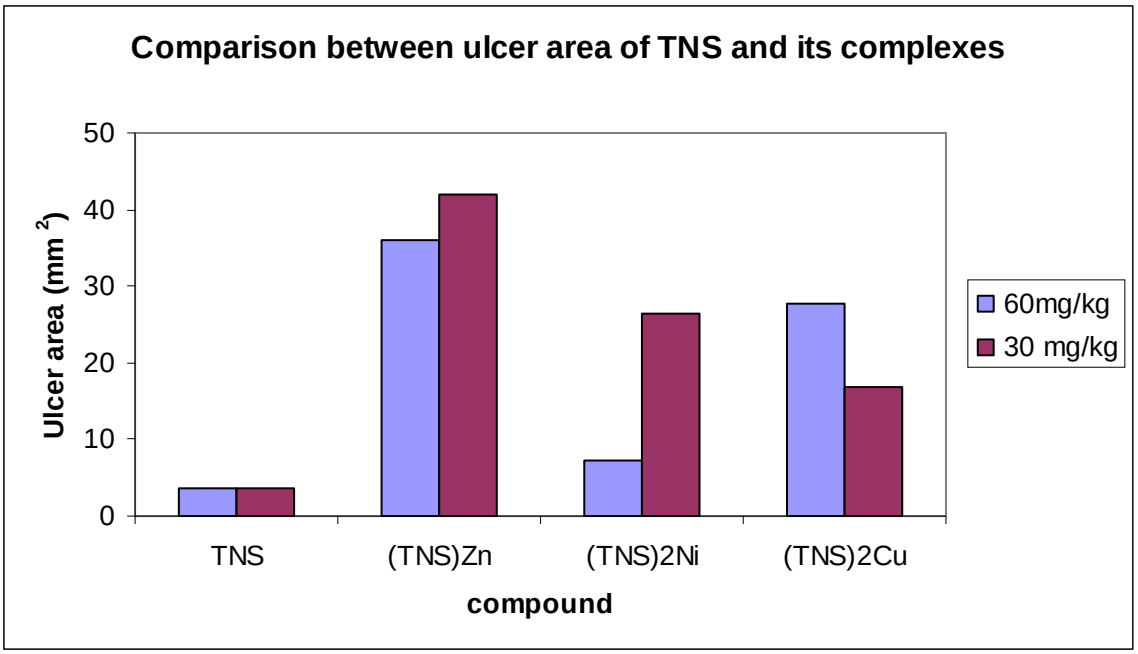

Figure 4.8: Comparison of ulcer areas (mm^2) among TNS and its complexes.

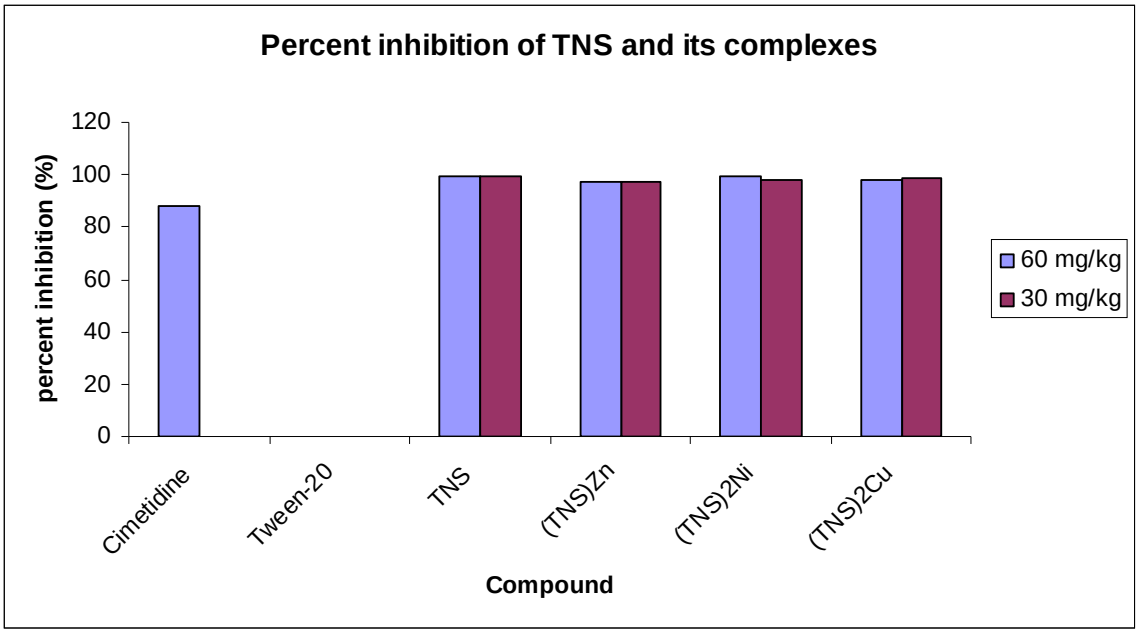

Figure 4.9: Percent inhibition for TNS and its Zn, Ni and Cu complexes.

In contrast to TCS and its complexes, TNS ligand is more effective as anti-ulcer drug than its zinc, nickel and copper complexes, yet, the ligands and complexes can be considered as potential anti-ulcer drugs compared to Cimetidine as shown in figure (4.8). This can be explained in the bases of reducing the acidity of the stomach juice as it can be implied from the pH values. These results also confirm the antisecretory ability of these compounds as reflected from the significant reduction of gastric juice volume and acid output, beside the enhancement of mucus secretion. However, $(TNS)_2Cu$ complex ranks on top of its counterparts, $(TNS)_2Ni$ complex comes at the second close, whereas zinc complex is the least effective. It has been reported that the gastric cytoprotection might be mediated by at least two different mechanisms: one of them through prostaglandine synthesis, and the second one by increasing the mucosal glycoproteins production [103, 104]. Copper complexes were shown to enhance the formation of prostaglandine E_2 and are likely to participate in gastroprotective activity [105,106]. The unusual feature in figure (4.8) is that, with respect to $(TNS)_2Cu$ complex, the low dose appear to have more better effect in reducing ulcer areas than the high dose and can be considered as the optimum dose, more higher doses will affect the physiological properties and lead to more bleeding and damage.

4.7 Histological evaluation of gastric lesions:

Histological observation of ethanol induced gastric lesions in ulcer control group pre-treated with 10% Tween 20, showed comparatively extensive damage to the gastric mucosa, and oedema and leucocytes infiltration of the submucosal layer (Appendix D, d-f). Rats that received pre-treatment with synthesized Schiff bases and complexes had comparatively better protection of the gastric mucosa as seen by reduction in ulcer area,

reduced or absence of submucosal edema and leucocytes infiltration (Appendix D 1e and f). The synthesized Schiff bases and complexes have been shown to exert the cytoprotective effects in a dose-dependent manner.

4.8 Anti-oxidant activity:

4.8.1 DPPH assay:

The total free radical scavenging capacity of the Schiff bases and complexes studied was estimated and compared to Vit C and BHT as standards.

Freshly prepared DPPH solution (100 μM) in DMSO was used in the determination. 5 μL of the samples (with a concentration range between 50-250 μM) and standards were added to 195 μL of DPPH reagent to start the reaction. The final concentration was 97.5 μM for DPPH and varies between 50-250 μM for the test compounds. This has been done to determine the optimum concentration that achieves maximum inhibition of DPPH. The plate was read at 515 nm for 3 hours with 20 minutes intervals to reach a steady state against DMSO as a blank. The percentage DPPH quenched was calculated according to the equation:

DPPH quenched (%) = (Abs. blank – Abs. sample)/ Abs. blank × 100.

All tests were conducted in triplicate, and the curves were shown in appendix (E).

4.8.2 Scavenging capacities for the series of tryptamine-salicylaldehydes and their complexes:

The total DPPH scavenging capacities of each of the compounds at 200 μM concentration were measured and compared to vitamin C and BHT (butylated

hydroxytoluene). Moderate DPPH radical scavenging capacity was detected in the complexes, but weak in the case of the ligands at the selected concentration, although the tested compounds differ in their activity to react and quench DPPH radicals (Fig 4.10).

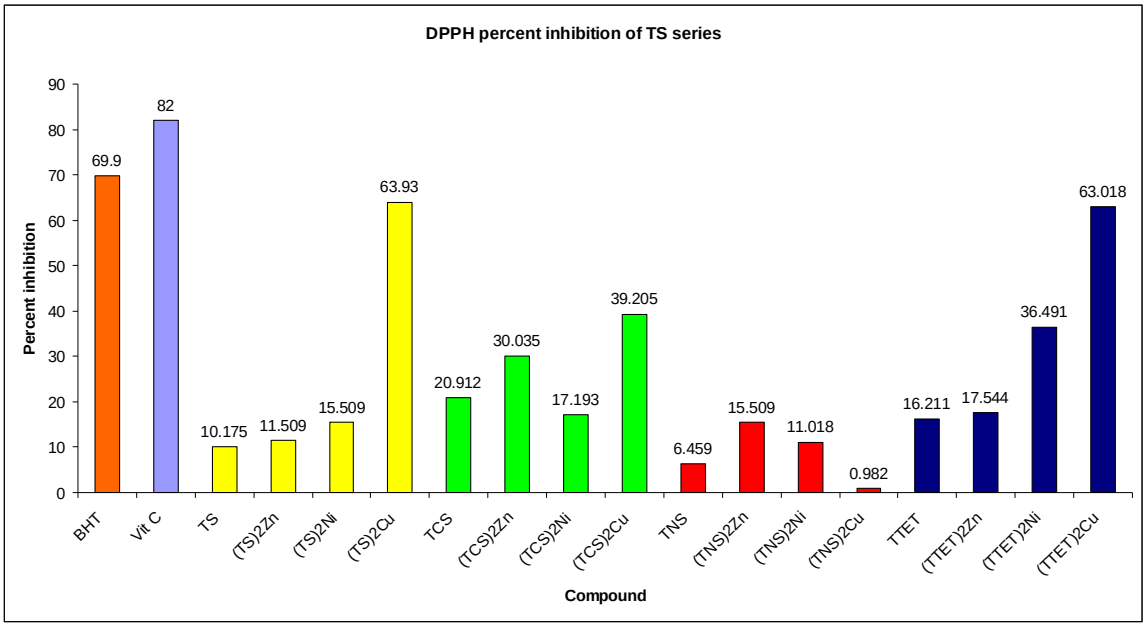

Figure 4.10: DPPH inhibition percentages amongst TS series compounds

In general, the complexes show comparable scavenging activity against DPPH radical than do the ligands. However, none of the compounds were found to be better than vitamin C or BHT. $(TS)_2Cu$ and $(TTET)_2Cu$ reveals the strongest radical scavenging activity among the series, whereas $(TNS)_2Cu$ complex represents the least. The different relative scavenging capacity of individual compounds against different radicals may be explained by the different mechanisms involved in the radical-antioxidant reactions. Chemical compounds that inhibit the peroxidase activity may reduce the DPPH. Other factors, such as stereoselectivity of the radicals or the solubility of these compounds in different testing systems, may also affect the capacity of individual compounds to react

and quench different radicals. This observation was supported by the study of Wang and Jiao [107] who evaluated the radical scavenging capacity of berry corps using superoxide radicals, hydroxyl radicals, and other reactive oxygen species. The berry corp that had a greater scavenging activity against superoxide radicals did not necessarily have a higher activity to quench hydroxyl radicals.

4.8.3 Scavenging capacities for the series of tryptamine-hydroxyacetophenones and their complexes:

Through the series of tryptamine-hydroxyacetophenones either ligands or complexes, none of them show a potent anti-oxidant property to suppress DPPH radicals as do vitamin C. Among the series, copper complexes were the most effective anti-oxidants, and their activity varies with concentration as shown in appendix E. The compounds in this series does not act as an efficient radical scavengers in any way comparable to other compounds of TS series, and even $(TMeHAP)_2Cu$ complex functions more as a prooxidant in high concentrations.

4.8.4 FRAP Assay:

Total anti-oxidant activity is measured by ferric reducing anti-oxidant power (FRAP) assay of Benzie and Strain [108]. Frap assay uses anti-oxidants as reductants in a redox-linked colorimetric method, employing an easily reduced oxidant system present in stoichiometric excess.

At low pH, reduction of ferric tripyridyl triazine (Fe III TPTZ) complex to ferrous form (which has an intense blue color) can be monitored by measuring the change in absorption at 593 nm. The reaction is non specific, in that any half reaction that has lower redox potential, under reaction conditions, than that of ferric-ferrous half reaction, will

derive the ferrous (Fe III to Fe II) ion formation. The change in absorbance is therefore, directly proportional to the combined or total reducing power of the electron donating anti-oxidants present in the reaction mixture.

The FRAP reagent was prepared by mixing 50 ml of 300 mmol/L sodium acetate buffer (pH 3.6), with 5 ml of 10 mmol/L TPTZ in 40 mmol/L HCl and 5 ml of 20 mmol/L $FeCl_3.6H_2O$. Samples (10 µL) and standards (Vit. C and BHT) were mixed with 300 µL of the working FRAP reagent, and the absorbance at 593 nm was measured at 0 minute after mixing and 4 minutes. Each test was carried out in triplicates.

The FRAP value was calculated as ferrous equivalents which obtained by comparing the absorbance change in the test reaction mixture with those containing known concentrations of ferrous ions (Standard). Calibration curve was shown in appendix (E).

4.8.5 FRAP results for TS series:

The Frap values of TS and its substituted derivatives expressed in µM ferrous equivalents in comparison with Vitamin C and BHT were given in figures (4.11 and 4.12).

In general, it is clearly evident that the complexes show more prominent efficacy as ferric reducing compounds than do the free ligands. None of the compounds are more powerful than vitamin C; nevertheless, they show comparable results with BHT. The highest reducing ability being in TTET and its zinc and copper complexes, with a Frap value of more than 2000 µM ferrous equivalents, whilst TS and its zinc and copper complexes represent the bottom of the series with a Frap value of less than 500 µM ferrous equivalents. $(TTET)_2Zn$ and $(TTET)_2Cu$ complexes reveal better reducing abilities than BHT with a Frap values of 2627 and 2883 µM ferrous equivalents respectively in

comparison to only 2463 µM ferrous equivalent for BHT. The nitro-substituted complexes, with the exception of nickel complex, appear to be more powerful anti-oxidants than the chloro-substituted counterparts with a Frap values lying between 1500-857 µM ferrous equivalents. However, the Frap values of chloro-substituted nickel complex is slightly under 1000 µM ferrous equivalent contrary to its group members which show just approximately half of its activity.

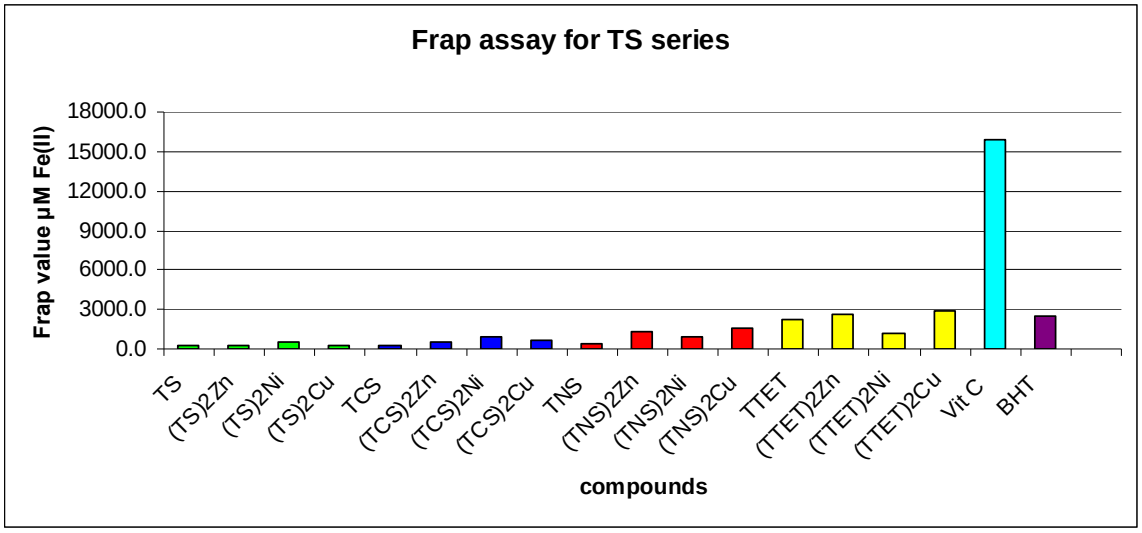

Figure 4.11: Frap assay for TS series in comparison with vitamin C and BHT

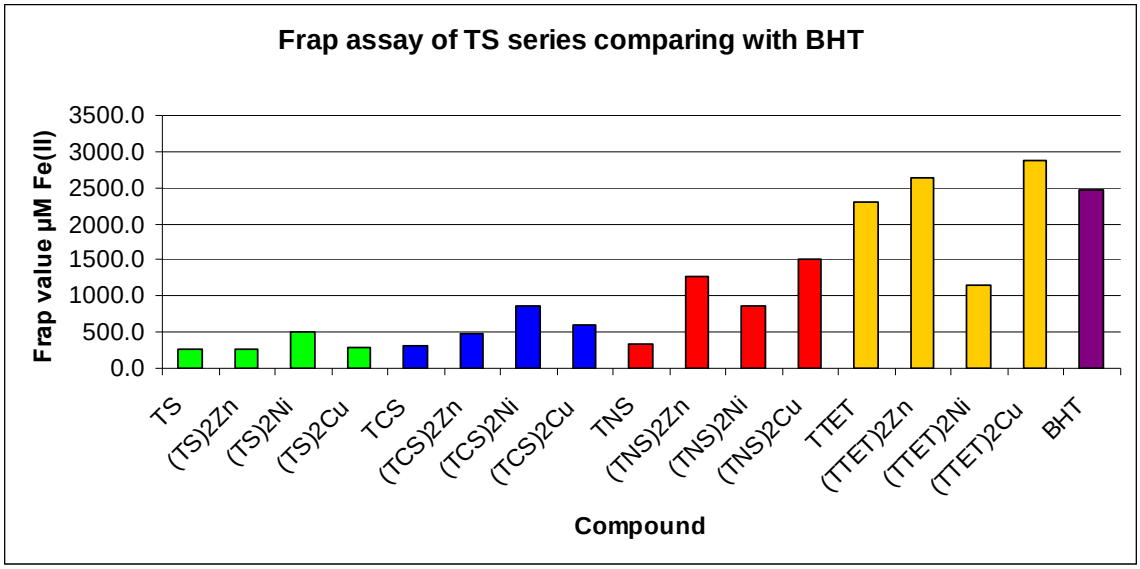

Figure 4.12: Frap assay of TS series in comparison with BHT only.

4.8.6 FRAP results for THAP series:

The column graph in figure (4.13) compares the proportions of ferric reducing abilities of THAP series with vitamin C and BHT as standards. In this series of compounds, the highest reducing ability have been found in TOMeHAP which accounts for 6570 µM ferrous equivalents four times as effective as BHT. This had decreased gradually from nickel to copper complexes of this ligand but still better than BHT. Likewise the trend has been observed for the methyl-substituted ligand and its copper complex. In this category the ligand shows a potency of approximately ten-fold of the corresponding copper complex, and approaches three times the activity of BHT.

For TBrHAP and its copper complex, the pattern is reversed. There are about 1955 µM ferrous equivalents Frap value for copper complex compared to only 876 µM for the free ligand. TBrHAP appears to be slightly effective anti-oxidant than BHT. Chloro-

substituted category and the un-substituted group have weak ferric reducing abilities of Frap values 1000 µM or less.

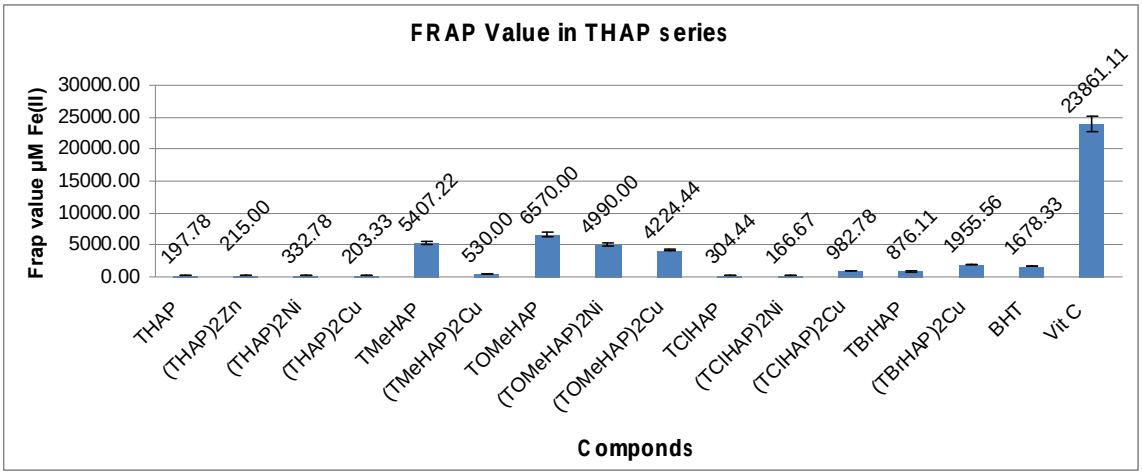

Figure 4.13: Frap values for THAP series in comparison with vitamin C and BHT

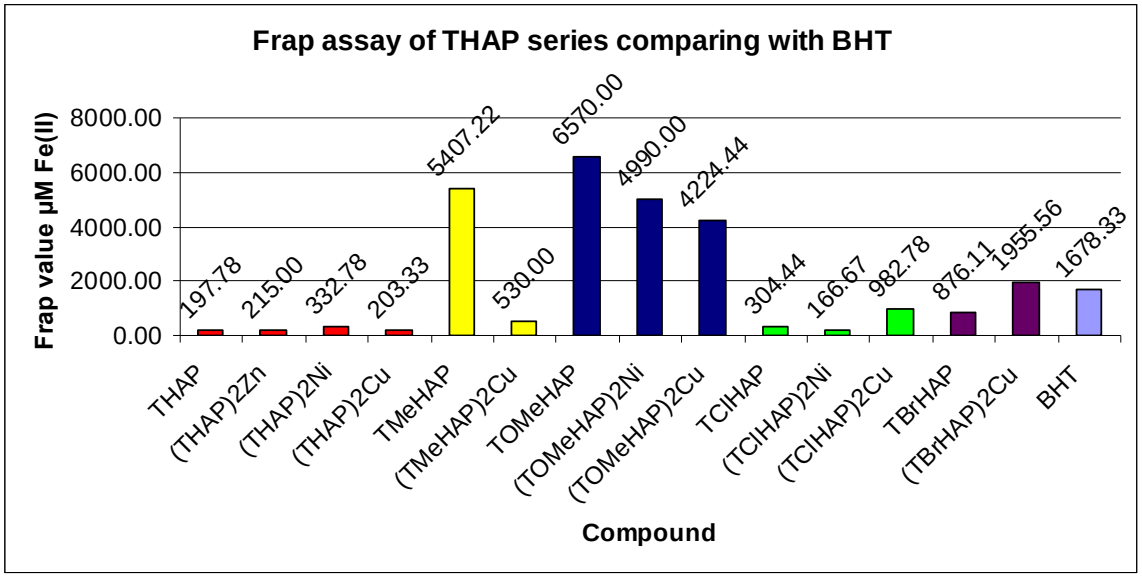

Figure 4.14: Frap values of THAP series in comparison with BHT only.

4.9 Acute toxicity study:

Table (4.4):

Physical observation for abnormalities or mortalities after test compounds administration.

Compounds	½ hour	1 hour	2 hours	3 hours	24 hours
TS	+	+	+	+	+
TCS	+	+	+	$D_{1/2}$	+
TNS	+	+	+	+	+
TTET	-	-	-	-	$D_{1/2}$
THAP	-	$D_{1/2}$	-	-	-
TMeHAP	+	+	+	+	+
TOMeHAP	+	+	+	+	+
TClHAP	+	+	+	+	+
TBrHAP	-	+	+	+	+

\+ Mice were active and did not show sign(s) of abnormalities.
\- Mice were less active.
\- $D_{1/2}$ half of the mice died.

For TS, TNS, TMeHAP, TOMeHAP and TClHAP the acute toxicity profile of the compounds for both genders could be considered favorable judging from the absence of adverse clinical manifestations in experimental animal after two week of observation. All the animals remain alive and did not manifest any significant visible signs of toxicity at these doses. There were no abnormal signs, behavioral changes, body weight changes, or macroscopic finding at any time of observation. There was no mortality in the above-mentioned doses at the end of 14 days of observation. Histology of liver and kidney, hematology and serum biochemistry revealed no significant differences between groups. It is concluded that acute toxicity study with a dose of 5g/kg did not manifest any toxicological signs in mice and that the oral lethal dose for male and female mice is in excess of 5g/kg. Based on these acute toxicity tests, the compounds were found safe.

For TCS no sign of physical abnormalities or mortality during the first two hours was observed, but after 3 hours, half of the mice died in the high dose group, and third of the total in the low dose group. This may imply that the LD_{50} value of this compound is around 5g/kg, and this must be taken into account if we are to consider the compound for bio activity.

TTET is by no means un-toxic. In spite of no death was recorded for the first half an hour after administration, physical abnormalities were observed and the mice tend to behave less active and their movement became very slow and they preferred to stay in their place for longer time during the subsequent 3 hours. After 24 hours, half of the mice were died in both high and low dose groups.

THAP can also be regarded as toxic only if it was administered in high dose. No toxicological symptoms were observed when it applied in low dose.

CONCLUSION

Conclusion

The condensation reaction of tryptamine with salicylaldehyde and its chloro, nitro and 3,5 di-tertiarybutyl derivatives; 2-hydroxyacetophenone, and its methyl, methoxy, chloro, and bromo derivatives afforded the corresponding Schiff base ligands with a good yield. Spectroscopic data proved the formation of the Schiff base ligands as ascertained by the appearance of the azomethine linkage between tryptamine and the carbonyl compound moieties.

Metal complexes of these ligands with Zn(II), Ni(II) and Cu(II) have been obtained with good stoichiometric yields. Spectroscopic studies revealed that zinc complexes adopt slightly distorted tetrahedral geometries through coordination of the zinc ion to phenolate oxygen and azomethine nitrogen atoms of two molecules of the Schiff base. Comparable results have been offered by X-ray crystal structure analysis of $(TCS)_2Zn$ and $(TTET)_2Zn$ complexes. The bond angle O1-Zn-O1$^{\backslash}$ in $(TCS)_2Zn$ (116.62) is closely similar to the same angle in $(TTET)_2Zn$ complex (116.04). Further more, the angle O1-Zn-N1 for $(TCS)_2Zn$ which is 95.57 was also comparable to the same angle in $(TTET)_2Zn$ (95.89). Similar observations were also detected for O1-Zn-N1 bond angles. The only remarkable difference was in the N1-Zn-N1$^{\backslash}$ bond angles which proved to be more wider in $(TTET)_2Zn$ complex (105.87) in comparison to (99.56) in $(TCS)_2Zn$ due to the steric effects exerted by the bulky tertiary butyl groups in position 3 and 5 in the salicylaldehyde moiety of $(TTET)_2Zn$ complex.

Nickel complexes adopt *trans* square planar geometries, rhombically distorted in the case of $(TS)_2Ni$ complex with longer axis along N-Ni-N and shorter along O-N-O direction.

All attempts to obtain suitable crystal for X-ray study of copper complexes were unsuccessful. It is believed that Cu(II) complexes adopt pseudotetrahedral geometry with the same mode of coordination of the Zn(II) and Ni(II) counterparts.

A considerable efforts have been put to obtain Zn(II) complexes of the ligands TOMeHAP, TClHAP; and Zn(II) and Ni(II) complexes for the ligands TMeHAP and TBrHAP, including modifications in the reaction conditions, the use of different deprotonating agents, etc but all were unsuccessful. This point here still deserves further consideration in the future of research to probe the reasons behind.

The anti-ulcerogenic activity of the ligands and complexes shows a potent effect for the compounds, in general, towards preventing gastric ulcer formation. Amongst TS, the nitro derivative TNS and their complexes, both the ligand and the complexes proved to be more effective in preventing gastric injuries than the positive control Cimetidine. TCS and its complexes were slightly less effective though $(TCS)_2Cu$ complex show high activity. The mechanism of ulcer prevention is complex, and need to be addressed for further investigations, although it is evident that, in principle, the compounds stimulate the production of more mucus and reduce the destructive gastric acidity.

Due to the interest in anti-oxidants, particularly in those intended to prevent the presumed deleterious effects of the free radicals in the human body, and to prevent the deterioration of fats and other constituents of foodstuffs, the anti-oxidant properties of the synthesized ligands and complexes have been tested through the popular methods based on the use of the stable free radical diphenylpicryl hydrazyl (DPPH) and ferric reducing anti-oxidant power (FRAP) assays.

Through the series of TS and its chloro, nitro, and tertiarybutyl derivatives, the complexes reveal a comparable scavenging activity in the DPPH assay as compared to Vitamin C and BHT standards. However, none of the compounds were found to be more effective than Vitamin C, but with the exception $(TNS)_2Cu$, copper complexes proved to have the strongest radical scavenging activity. The series of hydroxyacetophenones were far poorer in their scavenging capabilities for DPPH free radicals than TS counterparts. More efforts should be done to study the detailed structural conformations of these compounds towards their anti-oxidant activities.

In the FRAP assay, the complexes generally show more prominent efficacy as ferric reducing compounds than do the free ligands. TTET and its complexes represent the crest as compared to the standard anti-oxidant BHT. Likewise, TOMeHAP and its complexes reveal better anti-oxidant power in the FRAP assay than BHT.

The acute toxicity profile of the compounds could be considered favorable judging from the high oral lethal dose (LD_{50}) value obtained and the absence of adverse clinical manifestations in animal experiments after two week of observation. It is concluded that acute toxicity study with a dose of 2g/kg did not manifest any toxicological signs in mice and that the oral lethal dose for male and female mice is in excess of 2g/kg. Based on these acute toxicity tests, the compounds were found safe. This implies a high therapeutic index, which is ideal for any drug.

For future work, it is of interest to study the effects of modification in the ligand structures especially in the indole residue on the biological activities since it is obvious from the X-ray structures that this part of the whole molecule is not involved in

coordination. Also it is of value from biological point of view to enhance the aqueous solubility of these compounds for more relevant bioactivity.

APPENDICES

Appendix (A)

Physical properties of the compounds derived from TS and its derivatives:

No.	Name of the compound	Molecular formula	Molecular weight	Color	Melting point (°C)
1	TS	$C_{17}H_{16}N_2O$	264.32	Yellow	100
2	$(TS)_2Zn$	$C_{34}H_{30}N_4O_2Zn$	592.02	White	275 (decomposition)
3	$(TS)_2Ni$	$C_{34}H_{30}N_4O_2Ni$	585.33	Green	222 (decomposition)
4	$(TS)_2Cu$	$C_{34}H_{30}N_4O_2Cu$	590.18	Brown	214 (decomposition)
5	TCS	$C_{17}H_{15}N_2OCl$	298.77	Yellow	110
6	$(TCS)_2Zn$	$C_{34}H_{28}N_4O_2Cl_2Zn$	660.91	White	290
7	$(TCS)_2Ni$	$C_{34}H_{28}N_4O_2Cl_2Ni$	654.22	Green	247
8	$(TCS)_2Cu$	$C_{34}H_{28}N_4O_2Cl_2Cu$	687.13	Pale green	190 (decomposition)
9	TNS	$C_{17}H_{15}N_3O_3$	309.32	Yellow	170
10	$(TNS)_2Zn$	$C_{34}H_{28}N_6O_6Zn$	682.01	Bright yellow	310 (decomposition)
11	$(TNS)_2Ni$	$C_{34}H_{28}N_6O_6Ni$	675.32	Green	238 (decomposition)
12	$(TNS)_2Cu$	$C_{34}H_{28}N_6O_6Cu$	680.18	Green	264
13	TTET	$C_{25}H_{32}N_2O$	376.54	Pale yellow	100
14	$(TTET)_2Zn$	$C_{50}H_{62}N_4O_2Zn$	816.45	Pale yellow	205 (decomposition)
15	$(TTET)_2Ni$	$C_{50}H_{62}N_4O_2Ni$	809.76	Yellowish brown	232 (decomposition)
16	$(TTET)_2Cu$	$C_{50}H_{62}N_4O_2Cu$	814.61	Brown	182 (decomposition)

Physical properties of the compounds derived from THAP and its derivatives:

No.	Name of the compound	Molecular formula	Molecular weight	Color	Melting point (ºC)
1	THAP	$C_{18}H_{18}N_2O$	278.35	Yellow	112
2	$(THAP)_2Zn$	$C_{36}H_{34}N_4O_2Cl_2Zn$	690.98	Yellow	121
3	$(THAP)_2Ni$	$C_{36}H_{34}N_4O_2Ni$	613.38	Yellowish green	249 (decomposition)
4	$(THAP)_2Cu$	$C_{36}H_{34}N_4O_2Cu$	618.24	Brown	212 (decomposition)
5	TMeHAP	$C_{19}H_{20}N_2O$	292.38	Yellow	175
6	$(TMeHAP)_2Cu$	$C_{38}H_{38}N_4O_2Cu$	646.29	Brown	282 (decomposition)
7	TOMeHAP	$C_{19}H_{20}N_2O_2$	308.38	Bright yellow	179
8	$(TOMeHAP)_2Ni$	$C_{38}H_{38}N_4O_4Ni$	673.43	Brownish yellow	238 (decomposition)
9	$(TOMeHAP)_2Cu$	$C_{38}H_{38}N_4O_4Cu$	678.29	Brown	206
10	TClHAP	$C_{18}H_{17}N_2OCl$	296.80	Yellow	160
11	$(TClHAP)_2Ni$	$C_{36}H_{32}N_4O_2Cl_2Ni$	682.27	Yellowish green	280 (decomposition)
12	$(TClHAP)_2Cu$	$C_{36}H_{32}N_4O_2Cl_2Cu$	687.13	Brown	232
13	TBrHAP	$C_{18}H_{17}N_2OBr$	357.25	Yellow	182
14	$(TBrHAP)_2Cu$	$C_{36}H_{32}N_4O_2Br_2Cu$	776.03	Brown	238

Elemental Analysis (CHN) for the compounds derived from TS and its derivatives:

No.	Name of the compound	Molecular formula	Molecular weight	C% Calculated(Found)	H% Calculated(Found)	N% Calculated(Found)
1	TS	$C_{17}H_{16}N_2O$	264.32	77.17(76.99)	6.05(6.04)	10.59(10.23)
2	$(TS)_2Zn$	$C_{34}H_{30}N_4O_2Zn$	592.02	68.89(68.97)	5.06(4.96)	9.45(9.62)
3	$(TS)_2Ni$	$C_{34}H_{30}N_4O_2Ni$	585.33	69.70(70.09)	5.12(5.51)	9.56(9.33)
4	$(TS)_2Cu$	$C_{34}H_{30}N_4O_2Cu$	590.18	69.13(69.50)	5.08(5.46)	9.48(9.34)
5	TCS	$C_{17}H_{15}N_2OCl$	298.77	68.34(68.26)	5.06(4.96)	9.38(9.16)
6	$(TCS)_2Zn$	$C_{34}H_{28}N_4O_2Cl_2Zn$	660.91	61.72(61.48)	4.23(4.08)	8.47(8.20)
7	$(TCS)_2Ni$	$C_{34}H_{28}N_4O_2Cl_2Ni$	654.22	62.36(62.55)	4.28(4.37)	8.56(8.24)
8	$(TCS)_2Cu$	$C_{34}H_{28}N_4O_2Cl_2Cu$	687.13	61.90(61.78)	4.25(4.32)	8.49(8.52)
9	TNS	$C_{17}H_{15}N_3O_3$	309.32	66.01(65.97)	4.89(4.79)	13.58(13.63)
10	$(TNS)_2Zn$	$C_{34}H_{28}N_6O_6Zn$	682.01	59.82(59.67)	4.10(4.32)	12.31(12.65)
11	$(TNS)_2Ni$	$C_{34}H_{28}N_6O_6Ni$	675.32	60.41(60.32)	4.14(4.24)	12.43(12.21)
12	$(TNS)_2Cu$	$C_{34}H_{28}N_6O_6Cu$	680.18	59.98(59.62)	4.11(4.32)	12.35(12.17)
13	TTET	$C_{25}H_{32}N_2O$	376.54	79.75(79.58)	8.57(8.72)	7.44(7.22)
14	$(TTET)_2Zn$	$C_{50}H_{62}N_4O_2Zn$	816.45	73.48(73.24)	7.59(7.35)	6.85(6.80)
15	$(TTET)_2Ni$	$C_{50}H_{62}N_4O_2Ni$	809.76	74.09(74.15)	7.65(7.56)	6.91(6.78)
16	$(TTET)_2Cu$	$C_{50}H_{62}N_4O_2Cu$	814.61	73.65(73.38)	7.61(7.88)	6.87(6.90)

Elemental Analysis (CHN) for the compounds derived from THAP and its derivatives:

No.	Name of the compound	Molecular formula	Molecular weight	C% Calculated(Found)	H% Calculated(Found)	N% Calculated(Found)
1	THAP	$C_{18}H_{18}N_2O$	278.35	77.67(77.52)	6.52(6.25)	10.06(10.05
2	$(THAP)_2Zn$	$C_{36}H_{34}N_4O_2Cl_2Zn$	690.98	62.52(62.81)	4.92(4.68)	6.94(7.01)
3	$(THAP)_2Ni$	$C_{36}H_{34}N_4O_2Ni$	613.38	70.43(70.56)	5.54(5.20)	9.13(8.97)
4	$(THAP)_2Cu$	$C_{36}H_{34}N_4O_2Cu$	618.24	69.87(70.11)	5.49(5.77)	9.05(8.92)
5	TMeHAP	$C_{19}H_{20}N_2O$	292.38	77.90(77.62)	6.84(6.62)	9.57(9.83)
6	$(TMeHAP)_2Cu$	$C_{38}H_{38}N_4O_2Cu$	646.29	70.55(70.75)	5.87(5.57)	8.66(8.59)
7	TOMeHAP	$C_{19}H_{20}N_2O_2$	308.38	74.00(74.20)	6.54(6.19)	9.08(9.13)
8	$(TOMeHAP)_2Ni$	$C_{38}H_{38}N_4O_4Ni$	673.43	67.71(67.54)	5.64(5.48)	8.31(8.07)
9	$(TOMeHAP)_2Cu$	$C_{38}H_{38}N_4O_4Cu$	678.29	67.22(67.49)	5.60(5.90)	8.25(8.23)
10	TClHAP	$C_{18}H_{17}N_2OCl$	296.80	69.12(69.24)	5.48(5.75)	8.96(8.54)
11	$(TClHAP)_2Ni$	$C_{36}H_{32}N_4O_2Cl_2Ni$	682.27	63.31(63.09)	4.65(4.52)	8.15(7.92)
12	$(TClHAP)_2Cu$	$C_{36}H_{32}N_4O_2Cl_2Cu$	687.13	62.87(63.00)	4.65(4.38)	8.15(8.05)
13	TBrHAP	$C_{18}H_{17}N_2OBr$	357.25	60.52(60.11)	4.80(4.50)	7.84(7.73)
14	$(TBrHAP)_2Cu$	$C_{36}H_{32}N_4O_2Br_2Cu$	776.03	55.66(55.53)	4.12(4.16)	7.21(7.08)

Appendix (B)

Statistical analysis (One way AVONA)

1. TS series

Descriptive

Treatment	N	Mean	Std. Deviation	Std. Error	95% Confidence Interval for Mean		Minimum	Maximum
					Lower Bound	Upper Bound		
negative control	6	1438.0000	143.44895	58.56279	1287.4596	1588.5404	1238.00	1638.00
positive control	6	168.0000	12.06648	4.92612	155.3370	180.6630	150.00	184.00
TS(H)	6	.0000	.00000	.00000	.0000	.0000	.00	.00
TS(L)	6	.0000	.00000	.00000	.0000	.0000	.00	.00
(TS)2Zn(H)	6	.0000	.00000	.00000	.0000	.0000	.00	.00
(TS)2Zn(L)	6	.0000	.00000	.00000	.0000	.0000	.00	.00
(TS)2Ni(H)	6	9.6000	.46043	.18797	9.1168	10.0832	9.00	10.20
(TS)2Ni(L)	6	20.2333	.33862	.13824	19.8780	20.5887	19.90	20.70
(TS)2Cu(H)	6	2.4000	.30332	.12383	2.0817	2.7183	1.90	2.70
(TS)2Cu(L)	6	52.8000	.52154	.21292	52.2527	53.3473	52.00	53.40
Total	60	169.1033	431.47445	55.70311	57.6417	280.5650	.00	1638.00

ANOVA

Treatment	Sum of Squares	df	Mean Square	F	Sig.
Between Groups	1.088E7	9	1208935.850	583.354	.000
Within Groups	103619.453	50	2072.389		
Total	1.098E7	59			

Multiple Comparisons

Treatment

Bonferroni

(I) group	(J) group	Mean Difference (I-J)	Std. Error	Sig.	95% Confidence Interval	
					Lower Bound	Upper Bound
negative control	positive control	1270.00000*	26.28301	.000	1179.0379	1360.9621
	TS(H)	1438.00000*	26.28301	.000	1347.0379	1528.9621
	TS(L)	1438.00000*	26.28301	.000	1347.0379	1528.9621
	(TS)2Zn(H)	1438.00000*	26.28301	.000	1347.0379	1528.9621
	(TS)2Zn(L)	1438.00000*	26.28301	.000	1347.0379	1528.9621
	(TS)2Ni(H)	1428.40000*	26.28301	.000	1337.4379	1519.3621
	(TS)2Ni(L)	1417.76667*	26.28301	.000	1326.8046	1508.7287
	(TS)2Cu(H)	1435.60000*	26.28301	.000	1344.6379	1526.5621
	(TS)2Cu(L)	1385.20000*	26.28301	.000	1294.2379	1476.1621
positive control	negative control	-1270.00000*	26.28301	.000	-1360.9621	-1179.0379
	TS(H)	168.00000*	26.28301	.000	77.0379	258.9621
	TS(L)	168.00000*	26.28301	.000	77.0379	258.9621
	(TS)2Zn(H)	168.00000*	26.28301	.000	77.0379	258.9621
	(TS)2Zn(L)	168.00000*	26.28301	.000	77.0379	258.9621
	(TS)2Ni(H)	158.40000*	26.28301	.000	67.4379	249.3621
	(TS)2Ni(L)	147.76667*	26.28301	.000	56.8046	238.7287
	(TS)2Cu(H)	165.60000*	26.28301	.000	74.6379	256.5621
	(TS)2Cu(L)	115.20000*	26.28301	.003	24.2379	206.1621
TS(H)	negative control	-1438.00000*	26.28301	.000	-1528.9621	-1347.0379
	positive control	-168.00000*	26.28301	.000	-258.9621	-77.0379
	TS(L)	.00000	26.28301	1.000	-90.9621	90.9621
	(TS)2Zn(H)	.00000	26.28301	1.000	-90.9621	90.9621
	(TS)2Zn(L)	.00000	26.28301	1.000	-90.9621	90.9621
	(TS)2Ni(H)	-9.60000	26.28301	1.000	-100.5621	81.3621
	(TS)2Ni(L)	-20.23333	26.28301	1.000	-111.1954	70.7287
	(TS)2Cu(H)	-2.40000	26.28301	1.000	-93.3621	88.5621
	(TS)2Cu(L)	-52.80000	26.28301	1.000	-143.7621	38.1621

(I) group	(J) group	Mean Difference (I-J)	Std. Error	Sig.	95% Confidence Interval	
					Lower Bound	Upper Bound
TS(L)	negative control	-1438.00000*	26.28301	.000	-1528.9621	-1347.0379
	positive control	-168.00000*	26.28301	.000	-258.9621	-77.0379
	TS(H)	.00000	26.28301	1.000	-90.9621	90.9621
	(TS)2Zn(H)	.00000	26.28301	1.000	-90.9621	90.9621
	(TS)2Zn(L)	.00000	26.28301	1.000	-90.9621	90.9621
	(TS)2Ni(H)	-9.60000	26.28301	1.000	-100.5621	81.3621
	(TS)2Ni(L)	-20.23333	26.28301	1.000	-111.1954	70.7287
	(TS)2Cu(H)	-2.40000	26.28301	1.000	-93.3621	88.5621
	(TS)2Cu(L)	-52.80000	26.28301	1.000	-143.7621	38.1621
(TS)2Zn(H)	negative control	-1438.00000*	26.28301	.000	-1528.9621	-1347.0379
	positive control	-168.00000*	26.28301	.000	-258.9621	-77.0379
	TS(H)	.00000	26.28301	1.000	-90.9621	90.9621
	TS(L)	.00000	26.28301	1.000	-90.9621	90.9621
	(TS)2Zn(L)	.00000	26.28301	1.000	-90.9621	90.9621
	(TS)2Ni(H)	-9.60000	26.28301	1.000	-100.5621	81.3621
	(TS)2Ni(L)	-20.23333	26.28301	1.000	-111.1954	70.7287
	(TS)2Cu(H)	-2.40000	26.28301	1.000	-93.3621	88.5621
	(TS)2Cu(L)	-52.80000	26.28301	1.000	-143.7621	38.1621
(TS)2Zn(L)	negative control	-1438.00000*	26.28301	.000	-1528.9621	-1347.0379
	positive control	-168.00000*	26.28301	.000	-258.9621	-77.0379
	TS(H)	.00000	26.28301	1.000	-90.9621	90.9621
	TS(L)	.00000	26.28301	1.000	-90.9621	90.9621
	(TS)2Zn(H)	.00000	26.28301	1.000	-90.9621	90.9621
	(TS)2Ni(H)	-9.60000	26.28301	1.000	-100.5621	81.3621
	(TS)2Ni(L)	-20.23333	26.28301	1.000	-111.1954	70.7287
	(TS)2Cu(H)	-2.40000	26.28301	1.000	-93.3621	88.5621
	(TS)2Cu(L)	-52.80000	26.28301	1.000	-143.7621	38.1621
(TS)2Ni(H)	negative control	-1428.40000*	26.28301	.000	-1519.3621	-1337.4379
	positive control	-158.40000*	26.28301	.000	-249.3621	-67.4379
	TS(H)	9.60000	26.28301	1.000	-81.3621	100.5621
	TS(L)	9.60000	26.28301	1.000	-81.3621	100.5621
	(TS)2Zn(H)	9.60000	26.28301	1.000	-81.3621	100.5621

	(TS)2Zn(L)	9.60000	26.28301	1.000	-81.3621	100.5621
	(TS)2Ni(L)	-10.63333	26.28301	1.000	-101.5954	80.3287
	(TS)2Cu(H)	7.20000	26.28301	1.000	-83.7621	98.1621
	(TS)2Cu(L)	-43.20000	26.28301	1.000	-134.1621	47.7621
(TS)2Ni(L)	negative control	-1417.76667*	26.28301	.000	-1508.7287	-1326.8046
	positive control	-147.76667*	26.28301	.000	-238.7287	-56.8046
	TS(H)	20.23333	26.28301	1.000	-70.7287	111.1954
	TS(L)	20.23333	26.28301	1.000	-70.7287	111.1954
	(TS)2Zn(H)	20.23333	26.28301	1.000	-70.7287	111.1954
	(TS)2Zn(L)	20.23333	26.28301	1.000	-70.7287	111.1954
	(TS)2Ni(H)	10.63333	26.28301	1.000	-80.3287	101.5954
	(TS)2Cu(H)	17.83333	26.28301	1.000	-73.1287	108.7954
	(TS)2Cu(L)	-32.56667	26.28301	1.000	-123.5287	58.3954
(TS)2Cu(H)	negative control	-1435.60000*	26.28301	.000	-1526.5621	-1344.6379
	positive control	-165.60000*	26.28301	.000	-256.5621	-74.6379
	TS(H)	2.40000	26.28301	1.000	-88.5621	93.3621
	TS(L)	2.40000	26.28301	1.000	-88.5621	93.3621
	(TS)2Zn(H)	2.40000	26.28301	1.000	-88.5621	93.3621
	(TS)2Zn(L)	2.40000	26.28301	1.000	-88.5621	93.3621
	(TS)2Ni(H)	-7.20000	26.28301	1.000	-98.1621	83.7621
	(TS)2Ni(L)	-17.83333	26.28301	1.000	-108.7954	73.1287
	(TS)2Cu(L)	-50.40000	26.28301	1.000	-141.3621	40.5621
(TS)2Cu(L)	negative control	-1385.20000*	26.28301	.000	-1476.1621	-1294.2379
	positive control	-115.20000*	26.28301	.003	-206.1621	-24.2379
	TS(H)	52.80000	26.28301	1.000	-38.1621	143.7621
	TS(L)	52.80000	26.28301	1.000	-38.1621	143.7621
	(TS)2Zn(H)	52.80000	26.28301	1.000	-38.1621	143.7621
	(TS)2Zn(L)	52.80000	26.28301	1.000	-38.1621	143.7621
	(TS)2Ni(H)	43.20000	26.28301	1.000	-47.7621	134.1621
	(TS)2Ni(L)	32.56667	26.28301	1.000	-58.3954	123.5287
	(TS)2Cu(H)	50.40000	26.28301	1.000	-40.5621	141.3621

*. The mean difference is significant at the 0.05 level.

2. TCS series

Descriptive

Treatment	N	Mean	Std. Deviation	Std. Error	95% Confidence Interval for Mean		Minimum	Maximum
					Lower Bound	Upper Bound		
negative control	6	1438.0000	143.44895	58.56279	1287.4596	1588.5404	1238.00	1638.00
positive control	6	168.0000	12.06648	4.92612	155.3370	180.6630	150.00	184.00
TCS(H)	6	262.8000	2.03568	.83106	260.6637	264.9363	260.20	265.60
TCS(L)	6	.0000	.00000	.00000	.0000	.0000	.00	.00
(TCS)2Zn(H)	6	12.0000	.26077	.10646	11.7263	12.2737	11.70	12.40
(TCS)2Zn(L)	6	69.6000	.96540	.39412	68.5869	70.6131	68.00	70.70
(TCS)2Ni(H)	6	38.4000	.44272	.18074	37.9354	38.8646	37.90	39.00
(TCS)2Ni(L)	6	117.6000	2.56982	1.04913	114.9031	120.2969	114.20	121.00
(TCS)2Cu(H)	6	2.4000	.83905	.34254	1.5195	3.2805	1.00	3.40
(TCS)2Cu(L)	6	4.8000	.99398	.40579	3.7569	5.8431	3.60	6.00
Total	60	211.3600	422.58326	54.55526	102.1952	320.5248	.00	1638.00

ANOVA

Treatment	Sum of Squares	df	Mean Square	F	Sig.
Between Groups	1.043E7	9	1159148.416	558.980	.000
Within Groups	103684.180	50	2073.684		
Total	1.054E7	59			

Multiple Comparisons

Treatment

Bonferroni

(I) group	(J) group	Mean Difference (I-J)	Std. Error	Sig.	95% Confidence Interval	
					Lower Bound	Upper Bound
negative control	positive control	1270.00000*	26.29121	.000	1179.0095	1360.9905
	TCS(H)	1175.20000*	26.29121	.000	1084.2095	1266.1905
	TCS(L)	1438.00000*	26.29121	.000	1347.0095	1528.9905
	(TCS)2Zn(H)	1426.00000*	26.29121	.000	1335.0095	1516.9905
	(TCS)2Zn(L)	1368.40000*	26.29121	.000	1277.4095	1459.3905
	(TCS)2Ni(H)	1399.60000*	26.29121	.000	1308.6095	1490.5905
	(TCS)2Ni(L)	1320.40000*	26.29121	.000	1229.4095	1411.3905
	(TCS)2Cu(H)	1435.60000*	26.29121	.000	1344.6095	1526.5905
	(TCS)2Cu(L)	1433.20000*	26.29121	.000	1342.2095	1524.1905
positive control	negative control	-1270.00000*	26.29121	.000	-1360.9905	-1179.0095
	TCS(H)	-94.80000*	26.29121	.032	-185.7905	-3.8095
	TCS(L)	168.00000*	26.29121	.000	77.0095	258.9905
	(TCS)2Zn(H)	156.00000*	26.29121	.000	65.0095	246.9905
	(TCS)2Zn(L)	98.40000*	26.29121	.021	7.4095	189.3905
	(TCS)2Ni(H)	129.60000*	26.29121	.000	38.6095	220.5905
	(TCS)2Ni(L)	50.40000	26.29121	1.000	-40.5905	141.3905
	(TCS)2Cu(H)	165.60000*	26.29121	.000	74.6095	256.5905
	(TCS)2Cu(L)	163.20000*	26.29121	.000	72.2095	254.1905
TCS(H)	negative control	-1175.20000*	26.29121	.000	-1266.1905	-1084.2095
	positive control	94.80000*	26.29121	.032	3.8095	185.7905
	TCS(L)	262.80000*	26.29121	.000	171.8095	353.7905
	(TCS)2Zn(H)	250.80000*	26.29121	.000	159.8095	341.7905
	(TCS)2Zn(L)	193.20000*	26.29121	.000	102.2095	284.1905
	(TCS)2Ni(H)	224.40000*	26.29121	.000	133.4095	315.3905
	(TCS)2Ni(L)	145.20000*	26.29121	.000	54.2095	236.1905
	(TCS)2Cu(H)	260.40000*	26.29121	.000	169.4095	351.3905
	(TCS)2Cu(L)	258.00000*	26.29121	.000	167.0095	348.9905

(I) group	(J) group	Mean Difference (I-J)	Std. Error	Sig.	95% Confidence Interval	
					Lower Bound	Upper Bound
TCS(L)	negative control	-1438.00000*	26.29121	.000	-1528.9905	-1347.0095
	positive control	-168.00000*	26.29121	.000	-258.9905	-77.0095
	TCS(H)	-262.80000*	26.29121	.000	-353.7905	-171.8095
	(TCS)2Zn(H)	-12.00000	26.29121	1.000	-102.9905	78.9905
	(TCS)2Zn(L)	-69.60000	26.29121	.487	-160.5905	21.3905
	(TCS)2Ni(H)	-38.40000	26.29121	1.000	-129.3905	52.5905
	(TCS)2Ni(L)	-117.60000*	26.29121	.002	-208.5905	-26.6095
	(TCS)2Cu(H)	-2.40000	26.29121	1.000	-93.3905	88.5905
	(TCS)2Cu(L)	-4.80000	26.29121	1.000	-95.7905	86.1905
(TCS)2Zn(H)	negative control	-1426.00000*	26.29121	.000	-1516.9905	-1335.0095
	positive control	-156.00000*	26.29121	.000	-246.9905	-65.0095
	TCS(H)	-250.80000*	26.29121	.000	-341.7905	-159.8095
	TCS(L)	12.00000	26.29121	1.000	-78.9905	102.9905
	(TCS)2Zn(L)	-57.60000	26.29121	1.000	-148.5905	33.3905
	(TCS)2Ni(H)	-26.40000	26.29121	1.000	-117.3905	64.5905
	(TCS)2Ni(L)	-105.60000*	26.29121	.009	-196.5905	-14.6095
	(TCS)2Cu(H)	9.60000	26.29121	1.000	-81.3905	100.5905
	(TCS)2Cu(L)	7.20000	26.29121	1.000	-83.7905	98.1905
(TCS)2Zn(L)	negative control	-1368.40000*	26.29121	.000	-1459.3905	-1277.4095
	positive control	-98.40000*	26.29121	.021	-189.3905	-7.4095
	TCS(H)	-193.20000*	26.29121	.000	-284.1905	-102.2095
	TCS(L)	69.60000	26.29121	.487	-21.3905	160.5905
	(TCS)2Zn(H)	57.60000	26.29121	1.000	-33.3905	148.5905
	(TCS)2Ni(H)	31.20000	26.29121	1.000	-59.7905	122.1905
	(TCS)2Ni(L)	-48.00000	26.29121	1.000	-138.9905	42.9905
	(TCS)2Cu(H)	67.20000	26.29121	.615	-23.7905	158.1905
	(TCS)2Cu(L)	64.80000	26.29121	.774	-26.1905	155.7905
(TCS)2Ni(H)	negative control	-1399.60000*	26.29121	.000	-1490.5905	-1308.6095
	positive control	-129.60000*	26.29121	.000	-220.5905	-38.6095
	TCS(H)	-224.40000*	26.29121	.000	-315.3905	-133.4095
	TCS(L)	38.40000	26.29121	1.000	-52.5905	129.3905
	(TCS)2Zn(H)	26.40000	26.29121	1.000	-64.5905	117.3905

	(TCS)2Zn(L)	-31.20000	26.29121	1.000	-122.1905	59.7905
	(TCS)2Ni(L)	-79.20000	26.29121	.183	-170.1905	11.7905
	(TCS)2Cu(H)	36.00000	26.29121	1.000	-54.9905	126.9905
	(TCS)2Cu(L)	33.60000	26.29121	1.000	-57.3905	124.5905
(TCS)2Ni(L)	negative control	-1320.40000*	26.29121	.000	-1411.3905	-1229.4095
	positive control	-50.40000	26.29121	1.000	-141.3905	40.5905
	TCS(H)	-145.20000*	26.29121	.000	-236.1905	-54.2095
	TCS(L)	117.60000*	26.29121	.002	26.6095	208.5905
	(TCS)2Zn(H)	105.60000*	26.29121	.009	14.6095	196.5905
	(TCS)2Zn(L)	48.00000	26.29121	1.000	-42.9905	138.9905
	(TCS)2Ni(H)	79.20000	26.29121	.183	-11.7905	170.1905
	(TCS)2Cu(H)	115.20000*	26.29121	.003	24.2095	206.1905
	(TCS)2Cu(L)	112.80000*	26.29121	.004	21.8095	203.7905
(TCS)2Cu(H)	negative control	-1435.60000*	26.29121	.000	-1526.5905	-1344.6095
	positive control	-165.60000*	26.29121	.000	-256.5905	-74.6095
	TCS(H)	-260.40000*	26.29121	.000	-351.3905	-169.4095
	TCS(L)	2.40000	26.29121	1.000	-88.5905	93.3905
	(TCS)2Zn(H)	-9.60000	26.29121	1.000	-100.5905	81.3905
	(TCS)2Zn(L)	-67.20000	26.29121	.615	-158.1905	23.7905
	(TCS)2Ni(H)	-36.00000	26.29121	1.000	-126.9905	54.9905
	(TCS)2Ni(L)	-115.20000*	26.29121	.003	-206.1905	-24.2095
	(TCS)2Cu(L)	-2.40000	26.29121	1.000	-93.3905	88.5905
(TCS)2Cu(L)	negative control	-1433.20000*	26.29121	.000	-1524.1905	-1342.2095
	positive control	-163.20000*	26.29121	.000	-254.1905	-72.2095
	TCS(H)	-258.00000*	26.29121	.000	-348.9905	-167.0095
	TCS(L)	4.80000	26.29121	1.000	-86.1905	95.7905
	(TCS)2Zn(H)	-7.20000	26.29121	1.000	-98.1905	83.7905
	(TCS)2Zn(L)	-64.80000	26.29121	.774	-155.7905	26.1905
	(TCS)2Ni(H)	-33.60000	26.29121	1.000	-124.5905	57.3905
	(TCS)2Ni(L)	-112.80000*	26.29121	.004	-203.7905	-21.8095
	(TCS)2Cu(H)	2.40000	26.29121	1.000	-88.5905	93.3905

*. The mean difference is significant at the 0.05 level.

3. TNS

Descriptive

Treatment	N	Mean	Std. Deviation	Std. Error	95% Confidence Interval for Mean		Minimum	Maximum
					Lower Bound	Upper Bound		
negative control	6	1438.0000	143.44895	58.56279	1287.4596	1588.5404	1238.00	1638.00
positive control	6	168.0000	12.06648	4.92612	155.3370	180.6630	150.00	184.00
TNS(H)	6	3.6000	.48580	.19833	3.0902	4.1098	3.00	4.20
TNS(L)	6	3.6000	.46043	.18797	3.1168	4.0832	2.90	4.20
(TNS)2Zn(H)	6	36.0000	1.08628	.44347	34.8600	37.1400	34.60	37.30
(TNS)2Zn(L)	6	42.0000	1.36382	.55678	40.5688	43.4312	40.00	43.60
(TNS)2Ni(H)	6	7.2000	.77460	.31623	6.3871	8.0129	6.00	8.10
(TNS)2Ni(L)	6	26.4000	1.32212	.53975	25.0125	27.7875	24.50	28.00
(TNS)2Cu(H)	6	27.6000	.90774	.37059	26.6474	28.5526	26.70	29.00
(TNS)2Cu(L)	6	16.8000	1.43248	.58481	15.2967	18.3033	14.60	18.30
Total	60	176.9200	428.46392	55.31445	66.2360	287.6040	2.90	1638.00

ANOVA

treatment	Sum of Squares	df	Mean Square	F	Sig.
Between Groups	1.073E7	9	1191959.904	574.940	.000
Within Groups	103659.560	50	2073.191		
Total	1.083E7	59			

Multiple Comparisons

Treatment

Bonferroni

(I) group	(J) group	Mean Difference (I-J)	Std. Error	Sig.	95% Confidence Interval	
					Lower Bound	Upper Bound
negative control	positive control	1270.00000*	26.28809	.000	1179.0203	1360.9797
	TNS(H)	1434.40000*	26.28809	.000	1343.4203	1525.3797
	TNS(L)	1434.40000*	26.28809	.000	1343.4203	1525.3797
	(TNS)2Zn(H)	1402.00000*	26.28809	.000	1311.0203	1492.9797
	(TNS)2Zn(L)	1396.00000*	26.28809	.000	1305.0203	1486.9797
	(TNS)2Ni(H)	1430.80000*	26.28809	.000	1339.8203	1521.7797
	(TNS)2Ni(L)	1411.60000*	26.28809	.000	1320.6203	1502.5797
	(TNS)2Cu(H)	1410.40000*	26.28809	.000	1319.4203	1501.3797
	(TNS)2Cu(L)	1421.20000*	26.28809	.000	1330.2203	1512.1797
positive control	negative control	-1270.00000*	26.28809	.000	-1360.9797	-1179.0203
	TNS(H)	164.40000*	26.28809	.000	73.4203	255.3797
	TNS(L)	164.40000*	26.28809	.000	73.4203	255.3797
	(TNS)2Zn(H)	132.00000*	26.28809	.000	41.0203	222.9797
	(TNS)2Zn(L)	126.00000*	26.28809	.001	35.0203	216.9797
	(TNS)2Ni(H)	160.80000*	26.28809	.000	69.8203	251.7797
	(TNS)2Ni(L)	141.60000*	26.28809	.000	50.6203	232.5797
	(TNS)2Cu(H)	140.40000*	26.28809	.000	49.4203	231.3797
	(TNS)2Cu(L)	151.20000*	26.28809	.000	60.2203	242.1797
TNS(H)	negative control	-1434.40000*	26.28809	.000	-1525.3797	-1343.4203
	positive control	-164.40000*	26.28809	.000	-255.3797	-73.4203
	TNS(L)	.00000	26.28809	1.000	-90.9797	90.9797
	(TNS)2Zn(H)	-32.40000	26.28809	1.000	-123.3797	58.5797
	(TNS)2Zn(L)	-38.40000	26.28809	1.000	-129.3797	52.5797
	(TNS)2Ni(H)	-3.60000	26.28809	1.000	-94.5797	87.3797
	(TNS)2Ni(L)	-22.80000	26.28809	1.000	-113.7797	68.1797
	(TNS)2Cu(H)	-24.00000	26.28809	1.000	-114.9797	66.9797
	(TNS)2Cu(L)	-13.20000	26.28809	1.000	-104.1797	77.7797

(I) group	(J) group	Mean Difference (I-J)	Std. Error	Sig.	95% Confidence Interval	
					Lower Bound	Upper Bound
TNS(L)	negative control	-1434.40000*	26.28809	.000	-1525.3797	-1343.4203
	positive control	-164.40000*	26.28809	.000	-255.3797	-73.4203
	TNS(H)	.00000	26.28809	1.000	-90.9797	90.9797
	(TNS)2Zn(H)	-32.40000	26.28809	1.000	-123.3797	58.5797
	(TNS)2Zn(L)	-38.40000	26.28809	1.000	-129.3797	52.5797
	(TNS)2Ni(H)	-3.60000	26.28809	1.000	-94.5797	87.3797
	(TNS)2Ni(L)	-22.80000	26.28809	1.000	-113.7797	68.1797
	(TNS)2Cu(H)	-24.00000	26.28809	1.000	-114.9797	66.9797
	(TNS)2Cu(L)	-13.20000	26.28809	1.000	-104.1797	77.7797
(TNS)2Zn(H)	negative control	-1402.00000*	26.28809	.000	-1492.9797	-1311.0203
	positive control	-132.00000*	26.28809	.000	-222.9797	-41.0203
	TNS(H)	32.40000	26.28809	1.000	-58.5797	123.3797
	TNS(L)	32.40000	26.28809	1.000	-58.5797	123.3797
	(TNS)2Zn(L)	-6.00000	26.28809	1.000	-96.9797	84.9797
	(TNS)2Ni(H)	28.80000	26.28809	1.000	-62.1797	119.7797
	(TNS)2Ni(L)	9.60000	26.28809	1.000	-81.3797	100.5797
	(TNS)2Cu(H)	8.40000	26.28809	1.000	-82.5797	99.3797
	(TNS)2Cu(L)	19.20000	26.28809	1.000	-71.7797	110.1797
(TNS)2Zn(L)	negative control	-1396.00000*	26.28809	.000	-1486.9797	-1305.0203
	positive control	-126.00000*	26.28809	.001	-216.9797	-35.0203
	TNS(H)	38.40000	26.28809	1.000	-52.5797	129.3797
	TNS(L)	38.40000	26.28809	1.000	-52.5797	129.3797
	(TNS)2Zn(H)	6.00000	26.28809	1.000	-84.9797	96.9797
	(TNS)2Ni(H)	34.80000	26.28809	1.000	-56.1797	125.7797
	(TNS)2Ni(L)	15.60000	26.28809	1.000	-75.3797	106.5797
	(TNS)2Cu(H)	14.40000	26.28809	1.000	-76.5797	105.3797
	(TNS)2Cu(L)	25.20000	26.28809	1.000	-65.7797	116.1797
(TNS)2Ni(H)	negative control	-1430.80000*	26.28809	.000	-1521.7797	-1339.8203
	positive control	-160.80000*	26.28809	.000	-251.7797	-69.8203
	TNS(H)	3.60000	26.28809	1.000	-87.3797	94.5797
	TNS(L)	3.60000	26.28809	1.000	-87.3797	94.5797
	(TNS)2Zn(H)	-28.80000	26.28809	1.000	-119.7797	62.1797

	(TNS)2Zn(L)	-34.80000	26.28809	1.000	-125.7797	56.1797
	(TNS)2Ni(L)	-19.20000	26.28809	1.000	-110.1797	71.7797
	(TNS)2Cu(H)	-20.40000	26.28809	1.000	-111.3797	70.5797
	(TNS)2Cu(L)	-9.60000	26.28809	1.000	-100.5797	81.3797
(TNS)2Ni(L)	negative control	-1411.60000*	26.28809	.000	-1502.5797	-1320.6203
	positive control	-141.60000*	26.28809	.000	-232.5797	-50.6203
	TNS(H)	22.80000	26.28809	1.000	-68.1797	113.7797
	TNS(L)	22.80000	26.28809	1.000	-68.1797	113.7797
	(TNS)2Zn(H)	-9.60000	26.28809	1.000	-100.5797	81.3797
	(TNS)2Zn(L)	-15.60000	26.28809	1.000	-106.5797	75.3797
	(TNS)2Ni(H)	19.20000	26.28809	1.000	-71.7797	110.1797
	(TNS)2Cu(H)	-1.20000	26.28809	1.000	-92.1797	89.7797
	(TNS)2Cu(L)	9.60000	26.28809	1.000	-81.3797	100.5797
(TNS)2Cu(H)	negative control	-1410.40000*	26.28809	.000	-1501.3797	-1319.4203
	positive control	-140.40000*	26.28809	.000	-231.3797	-49.4203
	TNS(H)	24.00000	26.28809	1.000	-66.9797	114.9797
	TNS(L)	24.00000	26.28809	1.000	-66.9797	114.9797
	(TNS)2Zn(H)	-8.40000	26.28809	1.000	-99.3797	82.5797
	(TNS)2Zn(L)	-14.40000	26.28809	1.000	-105.3797	76.5797
	(TNS)2Ni(H)	20.40000	26.28809	1.000	-70.5797	111.3797
	(TNS)2Ni(L)	1.20000	26.28809	1.000	-89.7797	92.1797
	(TNS)2Cu(L)	10.80000	26.28809	1.000	-80.1797	101.7797
(TNS)2Cu(L)	negative control	-1421.20000*	26.28809	.000	-1512.1797	-1330.2203
	positive control	-151.20000*	26.28809	.000	-242.1797	-60.2203
	TNS(H)	13.20000	26.28809	1.000	-77.7797	104.1797
	TNS(L)	13.20000	26.28809	1.000	-77.7797	104.1797
	(TNS)2Zn(H)	-19.20000	26.28809	1.000	-110.1797	71.7797
	(TNS)2Zn(L)	-25.20000	26.28809	1.000	-116.1797	65.7797
	(TNS)2Ni(H)	9.60000	26.28809	1.000	-81.3797	100.5797
	(TNS)2Ni(L)	-9.60000	26.28809	1.000	-100.5797	81.3797
	(TNS)2Cu(H)	-10.80000	26.28809	1.000	-101.7797	80.1797

*. The mean difference is significant at the 0.05 level.

Appendix (C)

Gastric lesions and flattening of the folds inside rats stomachs

(a)

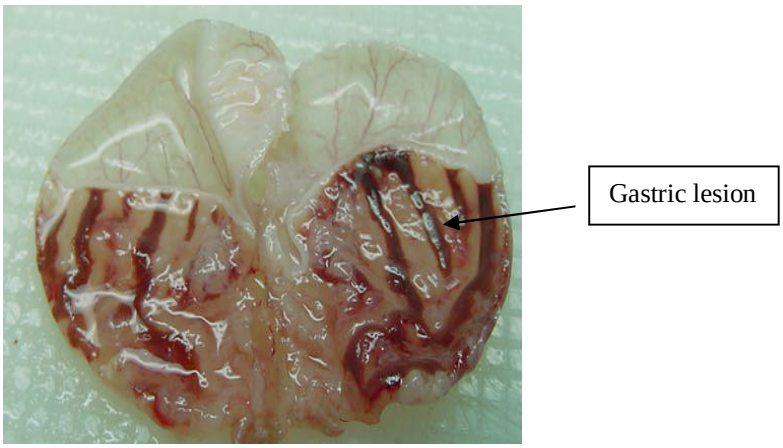

Gross appearance of the gastric mucosa in a rat pre-treated with 5 ml/kg of 10% Tween 20 (ulcer control). Severe injuries are seen in the gastric mucosa.

(b)

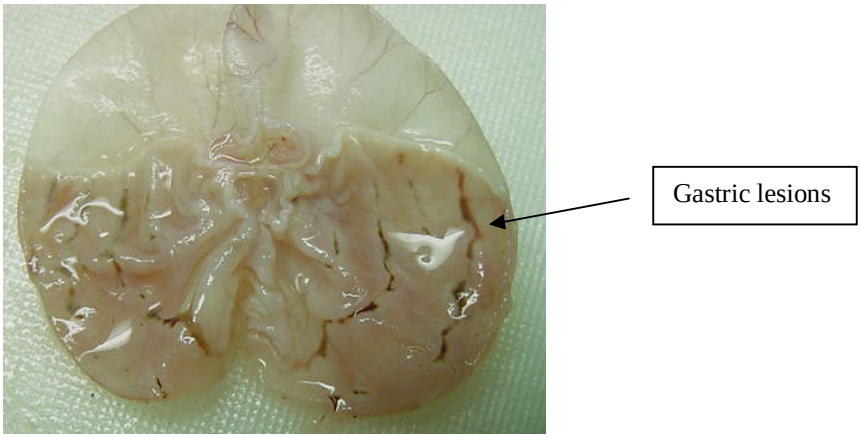

Gross appearance of the gastric mucosa in a rat pre-treated with 5 ml/kg of Cimedine (50 mg/kg). Injuries to the gastric mucosa are milder compared to the injuries seen in the negative control rat.

(c)

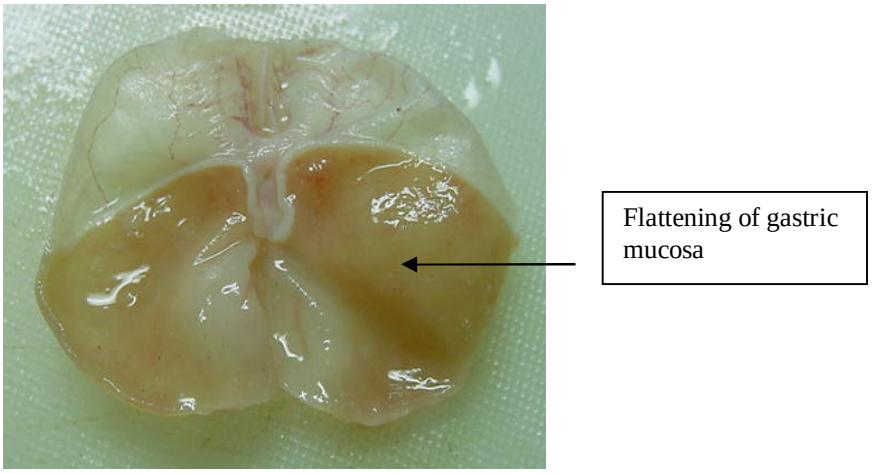

Gross appearance of the gastric mucosa in a rat pre-treated with 5 ml/kg of synthesized Schiff bases and complexes (60 mg/kg). No injuries to the gastric mucosa are seen, and showed flattening of gastric mucosa.

Appendix (D) Histology

(d)

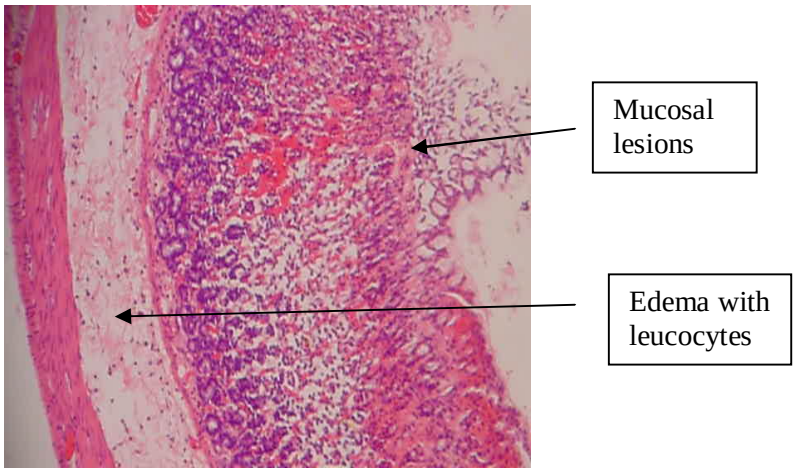

Histological section of gastric mucosa in a rat pre-treated with 5 ml/kg of 10% Tween 20 (ulcer control) only. There is severe disruption to the surface epithelium, and edema of the submucosa layer with leucocyte infiltration.

(e)

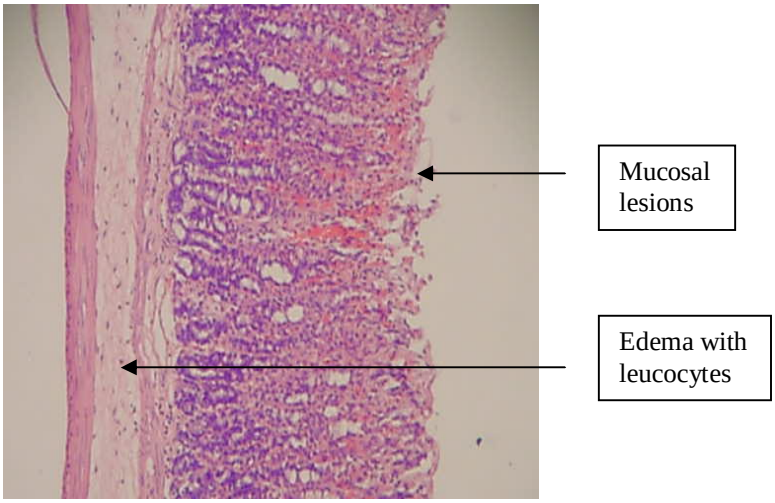

Histological section of gastric mucosa in a rat pre-treated with 5 ml/kg of Cimedine (50 mg/kg). There is mild disruption to the surface epithelium with mild edema and leucocytes infiltration of the submucosal layer.

(f)

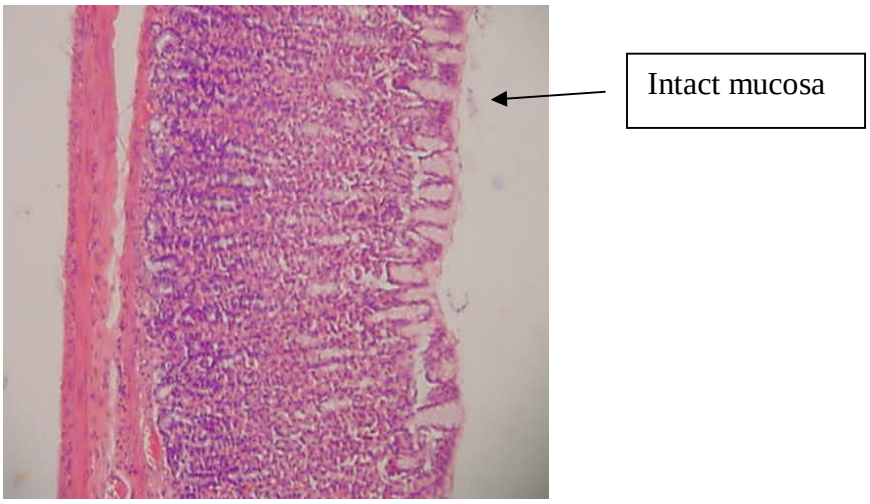

Histological section of gastric mucosa in a rat pre-treated with 5 ml/kg of Synthesized Schiff base t (250 mg/kg). There is no disruption to the surface epithelium with no edema and no leucocytes infiltration of the submucosal layer.

Appendix (E)

Standard curve for DPPH assay (TS series):

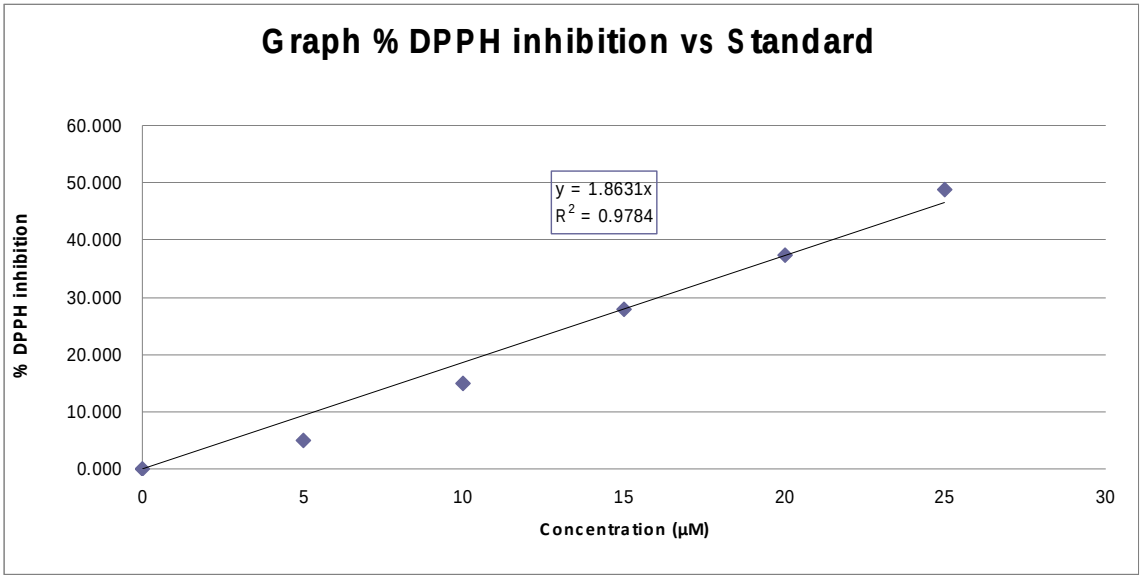

Standard curve show the percent inhibition of DPPH with various concentrations of Vitamin C.

Dose response curves for TS series:

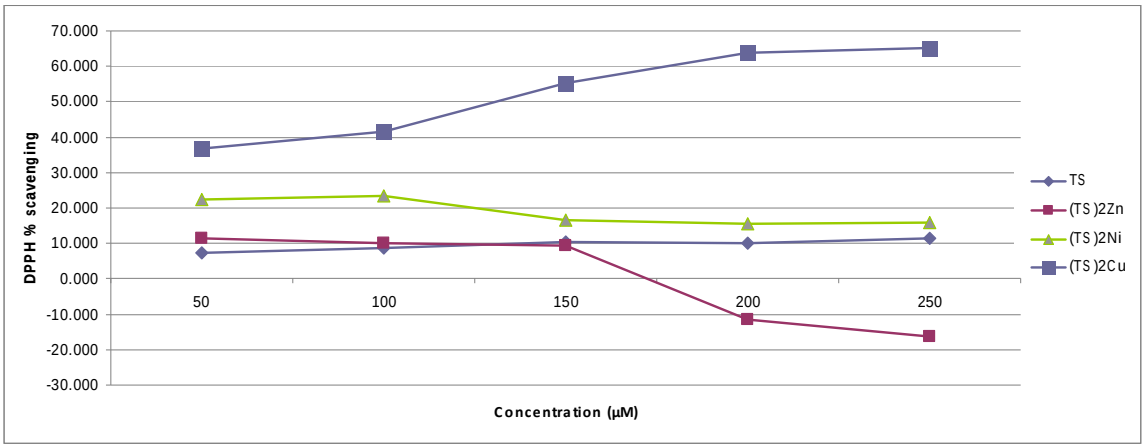

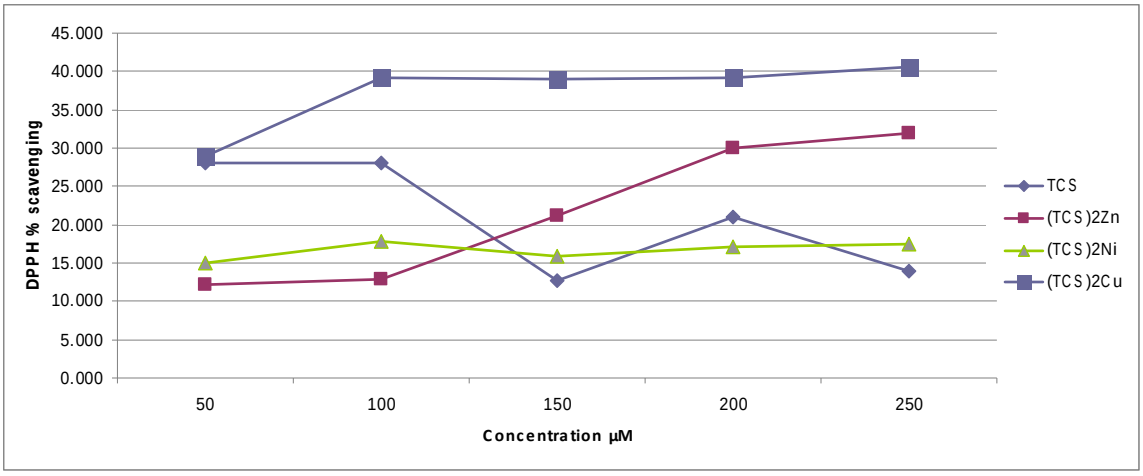
45.000
40.000
35.000
30.000
25.000
20.000
15.000
10.000
5.000
0.000
DPPH % scavenging
50
100
150
200
250
Concentration µM
TCS
(TCS)2Zn
(TCS)2Ni
(TCS)2Cu

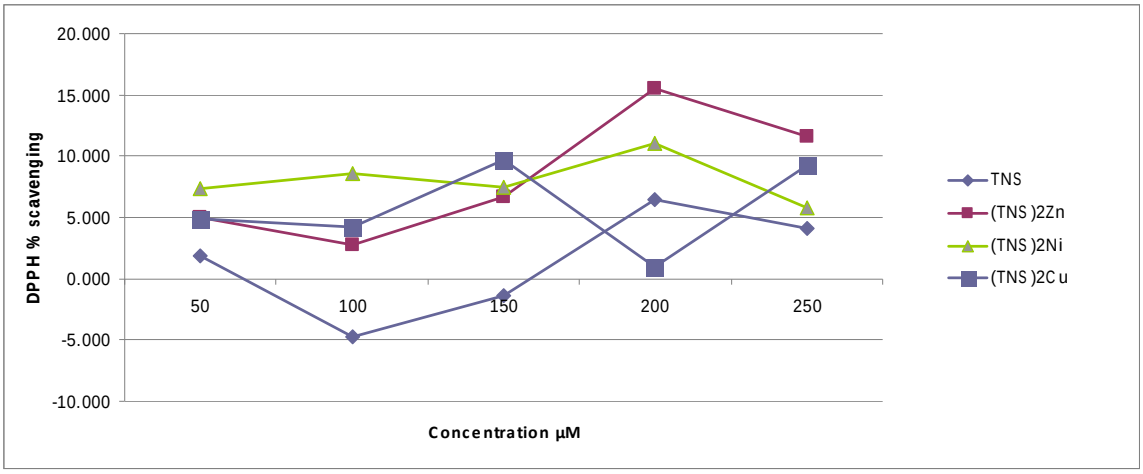
20.000
15.000
10.000
5.000
0.000
-5.000
-10.000
DPPH % scavenging
50
100
150
200
250
Concentration µM
TNS
(TNS)2Zn
(TNS)2Ni
(TNS)2Cu

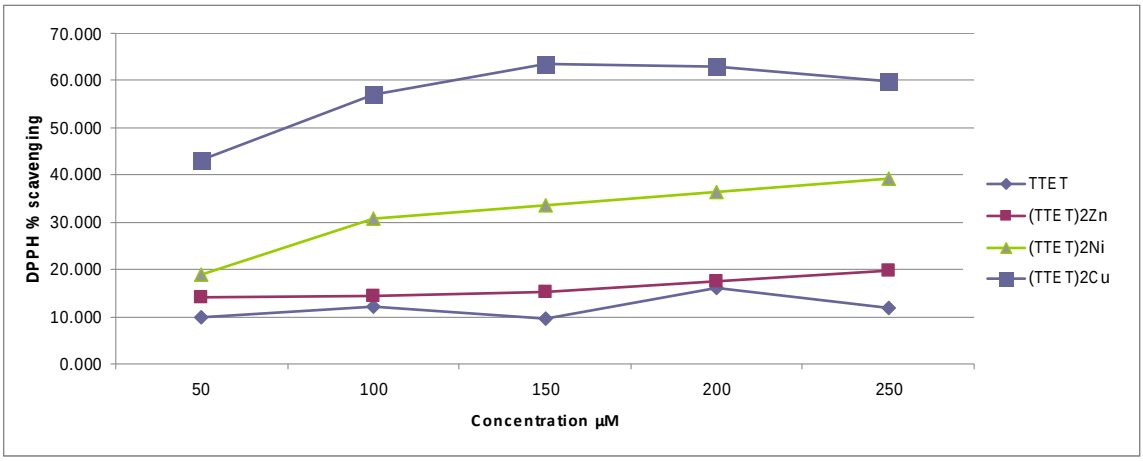
70.000
60.000
50.000
40.000
30.000
20.000
10.000
0.000
DPPH % scavenging
50
100
150
200
250
Concentration µM
TTET
(TTET)2Zn
(TTET)2Ni
(TTET)2Cu

Standard curve for DPPH assay (THAP series):

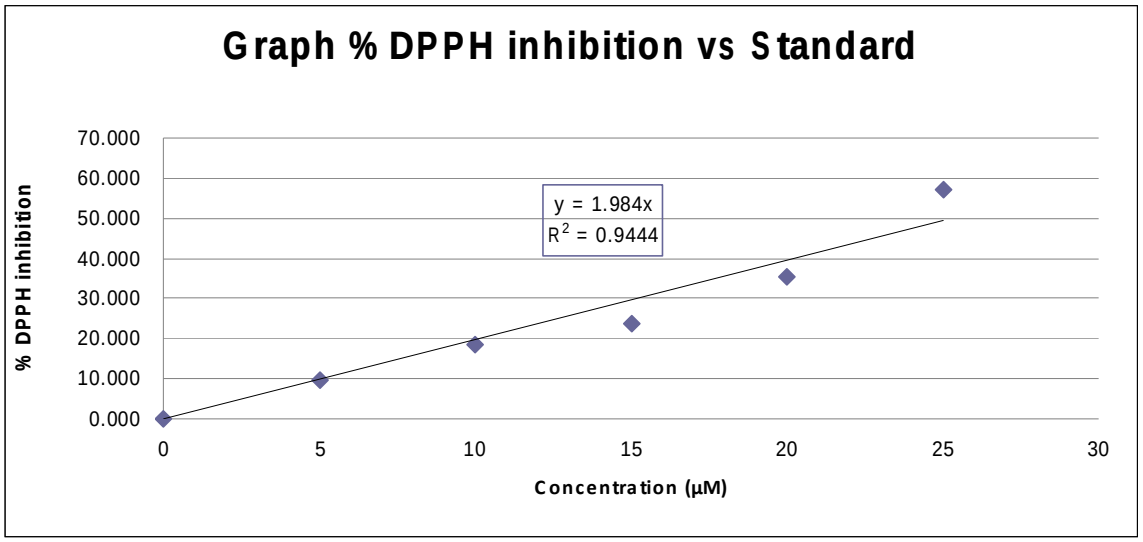

Standard curve show the percent inhibition of DPPH with various concentrations of Vitamin C.

Dose response curves for THAP series:

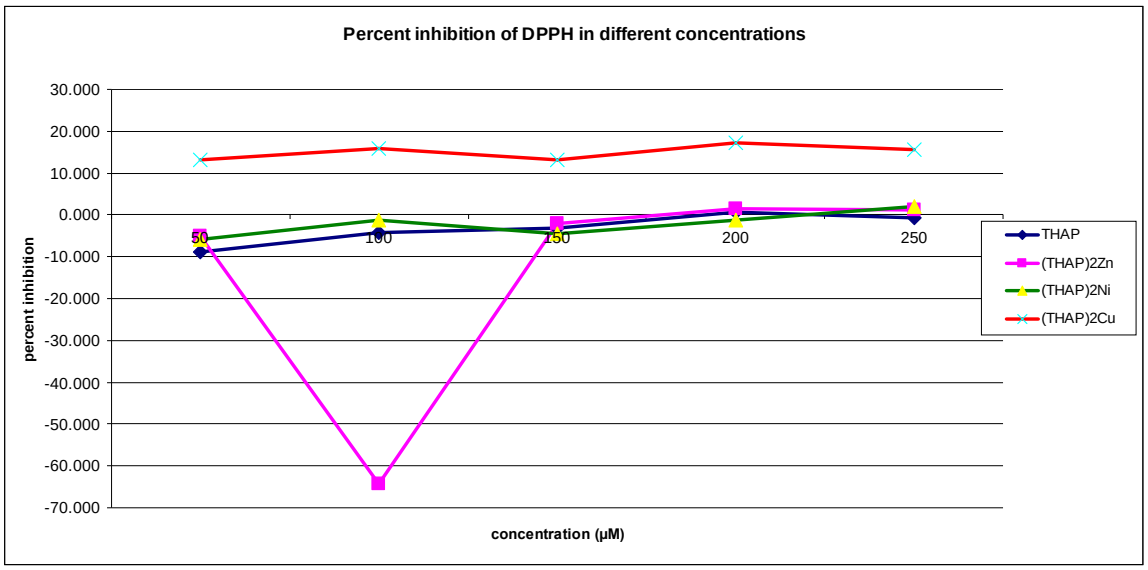

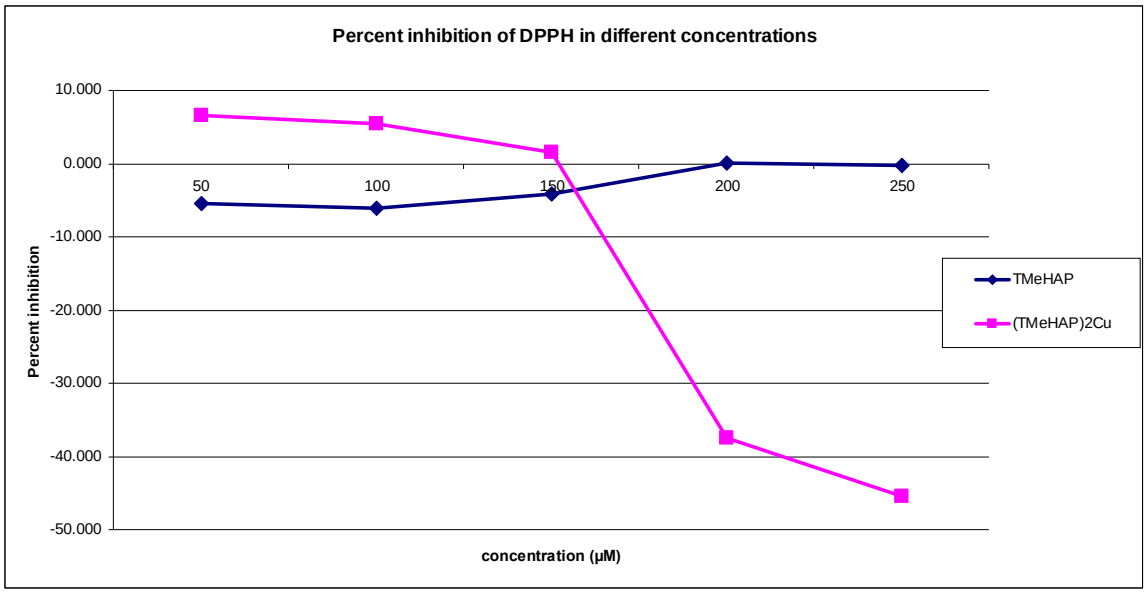
Percent inhibition of DPPH in different concentrations
10.000
0.000
-10.000
-20.000
-30.000
-40.000
-50.000
50
100
150
200
250
Percent inhibition
concentration (µM)
TMeHAP
(TMeHAP)2Cu

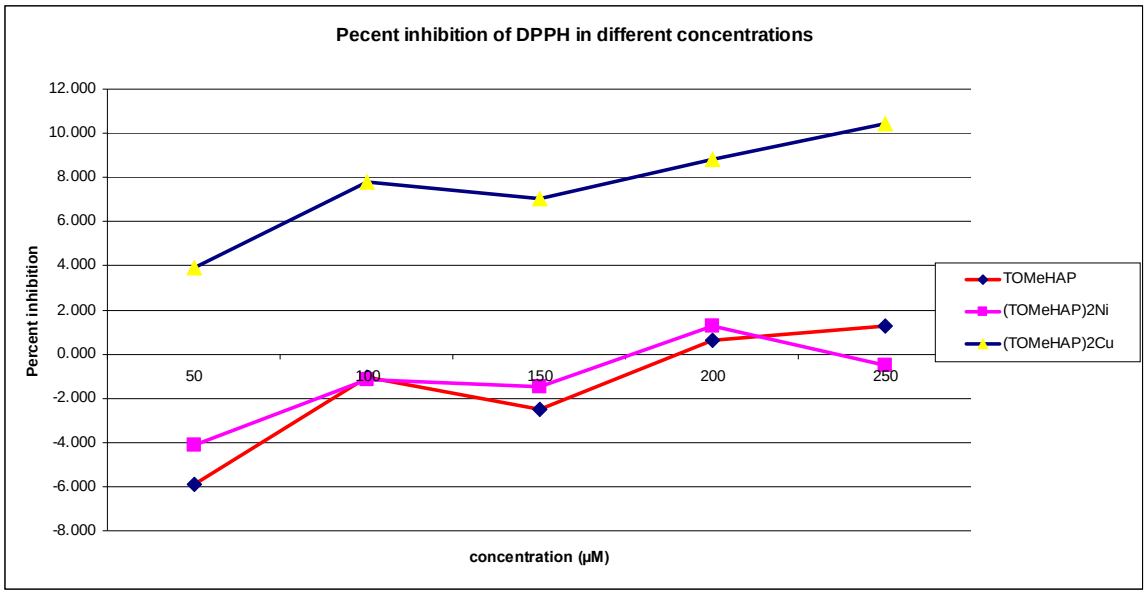
Pecent inhibition of DPPH in different concentrations
12.000
10.000
8.000
6.000
4.000
2.000
0.000
-2.000
-4.000
-6.000
-8.000
50
100
150
200
250
Percent inhibition
concentration (µM)
TOMeHAP
(TOMeHAP)2Ni
(TOMeHAP)2Cu

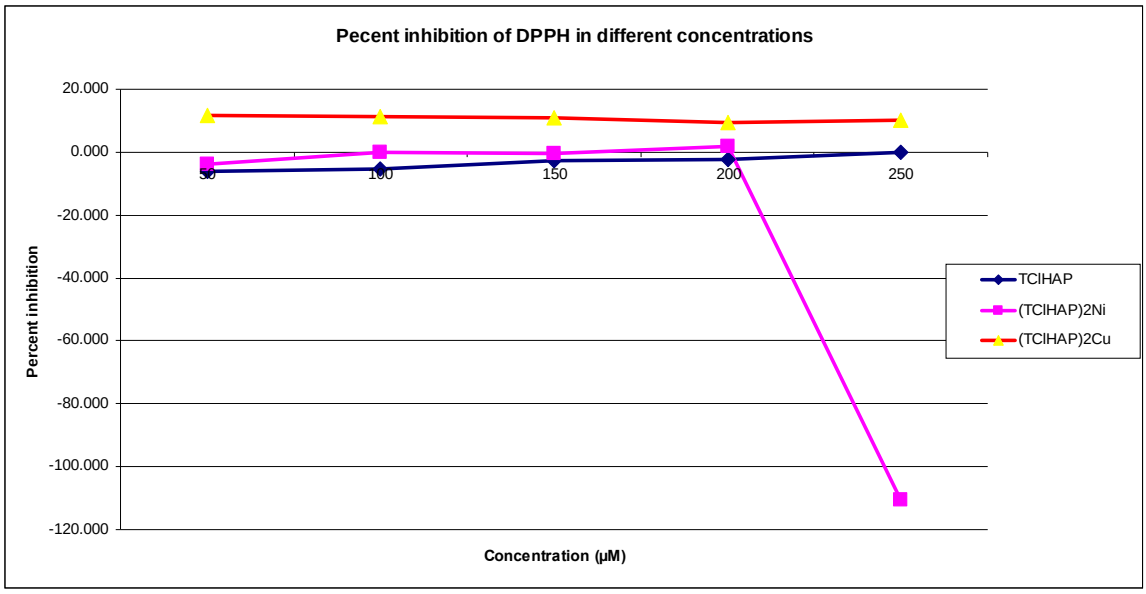
Pecent inhibition of DPPH in different concentrations
20.000
0.000
-20.000
-40.000
-60.000
-80.000
-100.000
-120.000
Percent inhibition
50
100
150
200
250
Concentration (µM)
TClHAP
(TClHAP)2Ni
(TClHAP)2Cu

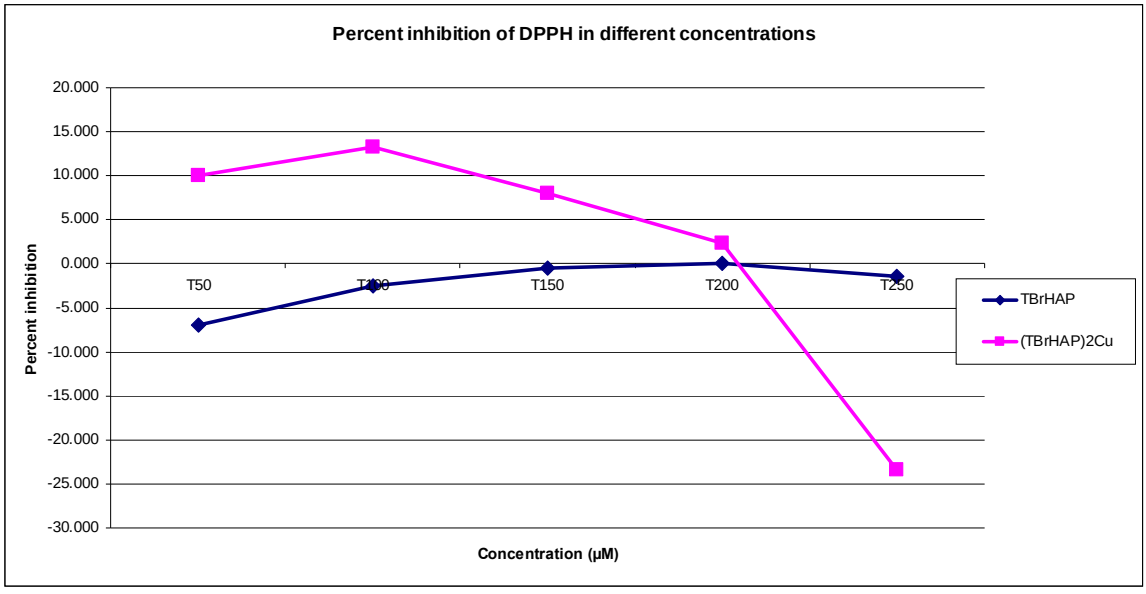
Percent inhibition of DPPH in different concentrations
20.000
15.000
10.000
5.000
0.000
-5.000
-10.000
-15.000
-20.000
-25.000
-30.000
Percent inhibition
T50
T100
T150
T200
T250
Concentration (µM)
TBrHAP
(TBrHAP)2Cu

FRAP standard curves:

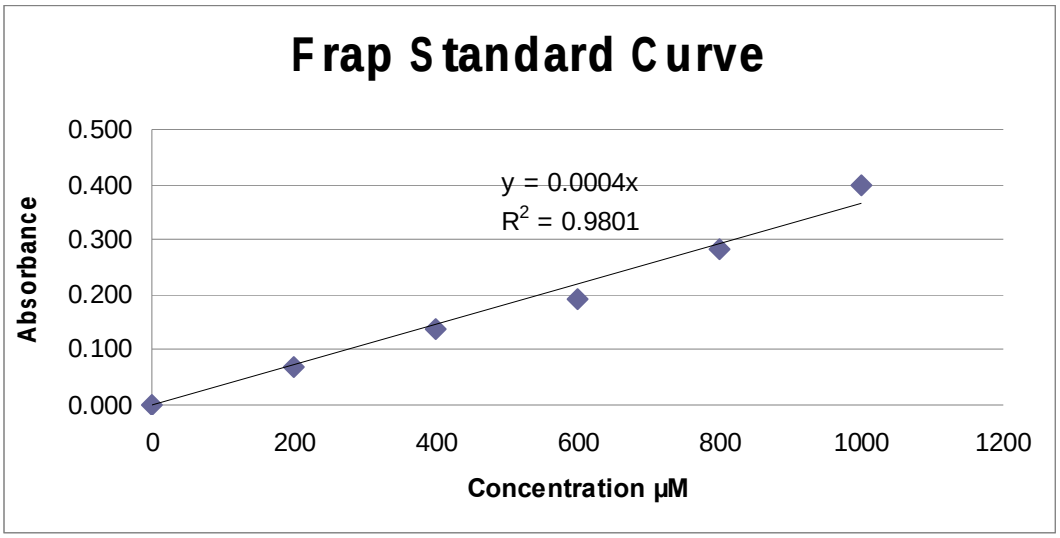

Standard curve shows the variation of absorbance of the FRAP reagent with changing the concentration of ascorbic acid (Vit. C) (Used in calculations of FRAP values for TS series)

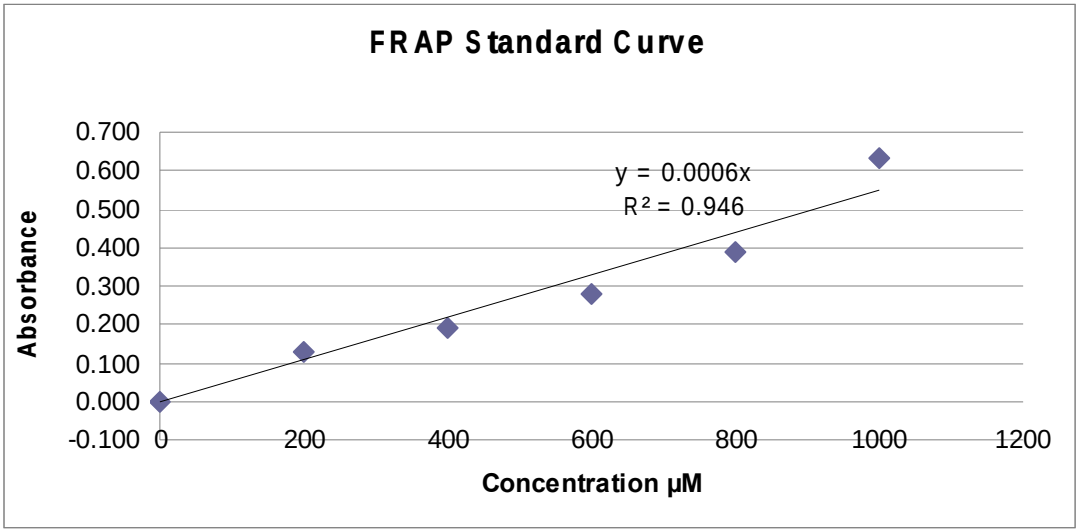

Standard curve shows the variation of absorbance of the FRAP reagent with changing the concentration of ascorbic acid (Vit. C) (Used in calculations of FRAP values for THAP series)

References

[1] H. Schiff; Ann Chem. 131 (1864) 118

[2] S. Yamada, Coord. Chem. Rev. 190–192 (1999) 537–555

[3] E.F.Pratt and M.J.Kamlet; J.Org Chem. 26 (1961) 4029

[4] P. Saul, The chemistry of the carbon–nitrogen double bond, John Wiley and sons, London, 1970

[5] L.Sacconi; Coord. Chem. Rev. 1 (1966) 192

[6] S. Yamada, Coord. Chem. Rev. 1 (1966) 415

[7] N.F Curtis, Coord. Chem. Rev. 3 (1968) 3

[8] R.H Holm, G.W Everett, and J. Chakravorthy, Progress in inorganic chemistry, Vol.7 Interscience, New York, 1966, p 83-214

[9] L.Sacconi, Coord. Chem. Rev 1 (1966) 126

[10] Haidue and Ional, Basic organometallic chemistry, W. de Gruyter, Berlin, 1985

[11] F. Dwyer and Meller, Chelating agents and metal chelates, Academic press, New York, 1964

[12] H. Schiff; Ann. Chem. 150 (1869) 193

[13] H. Schiff; Ann. Chem. 151 (1869) 186.

[14] L. Sacconi, M. Ciampolini, and G.P Speroni; J Am Chem. Soc 87 (1965) 3102

[15] A. Chakravorty; Inorg Chem. 4 (1965) 127

[16] J.B Willis, D.P Mellor; J Am Chem. Soc 69 (1947) 1237

[17] P.L Orioli, L. Sacconi, M. Di Vaira; Chem. Comm. (London) 1 (1965) 103

[18] L. Carbonaro, A. Gacomelli; Inorg Chim Acta 165 (1989) 197

[19] R. Butcher and E. Sinn; Inorg Chem., 15 (1976) 1604

[20] J. Costamagna, J. Vargas, R. Latorre, A. Alvarado, and G. Mena; Coord Chem. Rev; 119 (1992) 67

[21] M.G. Martin Reyes, P. Gili, P. Martin Zarza, A. Medina and M.C Diaz; Inorg Chim. Acta, 116 (1986) 153

[22] K. Ueno and A.E Martell; J Phys Chem. 61 (1957) 257

[23] A.B.P Lever; Inorganic electronic spectroscopy, Elsevier, Amsterdam, 1968 pp 320-343

[24] P.Gili, P. Martin Zarza, P. Nunez, A. Medina and M. G Martin; J Coord Chem. 20 (1989) 273

[25] P. Martin Zarza, A. Medina, A. Mederos and P. Gili; Transition Met Chem.15 (1990) 152

[26] P.Gili, M.L Rodriguez; Inorg Chim Acta, 176 (1990) 261

[27] P. Gili, C. Ruiz and F.V Lahoz; Polyhedron 11/17 (1992) 2171

[28] P.Gili, M.G Martin Reyes, P. Martin Zarza and A.J.L Pombeiro; Inorg Chim Acta 255 (1997) 279

[29] N.S Navaneetham, R.Kalyanasundaram and S.Soundararajan; Inorg. Chim Acta 110 (1985) 169

[30] Y. Tor, J. Libman, A. shanzer and S. Lifson; J. Am Chem. Soc 109 (1987) 6517

[31] R. Grigg and P. Armstrong; Tetrahedron 45 (1989) 23

[32] R.W Hay in D.R Williams Ed, An introduction to bioinorganic chemistry, Thomas, New York, 1976 Chap 4

[33] N.E Dixon, C. Gazzola; J. Am Chem. Soc 97 (1975) 4131

[34] H. Sigel and A. Sigel, Metal ions in biological systems, Vol. 23 , Dekker , New York, 1989

[35] C.T Walsh and W.H Orme Johnson; Biochemistry, 26 (1987) 4901

[36] L. Araya, J. Vargas and J. Costamagna; Transitiom Met Chem. 11 (1986) 312

[37] T. Sakura, and J. Hong; Inorg Chim Acta 46 (1980) 205

[38] J.H. Cameron, S.C Turner; J. Chem. Soc. Dalton Trans 23 (1992) 3285

[39] F.C Felicio, T.T.G. Cavalheiro, E.R Dockal; Polyhedron 20 (2001) 261

[40] S. Akmal Gaballa, S. Mohsen Asker, S. Atiat Barakat, S.M. Teleb; Spectrochim. Acta Part A, 67 (2007) 114

[41] D. Chen and A**.** E. Martell; Inorg. Chem. 26 (1987) 1026-1030

[42] E. Fenz; Munch. Med. Wschr 18 (1941) 398

[43] J.R.J Sorenson and W. Hangarter; Inflammation 2 (1977) 217

[44] J.R.J Sorenson; Inflammation 1 (1976) 317

[45] J.R.J Sorenson; J. Med. Chem. 19 (1976) 135

[46] J.R.J Sorenson; Prog. Med. Chem. 15 (1978) 211

[47] M. Peter and R. David in: Metal ions in biological systems, Vol 12, Helmut Sigel, New York, 1981 pp 283-317

[48] P.K Parashar, R.C. Sharma and G. Mohan; Biological Trace Element Res; 23 (1990) 145

[49] K.D Rainsford and M.W. Whitehouse; Experientia 32/9 (1976) 1172

[50] J. Vanco, J. Marek, Z. Travnicek and O. Svajlenova; J. Inorg Biochemistry, 102 (2008) 595

[51] P. Varughese, B. Murukan, B. Sindhu and K. Mohanan; Sectrochim. Acta Part A, 70 (2008) 403

[52] R.M Kelloggin, C.W Bird, G.W.H Cheeseman; Comprehensive heterocyclic chemistry, Vol 4, Oxford, 1984

[53] Z.H Chohan, M. Hassan, K.M Khan, C.T Supuran; J. Enz Inhib.Med.Chem 20 (2005) 183

[54] W. Zishen, L. Zhipping and Y. Zhenhaun; Transition Met. Chem. 18 (1993) 291

[55] C. Alaaddin, Y. Ibrahim, O. Habibe and A. Misir, Transition Met. Chem. 27 (2002) 171

[56] H. Dong; J. Organometallic Chem. 690 (2005) 3714

[57] M. A. Hapipah, S. Nadiah Abdul Halim, S. Puvaneswary, M. Sharifudin and I. Endom; Malaysian J. of Science 25/1 (2006) 99

[58] S.G. Gruber, C.M. Harris and E. Sinn, J. Inorg. Nucl. Chem 30 (1968) 1805

[59] G.C. Peroy, J. Inorg. Nucl. Chem 37 (1975) 2071

[60] S. Zolezzi, A. Decinti and E. Spodine, Polyhedron 18 (1999) 897

[61] D. M. Adams, Metal-ligand and related vibrations, Edward Arnold, London, 1967, pp 248 & 284

[62] S.A Abdel-Latif, H.B. Hassib and Y.A. Issa, Spectrochim. Acta Part A 67 (2007) 950-957

[63] L. Lindoy, W.E. Moody and D. Taylor, Inorg. Chem 16 (1977) 1962

[64] J. A. Faniran, K.S. Patel and L.O. Nelson, J Inogr. Nucl. Chem 38 (1976) 77

[65] A. D. Cross and R. Alan Jones, An introduction to practical infrared spectroscopy, Butterworths, London, 1969.

[66] H. M. Ali, M. I. Mohamed Mustafa, M. R. Rizal and S. W. Ng, Acta Cryst E 64 (2008) m718-719.

[67] D.L. Pavia, G.M. Lampman and G.S. Kriz, Introduction to spectroscopy, Thomson Learning, Washington, 2001

[68] D. Todor, and Carmy Lim, J Am. Chem Soc. 122 (2000) 11146

[69] G. D. Christian, Analytical Chemistry, Third edition, Jonn Wiley and sons, New York, 1980

[70] M. Kato, K. Imai, Y. Muto, T. Tokii and H.B.J. Jonassen, J Inorg. Nucl. Chem. 35 (1973) 109.

[71] B. Harry and C.J. Ballhausen, J. Am. Chem. Soc. 85 (1963) 260

[72] M. A. Ali, A.H. Mirza M. H. Hamid P. V. Bernhardt, O. Atchade, X. Song. G. Eng and L.May, Polyhedron 27 (2008) 977-984.

[73] L. Casella, M. Gullotti and G.Pacchiani, J. Am Chem. Soc. 104 (1982) 2386

[74] H. M. Ali, M. I. Mohamed Mustafa, M. R. Rizal and S. W. Ng, Acta Cryst E 64 (2008) o913.

[75] M.L Rodriguez, E. Medina, P.Gili and M.C Diaz; Acta Cryst C43 (1987) 134

[76] A. Wakahara, T. Fujiwara, and K. Tomita; Bull. Chem.. Soc. Jpn 46 (1973) 2481

[77] L.Sacconi, P. Paoletti and F. Maggio; J. Am. Chem. Soc. 79 (1957) 4067

[78] N.H Cromwell and F.A Miller; J. Am. Chem. Soc. 71 (1949) 3337

[79] H. M. Ali, M. I. Mohamed Mustafa, M. R. Rizal and S. W. Ng, Acta Cryst. E 64 (2008) m787.

[80] M.A. Hapipah, M. I Mohamed Mustafa, M. R. Rizal and Ng. Seik Weng, Acta Cryst. E 64 (2008) m421

[81] H. M. Ali, M. I. Mohamed Mustafa, M. R. Rizal and S. W. Ng, Acta Cryst. E64 (2008) m718-m719

[82] A. Robert, J.E. Nezamis, C. Lancaster, A.J. Hanchar, Gastroenterology 77 (1979) 433-443.

[83] D. W. Piper and D. Stiel, Medical Progress 2 (1986) 7-10

[84] T.H. Baron, M.T.S. and C. Wastell, Recent Advances in Gastroenterology, Churehill Livingstone, London, 1980 pp. 23-29.

[85] S. Kato, T. Kawase, J. Alderman, N. Inatomi, C.S. Lieber, Gastroenterology, 98 (1990) 203-210.

[86] R. Nordmann, Alcohol 29 (1994) 513-522.

[87] S. Szabo, S. Kusstatscher, G. Sakoulas, Z. Sandor, A. Vincze and M. Jadus, J. Gastroenterology 210 (1995) 15-18.

[88] E. Marhuenda, M.J. Martin and C. Alarcon de la Lastra, Phytotherapy Res. 7 (1993) 13-16.

[89] H. Mutoh, H. Hiraishi, S. Ota, K.J. Ivey, A. Terano and T. Sugimoto, Am J. Physiol. 258 (1990) G603-G609.

[90] A.S. Salim, Digestion 47/1 (1990) 24-28.

[91] G.P. Garg, S.K. Nigam, C.W. Ogle, Planta Medica 59 (1993) 215-217

[92] L.A.F. Paiva, V.S.N. Rao, N.V. Gramosa and F.R. Silveira, J. Ethnopharmacology 62 (1998) 73-78

[93] S. Murakamu, H. Kijima, Y. Isob, Planta Medica 56 (1990) 360-363

[94] V. C. O. Njar, J.K. Adesanwo, and J. Raji, Planta Medica 61 (1995) 91-92

[95] H. Varley, A.H. Gowenlock, M. Bell, Practical Clinical Biochemistry, The Whitefrairs Press, London, 1980, pp 535-595

[96] H.U. Bergmeyer, Clinica Chim. Acta 105 (1980) 147-154

[97] N.W. Tietz, A.D. Rinker and L.M. Shaw, J. Clinical Chem. and Clinical Biochem. 21 (1983) 731-748

[98] L.Franco and D. Doria, Pharm. Res. 36/5 (1997) 395-399

[99] T. Garrick, S. Buack, P. Bass, Am J. Physiol. 250 (1986) 6191-6199.

[100] K. Takeuchi, K. Nishiwakki, S. Okabe, Digestive Diseases Sciences 31 (1987) 1100-1107.

[101] K. Takeuchi and Y. Nobuhara, Digestive Disease Sciences 30 (1985) 1181-1188.

[102] A.W. Mersereau, and E.J. Hinchey, Surgery 91 (1982) 150-155.

[103] T. Guardia, J. Guzm´an, M.J. Pestchanker, E. Guerreiro, O.S. Giordano, J. Nat. Products 57 (1994) 507–509.

[104] S. Laura, S. Favier, M.O. Alejandra Mar´ıa, H. Graciela Wendel, J. Eduardo Borkowski, S. Oscar Giordano, L. Pelzer, E.C. Tonn, J. Ethnopharmacology 100 (2005) 260–267

[105] L. Franco, and D. Doria, Pharmaco Res. 36/5 (1997) 359-399

[106] M. Alberghina, G. La Spina, A. Mangiameli, M. Gulisano, D. Sciotto and E. Rizzarelli, J. Inorg. Biochem. 45 (1992) 245-259

[107] S.Y. Wang and H. Jiao, J. Agric. Food. Chem. 48 (2000) 5677-5684.

[108] F.F Benzie and J.J Strain, Methods in enzymology, 299 (1999) 15-23.

Table 4.3: Observed ulcer area, mucus weight, pH and inhibition percentage in rats for TNS and its complexes:

Compound	Total ulcer area(mm^2) (Mean ± S.E.M)	Mucus weight (g)	pH	% inhibition
Tween-20 (-ve control)	1438 ± 58^a	0.58	7.00	-
Cimetidine (+ve control)	168 ± 5^b	0.61	7.00	88
TNS (HD)	3.6 ± 0.2^c	1.33	4.22	100
TNS (LD)	3.6 ± 0.2^c	1.60	4.11	100
$(TNS)_2Zn$ (HD)	36.0 ± 0.4^c	1.13	3.92	97
$(TNS)_2Zn$ (LD)	42.0 ± 0.5^c	1.10	3.15	97
$(TNS)_2Ni$ (HD)	7.2 ± 0.3^c	1.65	3.68	100
$(TNS)_2Ni$ (LD)	26.4 ± 0.5^c	2.00	3.05	98
$(TNS)_2Cu$ (HD)	27.6 ± 0.4^c	1.63	6.03	98
$(TNS)_2Cu$ (LD)	16.8 ± 0.6^c	4.00	3.81	99

All values are expressed as mean ± standard error mean. Means with different superscripts are significantly different. The mean difference is significant at the $p<0.05$ level.
HD (High dose: 60 mg/kg), LD (Low dose: 30 mg/kg)

Table 4.2: Observed ulcer area, mucus weight, pH and inhibition percentage in rats for TCS and its complexes:

Compound	Total ulcer area(mm^2) (Mean ± S.E.M)	Mucus weight (g)	pH	% inhibition
Tween-20 (-ve control)	1438 ± 58^{a}	0.58	7.00	-
Cimetidine (+ve control)	168 ± 5^{b}	0.61	7.00	88
TCS (HD)	262.8 ± 0.8^{c}	1.10	6.06	81
TCS (LD)	$Zero^{d}$	1.22	3.68	100
$(TCS)_2Zn$ (HD)	12.0 ± 0.1^{d}	1.44	3.66	99
$(TCS)_2Zn$ (LD)	69.6 ± 0.4^{d}	1.20	3.19	95
$(TCS)_2Ni$ (HD)	38.4 ± 0.2^{d}	1.58	3.69	97
$(TCS)_2Ni$ (LD)	117.6 ± 1.0^{ad}	1.18	4.02	92
$(TCS)_2Cu$ (HD)	2.4 ± 0.3^{d}	2.84	2.35	100
$(TCS)_2Cu$ (LD)	4.8 ± 0.4^{d}	2.04	2.80	100

All values are expressed as mean ± standard error mean. Means with different superscripts are significantly different. The mean difference is significant at the $p<0.05$ level.
HD (High dose: 60 mg/kg), LD (Low dose: 30 mg/kg)

Table 4.1: Observed ulcer area, mucus weight, pH and inhibition percentage in rats for TS and its complexes:

Compound	Total ulcer area(mm^2) (Mean ± S.E.M)	Mucus weight (g)	pH	% inhibition
Tween-20 (-ve control)	1438 ± 58^a	0.58	7.00	-
Cimetidine (+ve control)	168 ± 5^b	0.61	7.00	88
TS (HD)	$Zero^c$	0.88	3.61	100
TS (LD)	$Zero^c$	0.71	5.28	100
$(TS)_2Zn$ (HD)	$Zero^c$	1.31	5.00	100
$(TS)_2Zn$ (LD)	$Zero^c$	0.58	3.44	100
$(TS)_2Ni$ (HD)	9.6 ± 0.2^c	1.50	6.25	99
$(TS)_2Ni$ (LD)	20.4 ± 0.2^c	0.86	4.77	98
$(TS)_2Cu$ (HD)	2.4 ± 0.1^c	1.43	3.54	100
$(TS)_2Cu$ (LD)	52.8 ± 0.2^c	1.33	4.54	96

All values are expressed as mean ± standard error mean. Means with different superscripts are significantly different. The mean difference is significant at the $p<0.05$ level.
HD (High dose: 60 mg/kg), LD (Low dose: 30 mg/kg)